The η-η' system in large-N_c chiral perturbation theory

Dissertation
zur Erlangung des Grades
„Doktor der Naturwissenschaften"

am Fachbereich Physik, Mathematik und Informatik
der Johannes Gutenberg-Universität
in Mainz

Patricia Bickert
geboren in Fulda

Mainz, Oktober 2016

1. Berichterstatter:

2. Berichterstatter:

Datum der mündlichen Prüfung: 16. Februar 2017

D77 (Dissertation der Johannes Gutenberg-Universität Mainz)

Abstract

This thesis is concerned with calculations of processes involving the η-η' system in the framework of large-N_c chiral perturbation theory (LN_cChPT). The calculations are performed at the one-loop level up to and including next-to-next-to-leading order (NNLO) in the simultaneous expansion in external momenta, quark masses, and $1/N_c$.

First, a general expression for the η-η' mixing at NNLO is derived, including higher-derivative terms up to fourth order in the four momentum, kinetic and mass terms. In addition, the axial-vector decay constants of the η-η' system are determined at NNLO. The numerical analysis of the results is performed successively at LO, NLO, and NNLO. The influence of one-loop corrections as well as OZI-rule-violating parameters is studied.

The second part of the thesis deals with quantum corrections to the chiral anomaly accounted for by the Wess-Zumino-Witten action. The anomalous and normal Ward identities are explicitly confirmed at the one-loop level, both in SU(3) ChPT and LN_cChPT. To that end, the three-point Green function involving one axial-vector current and two vector currents (AVV) with all three legs off shell is calculated.

The anomalous decays $\eta^{(\prime)} \to \gamma^{(*)}\gamma^{(*)}$ and $\eta^{(\prime)} \to \pi^+\pi^-\gamma^{(*)}$ are calculated at the one-loop level up to NNLO in LN_cChPT. Both the decays to real photons and the decays involving virtual photons, providing access to the substructure of the mesons, are discussed. The results are numerically evaluated successively at LO, NLO, and NNLO. The appearing low-energy constants are determined through fits to the available experimental data. In the case of $\eta^{(\prime)} \to \gamma^{(*)}\gamma^{(*)}$, we investigate the decay widths to real photons, the widths of $\eta^{(\prime)} \to \gamma l^+l^-$, where $l = e,\ \mu$, and the single-virtual transition form factors. The considered observables of the decays $\eta^{(\prime)} \to \pi^+\pi^-\gamma^{(*)}$ are the spectra of the decays involving a real photon, $\eta^{(\prime)} \to \pi^+\pi^-\gamma$, as well as the spectra of $\eta^{(\prime)} \to \pi^+\pi^-l^+l^-$, where $l = e,\ \mu$, with respect to the invariant masses of the $\pi^+\pi^-$ and l^+l^- systems.

Zusammenfassung

Die vorliegende Dissertation befasst sich mit der Berechnung von Prozessen des η-η'-Systems im Rahmen der chiralen Störungstheorie für große Werte von N_c (*large-N_c chiral perturbation theory*, LN_cChPT). Die Rechnungen werden auf dem Einschleifenniveau bis einschließlich *next-to-next-to-leading order* (NNLO) Korrekturen in der simultanen Entwicklung nach externen Impulsen, Quarkmassen und $1/N_c$ durchgeführt.

Zunächst wird ein allgemeiner Ausdruck für die η-η'-Mischung bis einschließlich NNLO-Korrekturen hergeleitet, welcher höhere Ableitungsterme bis zur vierten Ordnung in Viererimpulsen, kinetische und Massenterme berücksichtigt. Zusätzlich werden die Axialvektorzerfallskonstanten des η-η'-Systems bis einschließlich NNLO-Korrekturen berechnet. Die numerische Auswertung der Ergebnisse wird sukzessive durchgeführt in der führenden Ordnung (*leading order*, LO), NLO und NNLO. Dabei wird der Einfluss der Einschleifenkorrekturen und der Parameter, die die OZI-Regel verletzen, untersucht.

Der zweite Teil der Arbeit beschäftigt sich mit Quantenkorrekturen zur chiralen Anomalie, die durch die Wess-Zumino-Witten Wirkung beschrieben wird. Die anomalen und die normalen Ward Identitäten werden auf dem Einschleifenniveau sowohl in SU(3)-ChPT als auch in LN_cChPT explizit bestätigt. Zu diesem Zweck wird die Green'sche Dreipunktfunktion, die einen Axialvektorstrom und zwei Vektorströme (AVV) enthält, für alle drei Beine jenseits der Massenschale berechnet.

Die anomalen Zerfälle $\eta^{(\prime)} \to \gamma^{(*)}\gamma^{(*)}$ und $\eta^{(\prime)} \to \pi^+\pi^-\gamma^{(*)}$ werden auf dem Einschleifenniveau bis einschließlich NNLO-Korrekturen in LN_cChPT berechnet. Die Zerfälle in reelle Photonen sowie die Zerfälle mit virtuellen Photonen, welche einen Zugang zur Substruktur der Mesonen bieten, werden diskutiert. Die numerische Auswertung der Ergebnisse wird sukzessive in der führenden Ordnung, NLO und NNLO durchgeführt. Dabei werden die auftretenden Niederenergiekonstanten durch Fits an die vorhandenen experimentellen Daten bestimmt. Im Falle von $\eta^{(\prime)} \to \gamma^{(*)}\gamma^{(*)}$ werden die Zerfallsbreiten der Zerfälle in reelle Photonen, die Breiten von $\eta^{(\prime)} \to \gamma l^+ l^-$, wobei $l = e,\ \mu$, und die einfach virtuellen Übergangsformfaktoren untersucht. Die betrachteten Observablen der Zerfälle $\eta^{(\prime)} \to \pi^+\pi^-\gamma^{(*)}$ sind die Spektren der Zerfälle mit einem reellen Photon, $\eta^{(\prime)} \to \pi^+\pi^-\gamma$, sowie die Spektren von $\eta^{(\prime)} \to \pi^+\pi^- l^+ l^-$, wobei $l = e,\ \mu$, in Bezug auf die invarianten Massen der $\pi^+\pi^-$- und l^+l^--Systeme.

Contents

Chapter 1

Introduction

The strong interaction is one of the four fundamental forces known today to describe physical phenomena. The other three forces are the electromagnetic and the weak interaction and gravitation. In the Standard Model (SM) of particle physics, the electromagnetic, weak, and strong interactions are formulated as quantum field theories, while the incorporation of gravitation has not been achieved so far. The by now established gauge theory of the strong interaction is called quantum chromodynamics (QCD) [FGL 73, GW 73a, Wei 73]. Quantum chromodynamics is based on the gauge group SU(3) with quarks being the fundamental matter fields. The quarks, which carry a so-called color charge that can take three values, interact with each other through the exchange of gauge bosons, the gluons, which carry color charge themselves. Due to the latter, the gluons also interact with each other through three- and four-gluon vertices.

Despite being the constituents of matter, no isolated free quarks have been observed so far. Instead only color-neutral bound states of quarks and gluons, so-called hadrons, seem to appear in nature. This phenomenon is known as confinement [GW 73b] and it is still an open question how it can be derived from QCD. Confinement might be related to another remarkable feature of QCD called asymptotic freedom [GW 73a, GW 73b, Pol 73]. It has been shown that the running coupling constant of QCD α_s decreases for increasing energies, thus allowing for a perturbative treatment of QCD in the high-energy regime with expansion parameter α_s. On the other hand, for lower energies, corresponding to large distances, the strong coupling constant increases, providing a possible explanation for confinement. In the low-energy regime for large values of the coupling constant, perturbation theory is no longer applicable.

One tool for the non-perturbative treatment of QCD is given by Lattice QCD, where one obtains numerical solutions of QCD by discretizing space-time [Wil 74, Cre 90]. While lattice calculations have made great progress, they are still limited by the available computing power and an analytical method for calculations in the low-energy regime remains desirable. One option –pursued in this work– is the use of an effective field theory (EFT), which is a (low-energy) approximation to a more fundamental theory. One constructs the most general Lagrangian consistent with the symmetries of the underlying theory [Wei 79], using effective degrees of freedom. In the low-energy region of QCD, those are the baryons and mesons instead of quarks and gluons. The most general Lagrangian consists of an infinite number of interaction terms, each accompanied by a low-energy coupling constant (LEC). In principle, the LECs could be calculated if one knew the solution of the underlying theory. In practice, however, when the fundamental theory is unknown or the connection to the EFT cannot be established directly, the LECs can be determined by comparison with experimental data. In the EFT framework, physical quantities are calculated in terms of an expansion in q/Λ, where q stands for momenta or masses that are small in comparison to some scale Λ. Therefore, the range of applicability of the EFT is limited as the expansion is no longer sensible for sufficiently large values of q. In addition, in actual calculations only a finite number of terms in the q/Λ expansion is taken into account, yielding an appropriate description only to finite accuracy.

The effective field theory of the strong interaction at low energies is called chiral perturbation theory (ChPT) [Wei 79, GL 84, GL 85]. In its SU(3) formulation, ChPT is based on the chiral $\mathrm{SU}(3)_L \times \mathrm{SU}(3)_R$ symmetry of the QCD Lagrangian in the chiral limit[1] and its spontaneous breaking to $\mathrm{SU}(3)_V$. The relevant degrees of freedom are given by the pseudoscalar-meson octet (π, K, η), which can be identified with the Goldstone bosons arising from the spontaneous chiral symmetry breaking. Since the interaction between the Goldstone bosons in the chiral limit vanishes for decreasing energies, the perturbation series is organized in terms of an expansion in small momenta and Goldstone-boson or quark masses. In the mesonic sector of ChPT, the decision which terms of the effective Lagrangian and which Feynman diagrams are relevant in a calculation up to a given order can be made by employing Weinberg's power counting scheme [Wei 79]. Here, one assigns a chiral order D to each diagram according to its behavior under rescaling of external momenta or quark masses. Diagrams with higher D are suppressed relative to those with lower D. Due to the arbitrary negative mass dimension of the LECs, ChPT is not renormalizable in the traditional sense, i.e., divergences appearing in the calculation of loop diagrams cannot be eliminated by redef-

[1] i.e., neglecting the heavy quarks and sending the masses of the light quarks to zero.

inition of a finite number of parameters up to infinite order. However, since the most general Lagrangian contains all terms compatible with the relevant symmetries of QCD and calculations are performed up to finite order, the infinities can be absorbed order by order. In this way, ChPT is said to be renormalizable in a "modern" sense [Wei 79]. Chiral perturbation theory can also be extended to include baryons or other heavy degrees of freedom such as vector mesons, but this will not be part of this thesis.

Due to the $U(1)_A$ anomaly the η' is no Goldstone boson. The $U(1)_A$ symmetry is only preserved at the classical level. Quantum corrections give rise to so-called anomalies, which destroy the symmetry. However, in the large-number-of-colors (LN_c) limit of QCD [Hoo 74a, Wit 79], the $U(1)_A$ anomaly disappears and the η' becomes a ninth Goldstone boson. The η' can be incorporated in the EFT by means of a simultaneous expansion in momenta, quark masses, and $1/N_c$. The corresponding EFT is referred to as large-N_c chiral perturbation theory (LN_cChPT) [Mou 95, Leu 96, Her+ 97, Leu 98, KL 98, Her 98, KL 00]. In the effective theory, the non-abelian $U(3)_L \times U(3)_R$ anomaly is accounted for by the Wess-Zumino-Witten (WZW) action [WZ 71, Wit 83], which represents the leading-order contribution in the so-called anomalous or odd-intrinsic-parity sector.

In the real world, due to the breaking of the SU(3) flavor symmetry, the physical η and η' states are mixed octet and singlet states. In early investigations, the connection between the physical and the octet and singlet states has been established by an orthogonal transformation parametrized by a single mixing angle θ. The mixing angle θ can be determined either by diagonalizing the leading-order mass matrix in ChPT or from phenomenology [Ams+ 14]. Some examples of processes used to extract the η-η' mixing angle are the anomalous two-photon decays $\eta^{(\prime)} \to \gamma\gamma$ [AF 89, VH 98], decays of J/Ψ [GK 87, BES 97, BFT 96], or electromagnetic decays of vector and pseudoscalar mesons [BES 99]. These studies yield mixing angles between $-13°$ [BES 99] and $-22°$ [VH 98]. Using the Gell-Mann-Okubo mass formula for the pseudoscalar mesons, Refs. [Isg 76, FJ 77] obtained $-10°$. In the more modern approach of LN_cChPT, a two-angle mixing scheme [KL 98, Leu 98, Her+ 98] has been proposed for the calculation of the pseudoscalar decay constants. The decay constants relate the physical fields with the (bare) octet and singlet fields. At NLO in LN_cChPT, it turns out that the relation is more complicated than a simple rotation with a single mixing angle θ. The two-angle scheme has been adopted in phenomenological analyses [FKS 98, FKS 99] and has become very popular resulting in well-established determinations of the mixing parameters [FKS 98, FKS 99, BDC 00, EF 05, EMS 11, EMS 14, EMS 15]. Those investigations found out that the phenomenological analysis with two different mixing angles leads to a more coherent picture than the treatment with a single angle.

The η-η' mixing is relevant for every process involving the η-η' system. Two interesting decay modes, which will be studied in this thesis, are the anomalous decays $\eta^{(\prime)} \to \gamma^{(*)}\gamma^{(*)}$ and $\eta^{(\prime)} \to \pi^+\pi^-\gamma^{(*)}$. The two-photon decays involving one or two virtual photons are described by so-called transition form factors (TFFs), which probe the substructure of the decaying pseudoscalar meson. In the time-like region, the single-virtual TFFs are experimentally accessible in so-called Dalitz decays $P \to \gamma l^+l^-$, where $l = e,\ \mu$, [Ber+ 11, Arn+ 09, Agu+ 14, Abl+ 15, Arn+ 16]. For the η', also data in the low-energy space-like region are provided, which were measured in the process $e^+e^- \to e^+e^-P$ [Acc+ 98]. The TFFs are of interest for precision tests of the SM. They enter as contributions to hadronic light-by-light (HLbL) scattering calculations [Col+ 14, Col+ 15], which play an important role in theoretical determinations of the anomalous magnetic moment of the muon, $(g-2)_\mu$, within the SM [JN 09, Nyf 16]. Currently, there exists a puzzle, since the theoretical SM prediction and the experimental value of $(g-2)_\mu$ differ by 3.2σ [JN 09]. In addition, discrepancies between theoretical and experimental determinations are observed for the decay rates of the rare decays to a lepton pair $P \to l^+l^-$, $l = e,\ \mu$, [HL 15, MS 16], where the TFFs of the corresponding pseudoscalar P enter as well. The TFFs have been studied in a variety of theoretical approaches, e.g., the vector-meson-dominance model [BM 81, Ame+ 83, PB 84], a constituent quark model [BM 81, Ame+ 83, PB 84], ChPT at the one-loop level [Ame+ 92], a coupled-channel analysis [BN 04a], chiral effective theory with resonances [Czy+ 12], a data-driven approach using Padé approximants [EMS 14, EMS 15], and a dispersive analysis [Han+ 15].

The decay spectra of $\eta^{(\prime)} \to \pi^+\pi^-\gamma$ have been measured in Refs. [Gor+ 70, Lay+ 73, Adl+ 12, Abe+ 97]. The decays involving a virtual photon can be probed in the processes $\eta^{(\prime)} \to \pi^+\pi^-l^+l^-$, where $l = e,\ \mu$. While the decay widths of $\eta^{(\prime)} \to \pi^+\pi^-e^+e^-$ have been determined experimentally [Oli+ 14], for the widths of $\eta^{(\prime)} \to \pi^+\pi^-\mu^+\mu^-$ only upper limits exist [Oli+ 14]. Theoretical approaches to the decays $\eta^{(\prime)} \to \pi^+\pi^-\gamma$ include one-loop ChPT [BBC 90, Hac 08], ChPT combined with a coupled-channel Bethe-Salpeter equation [BN 04b], a vector-meson-dominance model [Pic 92], calculations in the context of Hidden Local Symmetries [Ben+ 03, Ben+ 10], one-loop ChPT combined with an Omnes function [VH 98, Hol 02], and a dispersive framework [Sto+ 12, KP 15]. It turned out that higher-order corrections are very important for an adequate description of the experimental data. The decays involving a lepton pair $\eta^{(\prime)} \to \pi^+\pi^-l^+l^-$ have been studied in various models including vector mesons [PR 93, FFK 00, Pet 10] and in a chiral unitary approach [BN 07].

At leading order in ChPT, the aforementioned anomalous decays are driven by the chiral anomaly accounted for by the Wess-Zumino-Witten action. In this thesis higher-order corrections to the chiral anomaly are investigated. The anomalous decays of the η-η' system, $\eta^{(\prime)} \to \gamma^{(*)}\gamma^{(*)}$ and $\eta^{(\prime)} \to \pi^+\pi^-\gamma^{(*)}$, are calculated at the one-loop level in LN_cChPT, which corresponds to a next-to-next-to-leading order (NNLO) calculation in the combined chiral and $1/N_c$ expansions. To that end, an expression for the η-η' mixing is derived at NNLO including one-loop corrections. The anomalous Ward identities are studied at the one-loop level by means of a calculation of the three-point Green function involving one axial-vector current and two vector currents (AVV). We show that the Ward identities are satisfied by an explicit verification.

This thesis is organized as follows. In Chapter 2, the QCD Lagrangian is introduced and its symmetry properties are discussed. Chapter 3 provides an introduction to anomalies. Various approaches to derive the anomaly are considered as well as the physical origin of the anomaly. Large-N_c chiral perturbation theory is introduced in Chapter 4. After the basic features of the large-N_c expansion of QCD and ChPT are explained, the relevant Lagrangians of LN_cChPT are constructed. This chapter provides all Lagrangians needed for the calculations in this thesis, including those of the anomalous or odd-intrinsic-parity sector. In Chapter 5 an expression for the η-η' mixing at the one-loop level is derived and the numerical analysis of the mixing, pseudoscalar masses, and decay constants in performed. Chapter 6 contains the investigation of the anomalous Ward identities at the one-loop level. The two-photon decays of the η-η' system are studied in Chapter 7. The calculation, the numerical evaluation, and the results are presented. The anomalous decays $\eta^{(\prime)} \to \pi^+\pi^-\gamma^{(*)}$ are considered in Chapter 8. Finally, in Chapter 9, conclusions and an outlook are provided. Technical details of this work can be found in the Appendix. Besides the Gell-Mann matrices and loop integrals, additional information on the building blocks and their transformation behavior is provided. Explicit expressions of higher-order corrections for the quantities calculated in this thesis, additional results for the fit parameters, and supplementary plots are shown.

Chapter 2

Quantum chromodynamics

In this chapter, the foundations of quantum chromodynamics (QCD), which is the gauge theory of the strong interaction, are presented. The QCD Lagrangian is introduced, followed by a discussion of its symmetries in the chiral limit. Besides spontaneous symmetry breaking and the Goldstone theorem, Green functions and the Ward identities, which originate from the chiral symmetry, are discussed. This introduction is based on Ref. [SS 12].

2.1 The QCD Lagrangian

The strong interaction is described by the gauge theory quantum chromodynamics (QCD). Quantum chromodynamics is a non-abelian gauge theory with SU(3) as gauge group. Its matter fields are spin-1/2 fermions, the so-called quarks, and they interact with each other by the exchange of eight massless gauge bosons, which are the gluons. Quarks occur in six different flavors (u, d, s, c, b, t) in addition to three possible colors red (r), blue (b), and green (g) (see Tab. 2.1). The QCD Lagrangian is given by [MP 78, Alt 81]

Flavor	u	d	s
Charge [e]	$2/3$	$-1/3$	$-1/3$
Mass [MeV]	$2.3^{+0.7}_{-0.5}$	$4.8^{+0.5}_{-0.3}$	95 ± 5
Flavor	c	b	t
Charge [e]	$2/3$	$-1/3$	$2/3$
Mass [GeV]	1.275 ± 0.025	4.18 ± 0.03	$173.21 \pm 0.51 \pm 0.71$

Table 2.1: Charges and masses of the quarks [Oli+ 14].

$$\mathcal{L}_{\mathrm{QCD}} = \sum_f \bar{q}_f (i\not{D} - m_f) q_f - \frac{1}{4} \mathcal{G}_{\mu\nu,a} \mathcal{G}_a^{\mu\nu}. \tag{2.1}$$

For each quark flavor f, the Dirac spinor quark fields are written down as a color triplet

$$q_f = \begin{pmatrix} q_{f,r} \\ q_{f,g} \\ q_{f,b} \end{pmatrix}, \tag{2.2}$$

which transforms under local $\mathrm{SU}(3)_c$ gauge transformations, given by $\Theta(x) = [\Theta_1(x), \ldots, \Theta_8(x)]$, as

$$q_f \mapsto q_f' = \exp\left[-i \sum_{a=1}^{8} \Theta_a(x) \frac{\lambda_a^c}{2}\right] q_f = U[g(x)] q_f. \tag{2.3}$$

The eight Gell-Mann matrices λ_a^c are the generators of SU(3), given in Appendix A.1. The covariant derivative D_μ acting on q_f

$$D_\mu q_f = \partial_\mu q_f - ig \sum_{a=1}^{8} \frac{\lambda_a^c}{2} \mathcal{A}_{\mu,a} q_f \tag{2.4}$$

introduces the coupling of the quark fields to the eight gluon fields $\mathcal{A}_{\mu,a}$ with the coupling strength g. Demanding invariance under gauge transformations leads to the following transformation behavior of the gluon fields[1]

$$\frac{\lambda_a^c}{2} \mathcal{A}_{\mu,a}(x) \mapsto U[g(x)] \frac{\lambda_a^c}{2} \mathcal{A}_{\mu,a}(x) U^\dagger[g(x)] - \frac{i}{g} \partial_\mu U[g(x)] U^\dagger[g(x)], \tag{2.5}$$

and the covariant derivative has to transform as q_f, i.e.,

$$D_\mu q_f \mapsto D_\mu' q_f' = U[g(x)] D_\mu q_f. \tag{2.6}$$

In addition, the QCD Lagrangian contains the kinetic term of the gluons, which is given by the product of the field-strength tensors

$$\mathcal{G}_{\mu\nu,a} = \partial_\mu \mathcal{A}_{\nu,a} - \partial_\nu \mathcal{A}_{\mu,a} + g f_{abc} \mathcal{A}_{\mu,b} \mathcal{A}_{\nu,c}, \tag{2.7}$$

where f_{abc} are the structure constants of SU(3) (see Appendix A.1). The non-abelian part $g f_{abc} \mathcal{A}_{\mu,b} \mathcal{A}_{\nu,c}$ is responsible for the gluon self interaction.

[1] Here and in the following, a summation over repeated indices is implied.

2.2 QCD in the chiral limit

The six quark flavors can be divided into three light quarks u, d, s and three heavy quarks c, b, t (see Tab. 2.1) with $m_u, m_d, m_s << 1$ GeV $\leq m_c, m_b, m_t$. The scale of 1 GeV corresponds to the masses of the lightest hadrons containing light quarks, e.g., $m_\rho = 770$ MeV, which are not Goldstone bosons, and to the scale of spontaneous chiral symmetry breaking $\Lambda_\chi = 4\pi F_\pi = 1.170$ GeV. This suggests that a good approximate description of low-energy QCD is given by the QCD Lagrangian in the so-called chiral limit

$$\mathcal{L}^0_{\mathrm{QCD}} = \sum_{f=u,d,s} \bar{q}_f i \not{D} q_f - \frac{1}{4}\mathcal{G}_{\mu\nu,a}\mathcal{G}^{\mu\nu}_a, \tag{2.8}$$

where the heavy quarks are omitted and the light-quark masses are set to zero. Introducing the projection operators

$$P_R = \frac{1}{2}(\mathbb{1} + \gamma_5), \qquad P_L = \frac{1}{2}(\mathbb{1} - \gamma_5), \tag{2.9}$$

the Lagrangian can be written as

$$\mathcal{L}^0_{\mathrm{QCD}} = \sum_{f=u,d,s} (\bar{q}_{R,f} i \not{D} q_{R,f} + \bar{q}_{L,f} i \not{D} q_{L,f}) - \frac{1}{4}\mathcal{G}_{\mu\nu,a}\mathcal{G}^{\mu\nu}_a. \tag{2.10}$$

This Lagrangian exhibits a global $\mathrm{SU}(3)_L \times \mathrm{SU}(3)_R \times \mathrm{U}(1)_V \times \mathrm{U}(1)_A$ symmetry. The $\mathrm{U}(1)_V$ symmetry leads to the conservation of the baryon number, while the $\mathrm{U}(1)_A$ symmetry exists only at the classical level. Quantum fluctuations destroy the conservation of the singlet axial-vector current and generate so-called anomalies [AB 69, Adl 69, BJ 69]. The $\mathrm{SU}(3)_L \times \mathrm{SU}(3)_R$ symmetry is referred to as chiral symmetry. Considering only the symmetry of the Hamiltonian H^0_{QCD}, one would naively expect that the hadrons form approximately degenerate multiplets matching the dimensionalities of irreducible representations of the group $\mathrm{SU}(3)_L \times \mathrm{SU}(3)_R \times \mathrm{U}(1)_V$. For every multiplet one would expect the existence of a degenerate multiplet of opposite parity. However, this is not observed in the hadron spectrum, since, e.g., a degenerate baryon octet of negative parity does not exist in the low-energy baryon spectrum. Empirically one realizes that the hadron spectrum reflects only an $\mathrm{SU}(3)_V$ symmetry. Furthermore, the masses of the pseudoscalar-meson octet are small in comparison to the corresponding vector-meson octet with the same quark content. This points to the fact that the $\mathrm{SU}(3)_L \times \mathrm{SU}(3)_R$ symmetry is spontaneously broken to the $\mathrm{SU}(3)_V$ symmetry. A symmetry is said to be spontaneously broken if the ground state of the system is not invariant under the full symmetry group G of the Hamiltonian but only invariant under a subgroup H of G. The Goldstone theorem [Gol 61] then predicts the existence of $n_G - n_H$ massless Goldstone bosons, where n_G denotes the number of generators of the group G and n_H the number of generators of the group H. The symmetry properties of the Goldstone bosons are closely related to the ones of the $n_G - n_H$ generators which do not annihilate the vacuum. The group $\mathrm{SU}(3)_L \times \mathrm{SU}(3)_R$ has 16 generators, while the group $\mathrm{SU}(3)_V$, which leaves the ground state invariant, has eight generators. According to the Goldstone theorem, one expects eight Goldstone bosons which can be identified with the pseudoscalar-meson octet. The finite masses of the meson octet are a consequence of the explicit symmetry breaking due to the non-vanishing quark masses. The observed $\mathrm{SU}(3)_V$ symmetry is explained by Coleman's theorem [Col 66], which states that the symmetry of the spectrum is determined by the symmetry of the vacuum and not by the symmetry of the Hamiltonian.

2.3 QCD in the presence of external fields

In quantum field theory, one is interested in so-called Green functions, which are vacuum expectation values of time-ordered products. The Lehmann-Symanzik-Zimmermann (LSZ) reduction formalism [LSZ 55] connects the Green functions to physical scattering amplitudes. The symmetries of the theory impose relations between different Green functions. Those relations are called Ward-Fradkin-Takahashi identites [War 50, Fra 55, Tak 57], or denoted shortly as Ward identities. In the path-integral formalism, all Green functions can be elegantly combined in a generating functional. To that end, we introduce into the QCD Lagrangian the couplings of the vector- and axial-vector currents, the scalar and pseudoscalar quark densities, and the winding number density $\omega = \frac{g^2}{16\pi^2}\mathrm{tr}_c(G_{\mu\nu}\tilde{G}^{\mu\nu})$ to external c-number fields [GL 84, GL 85]

$$\mathcal{L} = \mathcal{L}^0_{\mathrm{QCD}} + \mathcal{L}_{\mathrm{ext}} = \mathcal{L}^0_{\mathrm{QCD}} + \bar{q}\gamma_\mu\left(v^\mu + \gamma_5 a^\mu\right)q - \bar{q}\left(s - i\gamma_5 p\right)q - \theta\,\omega, \tag{2.11}$$

where

$$v^\mu = \sum_{a=0}^{8} v_a^\mu \frac{\lambda_a}{2},\ a^\mu = \sum_{a=0}^{8} a_a^\mu \frac{\lambda_a}{2},\ s = \sum_{a=0}^{8} s_a\lambda_a,\ p = \sum_{a=0}^{8} p_a\lambda_a, \tag{2.12}$$

with $\lambda_0 = \sqrt{2/3}\,\mathbb{1}$, and θ is a real field. The original QCD Lagrangian is recovered for

$$v^\mu = a^\mu = p = 0, \quad s = \mathrm{diag}(m_u, m_d, m_s), \quad \theta = \theta_0, \tag{2.13}$$

where θ_0 is the QCD vacuum angle, which is found to be very small $|\theta_0| \leq 10^{-10}$ [Oli+ 14, Bak 06]. Defining the generating functional

$$\exp\left(iZ[v,a,s,p,\theta]\right) = \langle 0|T\, \exp\left[i\int d^4x \mathcal{L}_{\text{ext}}(x)\right]|0\rangle\,, \tag{2.14}$$

each Green function can be calculated through a functional derivative of the generating functional with respect to the corresponding external fields. In the absence of anomalies, the Ward identities which are obeyed by the Green functions are equivalent to the invariance of the generating functional under local chiral transformations [Leu 94]. The invariance of the Lagrangian in Eq. (2.11) under local chiral transformations can be achieved if the external fields transform according to

$$\begin{aligned}
r^\mu &\mapsto V_R r^\mu V_R^\dagger + iV_R\partial^\mu V_R^\dagger,\\
l^\mu &\mapsto V_L l^\mu V_L^\dagger + iV_L\partial^\mu V_L^\dagger,\\
s+ip &\mapsto V_R(s+ip)V_L^\dagger,\\
s-ip &\mapsto V_L(s-ip)V_R^\dagger,\\
\theta &\mapsto \theta + i\ln\det V_R - i\ln\det V_L,
\end{aligned} \tag{2.15}$$

with $(V_L, V_R) \in \mathrm{U}(3)_L \times \mathrm{U}(3)_R$ and

$$r^\mu = v^\mu + a^\mu, \quad l^\mu = v^\mu - a^\mu. \tag{2.16}$$

In addition, local invariance allows to couple external gauge fields, e.g., the electromagnetic field, to the effective degrees of freedom [GL 84, GL 85].

Chapter 3

Anomalies

An anomaly is said to appear if a symmetry that exists at the classical level is destroyed by quantum corrections. Anomalies can give rise to a violation of global symmetries as well as local symmetries. In the latter case, the theory is no longer renormalizable and becomes inconsistent. One then constrains the theory by imposing the cancellation of the anomalies. In this chapter, we will outline different approaches to understand the origin of the anomaly. This discussion closely follows Ref. [BH 13].

3.1 Perturbation theory

We start with the most intuitive method of the derivation of the anomaly within perturbation theory, following Ref. [BH 13]. This approach was employed by the first investigators [AB 69, Adl 69, BJ 69]. We consider a massless spinor field ψ with a charge e coupled to the electromagnetic field A^μ. The Lagrangian is given by

$$\mathcal{L} = \bar{\psi}(i\partial\!\!\!/ - eA\!\!\!/)\psi - \frac{1}{4}F_{\mu\nu}F^{\mu\nu}, \tag{3.1}$$

which is invariant under the global transformations

$$\psi \mapsto \exp(i\alpha)\psi, \tag{3.2}$$

$$\psi \mapsto \exp(i\beta\gamma_5)\psi. \tag{3.3}$$

Noether's theorem implies the conservation of the corresponding vector and axial-vector currents,

$$J_\mu = \bar{\psi}\gamma_\mu\psi, \quad \text{with} \quad \partial^\mu J_\mu = 0, \tag{3.4}$$

and

$$J_{5\mu} = \bar{\psi}\gamma_\mu\gamma_5\psi, \quad \text{with} \quad \partial^\mu J_{5\mu} = 0, \tag{3.5}$$

respectively. Let us examine the axial-vector vector vector (AVV) three-point Green function

$$T^{\mu\nu\rho}(q_1, q_2) = -ie^2 \int d^4x d^4y e^{-iq_1\cdot x - iq_2\cdot y} \langle 0| T[J^\mu(x) J^\nu(y) J_5^\rho(0)] |0\rangle . \tag{3.6}$$

The requirement of the conservation of the vector and axial-vector currents leads to the Sutherland-Veltman theorem [Sut 67, Vel 67], which states that the $\pi^0 \to \gamma\gamma$ decay amplitude vanishes in this case. One starts by writing down the most general expression for $T_{\mu\nu\rho}(q_1, q_2)$ which satisfies Bose symmetry, parity conservation, and gauge invariance:[1]

$$\begin{aligned} T_{\mu\nu\rho}(q_1, q_2) = \epsilon_{\lambda\sigma\alpha\beta} \Big\{ & p_\rho g_\mu^\lambda g_\nu^\sigma q_1^\alpha q_2^\beta G_1(p^2) \\ & + \left(g_\mu^\sigma q_{2\nu} - g_\nu^\sigma q_{1\mu}\right) q_1^\alpha q_2^\beta g_\rho^\lambda G_2(p^2) \\ & + \left[\left(g_\mu^\sigma q_{1\nu} - g_\nu^\sigma q_{2\mu}\right) q_1^\alpha q_2^\beta - \frac{1}{2} p^2 g_\mu^\sigma g_\nu^\alpha (q_1 - q_2)^\beta \right] g_\rho^\lambda G_3(p^2) \Big\}, \end{aligned} \tag{3.7}$$

where $p = q_1 + q_2$ is the axial-current momentum. Demanding the conservation of the axial current yields

$$\begin{aligned} 0 &= p^\rho T_{\mu\nu\rho}(q_1, q_2) \\ &= \epsilon_{\mu\nu\alpha\beta} q_1^\alpha q_2^\beta p^2 \left[G_1(p^2) + G_3(p^2)\right]. \end{aligned} \tag{3.8}$$

We define the off-shell $\pi^0 \to \gamma\gamma$ amplitude as

$$\left\langle \gamma\gamma|\pi^0 \right\rangle = \epsilon_1^{\mu *} \epsilon_2^{\nu *} A_{\mu\nu}(q_1, q_2), \tag{3.9}$$

with

$$A_{\mu\nu}(q_1, q_2) = A(p^2) \epsilon_{\mu\nu\alpha\beta} q_1^\alpha q_2^\beta. \tag{3.10}$$

Using the LSZ reduction and the partially conserved axial-vector current (PCAC) condition, which asserts that the divergence of the axial current serves as an interpolating pion field,

$$\partial^\mu J_{5\mu}^a(x) = F_\pi M_\pi^2 \phi_\pi^a(x), \tag{3.11}$$

where $F_\pi = 92.2$ MeV, together with Eq. (3.8), we obtain

$$A(p^2) = \frac{(M_\pi^2 - p^2)}{F_\pi M_\pi^2} p^2 [G_1(p^2) + G_3(p^2)]. \tag{3.12}$$

[1] Note that we consider the expression for real photons, i.e., $q_1^2 = q_2^2 = 0$.

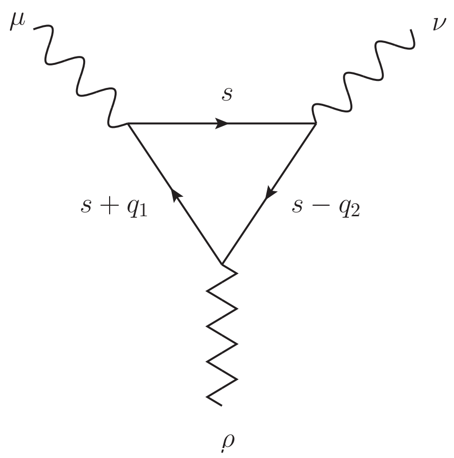

Figure 3.1: Perturbation theory Feynman diagram for the AVV three-point function. Wiggly lines refer to vector currents, the jagged line to the axial-vector current, and solid lines to quarks.

Since the appearance of poles of $G_1(p^2)$ and $G_3(p^2)$ at $p^2 = 0$ is excluded on physical grounds, we find that $A(0) = 0$ and the decay amplitude for $\pi^0 \to \gamma\gamma$ vanishes in the chiral limit, where $M_\pi^2 = 0$, thus proofing the Sutherland-Veltman theorem. To derive a value for the real word where $M_\pi^2 \neq 0$, we extrapolate from the chiral limit, which suggests an amplitude of the size

$$A(M_\pi^2) \sim \frac{e^2}{16\pi^2 F_\pi}\frac{M_\pi^2}{\Lambda_\chi^2}, \tag{3.13}$$

where $\Lambda_\chi \sim 4\pi F_\pi \sim 1$ GeV is the chiral scale. The factor $e^2/(4\pi)$ arises from the two-photon amplitude with a loop diagram, the "extra" $4\pi F_\pi$ is needed for dimensional purposes, and the factor M_π^2/Λ_χ^2 represents the chiral symmetry breaking correction by the quark masses to the vanishing lowest-order term. Equation (3.13) leads to a π^0 decay width of

$$\Gamma_{\pi^0} \sim 10^{13}\ \mathrm{s}^{-1}, \tag{3.14}$$

which is three orders of magnitude smaller than observed.

To examine this phenomenon further, we now study the π^0 decay in perturbation theory. Here, the three-point function is described by the triangle diagram in Fig. 3.1. The evaluation of the Feynman rules yields

$$T_{\mu\nu\rho}(q_1, q_2) = U_{\mu\nu\rho}(q_1, q_2) + U_{\nu\mu\rho}(q_2, q_1), \tag{3.15}$$

where

$$U_{\mu\nu\rho}(q_1, q_2) = -i\frac{e^2}{2}\int \frac{d^4 s}{(2\pi)^4}\mathrm{Tr}\left(\frac{1}{\not{s}+\not{q}_1}\gamma_\mu \frac{1}{\not{s}}\gamma_\nu \frac{1}{\not{s}-\not{q}_2}\gamma_\rho\gamma_5\right). \tag{3.16}$$

We can now check whether the current conservation in Eqs. (3.4) and (3.5) is valid on the quantum level. We start with the conservation of the vector current, which after some manipulations reads

$$q_1^\mu T_{\mu\nu\rho}(q_1, q_2) = -\frac{ie^2}{2}\int \frac{d^4 s}{(2\pi)^4}[W_{\nu\rho}(s+q_1) - W_{\nu\rho}(s+q_2)], \tag{3.17}$$

with

$$W_{\nu\rho}(s) = \mathrm{Tr}\left(\frac{1}{\not{s}}\gamma_\nu \frac{1}{\not{s}-\not{q}_1-\not{q}_2}\gamma_\rho\gamma_5\right). \tag{3.18}$$

We would be allowed to shift the integration variables in Eq. (3.17), if the integrals were convergent or no worse than logarithmically divergent. In this case, the two terms in Eq. (3.17) would cancel each other and the vector current would be conserved. However, since the integrals in Eq. (3.17) are linearly divergent at large s, one has to be more careful. Using Taylor's theorem

$$\int \frac{d^4 s}{(2\pi)^4}F(s+a) = \int \frac{d^4 s}{(2\pi)^4}[F(s) + a^\alpha \partial_\alpha F(s) + \dots], \tag{3.19}$$

we obtain

$$q_1^\mu T_{\mu\nu\rho}(q_1, q_2) = -\frac{ie^2}{2}(q_2 - q_1)^\alpha \int \frac{d^4 s}{(2\pi)^4}[\partial_\alpha W_{\nu\rho}(s) + \dots], \tag{3.20}$$

with vanishing higher-order terms, denoted by the ellipses. The remaining piece is evaluated via Gauss' theorem, leading to

$$q_1^\mu T_{\mu\nu\rho}(q_1, q_2) = \frac{-ie^2}{8\pi^2}\epsilon_{\mu\nu\rho\sigma} q_1^\mu q_2^\sigma. \tag{3.21}$$

In a similar way one finds

$$q_2^\nu T_{\mu\nu\rho}(q_1, q_2) = \frac{ie^2}{8\pi^2}\epsilon_{\mu\nu\rho\sigma} q_1^\nu q_2^\sigma \tag{3.22}$$

and

$$(q_1 + q_2)^\rho T_{\mu\nu\rho}(q_1, q_2) = 0. \tag{3.23}$$

Equations (3.21) and (3.22) show a violation of the electromagnetic gauge invariance, which is problematic if we want to consider interactions with photons. In addition, the finite divergence of the vector current leads to the non-conservation of the fermion number [Zee 03]. However, due to the linear divergence, the integral in Eq. (3.15) is not well defined. One can perform an appropriate shift of the integration variables such that the result $\tilde{T}_{\mu\nu\rho}(q_1, q_2)$ is manifestly crossing symmetric and the vector current is conserved [Zee 03]:

$$q_1^\mu \tilde{T}_{\mu\nu\rho}(q_1, q_2) = q_2^\nu \tilde{T}_{\mu\nu\rho}(q_1, q_2) = 0. \tag{3.24}$$

In this case the divergence of the axial-vector current reads

$$(q_1 + q_2)^\rho \tilde{T}_{\mu\nu\rho}(q_1, q_2) = \frac{ie^2}{4\pi^2} \epsilon_{\mu\nu\rho\sigma} q_1^\rho q_2^\sigma. \tag{3.25}$$

Demanding the conservation of the vector current results in the non-conservation of the axial-vector current. It is not possible to conserve both currents at the same time. The proper quantization of the theory has broken the classical axial symmetry and an anomaly exists. Equation (3.25) corresponds to the operator equation

$$\partial^\mu J^3_{5\mu} = \frac{e^2}{16\pi^2} F_{\mu\nu} \tilde{F}^{\mu\nu}, \tag{3.26}$$

where

$$\tilde{F}^{\mu\nu} = \frac{1}{2} \epsilon_{\mu\nu\alpha\beta} F^{\alpha\beta}. \tag{3.27}$$

Using the PCAC condition in Eq. (3.11) together with Eq. (3.26), we obtain

$$\langle \gamma\gamma | \pi^0 \rangle = \frac{e^2}{4\pi^2 F_\pi} \epsilon_{\mu\nu\alpha\beta} q_1^\mu \epsilon_1^{\nu *} q_2^\alpha \epsilon_2^{\beta *}, \tag{3.28}$$

which leads to the π^0 decay amplitude

$$A_{\pi^0\gamma\gamma} = \frac{e^2}{16\pi^2 F_\pi} \tag{3.29}$$

and a decay width of

$$\Gamma_{\pi^0} = \frac{M_\pi^3}{4\pi} |A_{\pi^0\gamma\gamma}|^2 = 1.18 \times 10^{16}\ \mathrm{s}^{-1}, \tag{3.30}$$

which is close to the experimental value $\Gamma_{\pi^0} = (1.16 \pm 0.02) \times 10^{16}\ \mathrm{s}^{-1}$.

Interestingly, already in 1949, Steinberger found a similar result in a pre-QCD theory when he calculated the π^0 decay amplitude from a triangle graph with a single proton loop [Ste 49], yielding

$$A_{\pi^0\gamma\gamma} = \frac{e^2 g_{\pi NN}}{16\pi^2 m_N}, \tag{3.31}$$

where $g_{\pi NN}$ is the strong pseudoscalar πNN coupling constant. Using the Goldberger-Treiman relation [GT 58]

$$g_{\pi NN} = \frac{m_N g_A}{F_\pi}, \tag{3.32}$$

where $g_A \simeq 1.27$ is the neutron axial decay constant, leads to a result which is similar to Eq. (3.29). Steinberger obtained nearly the correct result, because the answer is given by the triangle anomaly, which is proportional to

$$\mathrm{tr}[q^2\tau_3] = \frac{N_c e^2}{3}. \tag{3.33}$$

The trace has the same value for one proton as for quarks with three colors.

We have studied the anomaly in a simple (leading-order) perturbative calculation. In Ref. [AB 69], it was shown that the contributions of higher orders do not modify the chiral anomaly. The basic reason is that the higher-order effects remove the linear divergence of the triangle diagrams and render the diagrams more convergent. The study of anomalies has also been extended to non-abelian theories [Bar 69]. Here, anomalous Ward identities do not only arise from triangle diagrams but also from box and pentagon diagrams. Bardeen was able to identify the minimal form of the anomaly. Wess and Zumino [WZ 71] derived consistency or integrability relations which the anomalous Ward identities must satisfy. Those conditions follow from the structure of the gauge group and are largely independent of the details of the theory. Based on these relations, Wess and Zumino constructed an effective action involving the pseudoscalar octet which correctly produces the non-abelian anomaly. This procedure will be outlined in Sec. 4.4. Witten [Wit 83] has given a remarkable geometric interpretation of the Wess-Zumino effective action and constructed a closed form of the action in five dimensions. This will be discussed in more detail in Sec. 4.4 as well.

Alternative approaches

Alternative approaches to deal with the short-distance behavior are the Pauli-Villars regularization [PV 49, Gup 53] and point splitting [Tre+ 86]. The

Pauli-Villars regularization consists of using a Pauli-Villars regulator to render the results finite. The physical amplitude is defined as the difference of the amplitude calculated with massless fermions and the one calculated with fermions having a large mass M

$$T^{\text{physical}}_{\mu\nu\rho} = \lim_{M\to\infty} \left[T_{\mu\nu\rho}(q_1,q_2) - T^M_{\mu\nu\rho}(q_1,q_2)\right], \tag{3.34}$$

where $T^M_{\mu\nu\rho}(q_1,q_2)$ is identical to $T_{\mu\nu\rho}(q_1,q_2)$ but the massless fermion propagators are replaced by propagators having a mass M.

Difficulties arise when the field and its conjugate are at the same spacetime point. In the point-splitting approach, this problem is solved by defining the axial current via [Tre+ 86]

$$J^3_{5\mu}(x) = \lim_{\epsilon\to 0} \bar{\psi}\left(x+\frac{1}{2}\epsilon\right)\frac{1}{2}\tau_3\gamma_\mu\gamma_5\psi\left(x-\frac{1}{2}\epsilon\right)\exp\left(ie\int_{x-(1/2)\epsilon}^{x+(1/2)\epsilon} dy_\beta A^\beta(y)\right). \tag{3.35}$$

Because ψ and $\bar{\psi}$ have been placed at different points, a so-called Wilson line

$$\exp\left(ie\int_{x-(1/2)\epsilon}^{x+(1/2)\epsilon} dy_\beta A^\beta(y)\right) \tag{3.36}$$

has to be introduced in order to make the operator locally gauge invariant. Evaluating the divergence, taking the limit $\epsilon \to 0$, and using the short-distance behavior of the Dirac field [Tre+ 86] results once again in the axial-anomaly equation

$$\partial^\mu J^3_{5\mu} = \frac{e^2}{16\pi^2} F^{\mu\nu}\tilde{F}_{\mu\nu}. \tag{3.37}$$

3.2 Path integration

Another way of understanding the anomaly is provided in the path-integral formalism. Here, Ward identities are formulated via the variation of the generating functional under local symmetry transformations. In (gauge) theories with fermions, the path-integral measure is not invariant under axial transformations and the anomaly arises from nontrivial Jacobian factors in the path-integral measure [Fuj 79, Fuj 80]. Following Ref. [PS 95], this approach will be explained in more detail. Let us consider a theory of massless fermions described by a field $\psi(x)$ coupled to the electromagnetic field $A_\mu(x)$. The fermionic functional integral is given by

$$Z = \int \mathcal{D}\psi\mathcal{D}\bar{\psi}\exp\left[i\int d^4x\bar{\psi}(i\not{D})\psi\right], \tag{3.38}$$

with $\not{D} = \gamma_\mu D^\mu$. We perform a change of variables corresponding to a local axial transformation of the fermion field

$$\begin{aligned} \psi(x) &\to \psi'(x) = (1 + i\beta(x)\gamma^5)\psi(x), \\ \bar{\psi}(x) &\to \bar{\psi}'(x) = \bar{\psi}(x)(1 + i\beta(x)\gamma^5), \end{aligned} \tag{3.39}$$

which leads to

$$\int d^4x \bar{\psi}'(i\not{D})\psi' = \int d^4x \left[\bar{\psi}(i\not{D})\psi + \beta(x)\partial_\mu(\bar{\psi}\gamma^\mu\gamma^5\psi)\right]. \tag{3.40}$$

If the functional measure does not change under the change of variables from $\psi'(x)$ to $\psi(x)$, a variation of the Lagrangian with respect to $\beta(x)$ implies the conservation of the axial-vector current $J_{5\mu} = \bar{\psi}\gamma_\mu\gamma_5\psi$. However, this argument breaks down. To define the functional measure, we expand the fermion field in a basis of eigenstates of $\not{D}$

$$(i\not{D})\phi_m = \lambda_m\phi_m, \qquad \hat{\phi}_m(i\not{D}) = -iD_\mu\hat{\phi}_m\gamma^\mu = \lambda_m\hat{\phi}_m, \tag{3.41}$$

such that

$$\psi(x) = \sum_m a_m\phi_m(x), \qquad \bar{\psi}(x) = \sum_m \hat{a}_m\hat{\phi}_m(x), \tag{3.42}$$

with anticommuting coefficients a_m, $\hat{a}_m$ multiplying the c-number eigenfunctions. The functional measure is given by

$$\mathcal{D}\psi\mathcal{D}\bar{\psi} = \prod_m da_m d\hat{a}_m. \tag{3.43}$$

The expansion coefficients of ψ and ψ' are connected via an infinitesimal transformation $(1 + C)$, given by

$$a'_m = \sum_n \int d^4x \phi^\dagger_m(x)(1 + i\beta(x)\gamma^5)\phi_n(x)a_n = \sum_n(\delta_{mn} + C_{mn})a_n. \tag{3.44}$$

Then, the functional measure transforms as

$$\mathcal{D}\psi'\mathcal{D}\bar{\psi}' = \mathcal{J}^{-2}\mathcal{D}\psi\mathcal{D}\bar{\psi}, \tag{3.45}$$

where $\mathcal{J}$ is the Jacobian determinant of the transformation $(1 + C)$. We can evaluate $\mathcal{J}$ according to

$$\mathcal{J} = \det(1 + C) = \exp\left[\operatorname{tr}\log(1 + C)\right] = \exp\left[\sum_n C_{nn} + \dots\right], \tag{3.46}$$

where higher-order terms are neglected, because C is infinitesimal. We obtain

$$\log \mathcal{J} = i \int d^4x \beta(x) \sum_n \phi_n^\dagger(x) \gamma^5 \phi_n(x). \tag{3.47}$$

The sum over eigenstates n has to be regularized in a gauge-invariant way and a natural choice is

$$\sum_n \phi_n^\dagger(x) \gamma^5 \phi_n(x) = \lim_{M\to\infty} \sum_n \phi_n^\dagger(x) \gamma^5 \phi_n(x) e^{\lambda_n^2/M^2}. \tag{3.48}$$

For a fixed field A_μ the asymptotic form of the eigenvalues for large k is given by

$$\lambda_m^2 = k^2 = (k^0)^2 - (\vec{k})^2. \tag{3.49}$$

This implies that the sign of λ_m^2 will be negative at large momentum after a Wick rotation, which leads to the correct sign in the exponent of the convergence factor. Equation (3.48) can be written in an operator form

$$\begin{aligned}\sum_n \phi_n^\dagger(x) \gamma^5 \phi_n(x) &= \lim_{M\to\infty} \sum_n \phi_n^\dagger(x) \gamma^5 e^{(i\not{D})^2/M^2} \phi_n(x), \\ &= \lim_{M\to\infty} \langle x| \operatorname{tr}\left[\gamma^5 e^{(i\not{D})^2/M^2}\right] |x\rangle . \end{aligned} \tag{3.50}$$

To evaluate Eq. (3.50), we rewrite

$$(i\not{D})^2 = -D^2 + \frac{e}{2}\sigma^{\mu\nu} F_{\mu\nu}, \tag{3.51}$$

with $\sigma^{\mu\nu} = \frac{i}{2}[\gamma^\mu, \gamma^\nu]$. Since we want to take the limit $M \to \infty$, we can consider the asymptotic part of the spectrum, where the momentum k is large and we can expand in powers of the gauge field. The trace with γ_5 is only different from zero, if we bring down four Dirac matrices from the exponent. To obtain the leading term, we expand the exponent to order $(\sigma \cdot F)^2$, and then ignore the background field A_μ in the other terms. This leads to

$$\begin{aligned}&\lim_{M\to\infty} \langle x| \operatorname{tr}\left[\gamma^5 e^{(-\mathcal{D}^2 + (e/2)\sigma\cdot F)/M^2}\right] |x\rangle \\ &= \lim_{M\to\infty} \operatorname{tr}\left[\gamma^5 \frac{1}{2!}\left(\frac{e}{2M^2}\sigma^{\mu\nu}F_{\mu\nu}(x)\right)^2\right] \langle x| e^{-\partial^2/M^2} |x\rangle . \end{aligned} \tag{3.52}$$

We evaluate the matrix element via a Wick rotation

$$\begin{aligned}\langle x| e^{-\partial^2/M^2} |x\rangle &= \lim_{x\to y} \int \frac{d^4k}{(2\pi)^4} e^{-ik\cdot(x-y)} e^{k^2/M^2} \\ &= i \int \frac{d^4k_E}{(2\pi)^4} e^{-k_E^2/M^2} \\ &= i \frac{M^4}{16\pi^2}. \end{aligned} \tag{3.53}$$

Then, Eq. (3.52) reads[2]

$$\lim_{M\to\infty} \frac{-ie^2}{8\cdot 16\pi^2} M^4 \mathrm{tr}\left[\gamma^5\gamma^\mu\gamma^\nu\gamma^\lambda\gamma^\sigma \frac{1}{(M^2)^2} F_{\mu\nu}F_{\lambda\sigma}(x)\right]$$
$$= \frac{e^2}{32\pi^2}\epsilon^{\alpha\beta\mu\nu}F_{\alpha\beta}F_{\mu\nu}(x), \tag{3.54}$$

and the Jacobian determinant takes the form

$$\mathcal{J} = \exp\left[i\int d^4x\beta(x)\left(\frac{e^2}{32\pi^2}\epsilon^{\mu\nu\lambda\sigma}F_{\mu\nu}F_{\lambda\sigma}(x)\right)\right]. \tag{3.55}$$

Finally, after the change of variables in Eq. (3.39), the functional integral is given by

$$Z = \int \mathcal{D}\psi\mathcal{D}\bar{\psi}\exp\left[i\int d^4x\left(\bar{\psi}(i\not{D})\psi + \beta(x)\left\{\partial_\mu J_5^\mu - \frac{e^2}{16\pi^2}\epsilon^{\mu\nu\lambda\sigma}F_{\mu\nu}F_{\lambda\sigma}\right\}\right)\right]. \tag{3.56}$$

The variation with respect to $\beta(x)$ leads precisely to the anomaly equation

$$\partial_\mu J_5^\mu = \frac{e^2}{16\pi^2}\epsilon^{\mu\nu\lambda\sigma}F_{\mu\nu}F_{\lambda\sigma}. \tag{3.57}$$

3.3 Physics of the anomaly

After the formal derivation of the anomaly, we now turn to a discussion of the physics behind the anomaly. We start by studying the particularly simple model of massless electrodynamics in one plus one dimensions, which is called the Schwinger model [Sch 51]. Its Lagrangian is given by

$$\mathcal{L} = \bar{\psi}i\not{D}\psi - \frac{1}{4}F_{\mu\nu}F^{\mu\nu}, \tag{3.58}$$

where $D_\mu = \partial_\mu + ieA_\mu$ and the 2×2 Dirac matrices are represented in terms of the Pauli matrices via

$$\gamma^0 = \sigma_1 \quad \text{and} \quad \gamma^1 = i\sigma_2. \tag{3.59}$$

At the classical level, both the vector current

$$j_\mu = \bar{\psi}\gamma_\mu\psi \tag{3.60}$$

[2]Note that our convention $\epsilon_{0123} = 1$ has the opposite sign as the one used in Ref. [PS 95].

and the axial vector current

$$j^5_\mu = \bar{\psi}\gamma_\mu\gamma_5\psi \tag{3.61}$$

are conserved:

$$\partial^\mu j_\mu = 0 \quad \text{and} \quad \partial^\mu j^5_\mu = 0. \tag{3.62}$$

The currents are related via

$$j^5_\mu = \epsilon_{\mu\nu} j^\nu, \quad \text{with} \quad \gamma_5 = -\gamma^0\gamma^1 = \sigma_3, \tag{3.63}$$

where $\epsilon_{\mu\nu}$ is the two-dimensional Levi-Civita tensor. However, upon quantization it can be shown that the Lagrangian takes the form [Sch 62]

$$\mathcal{L} = \bar{\psi}' i\partial\!\!\!/ \psi' - \frac{1}{4}F_{\mu\nu}F^{\mu\nu} + \frac{e^2}{2\pi}A_\mu A^\mu. \tag{3.64}$$

This Lagrangian describes a non-interacting system of massless spin-1/2 particles and free "photons" with a squared mass of $m_\gamma^2 = e^2/\pi$. In addition, quantization destroys the conservation of the axial-vector current and leads to the anomaly

$$\partial^\mu j^5_\mu = -\frac{e}{2\pi}\epsilon^{\mu\nu}F_{\mu\nu}. \tag{3.65}$$

Widom and Srivastava [WS 88] have given an argument for the physical origin of the anomaly. According to Dirac, the vacuum state of the quantized theory can be described as a filled set of negative-energy states. If the external electric field is switched off, the electron states are evenly distributed with a constant level density of $dp/2\pi$ in momentum space between $p = -\infty$ and $p = \infty$ and there is no net current. The presence of a constant electric field E, however, gives rise to a net current flow. The current density j increases with time

$$\frac{dj}{dt} = e\int_{-\infty}^{\infty} \frac{dp}{2\pi}\frac{dv}{dt}. \tag{3.66}$$

The Lorentz force law, $dp/dt = eE$, yields

$$\frac{dv}{dt} = \frac{d}{dt}\frac{d}{dp}\sqrt{m^2 + p^2} = \frac{eEm^2}{(m^2 + p^2)^{3/2}}. \tag{3.67}$$

After the integration, we obtain

$$\frac{dj}{dt} = \frac{e^2 E}{\pi}, \tag{3.68}$$

which is independent of the mass. To calculate the divergence of the axial-vector current, we define $j^\mu = (\lambda, j)$ and apply Eq. (3.63). Furthermore, we make use of the fact that the vacuum charge density λ does not depend on the position, $d\lambda/dx = 0$, and obtain the result

$$e\,\partial^\mu j^5_\mu = -\frac{e^2}{2\pi}\epsilon^{\mu\nu}F_{\mu\nu}, \tag{3.69}$$

which is the chiral anomaly. We can rewrite the anomaly equation as

$$0 = \epsilon_{\mu\nu}\partial^\mu\left(ej^\nu + \frac{e^2}{\pi}A^\nu\right) \tag{3.70}$$

which leads in Lorenz gauge, i.e., $\partial^\mu A_\mu = 0$, to

$$j_\mu = -\frac{e}{\pi}A_\mu. \tag{3.71}$$

Inserting Eq. (3.71) into the classical equation of motion, $\Box A_\mu = ej_\mu$, yields

$$\left(\Box + \frac{e^2}{\pi}\right)A_\mu = 0. \tag{3.72}$$

This shows that the photon has developed a mass $m_\gamma^2 = e^2/\pi$. In this picture, the origin of the anomaly is the modification of the vacuum of the quantized system due to the presence of an external electromagnetic field.

An alternative way to understand this result consists in the discussion of solutions of the time-independent Dirac equation [Jac 86]

$$E\psi = \gamma_0\gamma_1\left(-i\frac{\partial}{\partial x} - eA\right)\psi. \tag{3.73}$$

For a constant vector potential A, we have two types of solutions,

$$\psi_+(x) = \begin{pmatrix} e^{ipx} \\ 0 \end{pmatrix}, \quad \text{with} \quad E = p - eA, \tag{3.74}$$

$$\psi_-(x) = \begin{pmatrix} 0 \\ e^{ipx} \end{pmatrix}, \quad \text{with} \quad E = -p + eA. \tag{3.75}$$

The subscript $\pm$ refers to the chirality of the solution, i.e., the eigenvalues of the operators $\frac{1}{2}(1 \pm \gamma_5)$. The vacuum consists of filled negative-energy states. If $A = 0$, the vacuum states are those with $p < 0$ for positive chirality and $p > 0$ for negative chirality, depicted in Fig. 3.2. Now we increase A adiabatically from $A = 0$ to a nonzero field $A = \epsilon$. In the presence of the field,

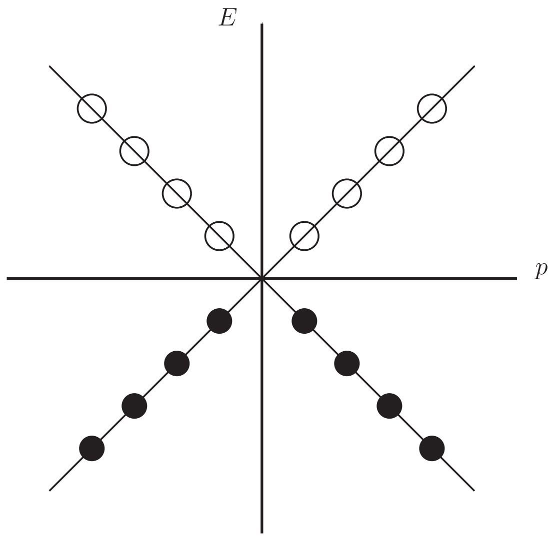

Figure 3.2: The Dirac sea in the case of a vanishing vector potential. Solid dots refer to filled states and empty dots to empty states.

the vacuum states change into those with $p < e\epsilon$ for positive chirality and $p > e\epsilon$ for negative chirality, which leads to a net chirality production of

$$\Delta\chi = 2\int_0^{e\epsilon} \frac{dp}{2\pi} = \frac{e\epsilon}{\pi}. \tag{3.76}$$

The axial charge is given by

$$Q_5 = \int dx \psi^\dagger \sigma_3 \psi, \tag{3.77}$$

which varies in time according to the axial anomaly

$$\frac{d}{dt} Q_5 = \frac{e}{\pi} E = \frac{e}{\pi}\frac{dA}{dt}. \tag{3.78}$$

The integration of both sides of Eq. (3.78) leads to

$$\Delta\chi = \frac{e}{\pi}\Delta A = \frac{e\epsilon}{\pi}, \tag{3.79}$$

which is in agreement with Eq. (3.76). Here, we can see again that the anomaly arises due to the modified vacuum in the presence of an applied electric field. This derivation can also be generalized to four space-time dimensions [Mue 90].

Chapter 4

Large-N_c chiral perturbation theory

The present chapter discusses large-N_c chiral perturbation theory (LN_cChPT), which is the effective theory of QCD at low energies including the singlet field. First, an introduction to QCD in the large-N_c limit is presented, mainly based on Refs. [Wit 79, Man 97, Leb 99]. We then derive the power-counting rules of LN_cChPT and construct the Lagrangians relevant for the calculations in this thesis. The discussion of the normal or even-intrinsic-parity sector is followed by a presentation of the anomalous or odd-intrinsic-parity sector.

4.1 The large-N_c expansion

The limit of an infinite number of color charges simplifies the physics of the strong interaction and provides a good starting point for understanding many features of the strong interaction. In the so-called large-N_c (LN_c) limit, QCD is generalized from an SU(3) gauge group with three colors to an SU(N_c) gauge group with N_c colors, and one considers the limit $N_c \to \infty$. Physical quantities are then calculated in this limit, and corrections are obtained from a systematic expansion in $1/N_c$. To determine the LN_c counting rules, one considers Feynman diagrams of QCD in the LN_c limit. At large N_c, combinatoric factors arise, which are responsible for the nature of the $1/N_c$ expansion. Let us consider the gluon contribution to the gluon vacuum polarization shown in Fig. 4.1. As will be explained below, if one specifies the color quantum numbers of the initial and final states, there are N_c possibilities for the quantum numbers of the intermediate-state gluon, and the diagram has a combinatoric factor of N_c. Each of the two interaction vertices contribute a factor of g, which is the strong coupling constant. If we

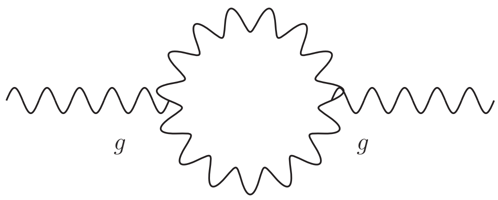

Figure 4.1: Gluon vacuum polarization at lowest order.

want the one-loop gluon vacuum polarization to have a smooth limit for LN_c, the coupling constant must be chosen to be $g/\sqrt{N_c}$, where g is held fixed as N_c becomes large.

The N_c scaling of g can also be understood from the renormalization group (RG) equation for the strong coupling constant

$$\mu \frac{dg}{d\mu} = -b_0 \frac{g^3}{16\pi^2} + \mathcal{O}(g^5), \tag{4.1}$$

where the leading coefficient of the β-function is given by

$$b_0 = \frac{11}{3} N_c - \frac{2}{3} N_f, \tag{4.2}$$

with N_f being the number of quark flavors. This equation does not exhibit a sensible LN_c limit, since $b_0 \sim \mathcal{O}(N_c)$. If we replace g by $g/\sqrt{N_c}$ in Eq. (4.1), the RG equation takes the form

$$\mu \frac{dg}{d\mu} = -\left(\frac{11}{3} - \frac{2}{3} \frac{N_f}{N_c} \right) \frac{g^3}{16\pi^2} + \mathcal{O}(g^5). \tag{4.3}$$

The β-function equation has now a well-defined limit as $N_c \to \infty$. Since N_c drops out of the equation for the running of g, the scale parameter of the strong interaction, Λ_{QCD}, is held fixed as $N_c \to \infty$. This is equivalent to holding the string tension, or a meson mass such as the ρ meson mass, fixed.

In the following, we consider the coupling constant to be $g/\sqrt{N_c}$, which scales $1/\sqrt{N_c}$. Then, one can show that, due to their combinatoric factors, a certain class of Feynman diagrams, which are called planar, dominates over others in the LN_c limit in possessing fewer powers of $1/\sqrt{N_c}$. To perform this combinatoric analysis, it is particularly convenient to employ 't Hooft's double-line notation. In this notation, quarks and antiquarks are represented as arrowed lines, where the anti-color flow is understood to be opposite the direction of the arrow. Gluons, which appear in the adjoint representation of SU(N_c), carry one color and one anti-color index, and are therefore drawn as two parallel lines whose arrows point in opposite directions, see Figs. 4.2 and

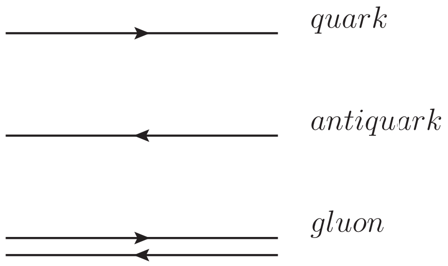

Figure 4.2: Double-line notation.

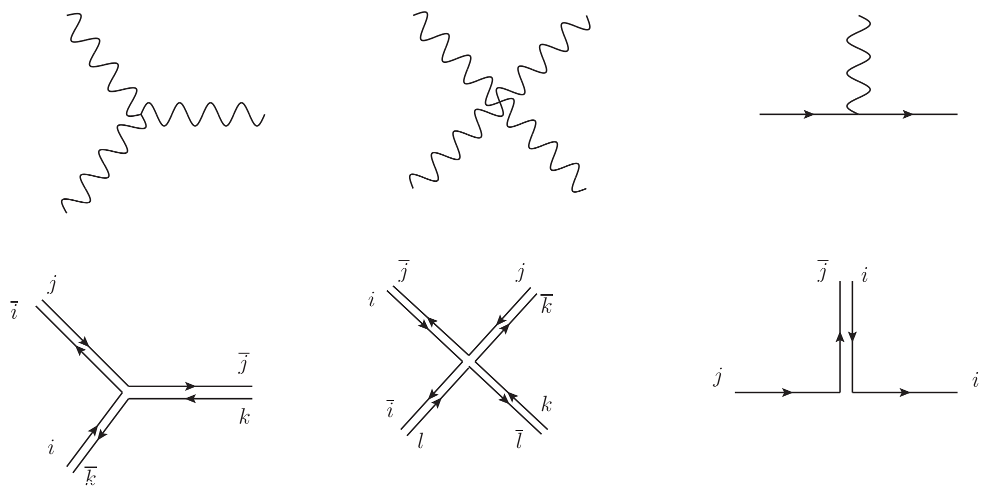

Figure 4.3: Vertices in ordinary and in double-line notation.

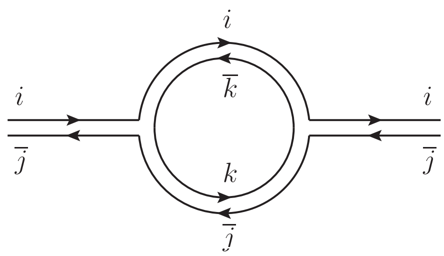

Figure 4.4: Lowest-order gluon vacuum polarization in double-line notation.

4.3. Figure 4.4 shows the gluon vacuum polarization diagram in double-line notation. The color-index lines at the edge are contracted with those of the initial and final states, and they are fixed once the states are specified. However, the closed color-line loop at the center is not fixed and the sum over k gives a factor of N_c, which is exactly the combinatoric factor of the diagram in Fig. 4.1. Using this technique one finds out that the leading diagrams are planar diagrams, which means that they can be drawn on the plane with line crossings only at interaction vertices. Non-planar diagrams are suppressed by factors of $1/N_c^2$. Examples for both types of diagrams are given in Fig. 4.5, where the planar diagram scales as $(1/\sqrt{N_c})^6 N_c^3 = N_c^0$ and the non-planar diagram as $(1/\sqrt{N_c})^6 N_c = 1/N_c^2$. Another selection rule is

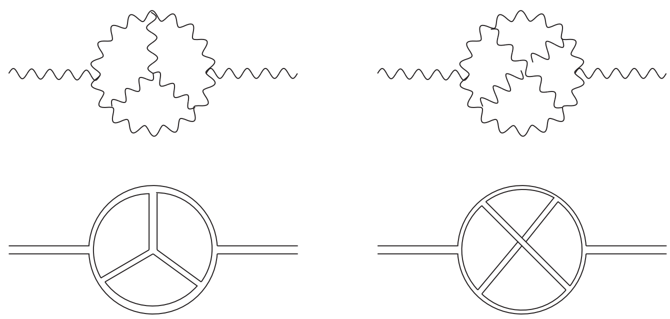

Figure 4.5: Example for a planar diagram (left) and a non-planar diagram (right) in ordinary and in double-line notation.

that internal quark loops are suppressed by factors of $1/N_c$, which is a result of the fact that for LN_c there are N_c^2 gluon states but only N_c quark states. This can be seen in Fig. 4.6, where the one-quark-loop contribution to the gluon propagator is shown. Compared to Fig. 4.4 the closed color line is

Figure 4.6: Quark contribution to the gluon self energy in ordinary and in double-line notation.

missing, and the diagram is suppressed by $1/N_c$ in comparison to Fig. 4.4.

In summary, the leading diagrams for LN_c are planar diagrams with a minimum number of quark loops. After having discussed the gluon propagator, we now turn to matrix elements of gauge-invariant operators such as quark bilinears. One finds that the dominant contributions to n-point functions of quark bilinears, such as $\bar{q}q$ or $\bar{q}\gamma^\mu q$, are planar diagrams with only one quark loop running at the edge. Since each quark loop is suppressed by $1/N_c$ and Green functions of quark bilinears contain at least one quark loop, their leading contributions are of the order of N_c. A typical leading diagram is shown in Fig. 4.7. The resummation of all the leading planar dia-

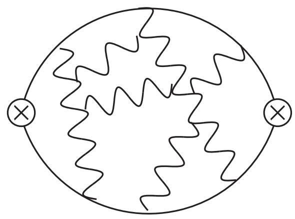

Figure 4.7: A typical leading-contribution diagram to $\langle JJ \rangle$.

grams has so far only been achieved in 1+1 dimensions [Hoo 74a, Hoo 74b]. This makes it difficult to obtain quantitative results in LN_cQCD. However, a qualitative picture of a variety of QCD phenomena emerges in the LN_c limit. The assumption that the color confinement persists in the LN_c limit combined with the knowledge that planar diagrams are dominating for LN_c leads to a successful picture of the meson world. Let us consider a generic n-point function of local quark bilinears $J = \bar{q}\Gamma q$:

$$\langle T(J_1 \cdots J_n) \rangle \sim \mathcal{O}(N_c). \tag{4.4}$$

Performing the diagrammatic analysis one finds that at LN_c the only singularities are one-meson poles. For example, a two-point function takes the form

$$\langle J(k)J(-k) \rangle = \sum_n \frac{a_n^2}{k^2 - M_n^2}, \tag{4.5}$$

where the sum runs over meson states only. The mass M_n^2 is the mass of the nth meson, and $a_n = \langle 0 | J | n \rangle$ is the matrix element for J to create the nth meson from the vacuum. Since the left-hand side has a smooth limit for LN_c, the meson masses have smooth limits as well, independent of N_c, $M_n^2 = \mathcal{O}(1)$. Furthermore, in the perturbative regime, $\langle J(k)J(-k) \rangle$ behaves logarithmically for large k^2. Therefore, the number of meson states is infinite, since a finite sum on the right-hand side of Eq. (4.5) would lead to a $1/k^2$ behavior for large k^2. In addition, the meson states are stable for $N_c \to \infty$, because the one-particle poles in Eq. (4.5) have to be on the real axis. Poles off the real axis would violate the spectral representation. Finally, the N_c dependence of a_n can be determined. Since the Green function $\langle J(k)J(-k) \rangle \sim \mathcal{O}(N_c)$, the matrix element for the operator J to create a meson from the vacuum, $a_n = \langle 0| J |n\rangle$, is $\mathcal{O}(\sqrt{N_c})$. Analyzing four-point functions, one finds that at LN_c mesons are free and non-interacting, and QCD at $N_c = \infty$ is a free field theory. In general, at LN_c the n-point functions are given by sums of tree diagrams with free meson propagators and effective local interaction vertices among m meson, which scale as $V_m \sim \mathcal{O}(N_c^{1-m/2})$. The amplitude for a bilinear current to create m mesons from the vacuum is $\langle 0| J |M_1 \cdots M_m\rangle \sim \mathcal{O}(N_c^{1-m/2})$.

The analysis can also be extended to gluonic bound states (glueballs). To that end, one includes gauge invariant operators J_G constructed from gluon fields, such as $\mathrm{Tr}(G_{\mu\nu}G^{\mu\nu})$ or $\mathrm{Tr}(G_{\mu\nu}\tilde{G}^{\mu\nu})$. From $\langle T(J_{G_1} \cdots J_{G_n})\rangle \sim \mathcal{O}(N_c^2)$ one can obtain the LN_c counting rules $\langle 0| J_G |G_1 \cdots G_m\rangle \sim \mathcal{O}(N_c^{2-m})$ and for the vertices $V[G_1, \dots, G_m] \sim \mathcal{O}(N_c^{2-m})$, meaning that, in the L$N_c$ limit, glueballs are also free, stable, non-interacting, and infinite in number. Considering the mixed correlators, which scale as $\langle T(J_1 \cdots J_n J_{G_1} \cdots J_{G_m})\rangle \sim \mathcal{O}(N_c)$, it can be shown that vertices behave as $V[M_1, \dots, M_p; G_1, \dots, G_q] \sim \mathcal{O}(N_c^{1-q-p/2})$. This means that glueballs and mesons decouple at LN_c and their mixing is suppressed by a factor $1/\sqrt{N_c}$.

This qualitative picture of QCD in the LN_c limit explains many aspects of hadron phenomenology, thus supporting the $1/N_c$ expansion to be valid for $1/N_c = 1/3$. Some of these aspects are: Mesons are approximately pure $q\bar{q}$ states and the additional $q\bar{q}$ sea leading to $q\bar{q}q\bar{q}$ exotics is suppressed; multiparticle decays proceed dominantly to resonant two-body final states; the success of Regge phenomenology, where the strong interaction is described in terms of tree diagrams with physical hadrons exchanged; the existence of resonances with a narrow width; and the Okubo-Zweig-Iizuka (OZI) rule [Oku 63, Oku 77, IKS 66, Iiz 66, Zwe 84]. The OZI rule states that strong decays are suppressed if their Feynman diagrams can be split in two by cutting only internal gluon lines. Annihilation graphs, as the one shown in Fig. 4.8, are suppressed. One consequence of this rule is that mesons appear in nonets

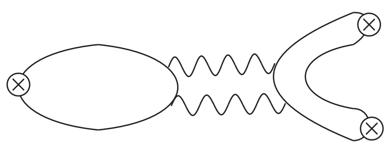

Figure 4.8: Annihilation graph. Solid lines refer to quarks and wiggly lines to gluons.

for three light quarks, because the diagrams that create a mass difference between singlet and octet involve $q\bar{q}$ annihilation and are $\mathcal{O}(1/N_c)$. As a further example, the OZI rule explains why the ϕ meson decays dominantly into $K\bar{K}$ instead of $\phi \to \rho\pi$ or $\phi \to \pi\pi\pi$.

The $\mathrm{U}(1)_A$ symmetry is broken by an anomaly. In the chiral limit, the divergence of the singlet axial-vector current is given by

$$\partial_\mu A_0^\mu = \frac{3g^2}{32\pi^2}\epsilon_{\mu\nu\rho\sigma}G_a^{\mu\nu}G_a^{\rho\sigma}. \tag{4.6}$$

In the LN_c limit however, since g^2 scales as $1/N_c$, the anomaly disappears. In this limit, the $\mathrm{U}(1)_A$ symmetry is restored and the spontaneous breaking of the chiral symmetry leads to a ninth Goldstone boson, which can be identified with the η'.

4.2 Chiral perturbation theory

In the low-energy regime, QCD cannot be treated by conventional perturbation theory, because the renormalized strong coupling constant becomes large. One possibility to solve this problem is to use an effective field theory (EFT). The effective field theory of the strong interaction at low energies is called chiral perturbation theory (ChPT) [Wei 79, GL 84, GL 85]. An extensive introduction to ChPT can be found in Ref. [SS 12]. One uses the effective degrees of freedom that are relevant to the energy region of interest. For strong-interaction processes below 1 GeV, those are the hadrons, mesons and baryons, instead of quarks and gluons, which are the fundamental degrees of freedom. Physical quantities are then calculated in terms of an expansion in q/Λ, where q stands for external momenta or masses that are small in comparison to the scale of spontaneous chiral symmetry breaking $\Lambda \approx 1$ GeV. The foundation for the construction of effective field theories is a "theorem" by Weinberg, which can be summarized in the following way: The perturbative description in terms of the most general Lagrangian that is compatible with the symmetries of the underlying theory yields "the most general possible S-matrix consistent with analyticity, perturbative unitarity, cluster decomposition and the assumed symmetry principles" [Wei 79]. In the case of ChPT, one constructs the most general Lagrangian compatible with the symmetries of QCD. Those are the (spontaneously broken) chiral symmetry, invariance under time-reversal, parity, and charge conjugation, and Lorentz invariance. In addition, one demands the Lagrangian to be Hermitian. The most general effective Lagrangian contains an infinite number of terms, and each term is accompanied by a coefficient, the so-called low-energy constant

(LEC). Therefore, one needs a scheme to organize the Lagrangian and to predict the importance of terms in the calculation of physical matrix elements. The mesonic chiral Lagrangian can be ordered according to the number of derivatives and quark-mass terms,

$$\mathcal{L}_{\text{eff}} = \mathcal{L}_2 + \mathcal{L}_4 + \mathcal{L}_6 + \dots, \tag{4.7}$$

where the subscripts refer to the order in the momentum and quark-mass expansion. The importance of Feynman diagrams can be determined by Weinberg's power counting [Wei 79]. One considers the behavior of the invariant amplitude of a given Feynman diagram under linear rescaling of the external momenta, $p_i \mapsto tp_i$, and quadratic rescaling of the quark masses, $m_q \mapsto t^2 m_q$,

$$\mathcal{M}(p_i, m_q) \mapsto \mathcal{M}(tp_i, t^2 m_q) = t^D \mathcal{M}(p_i, m_q), \tag{4.8}$$

where the chiral order D is assigned to the diagram. The chiral order D is given by

$$D = 2 + 2N_L + \sum_{k=1}^{\infty} 2(k-1) N_{2k}, \tag{4.9}$$

where N_L is the number of independent loops and N_{2k} is the number of vertices derived from $\mathcal{L}_{2k}$. If the masses and momenta are small enough, diagrams with increasing D become less important and diagrams with small D dominate.

The low-energy constants contain information on the underlying theory, and should, in principle, be calculable from QCD. In practice, they have so far been fitted to experimental data, determined by QCD inspired models, or predicted by lattice QCD [Nec 09, Col+ 11, Aok+ 14] .

4.3 Large-N_c chiral perturbation theory

Our aim is to include the η' in the framework of an EFT. Due to the $\mathrm{U}(1)_A$ anomaly, the η' remains massive even in the chiral limit. For that reason, in the low-energy expansion of conventional $\mathrm{SU}(3)_L \times \mathrm{SU}(3)_R$ ChPT, the η' does not play a special role as compared to other states such as the ρ meson [GL 85]. However, invoking the LN_c limit of QCD [Hoo 74a, Wit 79], the $\mathrm{U}(1)_A$ anomaly disappears, and the assumption of an $\mathrm{SU}(3)_V \times \mathrm{U}(1)_V$ symmetry of the ground state implies that the singlet state is also massless. This means that, in the combined chiral and LN_c limits, QCD at low energies is expected to generate the nonet (π, K, η_8, η_1) as the Goldstone bosons

[CW 80]. The combined chiral and LN_c limits may serve as a starting point for large-N_c chiral perturbation theory (LN_cChPT) as the EFT of QCD at low energies including the singlet field [Mou 95, Leu 96, Her+ 97, Leu 98, KL 98, Her 98, KL 00, Bor 04, Guo+ 15], which we will also refer to as U(3) effective theory.

In the framework of LN_cChPT, one performs a simultaneous expansion of (renormalized) Feynman diagrams in terms of momenta p, quark masses m, and $1/N_c$.[1] The three expansion variables are counted as small quantities of order [Leu 96]

$$p = \mathcal{O}(\sqrt{\delta}), \quad m = \mathcal{O}(\delta), \quad 1/N_c = \mathcal{O}(\delta). \tag{4.10}$$

The most general Lagrangian of LN_cChPT is organized as an infinite series in terms of derivatives, quark-mass terms, and, implicitly, powers of $1/N_c$, with the scaling behavior given in Eq. (4.10):

$$\mathcal{L}_{\text{eff}} = \mathcal{L}^{(0)} + \mathcal{L}^{(1)} + \mathcal{L}^{(2)} + \ldots, \tag{4.11}$$

where the superscripts (i) denote the order in δ. The rules for the assignments of these orders will be explained in a moment.

The dynamical degrees of freedom are collected in the unitary 3×3 matrix

$$U(x) = \exp\left(i\frac{\phi(x)}{F}\right), \tag{4.12}$$

where

$$\phi = \sum_{a=0}^{8}\phi_a\lambda_a = \begin{pmatrix} \pi^0 + \frac{1}{\sqrt{3}}\eta_8 + \sqrt{\frac{2}{3}}\eta_1 & \sqrt{2}\pi^+ & \sqrt{2}K^+ \\ \sqrt{2}\pi^- & -\pi^0 + \frac{1}{\sqrt{3}}\eta_8 + \sqrt{\frac{2}{3}}\eta_1 & \sqrt{2}K^0 \\ \sqrt{2}K^- & \sqrt{2}\bar{K}^0 & -\frac{2}{\sqrt{3}}\eta_8 + \sqrt{\frac{2}{3}}\eta_1 \end{pmatrix} \tag{4.13}$$

contains the pseudoscalar octet fields and the pseudoscalar singlet field η_1, the λ_a ($a = 1,\ldots,8$) are the Gell-Mann matrices, given in Appendix A.1, and $\lambda_0 = \sqrt{2/3}\,\mathbb{1}$.

In Eq. (4.12), F denotes the pion-decay constant in the three-flavor chiral limit and, in accordance with the rules derived in Sec. 4.1, is counted as $F = \mathcal{O}(\sqrt{N_c}) = \mathcal{O}(1/\sqrt{\delta})$. The pseudoscalar fields ϕ_a ($a = 0,\ldots,8$) count as $\mathcal{O}(\sqrt{N_c})$ such that the argument of the exponential function is $\mathcal{O}(\delta^0)$ and,

[1] It is understood that dimensionful variables need to be small in comparison with an energy scale.

thus, $U = \mathcal{O}(\delta^0)$. Besides the dynamical degrees of freedom of Eq. (4.13), the effective Lagrangian also contains a set of external fields $(s, p, l_\mu, r_\mu, \theta)$. The fields s, p, l_μ, and r_μ are Hermitian, color-neutral 3×3 matrices coupling to the corresponding quark bilinears, and θ is a real field coupling to the winding number density [GL 85]. The covariant derivative acting on U is defined as

$$D_\mu U = \partial_\mu U - i r_\mu U + i U l_\mu. \tag{4.14}$$

The external scalar and pseudoscalar fields s and p are combined in the definition $\chi \equiv 2B(s+ip)$ [GL 85]. The LEC B is related to the scalar singlet quark condensate $\langle\bar{q}q\rangle_0$ in the three-flavor chiral limit and is of $\mathcal{O}(N_c^0)$. Setting $s = M$ and $p = 0$, the (isospin-symmetric) quark-mass matrix $M = \mathrm{diag}(\hat{m}, \hat{m}, m_s)$, $\hat{m} = (m_u+m_d)/2$, is contained in $\chi = 2BM$. Finally, we introduce a dimensionless field variable $\psi = \sqrt{6}\eta_1/F$ such that $\det(U) = \exp(i\psi)$.

To construct chirally invariant Lagrangians, the transformation properties of the building blocks under chiral $\mathrm{U}(3)_L\times\mathrm{U}(3)_R$ transformations need to be known. The matrix U transforms under $(V_L, V_R) \in \mathrm{U}(3)_L\times\mathrm{U}(3)_R$ as

$$U \mapsto V_R U V_L^\dagger, \tag{4.15}$$

while the transformation behavior of the other building blocks is given by

$$\begin{aligned}
\psi &\mapsto \psi - i\ln(\det(V_R)) + i\ln(\det(V_L)) \\
&\quad = \psi - (\theta_R - \theta_L), \\
D_\mu U &\mapsto V_R D_\mu U V_L^\dagger, \\
D_\mu \psi &= \partial_\mu\psi - 2\langle a_\mu\rangle \mapsto D_\mu\psi, \\
D_\mu \theta &= \partial_\mu\theta + 2\langle a_\mu\rangle \mapsto D_\mu\theta, \\
\chi &\mapsto V_R \chi V_L^\dagger, \\
\theta &\mapsto \theta + (\theta_R - \theta_L).
\end{aligned} \tag{4.16}$$

We now apply the power-counting rules of Eq. (4.10) to the construction of the effective Lagrangian in the LN_c framework. First, there is the momentum and quark-mass counting which proceeds as in conventional $\mathrm{SU}(3)_L\times\mathrm{SU}(3)_R$ ChPT [GL 85]: (covariant) derivatives count as $\mathcal{O}(p)$, χ counts as $\mathcal{O}(p^2)$, etc. (see Table 4.1). We denote the corresponding chiral order by D_p. The discussion of the $\mathrm{U}(3)_L\times\mathrm{U}(3)_R$ case results in three major modifications in comparison with $\mathrm{SU}(3)_L\times\mathrm{SU}(3)_R$ [Leu 96, Her+ 97, KL 00]: First, the determinant of U is no longer restricted to have the value 1, second, additional external fields appear. Third, since, according to Eqs. (4.16), the sum $(\psi+\theta)$ remains invariant under chiral $\mathrm{U}(3)_L\times\mathrm{U}(3)_R$ transformations, the conventional structures of $\mathrm{SU}(3)_L\times\mathrm{SU}(3)_R$ ChPT will be multiplied by coefficients which are functions of the linear combination $(\psi+\theta)$. For example, denoting the SU(3) matrix of ordinary chiral perturbation theory by $\hat{U}$, i.e.,

$$U = e^{\frac{i}{3}\psi}\hat{U}, \tag{4.17}$$

the leading-order Lagrangian reads [GL 85]

$$\mathcal{L}_2 = \frac{F^2}{4}\langle D_\mu \hat{U} D^\mu \hat{U}^\dagger\rangle + \frac{F^2}{4}\langle \chi \hat{U}^\dagger + \hat{U}\chi^\dagger\rangle,$$

where the symbol $\langle\ \rangle$ denotes the trace over flavor indices and the covariant derivatives are defined in Appendix A.3 in Eqs. (A.23). This expression is replaced by [Her+ 97]

$$W_1\langle D_\mu U D^\mu U^\dagger\rangle + W_2\langle \chi U^\dagger + U\chi^\dagger\rangle, \tag{4.18}$$

where W_1 and W_2 are functions of $(\psi+\theta)$ and are also referred to as potentials [KL 00]. In the limit $N_c \to \infty$, these functions reduce to constants [Leu 96]. However, for N_c finite, the functions may be expanded in $(\psi+\theta)$ with well-defined assignments for the LN_c scaling behavior of the expansion coefficients.

In addition to the potentials, also new additional structures show up which do not exist in the $\mathrm{SU}(3)_L \times \mathrm{SU}(3)_R$ case. For example, in ordinary chiral perturbation theory one finds for the trace $\langle D_\mu \hat{U}\hat{U}^\dagger\rangle = 0$ [SS 12], whereas in the $\mathrm{U}(3)_L \times \mathrm{U}(3)_R$ case one has

$$\langle D_\mu U U^\dagger\rangle = iD_\mu\psi, \tag{4.19}$$

giving rise to a new term of the type $-W_4 D_\mu\psi D^\mu\psi$ [Her+ 97].

To assign LN_c counting rules, one compares the Green functions evaluated from the effective Lagrangian to those obtained in LN_cQCD (see Refs. [Her+ 97, KL 00] for a detailed account). As explained in Sect. 4.1, the leading contribution to a quark correlation function contains one quark loop and is of $\mathcal{O}(N_c)$. Each flavor trace in the effective theory amounts to a sum over quark flavors, which arises in QCD only in a quark loop and is therefore suppressed by $1/N_c$. In general, diagrams with r quark loops and thus r flavor traces are of order N_c^{2-r}. Terms in the Lagrangian without traces correspond to the purely gluonic theory and count at leading order as N_c^2. This argument is transferred to the level of the effective Lagrangian, i.e., single-trace terms are of order N_c, double-trace terms of order unity etc.[2] In other words, we need to identify the number N_{tr} of flavor traces. In

[2] When applying these counting rules, one has to account for the so-called trace relations connecting single-trace terms with products of traces (see, e.g., Appendix A of Ref. [FS 96]).

particular, because of Eq. (4.16), the expression $D_\mu\psi$ implicitly involves a flavor trace (see footnote 7 of Ref. [KL 00]). The external field θ couples to the winding number density with strength $1/N_c$. Therefore, when expanding the potentials, each power $(\psi+\theta)^n$ is accompanied by a coefficient of order $\mathcal{O}(N_c^{-n})$. In a similar fashion, $D_\mu\theta$ (as well as multiple derivatives) are related to expressions with $\mathcal{O}(N_c^{-1})$.[3] Denoting the number of $(\psi+\theta)$ and $D_\mu\theta$ terms by N_θ, the LN_c order reads [Her+ 97, KL 00]

$$D_{N_c^{-1}} = -2 + N_{tr} + N_\theta. \tag{4.20}$$

The combined order of an operator is then given by

$$D_\delta = \frac{1}{2}D_p + D_{N_c^{-1}}. \tag{4.21}$$

In particular, using Eq. (4.21) allows us to identify the LN_c scaling behavior of the LEC multiplying the corresponding operator.

The leading-order Lagrangian is given by [Leu 96, KL 00]

$$\mathcal{L}^{(0)} = \frac{F^2}{4}\langle D_\mu U D^\mu U^\dagger\rangle + \frac{F^2}{4}\langle \chi U^\dagger + U\chi^\dagger\rangle - \frac{1}{2}\tau(\psi+\theta)^2. \tag{4.22}$$

Comparing with Eq. (4.18), we identify

$$\frac{F^2}{4} = W_1(0) = W_2(0) \tag{4.23}$$

as the leading-order term of the expansion of the functions W_1 and W_2 which, because of parity, are even functions. On the other hand, the last term of Eq. (4.22) originates from the second-order term of the expansion of W_0. The constant $\tau = \mathcal{O}(N_c^0)$ is the topological susceptibility of the purely gluonic theory [Leu 96]. Counting the quark mass as $\mathcal{O}(p^2)$, the first two terms of $\mathcal{L}^{(0)}$ are of $\mathcal{O}(N_c p^2)$, while the third term is of $\mathcal{O}(N_c^0)$, i.e., all terms are of $\mathcal{O}(\delta^0)$. The leading-order Lagrangian contains 3 LECs, namely, F, B, and τ.

To explain the power counting of the interaction vertices, we set $r_\mu = l_\mu = 0$ and $\chi = 2BM$, where $M = \mathrm{diag}(m_u, m_d, m_s)$ denotes the quark-mass matrix. For this case, the leading-order Lagrangian contains only even powers of the pseudoscalar fields. Expanding the first two terms of Eq. (4.22) in terms of the pseudoscalar fields results in Feynman rules for the *interaction* vertices of the order $p^2 N_c^{1-k/2}$, where $k = 4, 6, \ldots$ is the number of interacting

[3]Note that we do not directly book the quantities $(\psi+\theta)$ or $D_\mu\theta$ as $\mathcal{O}(N_c^{-1})$, but rather attribute this order to the coefficients coming with the terms.

pseudoscalar fields [KL 00]. The dependence on N_c and p originates from the powers of F and the two derivatives, respectively. When discussing QCD Green functions of, say, pseudoscalar quark bilinears, there will be a factor $BF = \mathcal{O}(\sqrt{N_c})$ at each external source (see Sec. 4.6.2 of Ref. [Sch 03]), such that an n-point function is of the order $p^2 N_c$. Taking $\phi_a = \mathcal{O}(\sqrt{N_c})$, the interaction Lagrangian count as $\mathcal{O}(p^2 N_c)$ which is consistent with referring to the Lagrangian as $\mathcal{O}(\delta^0)$, with the leading-order contributions of quark loops being $\mathcal{O}(N_c)$ and the leading chiral order being $\mathcal{O}(p^2)$. On the other hand, it is also consistent with the expectation of the effective meson vertices containing k external lines being of the order $N_c^{1-k/2}$, see Sec. 4.1.

The NLO Lagrangian $\mathcal{L}^{(1)}$ was constructed in Refs. [Leu 96, Her+ 97, KL 00] and receives contributions of $\mathcal{O}(N_c p^4)$, $\mathcal{O}(p^2)$, and $\mathcal{O}(N_c^{-1})$. The terms that are of the same structure as those in $\mathcal{L}^{(0)}$ may be absorbed in the coupling constants F, B, and τ [KL 00]. In particular, τ now has to be distinguished from the topological susceptibility of gluodynamics. We only display the terms relevant for our calculation, in particular, we set $v_\mu \equiv (r_\mu + l_\mu)/2 = 0$ and keep only $a_\mu \equiv (r_\mu - l_\mu)/2$, which is needed for the calculation of the axial-vector matrix elements:

$$\begin{aligned}\mathcal{L}^{(1)} &= L_5\langle D_\mu U D^\mu U^\dagger(\chi U^\dagger + U\chi^\dagger)\rangle + L_8\langle \chi U^\dagger \chi U^\dagger + U\chi^\dagger U\chi^\dagger\rangle \\ &\quad + \frac{F^2}{12}\Lambda_1 D_\mu\psi D^\mu\psi - i\frac{F^2}{12}\Lambda_2(\psi+\theta)\langle\chi U^\dagger - U\chi^\dagger\rangle + \ldots,\end{aligned} \tag{4.24}$$

where the ellipsis refers to the suppressed terms. The first two terms of $\mathcal{L}^{(1)}$ count as $\mathcal{O}(N_c p^4)$ and are obtained from the standard $\mathrm{SU}(3)_L\times\mathrm{SU}(3)_R$ ChPT Lagrangian of $\mathcal{O}(p^4)$ [GL 85] by retaining solely terms with a single trace and keeping only the constant terms of the potentials. With $D_p = 4$ and $D_{N_c^{-1}} = -1$, Eq. (4.21) implies that L_5 and L_8 are of $\mathcal{O}(N_c)$. According to Eqs. (4.16), the expression $D_\mu\psi D^\mu\psi$ implicitly involves two flavor traces (see footnote 7 of Ref. [KL 00]), with the result that the corresponding term is $\mathcal{O}(N_c^0)$. Since $F = \mathcal{O}(\sqrt{N_c})$, the coupling Λ_1 scales as $\mathcal{O}(N_c^{-1})$ and has to vanish in the LN_c limit. Finally, the structure proportional to Λ_2 is the leading-order term of the expansion of the potential W_3. With $D_p = 2$ and $D_{N_c^{-1}} = 0$ ($N_{tr} = N_\theta = 1$), the LEC Λ_2 scales as $\mathcal{O}(N_c^{-1})$.

The $\mathrm{SU}(3)_L\times\mathrm{SU}(3)_R$ Lagrangian of $\mathcal{O}(p^6)$ was discussed in Refs. [FS 96, BCE 99, EFS 02, BGT 02], and the generalization to the $\mathrm{U}(3)_L\times\mathrm{U}(3)_R$ case has recently been obtained in Ref. [JGW 14]. For the present purposes, at NNLO, the relevant pieces of $\mathcal{L}^{(2)}$ can be split into three different contributions of $\mathcal{O}(N_c^{-1}p^2)$, $\mathcal{O}(p^4)$, and $\mathcal{O}(N_c p^6)$, respectively:

$$\mathcal{L}^{(2,N_c^{-1}p^2)} = -\frac{F^2}{4} v_2^{(2)} (\psi+\theta)^2 \langle \chi U^\dagger + U\chi^\dagger \rangle, \tag{4.25}$$

$$\begin{aligned}\mathcal{L}^{(2,p^4)} = {} & L_4 \langle D_\mu U D^\mu U^\dagger \rangle \langle \chi U^\dagger + U\chi^\dagger \rangle + L_6 \langle \chi U^\dagger + U\chi^\dagger \rangle^2 + L_7 \langle \chi U^\dagger - U\chi^\dagger \rangle^2 \\ & + iL_{18} D_\mu \psi \langle \chi D^\mu U^\dagger - D^\mu U \chi^\dagger \rangle + iL_{25}(\psi+\theta) \langle \chi U^\dagger \chi U^\dagger - U\chi^\dagger U \chi^\dagger \rangle \\ & + iL_{46} D_\mu \theta \langle D^\mu U U^\dagger (\chi U^\dagger + U\chi^\dagger) \rangle + iL_{53} \partial_\mu D^\mu \theta \langle \chi U^\dagger - U\chi^\dagger \rangle + \ldots ,\end{aligned} \tag{4.26}$$

$$\begin{aligned}\mathcal{L}^{(2,N_c p^6)} = {} & C_{12} \langle \chi_+ h_{\mu\nu} h^{\mu\nu} \rangle + C_{14} \langle u_\mu u^\mu \chi_+^2 \rangle + C_{17} \langle \chi_+ u_\mu \chi_+ u^\mu \rangle + C_{19} \langle \chi_+^3 \rangle \\ & + C_{31} \langle \chi_-^2 \chi_+ \rangle + \ldots ,\end{aligned} \tag{4.27}$$

where

$$\begin{aligned} \chi_\pm &= u^\dagger \chi u^\dagger \pm u \chi^\dagger u, \\ u &= \sqrt{U}, \\ u_\mu &= i\left[u^\dagger(\partial_\mu - ir_\mu)u - u(\partial_\mu - il_\mu)u^\dagger\right] = iu^\dagger D_\mu U u^\dagger, \\ h_{\mu\nu} &= \nabla_\mu u_\nu + \nabla_\nu u_\mu, \\ \nabla_\mu X &= \partial_\mu X + [\Gamma_\mu, X], \\ \Gamma_\mu &= \frac{1}{2}\left[u^\dagger(\partial_\mu - ir_\mu)u + u(\partial_\mu - il_\mu)u^\dagger\right]. \end{aligned} \tag{4.28}$$

The coupling $v_2^{(2)}$ of Eq. (4.25) scales like $\mathcal{O}(N_c^{-2})$ and originates from the expansion of the potentials of Refs. [Leu 96, KL 00] up to and including terms of order $(\psi+\theta)^2$. The first three terms of Eq. (4.26) stem from the standard $\mathrm{SU}(3)_L \times \mathrm{SU}(3)_R$ ChPT Lagrangian of $\mathcal{O}(p^4)$ with two traces and are $1/N_c$ suppressed compared to the single-trace terms in Eq. (4.24). The remaining terms of Eq. (4.26) are genuinely related to the LN_c $\mathrm{U}(3)_L \times \mathrm{U}(3)_R$ framework, since they contain interactions involving the singlet field or the singlet axial-vector current. Finally, the C_i terms of Eq. (4.27) are obtained from single-trace terms of the $\mathrm{SU}(3)_L \times \mathrm{SU}(3)_R$ Lagrangian of $\mathcal{O}(p^6)$ [BCE 99]. As there is, at present, no satisfactory unified nomenclature for the coupling constants, for easier reference we choose the names according to the respective references from which the Lagrangians were taken.

Last but not least, we summarize the power-counting rules for a given Feynman diagram, which has been evaluated by using the interaction vertices derived from the effective Lagrangians of Eq. (4.11). Using the δ counting introduced in Eq. (4.10), we assign to any such diagram an order D which is obtained from the following ingredients: Meson propagators for both octet and singlet fields count as $\mathcal{O}(\delta^{-1})$. Since meson fields are always divided by

$F = \mathcal{O}(\sqrt{N_c}) = \mathcal{O}(\delta^{-\frac{1}{2}})$, a vertex with k meson fields derived from $\mathcal{L}^{(i)}$ is $\mathcal{O}(\delta^{i+k/2})$. The integration of a loop counts as δ^2. The order D is obtained by adding up the contributions of the individual building blocks. Figure 4.9 provides two examples of the application of the power-counting rules. Since the tree-level diagram of Fig. 4.9 (a) consists of a single vertex derived from $\mathcal{L}^{(0)}$ with four external meson lines, it has $D = 2$. On the other hand, the one-loop diagram of Fig. 4.9 (b) has two vertices from $\mathcal{L}^{(0)}$ with four legs, two meson propagators, and one loop: $D = 2 + 2 - 1 - 1 + 2 = 4$. As expected, the loop increases the order by two units. The power-counting rules are summarized in Table 4.1.

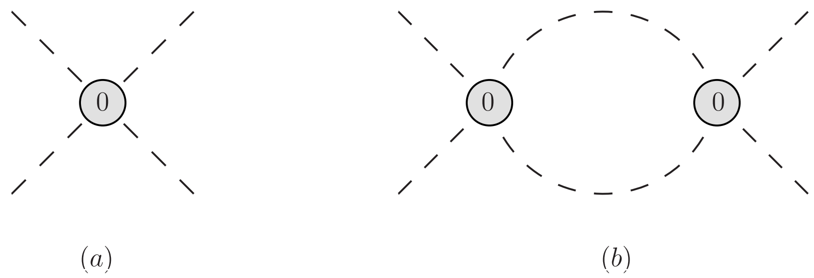

Figure 4.9: Illustration of the power counting in LN_cChPT. The number 0 in the interaction blobs refers to $\mathcal{L}^{(0)}$.

4.4 Odd-intrinsic-parity sector

The Lagrangians discussed so far, $\mathcal{L}^{(0)}$–$\mathcal{L}^{(2)}$, possess a larger symmetry than QCD [Wit 83]. If we consider pure QCD, i.e., no external fields except for $\chi = 2BM$, or only electromagnetic reactions, the Lagrangians $\mathcal{L}^{(0)}$–$\mathcal{L}^{(2)}$ are invariant under the transformation $\phi(x) \mapsto -\phi(x)$. This transformation is called intrinsic parity P, which is the normal parity transformation neglecting the transformation part of space-time x itself. The aforementioned Lagrangians contain only interaction terms with an even number of Goldstone bosons, which means that they are of even intrinsic parity. Processes with an odd number of Goldstone bosons are said to be of odd intrinsic parity. However, odd-intrinsic-parity processes such as $K^+K^- \to \pi^+\pi^-\pi^0$, $\eta \to \pi^+\pi^-\gamma$, or $\pi^0 \to \gamma\gamma$ are allowed by QCD and appear in nature. Those processes are related to the chiral anomaly. At leading order, they are described by the effective Wess-Zumino-Witten action [WZ 71, Wit 83].

Quantity	N_c	p	δ
Momenta/Derivatives p/∂_μ	1	p	$\delta^{\frac{1}{2}}$
$1/N_c$	N_c^{-1}	1	δ
Quark masses m	1	p^2	δ
Dynamical fields ϕ_a ($a = 1, \dots, 8$)	$\sqrt{N_c}$	1	$\delta^{-\frac{1}{2}}$
Dynamical field ψ	1	1	1
External field θ	1	1	1
External currents v_μ and a_μ	1	p	$\delta^{\frac{1}{2}}$
External fields s and p	1	p^2	δ
Pion-decay constant F (chiral limit)	$\sqrt{N_c}$	1	$\delta^{-\frac{1}{2}}$
Topological susceptibility τ	1	1	1
$M^2_{\eta'}$ (chiral limit)	N_c^{-1}	1	δ
Octet-meson propagator	1	p^{-2}	δ^{-1}
Singlet-η_1 propagator (chiral limit)	a)	a)	δ^{-1}
Loop integration	1	p^4	δ^2
k-meson vertex from $\mathcal{L}^{(i)}$	b)	b)	$\delta^{i+k/2}$

Table 4.1: Power-counting rules in LN_cChPT. a) The inverse of the singlet η_1 propagator is of order $1/N_c$ and p^2. b) The assignment i in $\mathcal{L}^{(i)}$ receives contributions from both $1/N_c$ and p^2.

4.4.1 Wess-Zumino-Witten action

Whereas normal Ward identities correspond to the invariance of the generating functional under local transformations of the external fields, the anomalous Ward identities give rise to a particular form of the variation of the generating functional. Let us consider an infinitesimal chiral transformation

$$\begin{aligned} V_R(x) &= 1 + i\alpha(x) + i\beta(x) + \ldots, \\ V_L(x) &= 1 + i\alpha(x) - i\beta(x) + \ldots. \end{aligned} \tag{4.29}$$

If one simultaneously transforms the external field $\theta(x)$, the variation of the generating functional Z due to the anomalies is given by [GL 85]

$$\begin{aligned} \delta\theta(x) &= -2\langle\beta(x)\rangle, \\ \delta Z &= -\int d^4x \langle\beta(x)\Omega(x)\rangle, \\ \Omega(x) &= \frac{N_c}{16\pi^2}\epsilon^{\alpha\beta\mu\nu}\Big[v_{\alpha\beta}v_{\mu\nu} + \frac{4}{3}\nabla_\alpha a_\beta \nabla_\mu a_\nu + \frac{2}{3}i\{v_{\alpha\beta}, a_\mu a_\nu\} + \frac{8}{3}i a_\mu v_{\alpha\beta} a_\nu \\ &\quad + \frac{4}{3} a_\alpha a_\beta a_\mu a_\nu\Big], \\ v_{\alpha\beta} &= \partial_\alpha v_\beta - \partial_\beta v_\alpha - i[v_\alpha, v_\beta], \\ \nabla_\alpha a_\beta &= \partial_\alpha a_\beta - i[v_\alpha, a_\beta], \end{aligned} \tag{4.30}$$

where the symbol $\langle\ \rangle$ denotes the trace over flavor indices and N_c is the number of colors. Wess and Zumino showed that the anomalies satisfy consistency or integrability relations [WZ 71]. Based on these relations, they constructed a functional Z_A involving the pseudoscalar octet which correctly produces the non-abelian anomaly. In the following, an outline of the construction will be provided [WZ 71, GL 85]. The generator $D(\beta)$ of an infinitesimal chiral transformation, specified in Eq. (4.29), of the generating functional is given by

$$\begin{aligned} D(\beta)f(v,a,s,p,\theta) = \int d^4x \Big[&\langle i[\beta, a_\mu]\frac{\delta f}{\delta v_\mu(x)} + \nabla_\mu\beta\frac{\delta f}{\delta a_\mu(x)} \\ &-\{\beta,p\}\frac{\delta f}{\delta s(x)} + \{\beta,s\}\frac{\delta f}{\delta p(x)}\rangle - 2\langle\beta\frac{\delta f}{\delta\theta(x)}\rangle\Big]. \end{aligned} \tag{4.31}$$

The condition in Eq. (4.30) then leads to

$$D(\beta)Z_A = -\int d^4x \langle\beta(x)\Omega(x)\rangle, \tag{4.32}$$

where Ω is given in Eq. (4.30). One can verify that the action of the operator $\exp(D(\beta))$ on the external fields takes the form

$$\begin{aligned}
e^{D(\beta)}\left[v_\mu(x)+a_\mu(x)\right] &= e^{i\beta(x)}\left[i\partial_\mu+v_\mu(x)+a_\mu(x)\right]e^{-i\beta(x)},\\
e^{D(\beta)}\left[v_\mu(x)-a_\mu(x)\right] &= e^{-i\beta(x)}\left[i\partial_\mu+v_\mu(x)-a_\mu(x)\right]e^{i\beta(x)},\\
e^{D(\beta)}\left[s(x)+ip(x)\right] &= e^{i\beta(x)}\left[s(x)+ip(x)\right]e^{i\beta(x)},\\
e^{D(\beta)}\theta(x) &= \theta(x)-2\langle\beta(x)\rangle.
\end{aligned} \tag{4.33}$$

The comparison with Eq. (2.15) in Sec. 2.3 shows that the operator $\exp(D(\beta))$ generates the global transformation

$$V_R(x)=V_L^\dagger(x)=\exp(i\beta(x)). \tag{4.34}$$

The field $U(x)$, given in Eq. (4.12) transforms according to

$$e^{D(\beta)}U(x)=e^{i\beta(x)}U(x)e^{i\beta(x)} \tag{4.35}$$

under chiral transformation of the external fields. Using this property, $U(x)$ can be transformed into the unit matrix if one chooses the matrix $\beta(x)$ such that

$$e^{-2i\beta(x)}=U(x). \tag{4.36}$$

Equation (4.32) can be solved with a functional Z_A which depends on the external fields only through v_μ, a_μ, and U:

$$Z_A=Z_A(v,a,U). \tag{4.37}$$

The condition Eq. (4.32) leads to a differential equation that determines the dependence of Z_A on the field U, and adding the boundary condition

$$Z_A(v,a,\mathbb{1})=0 \tag{4.38}$$

determines the functional uniquely. This boundary condition is consistent with the invariance of Z_A under gauge transformations generated by the vector current. Indeed, performing a global chiral transformation which satisfies Eq. (4.36) leads to

$$e^{D(\beta)}Z_A(v,a,U)=0=Z_A(v,a,\mathbb{1}). \tag{4.39}$$

The differential equation (4.32) can be solved by

$$Z_A(v,a,U)=\sum_{n=1}^{\infty}\frac{1}{n!}\int d^4x\langle\beta(x)[D(\beta)]^{n-1}\Omega(x)\rangle. \tag{4.40}$$

The first term of this series contains the anomaly. The higher-order terms do not vanish, even if the external vector and axial-vector fields are switched off, and the anomaly gives rise to interactions between five or more Goldstone bosons. The structure $Z_A(0,0,U)$ has been given a remarkable geometric interpretation by Witten [Wit 83].

In Witten's construction, he added to the lowest-order equation of motion the simplest term possible which breaks the symmetry of having only an even number of Goldstone bosons at the Lagrangian level. In the case of massless Goldstone bosons without any external fields the modified equation of motion reads

$$\partial_\mu\left(\frac{F^2}{2}U\partial^\mu U^\dagger\right) + \lambda\epsilon^{\mu\nu\rho\sigma}U\partial_\mu U^\dagger U\partial_\nu U^\dagger U\partial_\rho U^\dagger U\partial_\sigma U^\dagger = 0, \tag{4.41}$$

where λ is a (purely imaginary) constant and $\epsilon_{0123} = 1$. A term which is even (odd) in the Lagrangian leads to a term which is odd (even) in the equation of motion. As Wess and Zumino [WZ 71] already emphasized, the action functional generating the new term cannot be written down as the four-dimensional integral of a Lagrangian expressed in terms of U and its derivatives. To construct an action corresponding to Eq. (4.41), one has to extend the domain of definition of U to a (hypothetical) fifth dimension,

$$U(y) = \exp\left(i\alpha\frac{\phi(x)}{F}\right),\quad y^i = (x^\mu,\alpha),\ i = 0,\ldots,4,\ 0 \le \alpha \le 1, \tag{4.42}$$

where Minkowski space is defined as the surface of the five-dimensional space for $\alpha = 1$. In the absence of external fields (denoted by the superscript 0), the effective Wess-Zumino-Witten action is given by

$$\begin{aligned} S^0_{\text{ano}} &= n\, S^0_{\text{WZW}}, \\ S^0_{\text{WZW}} &= -\frac{i}{240\pi^2}\int_0^1 d\alpha \int d^4x\epsilon^{ijklm}\langle\mathcal{U}^L_i\mathcal{U}^L_j\mathcal{U}^L_k\mathcal{U}^L_l\mathcal{U}^L_m\rangle, \end{aligned} \tag{4.43}$$

where the indices $i,\ldots,m$ run from 0 to 4, $y_4 = y^4 = \alpha$, ϵ_{ijklm} is the completely antisymmetric (five-dimensional) tensor with $\epsilon_{01234} = -\epsilon^{01234} = 1$, and $\mathcal{U}^L_i = U^\dagger\partial U/\partial y^i$. The relation between the constant λ of Eq. (4.41) and n of Eq. (4.43) is $\lambda = in/(48\pi^2)$. Using topological arguments, Witten could show that the constant n must be an integer. Later, in the case of QCD, n will be identified with the number of colors N_c.

The expansion of $U(y)$ in terms of Goldstone boson fields, $U(y) = 1 + i\alpha\phi(x)/F + \mathcal{O}(\phi^2)$, leads to an infinite series of terms. Each term contains an odd number of Goldstone bosons, i.e., the WZW action S^0_{WZW} is of odd intrinsic parity. The α integration can be performed explicitly for each individual term and one obtains an ordinary action in terms of a four-dimensional integral of a local Lagrangian. As an example, let us consider the term with the smallest number of Goldstone bosons

$$
\begin{aligned}
S^{5\phi}_{\mathrm{WZW}} &= \frac{1}{240\pi^2 F^5}\int_0^1 d\alpha \int d^4x \epsilon^{ijklm}\langle \partial_i(\alpha\phi)\partial_j(\alpha\phi)\partial_k(\alpha\phi)\partial_l(\alpha\phi)\partial_m(\alpha\phi)\rangle \\
&= \frac{1}{240\pi^2 F^5}\int_0^1 d\alpha \int d^4x \epsilon^{ijklm}\partial_i\langle \alpha\phi\partial_j(\alpha\phi)\partial_k(\alpha\phi)\partial_l(\alpha\phi)\partial_m(\alpha\phi)\rangle .
\end{aligned}
\tag{4.44}
$$

Exactly one index can take the value 4. Integrating the term involving $i = 4$ with respect to α, one obtains

$$
S^{5\phi}_{\mathrm{WZW}} = \frac{1}{240\pi^2 F^5}\int d^4x \epsilon^{\mu\nu\rho\sigma}\langle \phi\partial_\mu\phi\partial_\nu\phi\partial_\rho\phi\partial_\sigma\phi\rangle, \tag{4.45}
$$

where the other terms cancel each other, because the ϵ tensor in four dimensions is antisymmetric under a cyclic permutation of the indices whereas the trace is symmetric under a cyclic permutation. Equation (4.45) shows that, without external fields, the WZW action starts with the interaction of five Goldstone boson fields. In the presence of external fields, the anomalous action receives an additional term [Man 85, Bij 93]

$$
S_{\mathrm{ano}} = n(S^0_{\mathrm{WZW}} + S^{\mathrm{ext}}_{\mathrm{WZW}}) \tag{4.46}
$$

given by

$$
S^{\mathrm{ext}}_{\mathrm{WZW}} = -\frac{i}{48\pi^2}\int d^4x \epsilon^{\mu\nu\rho\sigma}\left\{\langle Z_{\mu\nu\rho\sigma}(U,l,r)\rangle - \langle Z_{\mu\nu\rho\sigma}(\mathbb{1},l,r)\rangle\right\}, \tag{4.47}
$$

with

$$
\begin{aligned}
&Z_{\mu\nu\rho\sigma}(U,l,r) \\
&= \frac{1}{2}Ul_\mu U^\dagger r_\nu U l_\rho U^\dagger r_\sigma + U l_\mu l_\nu l_\rho U^\dagger r_\sigma - U^\dagger r_\mu r_\nu r_\rho U l_\sigma \\
&\quad + iU\partial_\mu l_\nu l_\rho U^\dagger r_\sigma - iU^\dagger \partial_\mu r_\nu r_\rho U l_\sigma + i\partial_\mu r_\nu U l_\rho U^\dagger r_\sigma - i\partial_\mu l_\nu U^\dagger r_\rho U^\dagger l_\sigma \\
&\quad - i\mathcal{U}_{L\mu} l_\nu U^\dagger r_\rho U l_\sigma + i\mathcal{U}_{R\mu} r_\nu U l_\rho U^\dagger r_\sigma - i\mathcal{U}_{L\mu} l_\nu l_\rho l_\sigma + i\mathcal{U}_{R\mu} r_\nu r_\rho r_\sigma \\
&\quad + \frac{1}{2}\left(\mathcal{U}_{L\mu}U^\dagger\partial_\nu r_\rho U l_\sigma - \mathcal{U}_{R\mu}U\partial_\nu l_\rho U^\dagger r_\sigma + \mathcal{U}_{L\mu}U^\dagger r_\nu U\partial_\rho l_\sigma - \mathcal{U}_{R\mu}U l_\nu U^\dagger \partial_\rho r_\sigma\right) \\
&\quad - \mathcal{U}_{L\mu}\mathcal{U}_{L\nu}U^\dagger r_\rho U l_\sigma + \mathcal{U}_{R\mu}\mathcal{U}_{R\nu}U l_\rho U^\dagger r_\sigma + \frac{1}{2}\mathcal{U}_{L\mu} l_\nu U\mathcal{U}_{L\rho} l_\sigma - \frac{1}{2}\mathcal{U}_{R\mu} r_\nu \mathcal{U}_{R\rho} r_\sigma \\
&\quad + \mathcal{U}_{L\mu} l_\nu \partial_\rho l_\sigma - \mathcal{U}_{R\mu} r_\nu \partial_\rho r_\sigma + \mathcal{U}_{L\mu}\partial_\nu l_\rho l_\sigma - \mathcal{U}_{R\mu}\partial_\nu r_\rho r_\sigma \\
&\quad - i\mathcal{U}_{L\mu}\mathcal{U}_{L\nu}\mathcal{U}_{L\rho} l_\sigma + i\mathcal{U}_{R\mu}\mathcal{U}_{R\nu}\mathcal{U}_{R\rho} r_\sigma ,
\end{aligned}
\tag{4.48}
$$

where $\mathcal{U}_{L\mu} \equiv U^\dagger \partial_\mu U$ and $\mathcal{U}_{R\mu} \equiv U \partial_\mu U^\dagger$. The subtraction of the $\langle Z_{\mu\nu\rho\sigma}(\mathbb{1}, l, r)\rangle$ term is necessary to satisfy the boundary condition in Eq. (4.38) leading to an action that is consistent with the conservation of the vector current.

For the purpose of determining the quantum number n in QCD, we consider the coupling to an external electromagnetic four-vector potential $\mathcal{A}_\mu$ by setting

$$r_\mu = l_\mu = -e\mathcal{A}_\mu Q, \tag{4.49}$$

where Q is the quark-charge matrix. We examine the interaction Lagrangian which is responsible for the decay $\pi^0 \to \gamma\gamma$. As Bär and Wiese pointed out [BW 01], in order for the Standard Model to be consistent for arbitrary N_c, the ordinary quark-charge matrix should be replaced by

$$Q = \begin{pmatrix} \frac{2}{3} & 0 & 0 \\ 0 & -\frac{1}{3} & 0 \\ 0 & 0 & -\frac{1}{3} \end{pmatrix} \to \begin{pmatrix} \frac{1}{2N_c} + \frac{1}{2} & 0 & 0 \\ 0 & \frac{1}{2N_c} - \frac{1}{2} & 0 \\ 0 & 0 & \frac{1}{2N_c} - \frac{1}{2} \end{pmatrix}. \tag{4.50}$$

From Eq. (4.46) one can derive the leading-order Lagrangian for the $\pi^0 \to \gamma\gamma$ decay

$$\mathcal{L}_{\pi^0\to\gamma\gamma} = -\frac{n}{N_c}\frac{e^2}{32\pi^2}\epsilon^{\mu\nu\rho\sigma}\mathcal{F}_{\mu\nu}\mathcal{F}_{\rho\sigma}\frac{\pi^0}{F_0}, \tag{4.51}$$

which leads to the decay rate

$$\Gamma_{\pi^0\to\gamma\gamma} = \frac{\alpha^2 M_{\pi^0}^3}{64\pi^3 F_0^2}\frac{n^2}{N_c^2} = 7.6 \text{ eV} \times \left(\frac{n}{N_c}\right)^2, \tag{4.52}$$

where $\alpha = e^2/(4\pi)$ is the fine-structure constant. This result is in good agreement with the experimental value of $\Gamma_{\pi^0\to\gamma\gamma} = (7.63 \pm 0.16)$ eV [Oli+ 14] for $n = N_c$. However, one cannot conclude that $N_c = 3$. Bär and Wiese suggested to obtain the value of N_c rather from three-flavor processes such as $\eta \to \pi^+\pi^-\gamma$ or $K\gamma \to K\pi$. However, Borasoy and Lipartia [BL 05] have investigated the corresponding η and η' decays up to NLO in LN_cChPT and concluded that, due to the importance of NLO corrections which are needed to describe the experimental spectra and decay widths, the number of colors cannot be determined from these decays.

4.4.2 Higher-order Lagrangians

In this thesis, we want to consider anomalous decays including the η'. At leading order, anomalous decays are driven by the WZW action, which has been discussed in Sec. 4.4.1 in SU(3) ChPT. Since our aim is the inclusion of the η', we need the expression for the WZW action including the singlet η_1 field. The WZW action in U(3) ChPT can be obtained from the SU(3) WZW action by simply replacing the SU(3) matrices U, r_μ, and l_μ by the corresponding U(3) expressions. The WZW term accounts for the anomaly. The rest of the unnatural parity Lagrangian, without the WZW term, becomes invariant under local $\mathrm{U}(3)_L \times \mathrm{U}(3)_R$ transformations. At $\mathcal{O}(p^4)$, there exist six independent invariants which obey charge conjugation invariance, and the effective Lagrangian at $\mathcal{O}(p^4)$ reads [KL 00]

$$\begin{aligned}\mathcal{L}_\epsilon^{(p^4)} = \mathcal{L}_{\mathrm{WZW}} &+ \tilde{V}_1\, i\langle \tilde{R}^{\mu\nu} D_\mu U D_\nu U^\dagger + \tilde{L}^{\mu\nu} D_\mu U^\dagger D_\nu U\rangle + \tilde{V}_2\,\langle \tilde{R}^{\mu\nu} U L_{\mu\nu} U^\dagger\rangle \\ &+ \tilde{V}_3\,\langle \tilde{R}^{\mu\nu} R_{\mu\nu} + \tilde{L}^{\mu\nu} L_{\mu\nu}\rangle + \tilde{V}_4\, i D_\mu\theta\,\langle \tilde{R}^{\mu\nu} D_\nu U U^\dagger - \tilde{L}^{\mu\nu} U^\dagger D_\nu U\rangle \\ &+ \tilde{V}_5\,(\langle \tilde{R}^{\mu\nu}\rangle\langle R_{\mu\nu}\rangle + \langle \tilde{L}^{\mu\nu}\rangle\langle L_{\mu\nu}\rangle) + \tilde{V}_6\,\langle \tilde{R}^{\mu\nu}\rangle\langle L_{\mu\nu}\rangle, \end{aligned} \tag{4.53}$$

where

$$\begin{aligned} R_{\mu\nu} &= \partial_\mu r_\nu - \partial_\nu r_\mu - i[r_\mu, r_\nu], \\ L_{\mu\nu} &= \partial_\mu l_\nu - \partial_\nu l_\mu - i[l_\mu, l_\nu], \\ \tilde{F}^{\mu\nu} &= \frac{1}{2}\epsilon^{\mu\nu\rho\sigma} F_{\rho\sigma}. \end{aligned} \tag{4.54}$$

Due to parity, all potentials are odd functions of $(\psi+\theta)$, except for V_4 which is even.

In the combined LN_c and chiral expansions, the WZW term starts contributing at $\mathcal{O}(N_c p^4) = \mathcal{O}(\delta)$. In this thesis, the anomalous processes are supposed to be studied at the one-loop level, which corresponds to a NNLO calculation in the δ counting. Therefore, we need the odd-intrinsic-parity Lagrangians at NLO and NNLO. Up to NNLO, the effective odd-intrinsic-parity Lagrangian is denoted by

$$\mathcal{L}_\epsilon = \mathcal{L}_{\mathrm{WZW}}^{(1)} + \mathcal{L}_\epsilon^{(2)} + \mathcal{L}_\epsilon^{(3)}, \tag{4.55}$$

where the superscripts (i) refer to the order in δ. The NLO Lagrangian $\mathcal{L}_\epsilon^{(2)}$ receives contributions from $\mathcal{O}(p^4)$ and $\mathcal{O}(N_c p^6)$. From Eq. (4.53) one can extract [KL 00]

$$\begin{aligned}\mathcal{L}_\epsilon^{(2,p^4)} = \tilde{L}_1\, i\,(\psi+\theta)&\langle \tilde{R}^{\mu\nu} D_\mu U D_\nu U^\dagger + \tilde{L}^{\mu\nu} D_\mu U^\dagger D_\nu U\rangle \\ &+ \tilde{L}_2(\psi+\theta)\langle \tilde{R}^{\mu\nu} U L_{\mu\nu} U^\dagger\rangle + \tilde{L}_3(\psi+\theta)\langle \tilde{R}^{\mu\nu} R_{\mu\nu} + \tilde{L}^{\mu\nu} L_{\mu\nu}\rangle \\ &+ \tilde{L}_4\, i D_\mu\theta\,\langle \tilde{R}^{\mu\nu} D_\nu U U^\dagger - \tilde{L}^{\mu\nu} U^\dagger D_\nu U\rangle. \end{aligned} \tag{4.56}$$

The odd-intrinsic-parity Lagrangian at $\mathcal{O}(p^6)$ has been constructed in SU(3) ChPT in Refs. [EFS 02, BGT 02]. Reference [JGW 14] provides the full

$\mathcal{O}(p^6)$ Lagrangian in U(3) ChPT. The $\mathcal{O}(N_c p^6)$ contributions are those terms of the $\mathcal{O}(p^6)$ Lagrangian which have only one flavor trace and do not contain the fields $(\psi+\theta)$ or $D_\mu\theta$. The NNLO Lagrangian $\mathcal{L}_\epsilon^{(3)}$ consists of terms of $\mathcal{O}(N_c p^8)$, $\mathcal{O}(p^6)$, and $\mathcal{O}(N_c^{-1}p^4)$. The $\mathcal{O}(p^8)$ Lagrangian has not been constructed so far. Order p^6 terms stem from the $\mathcal{O}(p^6)$ Lagrangian containing two flavor traces, the field $D_\mu\theta$, or are generated when expanding the potentials of the odd-parity terms of the $\mathcal{O}(p^6)$ Lagrangian up to linear order in $(\psi+\theta)$. Terms of $\mathcal{O}(N_c^{-1}p^4)$ could arise from the expansion of the potentials in $\mathcal{L}_\epsilon^{(p^4)}$, but they do not contribute to the anomalous processes we want to consider. Since especially the $\mathcal{O}(p^6)$ Lagrangian contains a lot of terms, in the following, we display only the terms needed for the calculations in this thesis. The relevant terms of the $\mathcal{O}(N_c p^6)$ and $\mathcal{O}(p^6)$ Lagrangians are shown in Tabs. 4.2 and 4.3, respectively. Since there is, at present, no satisfactory unified nomenclature for the coupling constants, for easier reference we choose the names according to the respective references from which the Lagrangians were taken.

The operators with the LECs $L_i^{6,\epsilon}$, which appear in SU(3) ChPT as well, are taken from Ref. [EFS 02]. They are given in terms of the building blocks

$$\begin{aligned}
(A)_\pm &= u^\dagger A u^\dagger \pm u A^\dagger u,\\
F_R^{\mu\nu} &= \partial_\mu r_\nu - \partial_\nu r_\mu - i[r_\mu, r_\nu],\\
F_L^{\mu\nu} &= \partial_\mu l_\nu - \partial_\nu l_\mu - i[l_\mu, l_\nu],\\
G^{\mu\nu} &= F_R^{\mu\nu} U + U F_L^{\mu\nu},\\
H^{\mu\nu} &= F_R^{\mu\nu} U - U F_L^{\mu\nu},\\
(D_\mu D_\nu U)_-^s &= \frac{1}{2}(\{D_\mu, D_\nu\}U)_-\\
&= (D_\mu D_\nu U)_- + \frac{i}{2}(H_{\mu\nu})_+,
\end{aligned}\tag{4.57}$$

where A refers to operators transforming under the chiral group G as $A \overset{G}{\to} V_R A V_L^\dagger$. The other terms, genuinely related to the U(3) sector, are taken from Ref. [JGW 14]. Here, the corresponding building blocks are the same as in Eq. (4.28) with the additional structures

$$f_\pm^{\mu\nu} = u F_L^{\mu\nu} u^\dagger \pm u^\dagger F_R^{\mu\nu} u.\tag{4.58}$$

4.5 Precision

In LN_cChPT, calculations are performed in the combined chiral and LN_c expansions with a common expansion parameter δ, specified in Eq. (4.10).

Process	LEC	Operator	SU(3)
$P\to\gamma^{(*)}\gamma^{(*)}$	$L_3^{6,\epsilon}$	$i\,\langle(\chi)_+\{(G_{\mu\nu})_+(H_{\alpha\beta})_+-\text{rev}\}\rangle\epsilon^{\mu\nu\alpha\beta}$	x
	$L_8^{6,\epsilon}$	$i\,\langle(\chi)_-(G_{\mu\nu})_+(G_{\alpha\beta})_+\rangle\epsilon^{\mu\nu\alpha\beta}$	x
	$L_{19}^{6,\epsilon}$	$i\,\langle(D^\lambda G_{\lambda\mu})_+\{(G_{\nu\alpha})_+(D_\beta U)_-+\text{rev}\}\rangle\epsilon^{\mu\nu\alpha\beta}$	x
$\eta^{(\prime)}\to\pi^+\pi^-\gamma^{(*)}$	$L_1^{6,\epsilon}$	$\langle(\chi)_+\{(H_{\mu\nu})_+(D_\alpha U)_-(D_\beta U)_-+\text{rev}\}\rangle\epsilon^{\mu\nu\alpha\beta}$	x
	$L_5^{6,\epsilon}$	$\langle(\chi)_-\{(G_{\mu\nu})_+(D_\alpha U)_-(D_\beta U)_--\text{rev}\}\rangle\epsilon^{\mu\nu\alpha\beta}$	x
	$L_6^{6,\epsilon}$	$\langle(\chi)_-(D_\mu U)_-(G_{\nu\alpha})_+(D_\beta U)_-\rangle\epsilon^{\mu\nu\alpha\beta}$	x
	$L_{13}^{6,\epsilon}$	$\langle(G_{\mu\nu})_+\{(D^\lambda D_\alpha U)_-^s(D_\beta U)_-(D_\lambda U)_--\text{rev}\}\rangle\epsilon^{\mu\nu\alpha\beta}$	x
	$L_{14}^{6,\epsilon}$	$\langle(G_{\mu\nu})_+\{(D_\lambda D_\alpha U)_-^s(D^\lambda U)_-(D_\beta U)_--\text{rev}\}\rangle\epsilon^{\mu\nu\alpha\beta}$	x

Table 4.2: Relevant terms of $\mathcal{L}_\epsilon^{(2,N_cp^6)}$.

Process	LEC	Operator	SU(3)
$P\to\gamma^{(*)}\gamma^{(*)}$	$L_9^{6,\epsilon}$	$i\,\langle(\chi)_-\rangle\langle(G_{\mu\nu})_+(G_{\alpha\beta})_+\rangle\epsilon^{\mu\nu\alpha\beta}$	x
	L_{237}	$\epsilon^{\mu\nu\lambda\rho}\langle f_{+\mu\nu}\rangle\langle f_{+\lambda}{}^\sigma h_{\rho\sigma}\rangle$	-
	L_{238}	$\epsilon^{\mu\nu\lambda\rho}\langle f_{+\mu\nu}\rangle\langle\nabla^\sigma f_{+\lambda\sigma}u_\rho\rangle$	-
	L_{239}	$\epsilon^{\mu\nu\lambda\rho}\langle f_{+\mu\nu}\nabla^\sigma f_{+\lambda\sigma}\rangle\langle u_\rho\rangle$	-
	L_{258}	$i\epsilon^{\mu\nu\lambda\rho}\langle f_{+\mu\nu}\rangle\langle f_{+\lambda\rho}\chi_-\rangle$	-
	Λ_{442}	$\epsilon^{\mu\nu\lambda\rho}(\psi+\theta)\langle f_{+\mu\nu}f_{+\lambda\rho}\chi_+\rangle$	-
AVV	L_{248}	$i\epsilon^{\mu\nu\lambda\rho}\langle F_{L\mu}{}^\sigma D_\sigma F_{L\nu\lambda}\rangle\nabla_\rho\hat{\theta}+\text{H.c.}$	-
	L_{249}	$i\epsilon^{\mu\nu\lambda\rho}\langle F_{L\mu\nu}D^\sigma F_{L\lambda\sigma}\rangle\nabla_\rho\hat{\theta}+\text{H.c.}$	-
	L_{236}	$\epsilon^{\mu\nu\lambda\rho}\langle f_{+\mu\nu}\rangle\langle f_{+\lambda}{}^\sigma f_{-\rho\sigma}\rangle$	-
$\eta^{(\prime)}\to\pi^+\pi^-\gamma^{(*)}$	$L_2^{6,\epsilon}$	$\langle(\chi)_+(D_\mu U)_-\rangle\langle(D_\nu U)_-(H_{\alpha\beta})_+\rangle\epsilon^{\mu\nu\alpha\beta}$	x
	$L_7^{6,\epsilon}$	$\langle(\chi)_-\rangle\langle(G_{\mu\nu})_+(D_\alpha U)_-(D_\beta U)_-\rangle\epsilon^{\mu\nu\alpha\beta}$	x
	L_{227}	$i\epsilon^{\mu\nu\lambda\rho}\langle\nabla^\sigma f_{+\mu\sigma}u_\nu u_\lambda\rangle\langle u_\rho\rangle$	-
	L_{228}	$i\epsilon^{\mu\nu\lambda\rho}\langle\nabla^\sigma f_{+\mu\nu}u_\sigma u_\lambda\rangle\langle u_\rho\rangle+\text{H.c.}$	-
	L_{229}	$i\epsilon^{\mu\nu\lambda\rho}\langle f_{+\mu}{}^\sigma h_{\nu\sigma}u_\lambda\rangle\langle u_\rho\rangle+\text{H.c.}$	-
	L_{230}	$i\epsilon^{\mu\nu\lambda\rho}\langle f_{+\mu\nu}h_\lambda{}^\sigma u_\sigma\rangle\langle u_\rho\rangle+\text{H.c.}$	-
	L_{233}	$i\epsilon^{\mu\nu\lambda\rho}\langle\nabla^\sigma f_{+\mu\sigma}\rangle\langle u_\nu u_\lambda u_\rho\rangle$	-
	L_{234}	$i\epsilon^{\mu\nu\lambda\rho}\langle f_{+\mu}{}^\sigma\rangle\langle u_\nu u_\lambda h_{\rho\sigma}\rangle$	-
	L_{242}	$\epsilon^{\mu\nu\lambda\rho}\langle u_\mu\rangle\langle u_\nu f_{-\lambda\rho}\chi_+\rangle+\text{H.c.}$	-
	L_{254}	$\epsilon^{\mu\nu\lambda\rho}\langle f_{+\mu\nu}\rangle\langle u_\lambda u_\rho\chi_-\rangle$	-
	L_{255}	$\epsilon^{\mu\nu\lambda\rho}\langle f_{+\mu\nu}\chi_-u_\lambda\rangle\langle u_\rho\rangle+\text{H.c.}$	-
	Λ_{437}	$(\psi+\theta)\,(i\epsilon^{\mu\nu\lambda\rho}\langle f_{+\mu\nu}\chi_+u_\lambda u_\rho\rangle+\text{H.c.})$	-
	Λ_{438}	$i\epsilon^{\mu\nu\lambda\rho}(\psi+\theta)\langle f_{+\mu\nu}u_\lambda\chi_+u_\rho\rangle$	-

Table 4.3: Relevant terms of $\mathcal{L}_\epsilon^{(3,p^6)}$.

Physical observables σ are then given as a series in terms of the expansion parameter δ with contributions from the different orders $\sigma^{(n)}$:

$$\sigma = \sigma^{(0)} + \delta\sigma^{(1)} + \delta^2\sigma^{(2)} + \delta^3\sigma^{(3)} + \dots\,. \tag{4.59}$$

Since actual calculations take only a finite number of terms into account, the result receives a systematic error introduced as δ^ϵ. The exponent ϵ is given by the difference of the order of the neglected contributions and the leading contributions with non-vanishing $\sigma^{(n)}$.

The processes in this thesis are calculated up to NNLO resulting in a systematic error of δ^3. A possible estimate for the expansion parameter is given by $\delta = 1/N_c = 1/3$. Corrections breaking the SU(3) symmetry are roughly given by

$$\frac{M_K^2}{\Lambda^2} = \frac{0.244\ \mathrm{GeV}^2}{1\ \mathrm{GeV}^2} \tag{4.60}$$

and are of the same order of magnitude as $1/N_c$. This means that, optimistically estimated, all NNLO results are affected by a systematic error of at least 4%, and NLO calculations receive a systematic error of at least 10%. These errors should be added to the (statistical) errors of all calculated quantities which will be provided in the following chapters.

Chapter 5

η-η' mixing

The mixing of states is a quantum-mechanical phenomenon which is intimately related to the symmetries of the underlying dynamics and the eventual mechanisms leading to their breaking. Prominent examples in the realm of subatomic physics include the K^0-$\bar{K}^0$ and B^0-$\bar{B}^0$ mixing and oscillations, neutrino mixing, the Cabibbo-Kobayashi-Maskawa quark-mixing matrix, and the Weinberg angle [Oli+ 14]. In the low-energy regime of QCD, we observe a fascinating interplay between the dynamical (spontaneous) breaking of chiral symmetry, the explicit symmetry breaking by the quark masses, and the axial $\mathrm{U}(1)_A$ anomaly. In this context, the pseudoscalar mesons η and η' represent an ideal laboratory for investigating the relevant symmetry-breaking mechanisms in QCD.

In this chapter, an expression for the η-η' mixing at the one-loop level up to and including NNLO is derived, followed by a successive numerical analysis of the mixing angle, pseudoscalar masses and decay constants at LO, NLO, and NNLO.

5.1 Calculation of the mixing angle

For $\hat{m} \neq m_s$, the physical η and η' mass eigenstates are linear combinations of the mathematical octet and singlet states η_8 and η_1. Our aim is to derive a general expression for the η-η' mixing at the one-loop level up to and including NNLO in the δ counting. To that end, we start from an effective Lagrangian in terms of the octet and singlet fields and perform successive transformations, resulting in a diagonal Lagrangian in terms of the physical fields. Because of the effective-field-theory nature of our approach, the starting Lagrangian will contain higher-derivative terms up to and including fourth order in the four momentum. The parameters of the

Lagrangian are obtained from a one-loop calculation of the self energies using the Lagrangians and power counting of Sec. 4.3. The Lagrangian after the transformations will have a standard "free-field" form.

Let us collect the fields η_8 and η_1 in the doublet

$$\eta_A \equiv \begin{pmatrix} \eta_8 \\ \eta_1 \end{pmatrix}. \tag{5.1}$$

In terms of η_A, at NNLO the most general effective Lagrangian quadratic in η_A is of the form

$$\mathcal{L}_{\text{eff}} = \mathcal{L}_A = \frac{1}{2}\partial_\mu \eta_A^T \mathcal{K}_A \partial^\mu \eta_A - \frac{1}{2}\eta_A^T \mathcal{M}_A^2 \eta_A + \frac{1}{2} \Box\, \eta_A^T \mathcal{C}_A \Box\, \eta_A. \tag{5.2}$$

The symmetric 2×2 matrices $\mathcal{K}_A$, $\mathcal{M}_A^2$, and $\mathcal{C}_A$ can be written as

$$\mathcal{K}_A = \begin{pmatrix} 1 + k_8 & k_{81} \\ k_{81} & 1 + k_1 \end{pmatrix}, \tag{5.3}$$

$$\mathcal{M}_A^2 = \begin{pmatrix} M_8^2 & M_{81}^2 \\ M_{81}^2 & M_1^2 \end{pmatrix}, \tag{5.4}$$

$$\mathcal{C}_A = \begin{pmatrix} c_8 & c_{81} \\ c_{81} & c_1 \end{pmatrix}. \tag{5.5}$$

Later on, we will provide the one-loop expressions for the matrices $\mathcal{K}_A$ and $\mathcal{M}_A^2$. The last term in Eq. (5.2), containing higher derivatives of η_A, originates from the C_{12} term of the $\mathcal{O}(\delta^2)$ Lagrangian in Eq. (4.27). The matrix $\mathcal{C}_A$ is given in Eqs. (B.6)–(B.8) of Appendix B.1. If we were to work at leading order, only, we would have to replace

$$\mathcal{K}_A \to \mathbb{1}, \quad \mathcal{M}_A^2 \to \mathcal{M}_A^{2\,(0)} = \begin{pmatrix} \mathring{M}_8^2 & \mathring{M}_{81}^2 \\ \mathring{M}_{81}^2 & \mathring{M}_1^2 + M_0^2 \end{pmatrix}, \quad \mathcal{C}_A \to 0.$$

The elements of the (leading-order) mass matrix $\mathcal{M}_A^{2\,(0)}$ read

$$\mathring{M}_8^2 = \frac{2}{3}B\,(\hat{m} + 2m_s) = \frac{1}{3}\Big(4\,\mathring{M}_K^2 - \mathring{M}_\pi^2\Big), \tag{5.6}$$

$$\mathring{M}_1^2 = \frac{2}{3}B\,(2\hat{m} + m_s) = \frac{1}{3}\Big(2\,\mathring{M}_K^2 + \mathring{M}_\pi^2\Big), \tag{5.7}$$

$$M_0^2 = 6\frac{\tau}{F^2}, \tag{5.8}$$

$$\mathring{M}_{81}^2 = -\frac{2\sqrt{2}}{3}B\,(m_s - \hat{m}) = -\frac{2\sqrt{2}}{3}\Big(\mathring{M}_K^2 - \mathring{M}_\pi^2\Big), \tag{5.9}$$

where $\overset{\circ}{M}{}^2_K = B\,(\hat{m} + m_s)$ and $\overset{\circ}{M}{}^2_\pi = 2B\hat{m}$ are the leading-order kaon and pion masses squared, respectively, and M_0^2 denotes the $\mathrm{U}(1)_A$ anomaly contribution to the η_1 mass squared. The mixing already shows up at leading order, because the mass matrix $\mathcal{M}_A^2$ is non-diagonal at that order.

Our first step is to perform a field redefinition to get rid of the higher-derivative structure in Eq. (5.2) [SF 95, FS 00],

$$\eta_A = \left(\mathbb{1} + \frac{1}{2}\mathcal{C}_A\Box\right)\eta_B. \tag{5.10}$$

The field transformation is constructed such that, after inserting Eq. (5.10) into Eq. (5.2), the last term is canceled by a term originating from the first term in Eq. (5.2). Moreover, we obtain additional terms originating from the "mass term" of Eq. (5.2) which now contribute to the new kinetic matrix. Finally, we neglect any terms generated by the field transformation which is beyond the accuracy of a NNLO calculation. Using the relation $\phi\,\Box\,\phi = \partial_\mu(\phi\partial^\mu\phi) - \partial_\mu\phi\partial^\mu\phi$ for the components of η_B, and neglecting total-derivative terms, the Lagrangian after the first field redefinition is of the form

$$\mathcal{L}_B = \frac{1}{2}\partial_\mu\eta_B^T\mathcal{K}_B\partial^\mu\eta_B - \frac{1}{2}\eta_B^T\mathcal{M}_B^2\eta_B, \tag{5.11}$$

where

$$\begin{aligned}
&\mathcal{K}_B \\
&= \mathcal{K}_A + \frac{1}{2}\begin{pmatrix} 2c_8\overset{\circ}{M}{}_8^2 + 2c_{81}\overset{\circ}{M}{}_{81}^2 & (c_1+c_8)\overset{\circ}{M}{}_{81}^2 + c_{81}(\overset{\circ}{M}{}_1^2 + M_0^2 + \overset{\circ}{M}{}_8^2) \\ (c_1+c_8)\overset{\circ}{M}{}_{81}^2 + c_{81}(\overset{\circ}{M}{}_1^2 + M_0^2 + \overset{\circ}{M}{}_8^2) & 2c_1(\overset{\circ}{M}{}_1^2 + M_0^2) + 2c_{81}\overset{\circ}{M}{}_{81}^2 \end{pmatrix} \\
&\equiv \begin{pmatrix} 1 + \delta_8^{(1)} + \delta_8^{(2)} & \delta_{81}^{(1)} + \delta_{81}^{(2)} \\ \delta_{81}^{(1)} + \delta_{81}^{(2)} & 1 + \delta_1^{(1)} + \delta_1^{(2)} \end{pmatrix},
\end{aligned} \tag{5.12}$$

where $\delta_j^{(i)}$ denotes corrections of $\mathcal{O}(\delta^i)$. The entries of the mass matrix $\mathcal{M}_B^2 = \mathcal{M}_A^2$ are given by

$$M_8^2 = \overset{\circ}{M}{}_8^2 + \Delta M_8^{2(1)} + \Delta M_8^{2(2)}, \tag{5.13}$$

$$M_1^2 = M_0^2 + \overset{\circ}{M}{}_1^2 + \Delta M_1^{2(1)} + \Delta M_1^{2(2)}, \tag{5.14}$$

$$M_{81}^2 = \overset{\circ}{M}{}_{81}^2 + \Delta M_{81}^{2(1)} + \Delta M_{81}^{2(2)}, \tag{5.15}$$

where $\Delta M_j^{2(i)}$ denotes corrections of $\mathcal{O}(\delta^i)$.

The next step consists of diagonalizing the kinetic matrix $\mathcal{K}_B$ in Eq. (5.12) up to and including $\mathcal{O}(\delta^2)$ through the field redefinition

$$\eta_B = \sqrt{Z}\eta_C, \tag{5.16}$$

such that

$$\sqrt{Z}^T \mathcal{K}_B \sqrt{Z} = \mathbb{1}. \tag{5.17}$$

Then, the matrix $\sqrt{Z}$ is given by

$$\sqrt{Z}$$
$$= \begin{pmatrix} 1 - \frac{1}{2}\delta_8^{(1)} + \frac{3}{8}\delta_8^{(1)^2} + \frac{3}{8}\delta_{81}^{(1)^2} - \frac{1}{2}\delta_8^{(2)} & -\frac{1}{2}\delta_{81}^{(1)} + \frac{3}{8}\delta_1^{(1)}\delta_{81}^{(1)} + \frac{3}{8}\delta_8^{(1)}\delta_{81}^{(1)} - \frac{1}{2}\delta_{81}^{(2)} \\ -\frac{1}{2}\delta_{81}^{(1)} + \frac{3}{8}\delta_1^{(1)}\delta_{81}^{(1)} + \frac{3}{8}\delta_8^{(1)}\delta_{81}^{(1)} - \frac{1}{2}\delta_{81}^{(2)} & 1 - \frac{1}{2}\delta_1^{(1)} + \frac{3}{8}\delta_1^{(1)^2} + \frac{3}{8}\delta_{81}^{(1)^2} - \frac{1}{2}\delta_1^{(2)} \end{pmatrix}. \tag{5.18}$$

In terms of η_C, the Lagrangian reads

$$\mathcal{L}_C = \frac{1}{2}\partial_\mu \eta_C^T \partial^\mu \eta_C - \frac{1}{2}\eta_C^T \mathcal{M}_C^2 \eta_C, \tag{5.19}$$

with the mass matrix given by

$$\mathcal{M}_C^2 = \sqrt{Z}^T \mathcal{M}_B^2 \sqrt{Z} \equiv \begin{pmatrix} \hat{M}_8^2 & \hat{M}_{81}^2 \\ \hat{M}_{81}^2 & \hat{M}_1^2 \end{pmatrix}. \tag{5.20}$$

Up to and including second order in the corrections $\delta_j^{(i)}$ and $\Delta M_j^{2(i)}$, the entries of the matrix $\mathcal{M}_C^2$ read

$$\begin{aligned} \hat{M}_8^2 = \mathring{M}_8^2 &\left(1 - \delta_8^{(1)} + \delta_8^{(1)^2} + \frac{3}{4}\delta_{81}^{(1)^2} - \delta_8^{(2)}\right) + \Delta M_8^{2(1)}\left(1 - \delta_8^{(1)}\right) + \Delta M_8^{2(2)} \\ &+ \mathring{M}_{81}^2\left(-\delta_{81}^{(1)} + \frac{3}{4}\delta_1^{(1)}\delta_{81}^{(1)} + \frac{5}{4}\delta_8^{(1)}\delta_{81}^{(1)} - \delta_{81}^{(2)}\right) + \Delta M_{81}^{2\,(1)}\left(-\delta_{81}^{(1)}\right) \\ &+ \frac{1}{4}\left(M_0^2 + \mathring{M}_1^2\right)\delta_{81}^{(1)^2}, \end{aligned} \tag{5.21}$$

$$\begin{aligned} \hat{M}_1^2 = &\left(M_0^2 + \mathring{M}_1^2\right)\left(1 - \delta_1^{(1)} + \delta_1^{(1)^2} + \frac{3}{4}\delta_{81}^{(1)^2} - \delta_1^{(2)}\right) + \Delta M_1^{2(1)}\left(1 - \delta_1^{(1)}\right) + \Delta M_1^{2(2)} \\ &+ \mathring{M}_{81}^2\left(-\delta_{81}^{(1)} + \frac{3}{4}\delta_8^{(1)}\delta_{81}^{(1)} + \frac{5}{4}\delta_1^{(1)}\delta_{81}^{(1)} - \delta_{81}^{(2)}\right) + \Delta M_{81}^{2\,(1)}\left(-\delta_{81}^{(1)}\right) + \frac{1}{4}\,\mathring{M}_8^2\,\delta_{81}^{(1)^2}, \end{aligned} \tag{5.22}$$

$$
\begin{aligned}
\hat{M}_{81}^2 = \overset{\circ}{M}{}_{81}^2 &\left(1 - \frac{1}{2}\delta_1^{(1)} - \frac{1}{2}\delta_8^{(1)} + \frac{3}{8}\delta_1^{(1)2} + \frac{1}{4}\delta_1^{(1)}\delta_8^{(1)} + \frac{3}{8}\delta_8^{(1)2} + \delta_{81}^{(1)2} - \frac{1}{2}\delta_1^{(2)} - \frac{1}{2}\delta_8^{(2)}\right) \\
&+ \Delta M_{81}^{2\,(1)}\left(1 - \frac{1}{2}\delta_1^{(1)} - \frac{1}{2}\delta_8^{(1)}\right) + \Delta M_{81}^{2\,(2)} \\
&+ \overset{\circ}{M}{}_8^2\left(-\frac{1}{2}\delta_{81}^{(1)} + \frac{3}{8}\delta_1^{(1)}\delta_{81}^{(1)} + \frac{5}{8}\delta_8^{(1)}\delta_{81}^{(1)} - \delta_{81}^{(2)}\right) + \Delta M_8^{2(1)}\left(-\frac{1}{2}\delta_{81}^{(1)}\right) \\
&+ \left(M_0^2 + \overset{\circ}{M}{}_1^2\right)\left(-\frac{1}{2}\delta_{81}^{(1)} + \frac{3}{8}\delta_8^{(1)}\delta_{81}^{(1)} + \frac{5}{8}\delta_1^{(1)}\delta_{81}^{(1)} - \delta_{81}^{(2)}\right) \\
&+ \Delta M_1^{2(1)}\left(-\frac{1}{2}\delta_{81}^{(1)}\right). \qquad (5.23)
\end{aligned}
$$

Finally, to obtain the physical mass eigenstates, we diagonalize the matrix $\mathcal{M}_C^2$ by means of an orthogonal transformation,

$$\eta_D = R\eta_C, \qquad (5.24)$$

$$R \equiv \begin{pmatrix} \cos\theta^{[2]} & -\sin\theta^{[2]} \\ \sin\theta^{[2]} & \cos\theta^{[2]} \end{pmatrix}, \qquad (5.25)$$

such that

$$R\mathcal{M}_C^2 R^T = \mathcal{M}_D^2 = \begin{pmatrix} M_\eta^2 & 0 \\ 0 & M_{\eta'}^2 \end{pmatrix}. \qquad (5.26)$$

The superscript [2] refers to corrections up to and including second order in the δ expansion. Introducing the nomenclature η_P for the physical fields and $\mathcal{M}_P^2$ for the diagonal mass matrix,

$$\eta_P = \eta_D = \begin{pmatrix} \eta \\ \eta' \end{pmatrix}, \qquad \mathcal{M}_P^2 = \begin{pmatrix} M_\eta^2 & 0 \\ 0 & M_{\eta'}^2 \end{pmatrix},$$

the Lagrangian is now of the “free-field” type,

$$\mathcal{L} = \mathcal{L}_D = \frac{1}{2}\partial_\mu\eta_P^T\partial^\mu\eta_P - \frac{1}{2}\eta_P^T\mathcal{M}_P^2\eta_P = \frac{1}{2}\partial_\mu\eta\partial^\mu\eta - \frac{1}{2}M_\eta^2\eta^2 + \frac{1}{2}\partial_\mu\eta'\partial^\mu\eta' - \frac{1}{2}M_{\eta'}^2\eta'^2.$$

Equation (5.26) yields three relations,

$$\hat{M}_8^2 = M_\eta^2\cos^2\theta^{[2]} + M_{\eta'}^2\sin^2\theta^{[2]}, \qquad (5.27)$$

$$\hat{M}_1^2 = M_\eta^2\sin^2\theta^{[2]} + M_{\eta'}^2\cos^2\theta^{[2]}, \qquad (5.28)$$

$$\hat{M}_{81}^2 = \left(M_{\eta'}^2 - M_\eta^2\right)\sin\theta^{[2]}\cos\theta^{[2]}, \qquad (5.29)$$

which define the mixing angle $\theta^{[2]}$ calculated up to and including $\mathcal{O}(\delta^2)$. First, from Eq. (5.29) we infer

$$\sin 2\theta^{[2]} = \frac{2\hat{M}_{81}^2}{M_{\eta'}^2 - M_\eta^2}. \qquad (5.30)$$

Further, we obtain from Eqs. (5.27)–(5.29)

$$M_{\eta'}^2 + M_\eta^2 = \hat{M}_8^2 + \hat{M}_1^2 \tag{5.31}$$

and

$$M_{\eta'}^2 - M_\eta^2 = \sqrt{\left(\hat{M}_8^2 - \hat{M}_1^2\right)^2 + 4\left(\hat{M}_{81}^2\right)^2}. \tag{5.32}$$

This equation implies that Eq. (5.30) can also be written as

$$\sin 2\theta^{[2]} = \frac{2\hat{M}_{81}^2}{\sqrt{\left(\hat{M}_8^2 - \hat{M}_1^2\right)^2 + 4\left(\hat{M}_{81}^2\right)^2}}. \tag{5.33}$$

The transformation from the octet fields η_A to the physical fields η_D can be summarized as

$$\eta_A = T\eta_D = \left(1 + \frac{1}{2}\mathcal{C}_A\Box\right)\sqrt{Z}R^T\eta_D, \tag{5.34}$$

where the transformation matrix T is given by

$$T = \begin{pmatrix} -A\sin\theta^{[2]} + B_8\cos\theta^{[2]} & A\cos\theta^{[2]} + B_8\sin\theta^{[2]} \\ A\cos\theta^{[2]} - B_1\sin\theta^{[2]} & A\sin\theta^{[2]} + B_1\cos\theta^{[2]} \end{pmatrix}, \tag{5.35}$$

with

$$A = -\delta_{81}^{(1)}\left(\frac{1}{2} - \frac{3}{8}\delta_1^{(1)} - \frac{3}{8}\delta_8^{(1)}\right) - \frac{1}{2}\delta_{81}^{(2)} + \frac{c_{81}}{2}\Box, \tag{5.36}$$

$$B_i = 1 - \frac{1}{2}\delta_i^{(1)} + \frac{3}{8}\delta_i^{(1)2} + \frac{3}{8}\delta_{81}^{(1)2} - \frac{1}{2}\delta_i^{(2)} + \frac{c_i}{2}\Box\,. \tag{5.37}$$

Up to this point, the procedure for defining a mixing angle in terms of successive transformations is rather general. We now turn to a determination of the quantities $\delta_i^{(j)}$ as well as the M_i^2 terms within LN_cChPT. To identify $\mathcal{K}_A$ and $\mathcal{M}_A^2$ at NNLO, we calculate the self-energy insertions $-i\Sigma_{ij}(p^2)$, $i,\ j = 1,\ 8$, corresponding to the Feynman diagrams in Fig. 5.1. The Feynman rules are derived from the Lagrangians $\mathcal{L}^{(0)}$, $\mathcal{L}^{(1)}$, and $\mathcal{L}^{(2)}$ of Eqs. (4.22), (4.24), and (4.25)–(4.27) in Sec. 4.3. The self energy calculated from the Lagrangian in Eq. (5.2) takes the form[1]

$$\Sigma(p^2) = \begin{pmatrix} \Sigma_{88}(p^2) & \Sigma_{81}(p^2) \\ \Sigma_{18}(p^2) & \Sigma_{11}(p^2) \end{pmatrix}, \tag{5.38}$$

[1]Since both the singlet and the octet states are massless in the combined chiral and $N_c \to \infty$ limits, we consider the lowest-order mass terms as part of the self-energy contributions.

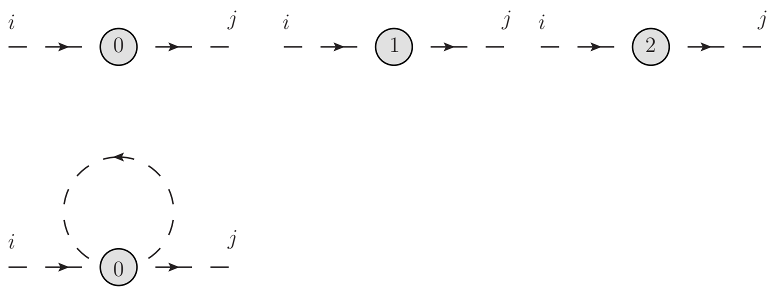

Figure 5.1: Self-energy diagrams up to and including $\mathcal{O}(\delta^2)$: Dashed lines refer to pseudoscalar mesons, and the numbers k in the interaction blobs refer to vertices derived from the corresponding Lagrangians $\mathcal{L}^{(k)}$.

where the $\Sigma_{ij}(p^2)$ are parametrized up to and including $\mathcal{O}(\delta^2)$ as

$$\Sigma_{88}(p^2) = -\left(k_8 + c_8 p^2\right) p^2 + M_8^2, \tag{5.39}$$

$$\Sigma_{81}(p^2) = \Sigma_{18}(p^2) = -\left(k_{81} + c_{81} p^2\right) p^2 + M_{81}^2, \tag{5.40}$$

$$\Sigma_{11}(p^2) = -\left(k_1 + c_1 p^2\right) p^2 + M_1^2. \tag{5.41}$$

We now obtain the elements of the kinetic matrix $\mathcal{K}_A$, the mass matrix $\mathcal{M}_A^2$, and the matrix $\mathcal{C}_A$ by comparing the results for the self energies calculated by means of the Feynman diagrams (Fig. 5.1) with the parametrization given in Eqs. (5.39)–(5.41).

The NLO contributions to the kinetic matrix read

$$\delta_8^{(1)} = \frac{8\,(4M_K^2 - M_\pi^2)\,L_5}{3F_\pi^2}, \tag{5.42}$$

$$\delta_1^{(1)} = \frac{8\,(2M_K^2 + M_\pi^2)\,L_5}{3F_\pi^2} + \Lambda_1, \tag{5.43}$$

$$\delta_{81}^{(1)} = -\frac{16\sqrt{2}\,(M_K^2 - M_\pi^2)\,L_5}{3F_\pi^2}, \tag{5.44}$$

where M_π, M_K, and F_π denote the physical pion and kaon masses, and the physical pion-decay constant, respectively. The difference between using physical values instead of leading-order expressions in Eqs. (5.42)–(5.44) is of NNLO and is compensated by an appropriate modification of the $\mathcal{O}(\delta^2)$ terms. The NNLO expressions for M_π, M_K, and F_π are displayed in Appendix B.1.

The entries of the mass matrix $\mathcal{M}_A^2$ are defined in Eqs. (5.13)–(5.15) in terms of leading-order, δ^1, and δ^2 pieces. The leading-order masses are given in Eqs. (5.6)–(5.9). In terms of the physical pion and kaon masses, and the physical pion-decay constant, the first-order corrections read

$$\Delta M_8^{2\,(1)} = \frac{16\left(8M_K^4 - 8M_\pi^2 M_K^2 + 3M_\pi^4\right)L_8}{3F_\pi^2}, \tag{5.45}$$

$$\Delta M_1^{2\,(1)} = \frac{16\left(4M_K^4 - 4M_\pi^2 M_K^2 + 3M_\pi^4\right)L_8}{3F_\pi^2} + \frac{2\Lambda_2}{3}\left(2M_K^2 + M_\pi^2\right), \tag{5.46}$$

$$\Delta M_{81}^{2\,(1)} = -\frac{64\sqrt{2}\left(M_K^2 - M_\pi^2\right)M_K^2 L_8}{3F_\pi^2} - \frac{2\sqrt{2}\Lambda_2}{3}(M_K^2 - M_\pi^2). \tag{5.47}$$

The corresponding NNLO expressions for the kinetic and the mass matrix elements can be found in Appendix B.1.

5.2 Decay constants

The decay constants of the η-η' system are defined via the matrix element of the axial-vector current operator $A_\mu^a = \bar{q}\gamma_\mu\gamma_5\frac{\lambda^a}{2}q$,

$$\langle 0|\, A_\mu^a(0)\,|P(p)\rangle = iF_P^a p_\mu, \tag{5.48}$$

where $a = 8,\ 0$ and $P = \eta,\ \eta'$. Since both mesons have octet and singlet components, Eq. (5.48) defines four independent decay constants, F_P^a. We parametrize them according to the convention in [Leu 98]

$$\{F_P^a\} = \begin{pmatrix} F_\eta^8 & F_\eta^0 \\ F_{\eta'}^8 & F_{\eta'}^0 \end{pmatrix} = \begin{pmatrix} F_8\cos\theta_8 & -F_0\sin\theta_0 \\ F_8\sin\theta_8 & F_0\cos\theta_0 \end{pmatrix}. \tag{5.49}$$

This parametrization is a popular way to define the η-η' mixing within the so-called two-angle scheme [FKS 98, FKS 99, BDC 00, EF 05, EMS 11, EMS 14, EMS 15]. The angles θ_8 and θ_0 and the constants F_8 and F_0 are given by

$$\tan\theta_8 = \frac{F_{\eta'}^8}{F_\eta^8}, \qquad \tan\theta_0 = -\frac{F_\eta^0}{F_{\eta'}^0}, \tag{5.50}$$

$$F_8 = \sqrt{\left(F_\eta^8\right)^2 + \left(F_{\eta'}^8\right)^2}, \qquad F_0 = \sqrt{\left(F_\eta^0\right)^2 + \left(F_{\eta'}^0\right)^2}. \tag{5.51}$$

To determine the decay constants F_P^a, we calculate the Feynman diagrams in Fig. 5.2. First, we calculate the coupling of the axial-vector current to the octet and singlet fields ϕ_b, collected in the doublet η_A, at the one-loop level

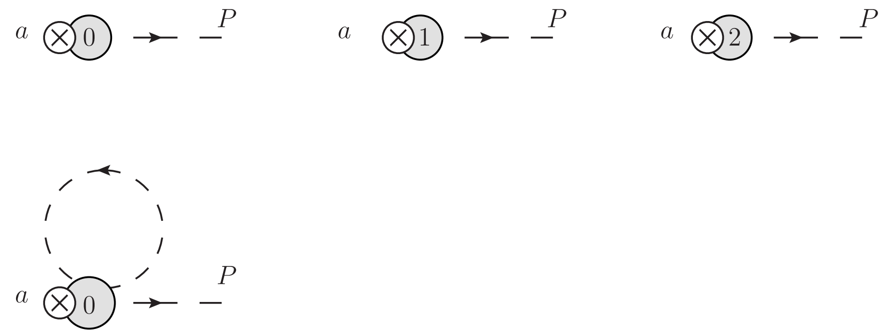

Figure 5.2: Feynman diagrams contributing to the calculation of the decay constants up to and including $\mathcal{O}(\delta^2)$. Dashed lines refer to pseudoscalar mesons, crossed dots to axial-vector sources, and the numbers k in the interaction blobs refer to vertices derived from the Lagrangians $\mathcal{L}^{(k)}$ in Sec. 4.3.

up to NNLO in the δ counting. The result, which should be interpreted as a Feynman rule, is represented by the "matrix elements" $\mathcal{F}_{ab} = \langle 0| A^a_\mu(0) |b\rangle$. In a next step, we transform the bare fields η_A to the physical states using the transformation T in Eq. (5.35). The decay constants F^a_P are then given by

$$\{F^a_P\}^T = \begin{pmatrix} F^8_\eta & F^0_\eta \\ F^8_{\eta'} & F^0_{\eta'} \end{pmatrix}^T = (\mathcal{F}\cdot T). \tag{5.52}$$

At leading order, the decay constants read

$$F^8_\eta = F^0_{\eta'} = F\cos\theta^{[0]}, \tag{5.53}$$

$$-F^0_\eta = F^8_{\eta'} = F\sin\theta^{[0]}, \tag{5.54}$$

in terms of the leading-order mixing angle $\theta^{[0]}$ given in Eq. (5.30). Equation (5.50) then yields $\theta_0 = \theta_8 = \theta^{[0]}$. The NLO decay constants are given by

$$F^8_\eta/F = \left(1+\frac{1}{2}\delta_8^{(1)}\right)\cos\theta^{[1]} - \frac{1}{2}\delta_{81}^{(1)}\sin\theta^{[1]}, \tag{5.55}$$

$$F^0_\eta/F = -\left(1+\frac{1}{2}\delta_1^{(1)}\right)\sin\theta^{[1]} + \frac{1}{2}\delta_{81}^{(1)}\cos\theta^{[1]}, \tag{5.56}$$

$$F^8_{\eta'}/F = \left(1+\frac{1}{2}\delta_8^{(1)}\right)\sin\theta^{[1]} + \frac{1}{2}\delta_{81}^{(1)}\cos\theta^{[1]}, \tag{5.57}$$

$$F^0_{\eta'}/F = \left(1+\frac{1}{2}\delta_1^{(1)}\right)\cos\theta^{[1]} + \frac{1}{2}\delta_{81}^{(1)}\sin\theta^{[1]}, \tag{5.58}$$

now in terms of the NLO mixing angle $\theta^{[1]}$. Using Eqs. (5.50) and (5.51), one obtains

$$F_8 = F\left(1 + \frac{\delta_8^{(1)}}{2}\right),$$
$$F_0 = F\left(1 + \frac{\delta_1^{(1)}}{2}\right), \tag{5.59}$$

and

$$\theta_8 = \theta^{[1]} + \arctan\left(\frac{\delta_{81}^{(1)}}{2}\right),$$
$$\theta_0 = \theta^{[1]} - \arctan\left(\frac{\delta_{81}^{(1)}}{2}\right). \tag{5.60}$$

The results for the decay constant at NNLO are lengthy and are given in Appendix B.1.

5.3 Dependence on the running scale of QCD

The singlet axial-vector current, $A^0_\mu = \bar{q}(1/2)\lambda_0\gamma_\mu\gamma_5 q$, carries anomalous dimension [Adl 69, Kod 80, ET 82]. To obtain finite correlation functions of this current, the operator A^0_μ receives multiplicative renormalization, and the decay constants associated with the singlet axial current depend on the renormalization scale μ of QCD.[2] The scale dependence of the operators is compensated by treating the external fields as scale-dependent quantities such that the effective action of QCD is rendered scale invariant [KL 00]. The renormalization of the singlet axial current and hence of the corresponding decay constants reads

$$A^{0\,\mathrm{ren}}_\mu = Z_A A^0_\mu, \tag{5.61}$$
$$F^{0\,\mathrm{ren}}_P = Z_A F^0_P, \quad P = \eta,\ \eta', \tag{5.62}$$

where the renormalization factor Z_A is determined by the anomalous dimension γ_A of the singlet axial current,

$$\mu\frac{dZ_A}{d\mu} = \gamma_A Z_A, \quad \gamma_A = -\frac{6N_f(N_c^2-1)}{N_c}\left(\frac{g}{4\pi}\right)^4 + \mathcal{O}(g^6). \tag{5.63}$$

[2]Here, we consider the scale dependence within QCD. This has to be distinguished from the scale used to renormalize loop corrections within the effective field theory.

These properties are then transferred to the effective Lagrangian resulting in effective coupling constants which depend on the running scale of QCD [KL 00]. In order for the effective Lagrangian to become invariant under a change of the QCD scale, the variables $(\psi+\theta)$ and $D_\mu\theta$ have to be renormalized according to

$$(\psi+\theta)^{\mathrm{ren}} = Z_A^{-1}(\psi+\theta), \tag{5.64}$$
$$(D_\mu\theta)^{\mathrm{ren}} = Z_A^{-1}D_\mu\theta, \tag{5.65}$$

leading to the following scaling laws for certain LECs,

$$\begin{aligned}
\tau^{\mathrm{ren}} &= Z_A^2\tau,\\
1+\Lambda_1^{\mathrm{ren}} &= Z_A^2(1+\Lambda_1),\\
1+\Lambda_2^{\mathrm{ren}} &= Z_A(1+\Lambda_2),\\
2L_5+3L_{18}^{\mathrm{ren}} &= Z_A(2L_5+3L_{18}),\\
2L_8-3L_{25}^{\mathrm{ren}} &= Z_A(2L_8-3L_{25}).
\end{aligned} \tag{5.66}$$

Since the triangle graph responsible for the anomalous dimension of the singlet axial current is suppressed by $1/N_c$, $Z_A = 1+\mathcal{O}(1/N_c)$. The renormalization is not always multiplicative, as can be seen in Eqs. (5.66). The individual Lagrangians $\mathcal{L}^{(0)}$–$\mathcal{L}^{(2)}$ are not invariant under the QCD renormalization group. However, the scaling rules above ensure that the sum $\mathcal{L}^{(0)}+\mathcal{L}^{(1)}+\dots$ is invariant.

The odd-intrinsic-parity Lagrangians are subject to this issue as well. In a similar way, one finds that the sum $\mathcal{L}_{\mathrm{WZW}}+\mathcal{L}_\epsilon^{(2)}$ is renormalization group invariant, provided $\tilde{L}_1,\dots,\tilde{L}_4$ are renormalized according to [KL 00]

$$\begin{aligned}
\tilde{L}_1^{\mathrm{ren}} &= Z_A\tilde{L}_1-\kappa,\\
\tilde{L}_2^{\mathrm{ren}} &= Z_A\tilde{L}_2-\kappa,\\
\tilde{L}_3^{\mathrm{ren}} &= Z_A\tilde{L}_3-\kappa,\\
\tilde{L}_4^{\mathrm{ren}} &= Z_A\tilde{L}_4+\kappa,
\end{aligned} \tag{5.67}$$

where $\kappa = N_c(Z_A-1)/144\pi^2$.

5.4 Numerical analysis

In the following, we perform the numerical evaluation of the mixing angle, the masses of the pseudoscalar mesons, and their decay constants. We present the results in a systematic way, order by order.

5.4.1 LO

At leading order, the mixing angle is given by Eq. (5.33) which reduces to

$$\sin 2\theta^{[0]} = \frac{-4\sqrt{2}\,(M_K^2 - M_\pi^2)}{\sqrt{12M_0^2\,(M_\pi^2 - M_K^2) + 36\,(M_K^2 - M_\pi^2)^2 + 9M_0^4}}. \tag{5.68}$$

This equation is well suited to study the two limits, the flavor-symmetric case, i.e., $M_\pi^2 = M_K^2$, and the limit $N_c \to \infty$. In the flavor-symmetric limit, the mixing angle vanishes, $\theta^{[0]} = 0$. On the other hand, in the LN_c limit, the U$(1)_A$ contribution to the η' mass vanishes, i.e., $M_0^2 = 0$, and the mixing angle becomes independent of the pseudoscalar masses

$$\sin 2\theta^{[0]} = -\frac{2\sqrt{2}}{3}, \tag{5.69}$$

which yields $\theta^{[0]} = -35.3°$. We then turn to the physical case. Employing Eqs. (5.31) and (5.32), we fix M_0^2 to the physical $M_{\eta'}^2$ mass

$$M_0^2 = \frac{3\left(M_{\eta'}^2 - M_\pi^2\right)\left(2M_K^2 - M_{\eta'}^2 - M_\pi^2\right)}{4M_K^2 - 3M_{\eta'}^2 - M_\pi^2}, \tag{5.70}$$

and obtain

$$\sin 2\theta^{[0]} = -\frac{4\sqrt{2}\,(M_K^2 - M_\pi^2)\left(-4M_K^2 + 3M_{\eta'}^2 + M_\pi^2\right)}{3\left[-8M_K^2\left(M_{\eta'}^2 + M_\pi^2\right) + 8M_K^4 + 3M_{\eta'}^4 + 2M_\pi^2 M_{\eta'}^2 + 3M_\pi^4\right]}. \tag{5.71}$$

Evaluating these results for physical masses M_π^2, M_K^2, and $M_{\eta'}^2$ yields

$$\theta^{[0]} = -19.6° \quad \text{and} \quad M_0 = 0.820 \text{ GeV}. \tag{5.72}$$

5.4.2 NLO

At NLO, still only tree diagrams contribute, since loop contributions are relegated to NNLO. Beyond F, $B\hat{m}$, Bm_s, and τ, the four NLO LECs L_5, L_8, Λ_1, Λ_2 appear and need to be fixed. Since there are, at present, no values for all of the NLO LECs in U(3) ChPT available in the literature, we follow two different strategies to fix the coupling constants:

1. We design a compact system of observables calculated within our framework of LN_cChPT and determine the LECs by fixing them to the physical values of the observables. Our set of observables consists of M_π^2,

M_K^2, F_K/F_π, M_η^2, $M_{\eta'}^2$. In addition, we need the quark mass ratio $m_s/\hat{m}$, which we take from [Aok+ 14]. The experimental values for the masses and decay constants are taken from Ref. [Oli+ 14] reading

$$\begin{aligned} &M_\pi = 0.135 \text{ GeV}, \quad M_K = 0.494 \text{ GeV}, \quad M_\eta = 0.548 \text{ GeV}, \\ &M_{\eta'} = 0.958 \text{ GeV}, \quad F_\pi = 0.0922(1) \text{ GeV}, \quad F_K/F_\pi = 1.198(6). \end{aligned} \tag{5.73}$$

2. We use phenomenological determinations of some constants obtained in SU(3) ChPT, for example Tab. 1 from Ref. [BE 14].

We start with the first strategy and begin by fixing M_0^2 to the physical $M_{\eta'}^2$ using the relation

$$\left(2M_{\eta'}^2 - \hat{M}_8^2 - \hat{M}_1^2\right)^2 = \left(\hat{M}_8^2 - \hat{M}_1^2\right)^2 + 4\left(\hat{M}_{81}^2\right)^2, \tag{5.74}$$

which follows from Eqs. (5.31) and (5.32). After expressing M_0^2 in terms of $M_{\eta'}^2$, the parameters Λ_1 and Λ_2 appear only in the QCD-scale-invariant combination $\tilde{\Lambda} = \Lambda_1 - 2\Lambda_2$ in the expressions for our observables and the mixing angle. Using the ratio $m_s/\hat{m} = 27.5$ from [Aok+ 14], the parameters $B\hat{m}$, L_5, L_8, $\tilde{\Lambda}$ can be unambiguously obtained from the NLO relations to the physical values of M_π^2, M_K^2, F_K/F_π, M_η^2, given in Appendix B.1. The results for the LECs are shown in Tab. 5.1 labeled NLO I. Notice that at this order no EFT-scale dependence is introduced yet, so these LECs are scale independent. We also display errors for all calculated quantities. These errors are only due to the input errors. We do not give estimates for the errors due to neglecting higher orders or particular assumptions of our models. As input errors we consider the errors of F_K/F_π, F_π, $m_s/\hat{m}$ and later, when we make use of LECs determined in SU(3) ChPT [BE 14], we also take their errors into account.

Once the set of LECs is determined, we can evaluate the LO pseudoscalar masses, the η-η' mixing angle, and the pseudoscalar decay constants. For the calculation of the parameters θ_8, θ_0, F_8, F_0, we use the simplified formula at NLO given in Eqs. (5.59) and (5.60). The quantities M_0^2 and F_0 depend on the QCD-renormalization scale (see Sec. 5.3). Therefore, we can only provide the QCD-scale-invariant quantities $M_0^2/(1+\Lambda_1)$ and $F_0/(1+\Lambda_1/2)$. We are not able to extract a value for Λ_1 from our observables, since physical observables do not depend on the QCD scale and we can only determine the invariant combination $\tilde{\Lambda} = \Lambda_1 - 2\Lambda_2$. The expressions for $M_0^2/(1+\Lambda_1)$ and $F_0/(1+\Lambda_1/2)$ are expanded up to NLO yielding results which depend on Λ_1 only through $\tilde{\Lambda}$. Table 5.2 shows the leading-order masses $\overset{\circ}{M}{}_\pi^2$, $\overset{\circ}{M}{}_K^2$, $M_0^2/(1+\Lambda_1)$, and M_η^2 for $\tilde{\Lambda} = 0$. The mixing angle $\theta^{[1]}$, the angles θ_8, θ_0 and the constants F_8, $F_0/(1+\Lambda_1/2)$ are shown in Tab. 5.3, again under the label NLO I.

The second scenario uses values for the LECs determined phenomenologically in the framework of SU(3) ChPT. Since our calculations are performed in U(3) ChPT, we apply the appropriate matching between the two EFTs [KL 00, Her 98] when we make use of SU(3) determinations. We set the matching scale of the two theories to be $\mu_0 = M_0 = 0.85$ GeV, which is basically the value of $M_{\eta'}$ in the chiral limit: $M_0^2 = 6\tau/F^2(1+\Lambda_1)$. Since SU(3) ChPT contains one-loop corrections already at NLO, the LECs depend on the scale of the effective theory μ. The SU(3) LECs are typically provided at $\mu_1 = 0.77$ GeV. To study the scale dependence of our results, we evaluate them at $\mu = 0.77$ GeV and at $\mu = 1$ GeV, which is the scale of $M_{\eta'}$. Combining the matching at μ_0 and the running from μ_1 to μ results in [KL 00, Her 98]:

$$\begin{aligned}
L_5^r(\mu) &= L_5^{\mathrm{SU}_3,r}(\mu_1) + \frac{3}{8}\frac{1}{16\pi^2}\ln\left(\frac{\mu_1}{\mu}\right), \\
L_8^r(\mu) &= L_8^{\mathrm{SU}_3,r}(\mu_1) + \frac{5}{48}\frac{1}{16\pi^2}\ln\left(\frac{\mu_1}{\mu}\right) + \frac{1}{12}\frac{1}{16\pi^2}\ln\left(\frac{\mu_0}{\mu}\right), \\
L_4^r(\mu) &= L_4^{\mathrm{SU}_3,r}(\mu_1) + \frac{1}{8}\frac{1}{16\pi^2}\ln\left(\frac{\mu_1}{\mu}\right), \\
L_6^r(\mu) &= L_6^{\mathrm{SU}_3,r}(\mu_1) + \frac{11}{144}\frac{1}{16\pi^2}\ln\left(\frac{\mu_1}{\mu}\right) + \frac{1}{72}\frac{1}{16\pi^2}\left(\frac{1}{2} - \ln\left(\frac{\mu_0}{\mu}\right)\right), \\
L_7^r(\mu) &= L_7^{\mathrm{SU}_3,r} + \frac{F^4(1+\Lambda_2)^2}{288\tau}, \\
L_{18}^r(\mu) &= L_{18}^r(\mu_2) - \frac{1}{4}\frac{1}{16\pi^2}\ln\left(\frac{\mu_2}{\mu}\right).
\end{aligned} \tag{5.75}$$

The constant L_{18} does not appear in SU(3) ChPT, but we include its running for completeness, since the running from the scale $\mu_2 = 1$ GeV will be needed later.

The LO quantities $\overset{\circ}{M}{}_\pi^2$, $\overset{\circ}{M}{}_K^2$, F are expressed in terms of the physical quantities M_π^2, M_K^2, F_π, and, again, M_0^2 is determined from the relation to $M_{\eta'}^2$ at this order. The parameters θ_8, θ_0, F_8, F_0 are calculated using Eqs. (5.59) and (5.60). For the LECs L_5 and L_8 we use the values determined at $\mathcal{O}(p^4)$ in SU(3) ChPT, i.e., column "p^4 fit" in Tab. 1 in Ref. [BE 14]. The OZI-rule-violating parameter $\tilde{\Lambda}$ is fixed to M_η^2. The results are given in Tabs. 5.1–5.3 labeled NLO II. The dependence of M_η^2 on $\tilde{\Lambda}$ is shown in Fig. 5.3.

	μ [GeV]	L_5 $[10^{-3}]$	L_8 $[10^{-3}]$	$\tilde{\Lambda}$
NLO I	-	1.86 ± 0.06	0.78 ± 0.05	-0.34 ± 0.05
NLO II	0.77	1.20 ± 0.10	0.55 ± 0.20	0.02 ± 0.13
NLO II	1	0.58 ± 0.10	0.24 ± 0.20	0.41 ± 0.13

Table 5.1: LECs at NLO.

	μ [GeV]	$\overset{\circ}{M}{}^2_\pi$	$\overset{\circ}{M}{}^2_K$	$\frac{M_0^2}{(1+\Lambda_1)}$	$M_\eta^2(\tilde{\Lambda}=0)$
NLO I	-	0.018 ± 0.000	0.261 ± 0.005	0.902 ± 0.013	0.326 ± 0.003
NLO II	0.77	0.018 ± 0.000	0.249 ± 0.023	0.871 ± 0.061	0.299 ± 0.010
NLO II	1	0.018 ± 0.000	0.249 ± 0.023	0.871 ± 0.061	0.269 ± 0.010

Table 5.2: Pseudoscalar masses at NLO in GeV^2.

	μ [GeV]	θ [°]	θ_8 [°]	θ_0 [°]	F_8/F_π	$\frac{F_0}{1+\Lambda_1/2}/F_\pi$
NLO I	-	-11.1 ± 0.6	-21.7 ± 0.7	-0.5 ± 0.7	1.26 ± 0.01	1.13 ± 0.00
NLO II	0.77	-12.6 ± 3.0	-19.5 ± 3.0	-5.7 ± 3.2	1.17 ± 0.01	1.09 ± 0.01
NLO II	1	-12.6 ± 3.0	-15.9 ± 3.0	-9.3 ± 3.2	1.08 ± 0.01	1.04 ± 0.01

Table 5.3: Mixing angles and decay constants at NLO.

	μ [GeV]	L_5 [10^{-3}]	L_8 [10^{-3}]	$\tilde{\Lambda}$
NLO+Lps I	0.77	1.37 ± 0.06	0.85 ± 0.05	0.52 ± 0.05
NLO+Lps I	1	0.75 ± 0.06	0.55 ± 0.05	1.09 ± 0.04
NLO+Lps II	0.77	1.20 ± 0.10	0.55 ± 0.20	1.34 ± 0.13
NLO+Lps II	1	0.58 ± 0.10	0.24 ± 0.20	1.34 ± 0.13

Table 5.4: LECs at NLO with loops added.

5.4.3 NLO+Loops

Before considering the full NNLO corrections, we first discuss the case where we just add the loop contributions to the NLO expressions. Since the loop corrections do not contain any unknown parameters, we can use exactly the same system of equations from the NLO I scenario in the previous section to obtain the desired LECs. We augment the system of linear equations with the one-loop corrections and extract the values of $B\hat{m}$, L_5, L_8, $\tilde{\Lambda}$. The results depend now on the scale of the effective theory and we choose to extract the LECs at $\mu = 1$ GeV. The parameters θ_8, θ_0, F_8, F_0 are obtained from Eqs. (B.23)–(B.26) in Appendix B.1, now also including the one-loop corrections. The results are given in Tabs. 5.4–5.6 labeled NLO+Lps I.

We compare the results with the values obtained in SU(3) ChPT. For L_5 and L_8 we use the same values as in the NLO II case. To compensate the scale dependence of the loop contributions we include the scale-dependent parts of the LECs L_4, L_6, L_7, L_{18} (see Eqs. (5.75)), which would appear only at NNLO. These constants are included without the SU(3)-U(3) matching and we choose $L_4^r = L_6^r = L_7^r = L_{18}^r = 0$ at $\mu_1 = 1$ GeV. Eventually, we again use M_η^2 to extract $\tilde{\Lambda}$. Equations (B.23)–(B.26) in Appendix B.1 provide then our values for θ_8, θ_0, F_8, F_0. The results can be found in Tabs. 5.4–5.6, denoted by NLO+Lps II. Figure 5.3 shows the dependence of M_η^2 on $\tilde{\Lambda}$ for the different scenarios discussed so far. We notice that the dependence is quite strong. After the inclusion of the loops and the scale-dependent parts of the $1/N_c$-suppressed L_i, M_η^2 is independent of the renormalization scale μ (compare solid and dashed red lines).

5.4.4 NNLO

At NNLO, there are too many unknown LECs, which cannot be determined from our chosen set of observables. This means that it is not possible to consistently determine all LECs appearing at NNLO within our framework of LN_cChPT. So we can only employ the second strategy and make use of

	μ [GeV]	$\overset{\circ}{M}{}_{\pi}^{2}$	$\overset{\circ}{M}{}_{K}^{2}$	$\frac{M_0^2}{(1+\Lambda_1)}$	$M_\eta^2(\tilde{\Lambda}=0)$
NLO+Lps I	0.77	0.018 ± 0.000	0.263 ± 0.005	0.927 ± 0.013	0.261 ± 0.003
NLO+Lps I	1	0.017 ± 0.000	0.240 ± 0.005	0.867 ± 0.012	0.218 ± 0.003
NLO+Lps II	0.77	0.019 ± 0.000	0.287 ± 0.023	0.933 ± 0.061	0.199 ± 0.010
NLO+Lps II	1	0.017 ± 0.000	0.265 ± 0.023	0.933 ± 0.061	0.199 ± 0.010

Table 5.5: Pseudoscalar masses at NLO with loops added in GeV^2.

	μ [GeV]	θ [°]	θ_8 [°]	θ_0 [°]	F_8/F_π	$\frac{F_0}{1+\Lambda_1/2}/F_\pi$
NLO+Lps I	0.77	-10.2 ± 0.6	-18.0 ± 0.7	-2.4 ± 0.7	1.31 ± 0.01	0.97 ± 0.00
NLO+Lps I	1	-13.4 ± 0.6	-17.7 ± 0.7	-9.1 ± 0.7	1.31 ± 0.01	0.87 ± 0.00
NLO+Lps II	0.77	-10.2 ± 2.9	-13.5 ± 2.9	-6.8 ± 3.1	1.28 ± 0.01	0.86 ± 0.01
NLO+Lps II	1	-10.2 ± 2.9	-13.5 ± 2.9	-6.8 ± 3.1	1.28 ± 0.01	0.86 ± 0.01

Table 5.6: Mixing angles and decay constants at NLO with loops added.

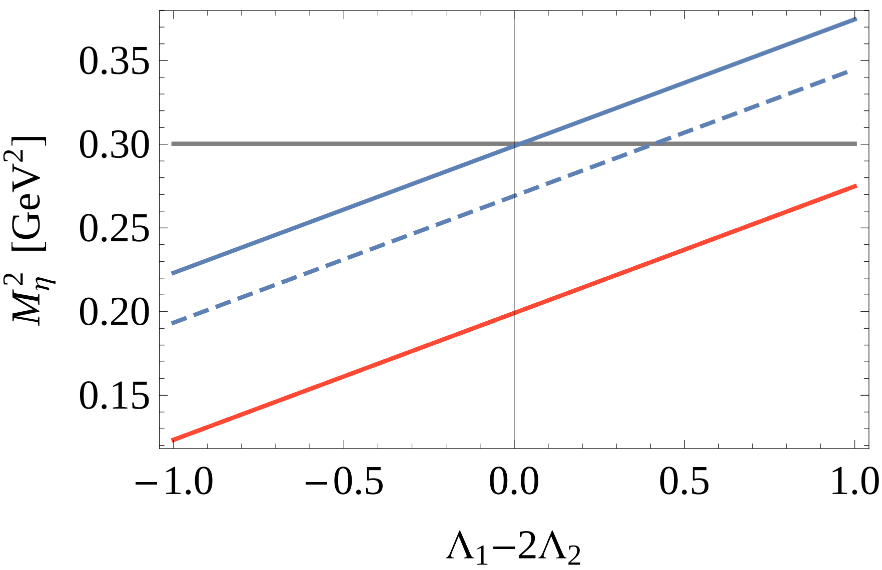

Figure 5.3: M_η^2 as a function of $\tilde{\Lambda} = \Lambda_1 - 2\Lambda_2$. Blue lines: NLO II, at 0.77 GeV (solid) and 1 GeV (dashed). Red lines: NLO+Loop II, at 0.77 GeV (solid) and 1 GeV (dashed). The two red lines coincide. Gray line: Physical value.

phenomenological determinations of the LECs L_i and C_i in SU(3) ChPT. We are then left with five completely unknown LECs, Λ_1, Λ_2, L_{18}, L_{25}, $v_2^{(2)}$, and the combination $L_{46} + L_{53}$, which are related to the singlet field. First, we investigate the case with $C_i = 0$. We match the L_i from SU(3) to U(3), according to Eq. (5.75), and take their values from the column "p^4 fit" in Tab. 1 in Ref. [BE 14]. Since a NNLO calculation in the δ counting includes contributions of the type NLO×NLO, e.g., products of L_i, the results depend on the EFT scale μ. We display results for two different scales, $\mu = 0.77$ GeV and $\mu = 1$ GeV. We choose $\Lambda_1 = \Lambda_2 = L_{18}^r = v_2^{(2)} = L_{46} = L_{53} = 0$ at $\mu_2 = 1$ GeV, which, together with the U(3)-SU(3) matching, results in $L_7^r \approx 0$ (at $\mu = 1$ GeV). We can then fix one OZI-rule-violating LEC, which we choose to be L_{25}, to the physical value of M_η^2. In this way, L_{25} accounts for the contributions to M_η^2 of all other OZI-rule-violating LECs, which are put to zero. At NNLO including C_{12} terms, the simplified expressions for θ_8, θ_0, F_8, F_0 in Eqs. (5.59) and (5.60) do no longer hold. We therefore use the general formulae in Eqs. (5.50) and (5.51) to calculate the parameters of the two-angle scheme in the NNLO scenarios. The results are given in Tabs. 5.7–5.9 labeled NNLO w/o Ci. Figure 5.4 shows M_η^2 as a function of L_{25}.

Finally, we include the contributions of the C_i. The L_i are treated as before in terms of running and matching, but now we use the $\mathcal{O}(p^6)$ values from Ref. [BE 14], i.e., column "BE14" in Tab. 3. For the C_i we employ the values from Tab. 4 in Ref. [BE 14]. We do not consider any matching between U(3) and SU(3) ChPT for the C_i, since we expect the matching to be a correction beyond the accuracy of our calculation. The dependence of M_η^2 on L_{25} is shown in Fig. 5.4, and eventually L_{25} is fixed to the physical value of M_η^2. The results are given in Tabs. 5.7–5.9 labeled NNLO w/ Ci.

Figure 5.4 shows a strong dependence of M_η^2 on L_{25}. The renormalization-scale dependence is now much smaller than in the NLO cases. The small residual scale dependence stems from products of L_5 and L_8, whose scale dependence would be compensated by products of one-loop terms in the full two-loop calculation. The inclusion of the one-loop corrections decreases the value of $M_\eta^2(L_{25} = 0)$ by about 30%. This would rather match the expected order of magnitude of a NLO correction. Taking the C_i into account, further drastically decreases $M_\eta^2(L_{25} = 0)$. The C_i couplings have a rather strong influence on our observables. However, they are not very well constrained in Ref. [BE 14]. Therefore, those values may only be suited for the SU(3) observables studied in Ref. [BE 14]. According to the δ counting, we would expect the value for L_{25} to be of the same order of magnitude as L_5 and L_8, since the operator structure is similar, with an additional $1/N_c$ suppression leading to $|L_{25}| \sim \frac{1}{3} \cdot 10^{-3}$. The fit to the physical M_η^2 demands slightly larger

	μ [GeV]	L_5 [10^{-3}]	L_8 [10^{-3}]	L_{25} [10^{-3}]
NNLO w/o Ci	0.77	1.20 ± 0.10	0.55 ± 0.20	0.55 ± 0.08
NNLO w/o Ci	1	0.58 ± 0.10	0.24 ± 0.20	0.50 ± 0.08
NNLO w/ Ci	0.77	1.01 ± 0.06	0.52 ± 0.10	0.84 ± 0.04
NNLO w/ Ci	1	0.39 ± 0.06	0.21 ± 0.10	0.80 ± 0.04

Table 5.7: LECs at NNLO.

	μ [GeV]	$\overset{\circ}{M}{}^2_\pi$	$\overset{\circ}{M}{}^2_K$	$\frac{M_0^2}{(1+\Lambda_1)}$	$M_\eta^2(L_{25}=0)$
NNLO w/o Ci	0.77	0.018 ± 0.007	0.277 ± 0.101	0.840 ± 0.154	0.186 ± 0.016
NNLO w/o Ci	1	0.016 ± 0.007	0.257 ± 0.102	0.841 ± 0.158	0.197 ± 0.017
NNLO w/ Ci	0.77	0.018 ± 0.001	0.308 ± 0.015	0.740 ± 0.054	0.124 ± 0.007
NNLO w/ Ci	1	0.017 ± 0.001	0.287 ± 0.016	0.736 ± 0.057	0.133 ± 0.008

Table 5.8: Pseudoscalar masses at NNLO in GeV^2.

values for L_{25} than expected. However, since we neglected the other OZI-rule-violating couplings Λ_1, Λ_2, L_{18}, $v_2^{(2)}$ in the NNLO scenarios, there could still exist a combination of values for those LECs which results in both a good description of M_η^2 and "natural" values for the LECs.

5.4.5 Discussion of the results

In the following, we discuss the summaries of our results in Tabs. 5.10–5.12. A summary of the LECs used in the different scenarios is provided in Tabs. C.1–C.3 in Appendix C. We start with the results for the masses summarized in Tab. 5.10. The values for the squared pion mass at LO are very close to the physical squared pion mass with deviations of ca. 10%. The LO squared kaon masses are larger than the physical value, up to about 25%. The sign of the NLO and NNLO corrections is in accordance with the

	μ [GeV]	θ [°]	θ_8 [°]	θ_0 [°]	F_8/F_π	$\frac{F_0}{1+\Lambda_1/2}/F_\pi$
NNLO w/o Ci	0.77	-9.6 ± 6.0	-11.7 ± 5.8	-6.6 ± 6.4	1.27 ± 0.02	0.85 ± 0.01
NNLO w/o Ci	1	-10.1 ± 6.3	-12.6 ± 6.1	-6.3 ± 6.5	1.28 ± 0.02	0.86 ± 0.01
NNLO w/ Ci	0.77	-17.3 ± 3.1	-15.5 ± 2.8	-13.7 ± 3.7	1.21 ± 0.02	0.82 ± 0.01
NNLO w/ Ci	1	-18.0 ± 3.3	-16.6 ± 3.1	-13.7 ± 3.8	1.23 ± 0.01	0.83 ± 0.01

Table 5.9: Mixing angles and decay constants at NNLO.

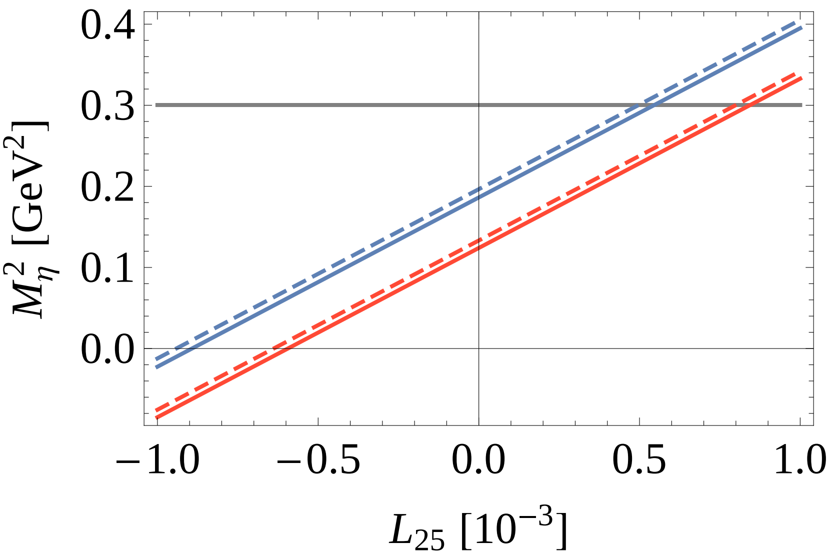

Figure 5.4: M_η^2 as a function of L_{25}. Blue lines: NNLO without C_i, at 0.77 GeV (solid) and 1 GeV (dashed). Red lines: NNLO with C_i, at 0.77 GeV (solid) and 1 GeV (dashed). Gray line: Physical value.

findings in Ref. [BE 14]. The LO squared pion and kaon masses, $2\hat{m}B$ and $(\hat{m} + m_s)B$, respectively, show a renormalization-scale dependence, which is caused by the renormalization of the parameter B in U(3) ChPT. The squared singlet mass in the chiral limit, $M_0^2/(1 + \Lambda_1)$, has its smallest value in the LO calculation and increases by about 30% in the other scenarios. However, a direct comparison to the LO value, M_0^2, remains difficult, since we do not know the value of Λ_1. The column $M_\eta^2(x = 0)$ shows the value of M_η^2 if the OZI-rule-violating parameter $\tilde{\Lambda}$ or L_{25}, which is fixed to the physical M_η^2, is switched off. Especially in the NNLO scenarios those values are only 30% to 50% of the physical M_η^2. Therefore, we conclude that employing the LECs determined in SU(3) ChPT is not sufficient in a LN_cChPT calculation and OZI-rule-violating couplings need to be included to adequately describe M_η^2. The contributions of the OZI-rule-violating parameters $\tilde{\Lambda}$ and L_{25} are very important. One should also keep in mind that we only retained L_{25} and omitted all other OZI-rule-violating LECs in the NNLO cases.

A summary of the results for the mixing angle θ is shown in Fig. 5.5. In comparison to the LO value $\theta = -19.6°$, θ gets shifted to values between $-9°$ and $-18°$. We display the results for the angles θ_8, θ_0 and constants F_8, F_0 in Figs. 5.6 and 5.7, respectively. They are compared to other phenomenological determinations. Reference [Leu 98] determined the mixing parameters at NLO in LN_cChPT using additional input from the two-photon decays of

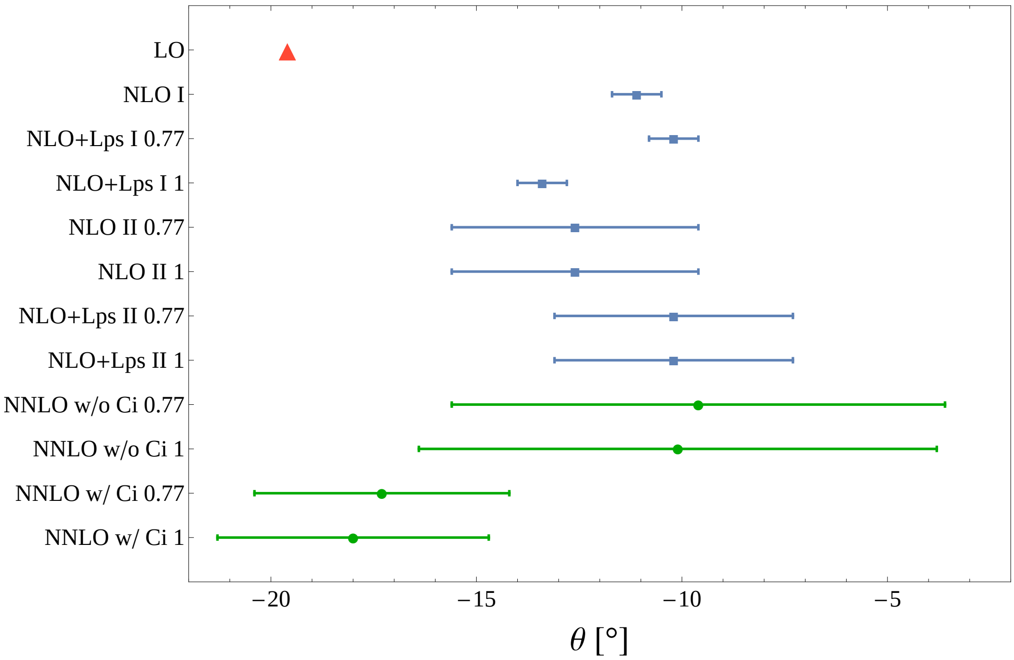

Figure 5.5: Results for the mixing angle θ.

η and η'. References [FKS 98, BDC 00, EF 05, EMS 15] employed the two-angle scheme to extract the mixing parameters phenomenologically from decays involving η and η', mostly the two-photon decays but other processes, e.g., $\eta^{(\prime)}V\gamma$ with vector mesons V, were used as well [BDC 00]. Note, however, these other determinations were performed only in a NLO framework and under certain assumptions, e.g., neglecting OZI-rule-violating couplings [FKS 98]. A study of the η-η' mixing at NNLO in LN_cChPT has been performed in Ref. [Guo+ 15], and the mixing parameters have been obtained from a fit to data from Lattice QCD and input from the two-photon decays. However, also this work is not able to determine all LECs at NNLO and some of them were put to zero. For θ_0, we find values between $-14°$ and $0°$, which agree approximately with the other calculations. For θ_8, our values range from $-22°$ to $-11°$, and their absolute values are slightly smaller than those obtained from phenomenology at NLO. Our values for F_8 agree with most of the other calculations. Note that F_8 depends only on LECs which appear in SU(3) ChPT as well and F_8 is not affected by neglecting unknown OZI-rule-violating LECs. The errors of F_8 and $F_0/(1+\Lambda_1/2)$ due to the errors of the input parameters are very small, and the variation of our values in the different scenarios could serve as a better estimate of our systematic errors. For $F_0/(1+\Lambda_1/2)$ we find smaller values than the other works. The constant

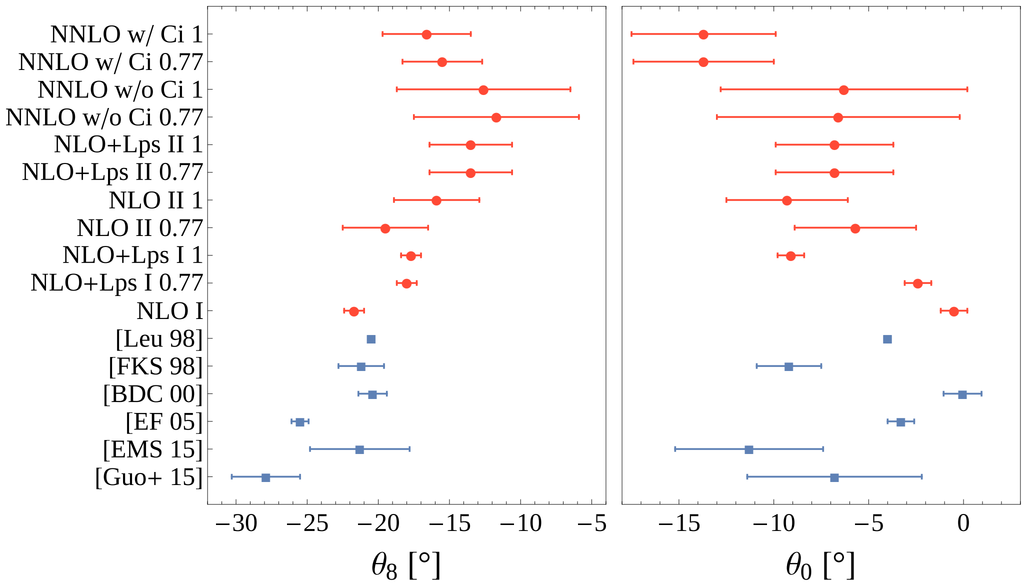

Figure 5.6: Results for θ_8 and θ_0.

F_0 depends on the OZI-rule-violating couplings Λ_1, L_{18}, $L_{46} + L_{53}$. In our NNLO scenarios, however, all of them are set to zero, since they cannot be determined independently from the observables we study. Allowing values for Λ_1 and L_{18} which are different from zero, e.g. $\Lambda_1 \approx 0.3$ and $L_{18} \approx 0.3 \cdot 10^{-3}$, shifts F_0 to higher values in the range of the determinations of the other works. The values for F are mostly smaller than the physical value. This is consistent with the findings in Ref. [BE 14].

The NLO I case is the most consistent scenario, since it is a full calculation up to NLO in LN_cChPT and does not rely on input from other theories with different degrees of freedom or a different power-counting scheme. However, our aim was a calculation of the mixing at the one-loop level up to NNLO in

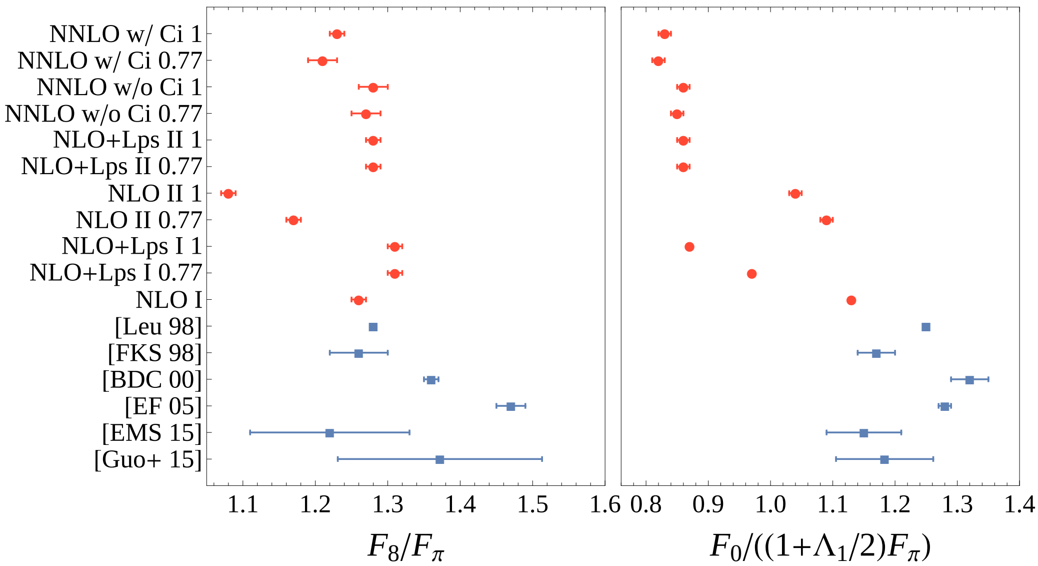

Figure 5.7: Results for F_8 and $F_0/(1+\Lambda_1/2)$.

	μ [GeV]	$\overset{\circ}{M}{}^2_\pi$	$\overset{\circ}{M}{}^2_K$	$\frac{M_0^2}{(1+\Lambda_1)}$	$M_\eta^2(x=0)$
LO	-	0.018 ± 0	0.244 ± 0	0.673 ± 0	0.244 ± 0
NLO I	-	0.018 ± 0.000	0.261 ± 0.005	0.902 ± 0.013	0.326 ± 0.003
NLO+Lps I	0.77	0.018 ± 0.000	0.263 ± 0.005	0.927 ± 0.013	0.261 ± 0.003
NLO+Lps I	1	0.017 ± 0.000	0.240 ± 0.005	0.867 ± 0.012	0.218 ± 0.003
NLO II	0.77	0.018 ± 0.000	0.249 ± 0.023	0.871 ± 0.061	0.299 ± 0.010
NLO II	1	0.018 ± 0.000	0.249 ± 0.023	0.871 ± 0.061	0.269 ± 0.010
NLO+Lps II	0.77	0.019 ± 0.000	0.287 ± 0.023	0.933 ± 0.061	0.199 ± 0.010
NLO+Lps II	1	0.017 ± 0.000	0.265 ± 0.023	0.933 ± 0.061	0.199 ± 0.010
NNLO w/o Ci	0.77	0.018 ± 0.007	0.277 ± 0.101	0.840 ± 0.154	0.186 ± 0.016
NNLO w/o Ci	1	0.016 ± 0.007	0.257 ± 0.102	0.841 ± 0.158	0.197 ± 0.017
NNLO w/ Ci	0.77	0.018 ± 0.001	0.308 ± 0.015	0.740 ± 0.054	0.124 ± 0.007
NNLO w/ Ci	1	0.017 ± 0.001	0.287 ± 0.016	0.736 ± 0.057	0.133 ± 0.008

Table 5.10: Summary of the results for the pseudoscalar masses in GeV^2. The parameter x denotes $\tilde{\Lambda}$ or L_{25}.

the δ counting. Among these scenarios, the most complete one is NNLO w/ Ci. Note that even in this case we could not fix all parameters and set five OZI-rule-violating LECs equal to zero.

	μ [GeV]	θ [°]	θ_8 [°]	θ_0 [°]
LO	-	-19.6 ± 0	-19.6 ± 0	-19.6 ± 0
NLO I	-	-11.1 ± 0.6	-21.7 ± 0.7	-0.5 ± 0.7
NLO+Lps I	0.77	-10.2 ± 0.6	-18.0 ± 0.7	-2.4 ± 0.7
NLO+Lps I	1	-13.4 ± 0.6	-17.7 ± 0.7	-9.1 ± 0.7
NLO II	0.77	-12.6 ± 3.0	-19.5 ± 3.0	-5.7 ± 3.2
NLO II	1	-12.6 ± 3.0	-15.9 ± 3.0	-9.3 ± 3.2
NLO+Lps II	0.77	-10.2 ± 2.9	-13.5 ± 2.9	-6.8 ± 3.1
NLO+Lps II	1	-10.2 ± 2.9	-13.5 ± 2.9	-6.8 ± 3.1
NNLO w/o Ci	0.77	-9.6 ± 6.0	-11.7 ± 5.8	-6.6 ± 6.4
NNLO w/o Ci	1	-10.1 ± 6.3	-12.6 ± 6.1	-6.3 ± 6.5
NNLO w/ Ci	0.77	-17.3 ± 3.1	-15.5 ± 2.8	-13.7 ± 3.7
NNLO w/ Ci	1	-18.0 ± 3.3	-16.6 ± 3.1	-13.7 ± 3.8

Table 5.11: Summary of the results for the mixing angles.

	μ [GeV]	F_8/F_π	$\frac{F_0}{1+\Lambda_1/2}/F_\pi$	F [MeV]
LO	-	1 ± 0	1 ± 0	92.2 ± 0.1
NLO I	-	1.26 ± 0.01	1.13 ± 0.00	90.73 ± 0.11
NLO+Lps I	0.77	1.31 ± 0.01	0.97 ± 0.00	79.31 ± 0.12
NLO+Lps I	1	1.31 ± 0.01	0.87 ± 0.00	74.77 ± 0.12
NLO II	0.77	1.17 ± 0.01	1.09 ± 0.01	91.25 ± 0.13
NLO II	1	1.08 ± 0.01	1.04 ± 0.01	91.74 ± 0.13
NLO+Lps II	0.77	1.28 ± 0.01	0.86 ± 0.01	74.91 ± 0.14
NLO+Lps II	1	1.28 ± 0.01	0.86 ± 0.01	74.91 ± 0.14
NNLO w/o Ci	0.77	1.27 ± 0.02	0.85 ± 0.01	79.46 ± 6.59
NNLO w/o Ci	1	1.28 ± 0.02	0.86 ± 0.01	79.45 ± 6.59
NNLO w/ Ci	0.77	1.21 ± 0.02	0.82 ± 0.01	73.02 ± 0.13
NNLO w/ Ci	1	1.23 ± 0.01	0.83 ± 0.01	73.02 ± 0.13

Table 5.12: Summary of the results for the decay constants.

Chapter 6

Anomalous Ward identities

At leading order in chiral effective field theory, anomalous processes such as $\eta^{(\prime)} \to \gamma^{(*)}\gamma^{(*)}$, $\eta^{(\prime)} \to \pi^+\pi^-\gamma^{(*)}$ are driven by the Wess-Zumino-Witten effective action [WZ 71, Wit 83], which accounts for the anomaly. Higher-order corrections are supposed to be chirally invariant again. In the following, we want to investigate this statement by means of an explicit verification of the anomalous Ward identities at the one-loop level. This calculation serves as a benchmark for studies of anomalous decays beyond the leading order and the investigation of the influence of vector-meson degrees of freedom on higher-order corrections.

6.1 Calculation in SU(3) ChPT

We first consider the anomalous Ward identities within ordinary ChPT and then extend the calculation to LN_cChPT. For that purpose, we calculate the three-point Green function involving one axial-vector current and two vector currents (AVV),

$$T^{\rho\mu\nu}_{cab}(p,q) = \int d^4x\, d^4y\, e^{ip\cdot x + iq\cdot y} \langle 0|T[A^\rho_c(0) V^\mu_a(x) V^\nu_b(y)]|0\rangle, \tag{6.1}$$

at $\mathcal{O}(q^6)$ in $\mathrm{SU}(3)_L \times \mathrm{SU}(3)_R$ ChPT with all three legs off shell. At $\mathcal{O}(p^6)$, we have to evaluate the Feynman diagrams shown in Fig. 6.1. The vertices are derived from the SU(3) versions of the Lagrangians given in Chapter 4. The Feynman diagrams are evaluated with the help of the *Mathematica* package FEYNCALC [MBD 91]. Since the expressions we obtain for the Green functions are very large, we do not display them here explicitly. However, upon request, they are available as *Mathematica* notebooks.

To confirm the Ward identities explicitly, we consider the diagonal components, $c = 3,\ 8$, for the axial-vector current A^ρ_c and for the vector currents the

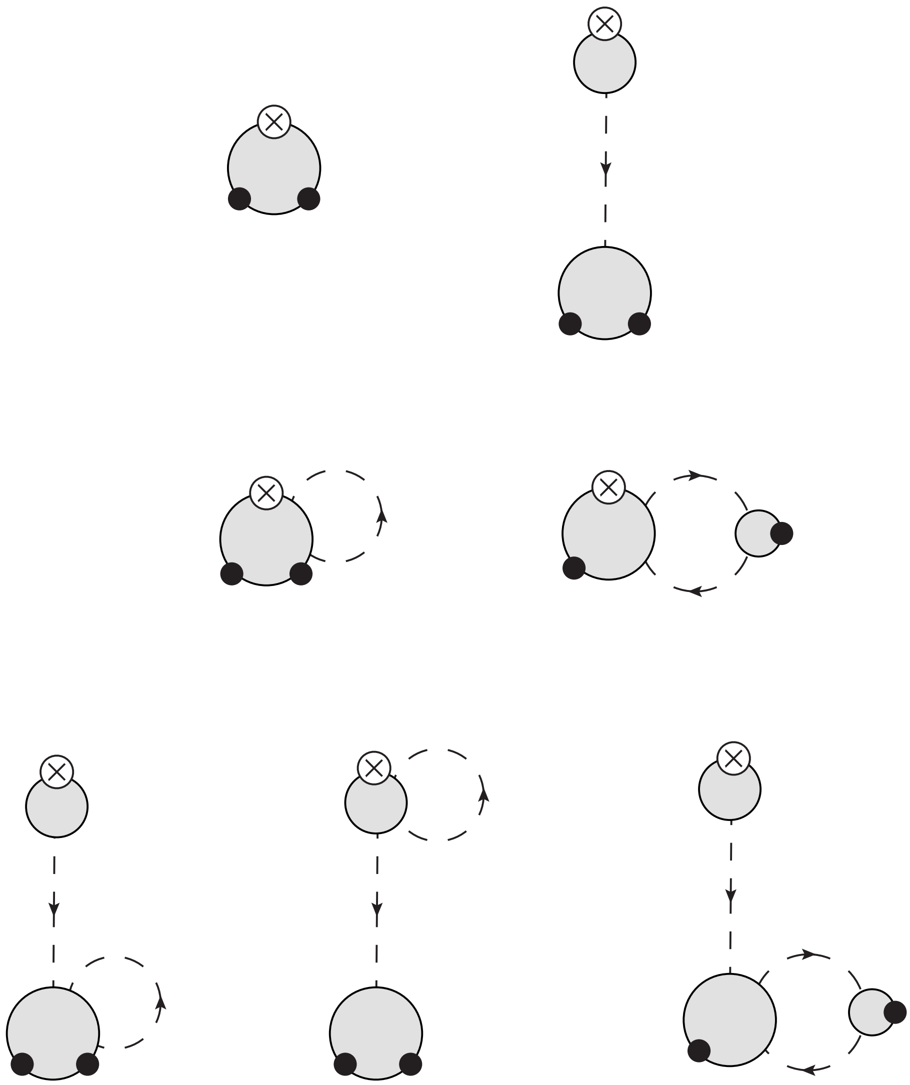

Figure 6.1: Topologies of the Feynman diagrams contributing to the AVV Green function. Solid dots refer to vector currents, crossed dots to the axial-vector current, and dashed lines to pseudoscalar mesons.

electromagnetic current operator $J^\mu = \bar{q}Q\gamma^\mu q$, where $Q = \mathrm{diag}(2/3, -1/3, -1/3)$ is the quark-charge matrix. These (diagonal) vector currents are conserved and the Green function

$$T^{\rho\mu\nu}_{c,\mathrm{em}}(p,q) = \int d^4x\, d^4y\, e^{ip\cdot x+iq\cdot y}\langle 0|T[A^{\rho,c}(0)J^\mu(x)J^\nu(y)]|0\rangle$$

satisfies the normal Ward identities:

$$p_\mu T^{\rho\mu\nu}_{c,\mathrm{em}}(p,q) = 0 \quad \text{and} \quad q_\nu T^{\rho\mu\nu}_{c,\mathrm{em}}(p,q) = 0. \tag{6.2}$$

The axial-vector current has an anomaly. The corresponding anomalous Ward identity for the AVV Green function can be derived from Eq. (4.40) in Sec. 4.4 and reads

$$\begin{aligned} i(p+q)_\rho T^{\rho\mu\nu}_{c,\mathrm{em}}(p,q) = {}& \frac{1}{3}(2\hat{m}+m_s)\Pi^{\mu\nu}_{c,\mathrm{em}}(p,q) + \frac{1}{\sqrt{3}}(\hat{m}-m_s)d_{cc8}\Pi^{\mu\nu}_{c,\mathrm{em}}(p,q) \\ & + \frac{\sqrt{2}}{3}(\hat{m}-m_s)\delta_{c8}\Pi^{\mu\nu}_{0,\mathrm{em}}(p,q) \\ & - \frac{N_c}{8\pi^2}\epsilon^{\mu\nu\alpha\beta}p_\alpha q_\beta\langle\lambda_c\{Q,Q\}\rangle, \end{aligned} \tag{6.3}$$

where

$$\Pi^{\mu\nu}_{c,\mathrm{em}}(p,q) = \int d^4x\, d^4y\, e^{ip\cdot x+iq\cdot y}\langle 0|T[P_c(0)J^\mu(x)J^\nu(y)]|0\rangle.$$

This Ward identity contains the three-point function involving two vector currents and one pseudoscalar source P, which we calculate in the same manner as the AVV Green function. We have explicitly verified that the Ward identities, Eqs. (6.2) and (6.3), are satisfied at the one-loop level for $c = 3,\ 8$.

6.2 Calculation in LN_cChPT

We then extend the calculation to LN_cChPT, including the η' and the singlet axial-vector current. Again, the aim is to investigate the anomalous Ward identities at the one-loop level. To that end, we calculate the AVV vertex at the one-loop level, which is NNLO in LN_cChPT. In order to determine the AVV Green function at NNLO, one has to evaluate the Feynman diagrams shown in Fig. 6.1. The vertices are derived from the Lagrangians in Chapter 4. In the Feynman diagrams, the pseudoscalar propagators are dressed propagators. To evaluate them, we employ the η-η' mixing at NNLO as introduced in Chapter 5. According to Ref. [BW 01] (see Sec. 4.4.1), for arbitrary N_c, the quark-charge matrix reads

$$Q(N_c) = \frac{1}{2}\mathrm{diag}\left(\frac{1}{N_c}+1, \frac{1}{N_c}-1, \frac{1}{N_c}-1\right). \tag{6.4}$$

We investigate the Ward identities not only for $Q(3)$, but also for the general case $Q(N_c)$ taking into account the N_c dependence of Q in the δ expansion.

We have again tested the normal and anomalous Ward identities for the diagonal components of the currents, given in Eqs. (6.2) and (6.3), and showed that they are satisfied at NNLO. We explicitly calculated the anomalous Ward identity for the singlet axial-vector current, which on top has the $\mathrm{U}(1)_A$ anomaly. The relevant Ward identity can again be derived from Eq. (4.40) in Sec. 4.4 and is given by

$$\begin{aligned} i(p+q)_\rho T^{\rho\mu\nu}_{0,\text{em}}(p,q) = {}& \sqrt{\frac{2}{3}}(2\hat{m}+m_s)\Pi^{\mu\nu}_{0,\text{em}}(p,q) + \frac{2}{\sqrt{3}}(\hat{m}-m_s)\Pi^{\mu\nu}_{8,\text{em}}(p,q) \\ & + \sqrt{6}\,\Omega^{\mu\nu}_{\text{em}}(p,q) - \frac{N_c}{8\pi^2}\epsilon^{\mu\nu\alpha\beta}p_\alpha q_\beta \langle\lambda_0\{Q,Q\}\rangle, \end{aligned} \tag{6.5}$$

where

$$\Omega^{\mu\nu}_{\text{em}}(p,q) = \int d^4x\, d^4y\, e^{ip\cdot x+iq\cdot y}\langle 0|T[\omega(0)J^\mu(x)J^\nu(y)]|0\rangle.$$

The Green functions involving a pseudoscalar source or the winding number density ω are calculated in the same manner as the AVV vertex.

Using the Lehmann-Symanzik-Zimmermann reduction formalism [LSZ 55], the AVV vertex can be related to the two-photon decays $\pi^0 \to \gamma^{(*)}\gamma^{(*)}$ and $\eta^{(\prime)} \to \gamma^{(*)}\gamma^{(*)}$. The divergence of the axial-vector current serves as an interpolating pseudoscalar-meson field, since it satisfies the relation

$$\langle 0|\,\partial^\mu A^c_\mu(x)\,|P(q)\rangle = M_P^2 F_P^c e^{-iq\cdot x}, \tag{6.6}$$

where M_P denotes the mass of the pseudoscalar and F_P^c the decay constant defined in Eq. (5.48) in Sec. 5.2. The matrix element $\mathcal{M}$ for the decay $P \to \gamma^{(*)}\gamma^{(*)}$ is then given by

$$\mathcal{M} = \frac{1}{M_P^2 F_P^c}\lim_{r^2\to M_P^2}\left(r^2 - M_P^2\right)(-ir_\rho)T^{\rho\mu\nu}_{c,\text{em}}(p,q), \tag{6.7}$$

where $r^\rho = -(p+q)^\rho$. We have checked our results with previous calculations of the two-photon decays [DW 89, BBC 88, BN 04a, Hac 08].

Chapter 7

Two-photon decays

Anomalous decays of the η-η' system are ideally suited to obtain important information on the symmetries of the strong interaction and its symmetry breaking mechanism. The decays are driven by an interplay of the dynamical (spontaneous) breaking of the chiral symmetry, the non-abelian anomaly, explicit symmetry breaking due to the quark masses, and the $\mathrm{U}(1)_A$ anomaly. Having successfully included the η' meson in the framework of LN_cChPT and obtained an expression for the η-η' mixing, we are now able to investigate the two-photon decays of the η-η' system and the decays $\eta^{(\prime)} \to \pi^+\pi^-\gamma^{(*)}$ at the one-loop level.

The decays $\eta^{(\prime)} \to \gamma^{(*)}\gamma^{(*)}$ can be studied for real as well as virtual photons. They are described by so-called transition form factors (TFF) $F_{P\gamma^*\gamma^*}(q_1^2, q_2^2)$, where $P = \eta,\ \eta'$, which depend on the photon virtualities q_1^2, q_2^2 and provide access to the substructure of the mesons. The single-virtual TFFs $F_{P\gamma^*\gamma}(q^2, 0)$ are experimentally accessible both in the space-like and in the time-like region. In the time-like region, they are measured in so-called single Dalitz decays $P \to \gamma l^+ l^-$, where $l = e,\ \mu$, in the low-energy range $4m_l^2 \leq q^2 \leq (M_P - 2m_l)^2$. The η TFF has been measured in the decay $\eta \to e^+e^-\gamma$ by the A2 collaboration at MAMI [Ber+ 11, Agu+ 14] and in the decay $\eta \to \mu^+\mu^-\gamma$ by the NA60 collaboration [Arn+ 09, Arn+ 16]. In the low-energy region, the time-like η' TFF has been obtained from measurements of $\eta' \to e^+e^-\gamma$ by the BESIII collaboration [Abl+ 15]. In the space-like region, the TFFs are accessed by e^+e^- colliders in two-photon-fusion reactions $e^+e^- \to e^+e^-P$ using the single-tag method. One outgoing lepton is tagged, having emitted a highly-virtual photon with $q_1^2 = -Q^2$, while the other untagged lepton is scattered at small angle with momentum transfer $q_2^2 \simeq 0$. Whereas for the space-like η TFF no data at low energies are available, the space-like η' TFF has been measured by the L3 collaboration at LEP1 [Acc+ 98].

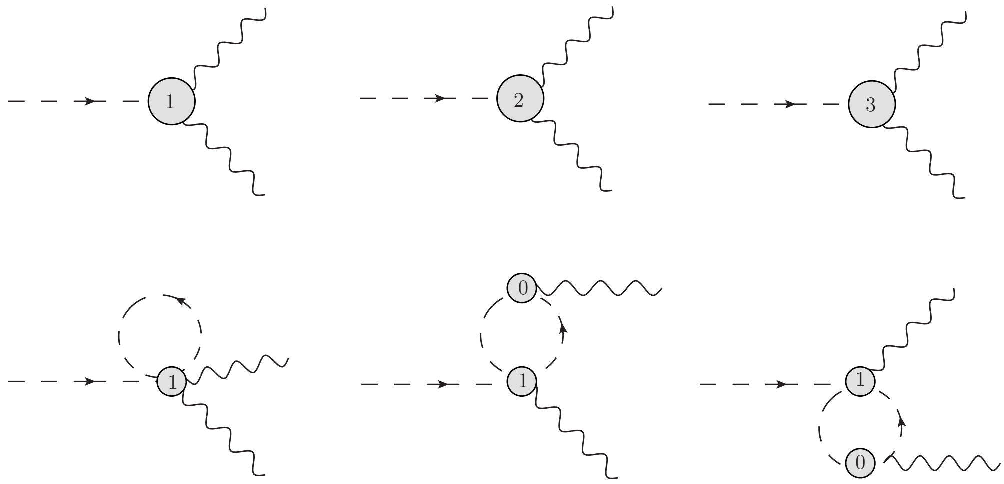

Figure 7.1: Feynman diagrams for $P \to \gamma^* \gamma^*$ up to NNLO. Dashed lines refer to pseudoscalar mesons and wiggly lines to photons. The numbers k in the interaction blobs refer to vertices derived from the corresponding Lagrangians $\mathcal{L}^{(k)}$.

The double-virtual form factors in the time-like region can be probed in double Dalitz decays $P \to l^+ l^- l^+ l^-$ [Amb+ 11], whereas their measurement in the space-like region remains still an experimental challenge.

7.1 Calculation of the invariant amplitude

The invariant amplitude can be parametrized by

$$\mathcal{M} = -iF_{P\gamma^*\gamma^*}(q_1^2, q_2^2)\epsilon_{\mu\nu\alpha\beta}\epsilon_1^\mu \epsilon_2^\nu q_1^\alpha q_2^\beta, \tag{7.1}$$

where q_1^μ, q_2^μ denote the photon momenta and ϵ_1^μ, ϵ_2^μ the polarization vectors of the photons. In order to determine the invariant amplitude up to NNLO, we need to calculate the Feynman diagrams shown in Fig. 7.1. The vertices are derived from the Lagrangians given in Chapter 4. The electromagnetic field couples to the electromagnetic current operator

$$J^\mu = \bar{q} Q \gamma^\mu q, \tag{7.2}$$

where Q is the quark-charge matrix. For $N_c = 3$, the quark-charge matrix is given by

$$Q(3) = \mathrm{diag}\left(\frac{2}{3}, -\frac{1}{3}, -\frac{1}{3}\right). \tag{7.3}$$

For arbitrary N_c, however, Q needs to be modified [BW 01] (see Sec. 4.4.1) and reads

$$Q(N_c) = \frac{1}{2}\mathrm{diag}\left(\frac{1}{N_c}+1, \frac{1}{N_c}-1, \frac{1}{N_c}-1\right). \tag{7.4}$$

The matrix element is calculated using both versions, $Q(3)$ and $Q(N_c)$. In the $Q(N_c)$ case, we first perform the δ expansion up to NNLO and then set $N_c = 3$. The Feynman diagrams are evaluated using the *Mathematica* package FEYNCALC [MBD 91]. Without the N_c expansion of Q, the results for the form factors of π^0, η, η' at LO and NLO read

$$F(\pi^0 \to \gamma^*\gamma^*)_{\mathrm{LO}} = \frac{1}{4\pi^2 F_\pi}, \tag{7.5}$$

$$F(\pi^0 \to \gamma^*\gamma^*)_{\mathrm{NLO}} = \frac{1}{4\pi^2 F_\pi}\left(1 - \frac{1024}{3}\pi^2 M_\pi^2 L_8^{6,\epsilon} - \frac{512}{3}\pi^2 L_{19}^{6,\epsilon}\left(q_1^2+q_2^2\right)\right), \tag{7.6}$$

$$F(\eta \to \gamma^*\gamma^*)_{\mathrm{LO}} = \frac{1}{4\sqrt{3}\pi^2 F_\pi}\left(\cos(\theta^{[0]}) - 2\sqrt{2}\sin(\theta^{[0]})\right), \tag{7.7}$$

$$\begin{aligned}
&F(\eta \to \gamma^*\gamma^*)_{\mathrm{NLO}} \\
&= \frac{1}{4\sqrt{3}\pi^2 F_\pi}\Bigg(\cos(\theta^{[1]}) - 2\sqrt{2}\sin(\theta^{[1]}) \\
&\quad + \frac{8\left(M_K^2 - M_\pi^2\right)\left(\sqrt{2}\sin(\theta^{[1]}) + 2\cos(\theta^{[1]})\right)}{3F_\pi^2} L_5 \\
&\quad + \frac{1024}{9}\pi^2\left(2\sqrt{2}\left(M_K^2 + 2M_\pi^2\right)\sin(\theta^{[1]}) + \left(4M_K^2 - 7M_\pi^2\right)\cos(\theta^{[1]})\right) L_8^{6,\epsilon} \\
&\quad + \sqrt{2}\sin(\theta^{[1]})\lambda_1 \\
&\quad - \frac{512}{3}\pi^2\left(\cos(\theta^{[1]}) - 2\sqrt{2}\sin(\theta^{[1]})\right) L_{19}^{6,\epsilon}\left(q_1^2+q_2^2\right)\Bigg),
\end{aligned} \tag{7.8}$$

$$F(\eta' \to \gamma^*\gamma^*)_{\mathrm{LO}} = \frac{1}{4\sqrt{3}\pi^2 F_\pi}\left(\sin(\theta^{[0]}) + 2\sqrt{2}\cos(\theta^{[0]})\right), \tag{7.9}$$

$$\begin{aligned}
&F(\eta' \to \gamma^*\gamma^*)_{\mathrm{NLO}} \\
&= \frac{1}{4\sqrt{3}\pi^2 F_\pi}\Bigg(\sin(\theta^{[1]}) + 2\sqrt{2}\cos(\theta^{[1]}) \\
&\quad + \frac{8\left(M_\pi^2 - M_K^2\right)\left(\sqrt{2}\cos(\theta^{[1]}) - 2\sin(\theta^{[1]})\right)}{3F_\pi^2} L_5 \\
&\quad - \frac{1024}{9}\pi^2\left(\left(7M_\pi^2 - 4M_K^2\right)\sin(\theta^{[1]}) + 2\sqrt{2}\left(M_K^2 + 2M_\pi^2\right)\cos(\theta^{[1]})\right) L_8^{6,\epsilon} \\
&\quad - \sqrt{2}\cos(\theta^{[1]})\lambda_1 \\
&\quad - \frac{512}{3}\pi^2\left(\sin(\theta^{[1]}) + 2\sqrt{2}\cos(\theta^{[1]})\right) L_{19}^{6,\epsilon}\left(q_1^2+q_2^2\right)\Bigg),
\end{aligned} \tag{7.10}$$

where $\theta^{[i]}$ is the corresponding mixing angle at LO (NLO) given in Eq. (5.33) in Sec. 5.1. The parameter λ_1 is a QCD-scale-invariant combination of OZI-rule-violating parameters, given by [KL 00]

$$\lambda_1 = \Lambda_1 - 2K_1 = \Lambda_1 + 16\pi^2(\tilde{L}_2 + 2\tilde{L}_3). \tag{7.11}$$

Including the N_c expansion of Q, the results at LO and NLO now take the form

$$F(\pi^0 \to \gamma^*\gamma^*)_{\text{LO}} = 0, \tag{7.12}$$

$$F(\pi^0 \to \gamma^*\gamma^*)_{\text{NLO}} = \frac{1}{4\pi^2 F_\pi}, \tag{7.13}$$

$$F(\eta \to \gamma^*\gamma^*)_{\text{LO}} = -\frac{3\sqrt{\frac{3}{2}}}{8\pi^2 F_\pi}\sin(\theta^{[0]}), \tag{7.14}$$

$$\begin{aligned}
&F(\eta \to \gamma^*\gamma^*)_{\text{NLO}} \\
&= \frac{3\sqrt{\frac{3}{2}}}{8\pi^2 F_\pi}\Big(-\sin(\theta^{[1]}) \\
&\quad + \frac{8\left(M_K^2 - M_\pi^2\right)\left(\sin(\theta^{[1]}) + \sqrt{2}\cos(\theta^{[1]})\right)}{3F_\pi^2}L_5 \\
&\quad + \frac{1024}{9}\pi^2\left(\left(2M_K^2 + M_\pi^2\right)\sin(\theta^{[1]}) + 2\sqrt{2}\left(M_K^2 - M_\pi^2\right)\cos(\theta^{[1]})\right)L_8^{6,\epsilon} \\
&\quad + \frac{\sin(\theta^{[1]})}{2}\lambda_1 + 384\sqrt{2}\pi^2\sin(\theta^{[1]})L_{19}^{6,\epsilon}\left(q_1^2 + q_2^2\right)\Big),
\end{aligned} \tag{7.15}$$

$$F(\eta' \to \gamma^*\gamma^*)_{\text{LO}} = \frac{3\sqrt{\frac{3}{2}}}{8\pi^2 F_\pi}\cos(\theta^{[0]}), \tag{7.16}$$

$$\begin{aligned}
&F(\eta' \to \gamma^*\gamma^*)_{\text{NLO}} \\
&= \frac{3\sqrt{\frac{3}{2}}}{8\pi^2 F_\pi}\Big(\cos(\theta^{[1]}) \\
&\quad + \frac{8\left(M_K^2 - M_\pi^2\right)\left(\sqrt{2}\sin(\theta^{[1]}) - \cos(\theta^{[1]})\right)}{3F_\pi^2}L_5 \\
&\quad + \frac{1024}{9}\pi^2\left(2\sqrt{2}\left(M_K^2 - M_\pi^2\right)\sin(\theta^{[1]}) - \left(2M_K^2 + M_\pi^2\right)\cos(\theta^{[1]})\right)L_8^{6,\epsilon} \\
&\quad - \frac{\cos(\theta^{[1]})}{2}\lambda_1 - 384\sqrt{2}\pi^2\cos(\theta^{[1]})L_{19}^{6,\epsilon}\left(q_1^2 + q_2^2\right)\Big).
\end{aligned} \tag{7.17}$$

At NNLO, the expressions for the form factors are quite long. Therefore, we do not display all terms explicitly. The loop contributions corresponding to the loop diagrams shown in Fig. 7.1 are provided in Appendix B.2. As an example, we show the full NNLO tree-level contributions to $F(\eta \to \gamma^*\gamma^*)$ in Eq. (B.33) in Appendix B.2. The expressions for the other form factors are available as *Mathematica* notebooks.

7.1.1 Observables

The decay amplitude for real photons is recovered by setting $q_1^2 = q_2^2 = 0$ in Eq. (7.1). The decay width is then given by [Hac 08]

$$\Gamma = \frac{1}{2!2M_P(2\pi)^2}\frac{\pi\sqrt{\lambda[M_P^2,0,0]}}{2M_P^2}\int d\Omega \sum |\mathcal{M}|^2. \tag{7.18}$$

Using $\sum_\lambda \epsilon^*_{(\lambda)\mu}\epsilon_{(\lambda)\mu'} = -g_{\mu\mu'}$, one obtains

$$\Gamma(P \to \gamma\gamma) = \frac{M_P^3}{64\pi}|F_{P\gamma\gamma}|^2. \tag{7.19}$$

The single-virtual TFF $F_{P\gamma^*\gamma}(q^2) := F_{P\gamma^*\gamma^*}(q^2,0)$ can be measured in single Dalitz decays $P \to \gamma l^+ l^-$. The *slope* of the TFF is defined as

$$\mathit{slope} := \frac{1}{F_{P\gamma\gamma}}\frac{d}{dq^2}\, F_{P\gamma^*\gamma}(q^2)\Big|_{q^2=0}. \tag{7.20}$$

One can also define the dimensionless quantity $b_P = M_P^2 \times \mathit{slope}$. The curvature is given by

$$\mathit{curv} := \frac{1}{2}\frac{1}{F_{P\gamma\gamma}}\frac{d^2}{d(q^2)^2}\, F_{P\gamma^*\gamma}(q^2)\Big|_{q^2=0}, \tag{7.21}$$

and the corresponding dimensionless quantity reads $c_P = M_P^4 \times \mathit{curv}$.

Experimental extractions of the slope parameter are often performed using a vector-meson-dominance model (VMD) [Sak 69] to fit the data. In this case, the TFF is given by a normalized single-pole term with an associated mass Λ_P [EMS 14]:

$$F_{P\gamma^*\gamma}(Q^2) = \frac{F_{P\gamma\gamma}(0)}{1 + Q^2/\Lambda_P^2}, \tag{7.22}$$

where $Q^2 = -q^2$. Expanding this expression in Q^2 leads to

$$F_{P\gamma^*\gamma}(Q^2) = F_{P\gamma\gamma}(0)\left(1 - \frac{Q^2}{\Lambda_P^2} + \frac{Q^4}{\Lambda_P^4} + \dots\right). \tag{7.23}$$

Now, we can read off the slope and curvature VMD predictions, which are given by

$$slope = \frac{1}{\Lambda_P^2}, \tag{7.24}$$

$$curv = \frac{1}{\Lambda_P^4}. \tag{7.25}$$

7.2 Numerical analysis

We perform the numerical analysis of our results successively at LO, NLO, and NNLO. In the following, we distinguish between two cases, using the normal quark-charge matrix for $N_c = 3$ and taking the N_c expansion of Q into account, denoted by Qexp. Performing the N_c expansion of Q shifts some of the LECs to higher orders. The LECs $L_8^{6,\epsilon}$ and $L_{19}^{6,\epsilon}$, stemming from the NLO Lagrangian in Tab. 4.2 in Sec. 4.4, appear only at NNLO in the expression for the two-photon decay of the π^0. At LO, no unknown LECs show up and we can calculate the desired quantities directly.

7.2.1 NLO

At NLO, we have to determine five LECs. From the even-intrinsic-parity sector L_5 and the NLO mixing angle $\theta^{[1]}$ contribute. Here, we employ the values for L_5 and $\theta^{[1]}$ determined in the NLO analysis of the η-η' mixing in Tabs. 5.1 and 5.3 in Sec. 5.4.2 labeled NLO I. From the odd-intrinsic-parity sector we have to fix $L_8^{6,\epsilon}$, $L_{19}^{6,\epsilon}$, and $\lambda_1 = \Lambda_1 - 2K_1$.

First, we consider the $Q(3)$ case. Since the decay width of the π^0 to two photons depends only on $L_8^{6,\epsilon}$, we start by fixing $L_8^{6,\epsilon}$ to the experimental value of $\Gamma_{\pi^0\to\gamma\gamma}$. We then fit λ_1 simultaneously to the experimental results for $\Gamma_{\eta\to\gamma\gamma}$ and $\Gamma_{\eta'\to\gamma\gamma}$. The experimental values for the decay widths are taken from Ref. [Oli+ 14] and are displayed in Tab. 7.2. Finally, the parameter $L_{19}^{6,\epsilon}$ is determined through a simultaneous fit to the experimental values of the π^0, η, and η' slopes, given in Tab. 7.3. For the fits we employ the *Mathematica* routine NonlinearModelFit. The errors of the fit parameters and of the results are the ones obtained from the fit routine. The different steps are performed successively and we do not take the errors of LECs determined in a previous step into account. We also do not consider the errors due to neglecting higher-order terms. Therefore, as explained in Sec. 4.5, a systematic error of at least 10% should be added to all quantities determined up to NLO. The results for the LECs are given in Tab. 7.1 and the results for the decay widths and slopes in Tabs. 7.2 and 7.3, respectively, labeled NLO 1.

	$L_8^{6,\epsilon}$ $[10^{-3}]$	$L_{19}^{6,\epsilon}$ $[10^{-3}]$	λ_1
NLO 1	0.16 ± 0.17	-1.31 ± 0.14	0.08 ± 0.18
NLO 2	0.86 ± 0.15	-1.31 ± 0.35	2.59 ± 0.18
NLO 3	0.80 ± 0.34	-1.09 ± 0.33	2.77 ± 0.38
NLO Qexp	0.23 ± 0.45	-1.63 ± 1.87	2.16 ± 1.13

Table 7.1: Results for the LECs determined at NLO.

Next, we examine the case where we fit $L_8^{6,\epsilon}$ and λ_1 simultaneously to all three decay widths $\Gamma_{\pi^0\to\gamma\gamma}$, $\Gamma_{\eta\to\gamma\gamma}$, and $\Gamma_{\eta'\to\gamma\gamma}$. The constant $L_{19}^{6,\epsilon}$ is then again fixed to the slopes of π^0, η, and η'. The results are shown in Tabs. 7.1–7.3, labeled NLO 2. To consistently take the errors of $L_8^{6,\epsilon}$, $L_{19}^{6,\epsilon}$, and λ_1 into account, we consider another scenario where we determine these three LECs through a simultaneous fit to the decay widths of π^0, η, η' and the slope parameters of π^0, η, η'. The results are given in Tabs. 7.1–7.3, labeled NLO 3.

In the $Q(N_c)$ case, the π^0 form factor at NLO is independent of $L_8^{6,\epsilon}$ and $L_{19}^{6,\epsilon}$, which are shifted to the NNLO expression. The width $\Gamma_{\pi^0\to\gamma\gamma}$ takes the LO value of the $Q(3)$ case, and the slope is equal to zero at NLO. Therefore, we determine $L_8^{6,\epsilon}$, $L_{19}^{6,\epsilon}$, and λ_1 via a simultaneous fit to $\Gamma_{\eta\to\gamma\gamma}$, $\Gamma_{\eta'\to\gamma\gamma}$, b_η, and b'_η. The results are displayed in Tabs. 7.1–7.3, labeled NLO Qexp.

The parameters L_5 and $\theta^{[1]}$ have been determined in the NLO analysis in Sec. 5.4.2 with a small error. Therefore, we have not taken these errors into account in the analysis of the two-photon decays. However, to obtain an estimate of the effect of the errors, we recalculate the quantities in the NLO 2 scenario varying L_5 and $\theta^{[1]}$ within their errors. This leads to only small variations in the last digit of the results for the decay widths and the slopes. We conclude that the influence of the errors of L_5 and θ_1 is very small, and we neglect them in the following.

Discussion of the results

In the NLO 1 case, we find quite small values for $L_8^{6,\epsilon}$ and λ_1. However, if we perform a simultaneous fit to the π^0, η, η' decay widths (NLO 2 and NLO 3), the values for $L_8^{6,\epsilon}$ and λ_1 become larger, with a drastic increase of the λ_1 value. Phenomenological studies [Leu 98, FKS 98, FKS 99, EGM 15] suggest that OZI-rule-violating parameters as, e.g., λ_1 should be small. For example, Ref. [Leu 98] determines[1] $\lambda_1 = \Lambda_1 - 2\Lambda_3 = 0.25$ and Ref. [EGM 15]

[1]In Ref. [Leu 98] the coupling K_1 is denoted by $\Lambda_3 = K_1$.

	Γ_{π^0} [eV]	Γ_η [keV]	$\Gamma_{\eta'}$ [keV]
LO	7.79 ± 0.02	0.62 ± 0.00	5.03 ± 0.01
LO Qexp	0 ± 0	0.20 ± 0.00	8.33 ± 0.02
NLO 1	7.63 ± 0.16	0.59 ± 0.40	3.95 ± 12.23
NLO 2	6.99 ± 1.71	0.50 ± 1.02	4.28 ± 13.17
NLO 3	7.04 ± 0.99	0.45 ± 0.55	5.06 ± 7.23
NLO Qexp	7.79 ± 0.02	0.52 ± 7.40	4.36 ± 94.40
Data [Oli+ 14]	7.63 ± 0.16	0.52 ± 0.02	4.36 ± 0.25

Table 7.2: Results for the two-photon decay widths at NLO.

	b_{π^0}	b_η	$b_{\eta'}$
LO	0 ± 0	0 ± 0	0 ± 0
LO Qexp	0 ± 0	0 ± 0	0 ± 0
NLO 1	0.04 ± 0.02	0.55 ± 0.26	2.53 ± 1.19
NLO 2	0.04 ± 0.05	0.51 ± 0.69	-2.09 ± 2.83
NLO 3	0.04 ± 0.04	0.52 ± 0.42	-1.86 ± 2.20
NLO Qexp	0 ± 0	0.29 ± 4.27	-3.62 ± 52.87
Data	0.03 ± 0.01	0.58 ± 0.02	1.30 ± 0.22

Table 7.3: Results for the slope parameters at NLO. The experimental value for b_{π^0} is taken from Ref. [Mas 12], b_η from Ref. [EMS 15], and $b_{\eta'}$ from Ref. [EMS 14].

finds $\Lambda_1 = 0.21(5)$, $\Lambda_3 = 0.05(3)$, yielding $\lambda_1 = \Lambda_1 - 2\Lambda_3 = 0.11(8)$. These results are in agreement with the NLO 1 case, whereas the scenarios NLO 2 and NLO 3 indicate very large OZI-rule-violating corrections. The values for $L_{19}^{6,\epsilon}$ do not exhibit large variations in the different scenarios. They can be compared to a VMD prediction yielding $L_{19}^{6,\epsilon} = -1 \times 10^{-3}$ [Hac 08]. Our absolute values are 30% larger than predicted by VMD, but agree mostly within their errors.

The LO values for the decay widths labeled LO agree within 20% with the experimental values. The slopes are equal to zero at that order. At LO, taking the N_c expansion of Q into account leads to results that are far from the experimental values. The NLO calculations improve the description of the decay widths. In the NLO 1 case, the π^0 decay width is equal to the experimental value, because $L_8^{6,\epsilon}$ is fixed to it. In the NLO 2 case, where the parameters where fitted to all three decay widths, the description of Γ_{π^0} worsens, while Γ_η and $\Gamma_{\eta'}$ come closer to the experimental values. Our NLO 1-3 results for the slope of the η agree well with the experimental value, which was determined in Ref. [EMS 15] with great precision. The description of the η' slope, however, is very bad. Due to the small error of b_η the fit favors this value, contributing to the poor description of $b_{\eta'}$. In the simultaneous fit to all decay widths and slope parameters (NLO 3), the results for the decay widths show larger deviations from the experimental values in comparison to NLO 2, marginally improving the values for the slopes. In the NLO Qexp scenario, the π^0 decay width is given by the leading-order value of the $Q(3)$ case. Since, then, the two parameters $L_8^{6,\epsilon}$ and λ_1 need to be fixed by Γ_η and $\Gamma_{\eta'}$ alone, we reproduce the experimental values for these widths. The results for b_η and $b_{\eta'}$ are very poor in this case. In the NLO Qexp case, the errors of the LECs and the results for the decay widths and slopes are very large. This further reflects the fact that the NLO Qexp calculation is not appropriate the describe the data, and the LECs cannot be fixed in a sensible way. We thus conclude that neglecting the N_c expansion of Q leads to a better description of the experimental data at LO and NLO. However, in general, the NLO calculation is not sufficient to adequately describe the decay widths and slopes of π^0, η, and η', which motivates taking higher-order corrections into account.

7.2.2 NNLO

At NNLO, a lot of new LECs appear both from the even-intrinsic-parity sector and the odd-intrinsic-parity sector. Moreover, our power counting demands taking terms of the $\mathcal{O}(p^8)$ Lagrangian into account, which has not been constructed yet. We therefore make the following ansatz for the q^2

dependence of the single-virtual TFFs up to NNLO:

$$F_{\eta\gamma^*\gamma}(q^2) = F^{\mathrm{LO}}_{\eta\gamma^*\gamma} + \frac{1}{4\sqrt{3}\pi^2 F_\pi}\left(A_\eta + B_\eta q^2 + C_\eta (q^2)^2\right) + loops_\eta(q^2), \tag{7.26}$$

$$F_{\eta'\gamma^*\gamma}(q^2) = F^{\mathrm{LO}}_{\eta'\gamma^*\gamma} + \frac{2\sqrt{2}}{4\sqrt{3}\pi^2 F_\pi}\left(A_{\eta'} + B_{\eta'} q^2 + C_{\eta'} (q^2)^2\right) + loops_{\eta'}(q^2). \tag{7.27}$$

The A_P and B_P are combinations of LECs from the higher-order Lagrangians in Chapter 4 and, in principle, receive contributions from the $\mathcal{O}(p^8)$ Lagrangian as well. The C_P stem solely from the $\mathcal{O}(p^8)$ Lagrangian. The expression $loops_P(q^2)$ denotes the q^2-dependent part of the loop corrections, while the q^2-independent parts are absorbed in the parameters A_P. At NNLO, we only consider the TFFs of η and η', since there are no data available for the π^0 TFF in the low-energy region. We determine the parameters A_P, B_P, C_P through a simultaneous fit to the decay widths to real photons $\Gamma_{P\to\gamma\gamma}$ and to the experimental data for the TFFs. In the following, we perform several fits for both the η and the η' TFF considering different NNLO contributions. We start by fitting the full NNLO expressions. Then, we consider the case without loops, which means switching of the q^2-dependent pieces $loops_P(q^2)$. To study the influence of the C_P terms, we also perform fits where we put $C_P = 0$. Finally, we discuss the case where both C_P and loops are neglected. In addition, we examine each of these four scenarios taking the N_c expansion of Q into account, denoted by Qexp. The fits are performed using the *Mathematica* routine NonlinearModelFit, and the errors of the fit parameters are the ones obtained by this routine. According to Sec. 4.5, a systematic error of at least 4% should be added to all results determined up to NNLO.

The TFF of the η is fitted to the time-like experimental data obtained in Refs. [Arn+ 09, Ber+ 11, Agu+ 14, Arn+ 16]. For each case, we perform fits up to three different values of the invariant mass of the lepton pair, $q = m(l^+l^-)$. The maximal q values are $q_1 = 0.47$ GeV, $q_2 = 0.40$ GeV, and $q_3 = 0.35$ GeV. The results for the parameters fitted up to 0.47 GeV are displayed in Tab. 7.4, and the results of the other fits can be found in Tab. C.4 in Appendix C. For the η' TFF there are also data points in the space-like low-energy region available. Therefore, we fit the TFF to the space-like data from Ref. [Acc+ 98] and to the time-like data from Ref. [Abl+ 15]. Here, we choose four fit regions for each scenario. The different fit ranges for the photon virtuality q^2 are $-0.53\ \mathrm{GeV}^2 \le q^2 \le 0.43\ \mathrm{GeV}^2$ (I), $-0.53\ \mathrm{GeV}^2 \le q^2 \le 0.40\ \mathrm{GeV}^2$ (II), $-0.50\ \mathrm{GeV}^2 \le q^2 \le 0.43\ \mathrm{GeV}^2$ (III), and $-0.50\ \mathrm{GeV}^2 \le q^2 \le 0.40\ \mathrm{GeV}^2$ (IV). Table 7.5 shows the results for the parameters fitted in the range $-0.53\ \mathrm{GeV}^2 \le q^2 \le 0.43\ \mathrm{GeV}^2$, and the results of the other fits are displayed in Tab. C.5 in Appendix C.

	A_η	B_η [GeV^{-2}]	C_η [GeV^{-4}]
Full	-0.17 ± 0.02	2.16 ± 0.18	11.57 ± 1.46
W/O loops	-0.17 ± 0.02	2.84 ± 0.17	12.30 ± 1.44
Cp=0	-0.17 ± 0.03	3.41 ± 0.12	0 ± 0
W/O loops Cp=0	-0.17 ± 0.03	4.17 ± 0.13	0 ± 0
Full Qexp	0.66 ± 0.02	2.23 ± 0.18	11.65 ± 1.46
W/O loops Qexp	0.66 ± 0.02	2.84 ± 0.17	12.30 ± 1.44
Cp=0 Qexp	0.66 ± 0.03	3.49 ± 0.12	0 ± 0
W/O loops Cp=0 Qexp	0.66 ± 0.03	4.17 ± 0.13	0 ± 0

Table 7.4: Fit parameters for the η TFF. The LECs were fitted up to 0.47 GeV.

	$A_{\eta'}$	$B_{\eta'}$ [GeV^{-2}]	$C_{\eta'}$ [GeV^{-4}]
Full	-0.06 ± 0.02	1.08 ± 0.18	1.18 ± 0.37
W/O loops	-0.06 ± 0.02	1.23 ± 0.18	1.30 ± 0.37
Cp=0	-0.06 ± 0.02	0.55 ± 0.10	0 ± 0
W/O loops Cp=0	-0.06 ± 0.02	0.64 ± 0.10	0 ± 0
Full Qexp	-0.29 ± 0.02	1.07 ± 0.18	1.17 ± 0.37
W/O loops Qexp	-0.29 ± 0.02	1.23 ± 0.18	1.30 ± 0.37
Cp=0 Qexp	-0.29 ± 0.02	0.54 ± 0.10	0 ± 0
W/O loops Cp=0 Qexp	-0.29 ± 0.02	0.64 ± 0.10	0 ± 0

Table 7.5: Fit parameters for the η' TFF. The LECs were fitted in the range -0.53 GeV$^2 \leq q^2 \leq 0.43$ GeV^2.

The q^2 dependence of the η TFF is shown in Fig. 7.2, where the TFF, normalized to 1 at $q^2 = 0$, is plotted as a function of the invariant mass of the lepton pair $m(l^+l^-)$ together with the experimental data. In this case, the TFF was fitted up to 0.47 GeV. The bands show the 1σ error bands obtained by the *Mathematica* fit routine NonlinearModelFit. Figure 7.3 shows the

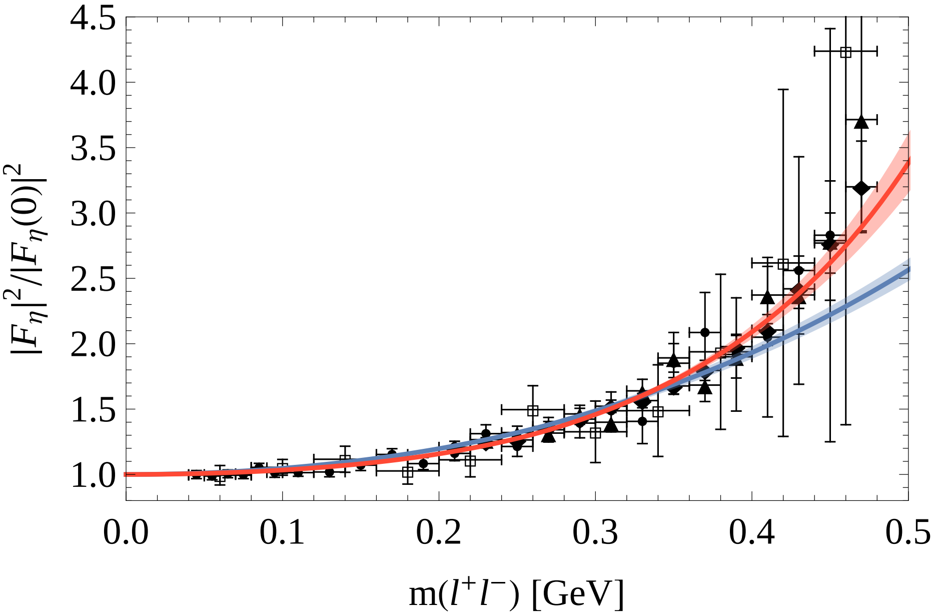

Figure 7.2: η TFF fitted up to 0.47 GeV. The red line is the full NNLO calculation and the blue line the NNLO result with $C_\eta = 0$. The experimental data are taken from Refs. [Arn+ 09] (▲), [Ber+ 11] (□), [Agu+ 14] (■), [Arn+ 16] (♦).

results of the fits for the different fit ranges. As the fit range is extended to higher $m(l^+l^-)$ values, the curves become steeper.

The q^2 dependence of the normalized η' TFF, fitted between -0.53 GeV^2 and 0.43 GeV^2, is shown in Fig. 7.4 together with the experimental data. The bands are the 1σ error bands due to the errors of the fit parameters. The results for the η' TFF fitted to different ranges are displayed in Fig. 7.5.

Discussion of the results

In the following, we will interpret the results of the NNLO analysis. We start with the discussion of the LECs determined at NNLO, shown in Tabs. 7.4 and 7.5. Switching on or off the loop contributions corresponds to considering

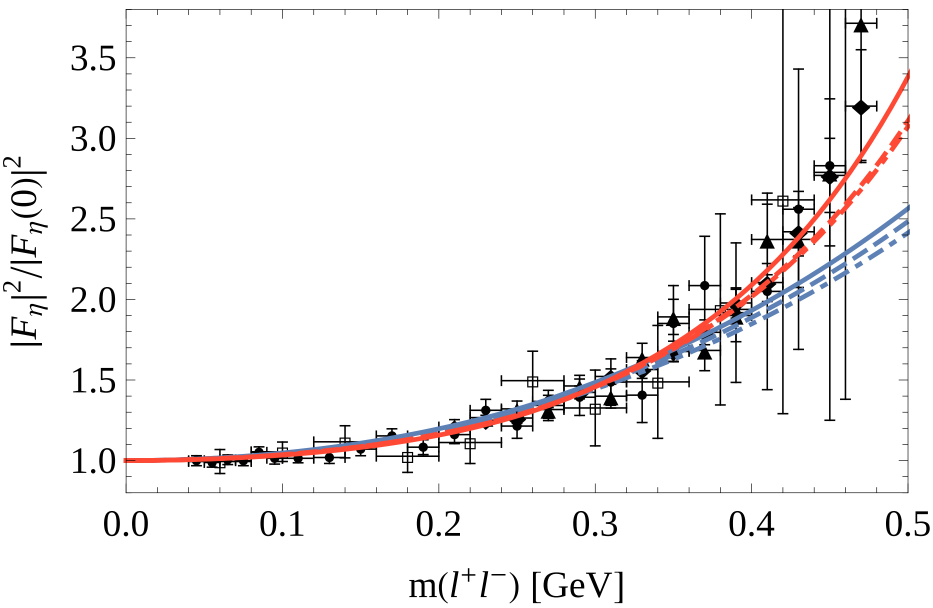

Figure 7.3: η TFF fitted up to 0.47 GeV (solid), 0.40 GeV (dashed), and 0.35 GeV (dash-dotted). The red lines are the full NNLO calculations and the blue lines the NNLO results with $C_\eta = 0$. The experimental data are taken from Refs. [Arn+ 09] (▲), [Ber+ 11] (□), [Agu+ 14] (■), [Arn+ 16] (♦).

the q^2-dependent parts, $loops_P(q^2)$, or neglecting them, respectively. As a result, the parameters A_P remain the same in both cases. The inclusion of the N_c expansion of Q has almost no visible effect on the shape of the TFFs. However, this expansion has an influence on the parameters A_P which change notably, since the LO expressions for the TFF (see Sec. 7.1) are different with or without the N_C expansion of Q. The q^2-dependent loop corrections $loops_P(q^2)$ give numerically quite similar contributions to the TFF with or without the N_c expansion of Q. Therefore, the parameters B_P and C_P do not vary very much in these two cases. As Figures D.1 and D.2 in Appendix D show, the influence of the loop contributions on the shape of the TFFs is very small. However, the effects of the loops can be seen in the variation of B_P and C_P with and without loops, where we observe rather small changes. Neglecting the loops leads to an increase of the values of B_P and C_P in order to compensate for the missing contributions, which add positively to the TFFs.

Table C.4 in Appendix C shows the variation of the fit parameters for the η TFF with decreasing fit range. If C_η is put to zero, the parameter B_η decreases as the fit range decreases. This behavior is in accordance with the fact that the curves become steeper as the fit range is extended to higher q^2

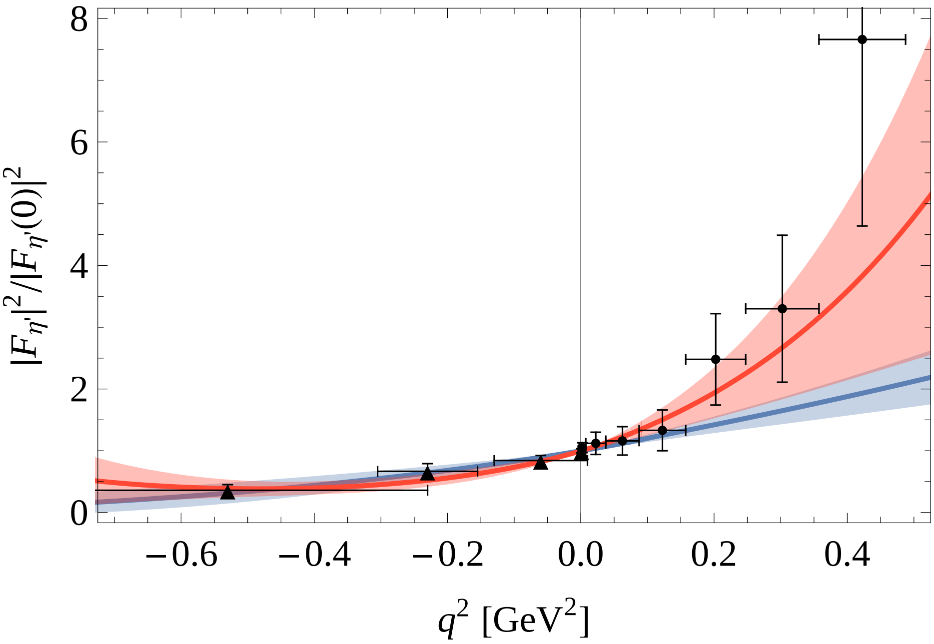

Figure 7.4: η' TFF fitted in the range -0.53 GeV$^2 \leq q^2 \leq 0.43$ GeV^2. The red line is the full NNLO calculation and the blue line the NNLO result with $C_{\eta'} = 0$. The time-like data are taken from Ref. [Abl+ 15] (•) and the space-like data from Ref. [Acc+ 98] (▲).

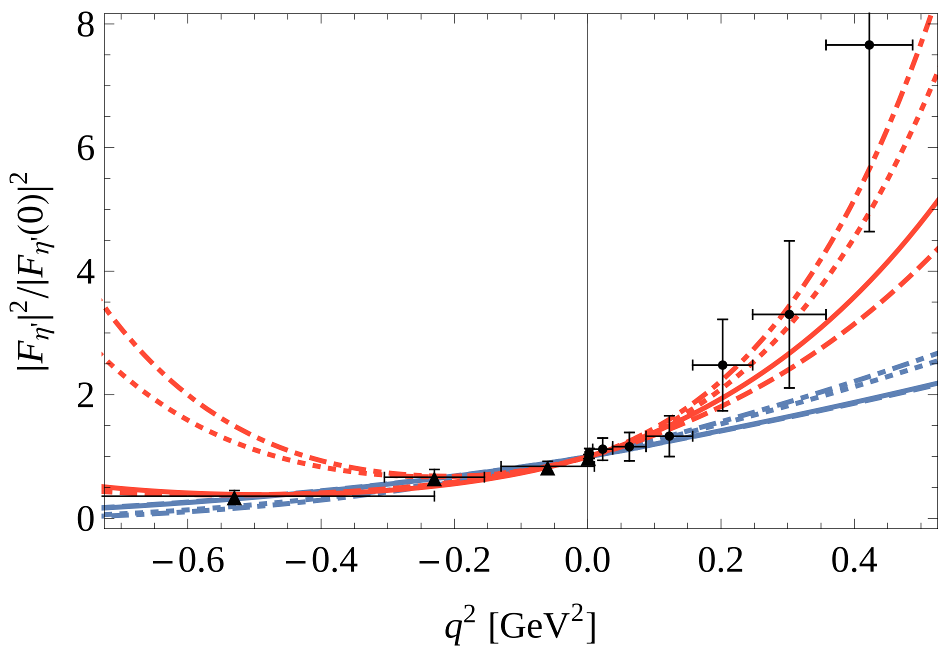

Figure 7.5: η' TFF fitted in the range -0.53 GeV$^2 \leq q^2 \leq 0.43$ GeV^2 (solid), -0.53 GeV$^2 \leq q^2 \leq 0.40$ GeV^2 (dashed), -0.50 GeV$^2 \leq q^2 \leq 0.43$ GeV^2 (dash-dotted), -0.50 GeV$^2 \leq q^2 \leq 0.40$ GeV^2 (dotted). The red lines are the full NNLO calculations and the blue lines the NNLO results with $C_{\eta'} = 0$. The time-like data are taken from Ref. [Abl+ 15] (•) and the space-like data from Ref. [Acc+ 98] (▲).

	$q_{\max}$ [GeV]	b_η	c_η
Full	0.47	0.48 ± 0.03	0.66 ± 0.08
Full	0.40	0.53 ± 0.04	0.49 ± 0.08
Full	0.35	0.53 ± 0.06	0.47 ± 0.08
Cp=0	0.47	0.70 ± 0.03	0.05 ± 0.00
Cp=0	0.40	0.67 ± 0.02	0.05 ± 0.00
Cp=0	0.35	0.64 ± 0.02	0.05 ± 0.00

Table 7.6: Results for the slope and the curvature of the η TFF at NNLO.

values. If we include the C_η term in the fit, there is an interplay between C_η and B_η. For decreasing fit range, the C_η values tend to decrease while B_η increases. In addition, the errors of B_η and C_η become larger. This is to be expected since less data points are included in the fit, there seems to be a correlation between B_η and C_η, and the C_η term becomes more important at higher values of q^2.

In the case of the η', the fit range is varied both in the time-like and the space-like region. The variation of the parameters is displayed in Tab. C.5 in Appendix C. Decreasing the time-like fit range yields smaller values for both $B_{\eta'}$ and $C_{\eta'}$. This is to be expected, since the TFF curves show less curvature as the fit range gets smaller. If we exclude the last space-like data point, the values for $B_{\eta'}$ and $C_{\eta'}$ increase. In this case, the fit focuses more on the time-like region and the parameters adjust to the steep rise of the time-like TFF.

Slope and curvature

Employing the results for the fit parameters, we calculate the slopes and the curvatures of the TFFs as defined in Eqs. (7.20) and (7.21). The errors are due to the errors of the fit parameters. As a first estimate we assume that the fit parameters are independent. Taking into account their correlations is beyond the scope of this thesis. The main results are given in Tabs. 7.6 and 7.7.

The values for the slopes with and without loop contributions agree within their uncertainties. This is the case, because the influence of the loops is already compensated by different values for the fit parameters B_P. The N_c expansion of the quark-charge matrix plays a negligible role. If we neglect the C_η term, B_η compensates for the missing contribution, and, as a result, the η slope increases. This effect is diminished if the fit range is restricted to lower q^2 values. In the case of the η', if we set $C_{\eta'} = 0$, the slope gets smaller.

	Fit range	$b_{\eta'}$	$c_{\eta'}$
Full	I	1.47 ± 0.22	1.58 ± 0.41
Full	II	1.32 ± 0.19	1.30 ± 0.41
Full	III	1.52 ± 0.13	3.46 ± 0.42
Full	IV	1.42 ± 0.13	2.95 ± 0.41
Cp=0	I	0.84 ± 0.12	0.28 ± 0.01
Cp=0	II	0.82 ± 0.10	0.28 ± 0.01
Cp=0	III	1.11 ± 0.25	0.28 ± 0.01
Cp=0	IV	1.04 ± 0.20	0.28 ± 0.01

Table 7.7: Results for the slope and the curvature of the η' TFF at NNLO. The fit ranges are: -0.53 GeV$^2 \leq q^2 \leq 0.43$ GeV^2 (I), -0.53 GeV$^2 \leq q^2 \leq 0.40$ GeV^2 (II), -0.50 GeV$^2 \leq q^2 \leq 0.43$ GeV^2 (III), -0.50 GeV$^2 \leq q^2 \leq 0.40$ GeV^2 (IV).

This behavior is different from the one of the η slope due to the inclusion of the space-like data. As a further check, we have investigated the case where the fit is performed only to the time-like data. Then, the η' slope increases if we put $C_{\eta'} = 0$, which is similar to the η case.

Our results for the slopes can be compared with other theoretical and experimental determinations. Experimental results for the η slope are: $b_\eta = 0.57(12)$ from Lepton-G [Dzh+ 80], $b_\eta = 0.61(14)$ from TPC [Aih+ 90], $b_\eta = 0.43(6)$ from CELLO [Beh+ 91], and $b_\eta = 0.50(6)$ from CLEO [Gro+ 98]. The NA60 collaboration determined $b_\eta = 0.59(5)$ [Arn+ 09] and $b_\eta = 0.59(2)$ [Usa+ 11]. Results from A2 are $b_\eta = 0.58(11)$ [Ber+ 11] and $b_\eta = 0.59(7)$ [Agu+ 14]. Experimental results for the η' slope are: $b_{\eta'} = 1.55(73)$ from Lepton-G [Dzh+ 79, Dzh+ 80], $b_{\eta'} = 1.27(21)$ from TPC [Aih+ 90], $b_{\eta'} = 1.47(15)$ from CELLO [Beh+ 91], $b_{\eta'} = 1.24(14)$ from CLEO [Gro+ 98], and $b_{\eta'} = 1.47(23)$ from BESIII [Abl+ 15]. The TFFs of the η-η' system have been studied in various theoretical approaches. The vector-meson-dominance model (VMD) [BM 81, Ame+ 83, PB 84] predicts $b_\eta = 0.53$ and $b_{\eta'} = 1.33$. The calculation of a triangle loop of the constituent quarks (Quark loop) [BM 81, Ame+ 83, PB 84] yields $b_\eta = 0.51$ and $b_{\eta'} = 1.30$, and the Brodsky-Lepage interpolation formula [BL 81] gives $b_\eta = 0.36$ and $b_{\eta'} = 2.11$. Chiral perturbation theory at the one-loop level (1-loop ChPT) using the leading-order η-η' mixing [Ame+ 92] provides $b_\eta = 0.51$ and $b_{\eta'} = 1.47$. A coupled-channel (CC) analysis [BN 04a] finds $b_\eta = 0.47$ and $b_{\eta'} = 1.64$, and chiral effective theory with resonances (RχT) [Czy+ 12] finds $b_\eta = 0.546(9)$ and $b_{\eta'} = 1.384(3)$. In Ref. [KOT 14], the axial anomaly is connected to the vector-meson-dominance model by means of anomaly sum rules (ASR) yielding $b_\eta = 0.54$ and $b_{\eta'} = 1.06$. An analysis of the data using Padé approximants gives $b_\eta = 0.576(15)$ [EMS 15] and $b_{\eta'} = 1.30(22)$ [EMS 14], and a dispersive analysis [Han+ 15] predicts $b_\eta = 0.62^{+0.07}_{-0.03}$ and $b_{\eta'} = 1.40^{+0.14}_{-0.07}$. Figures 7.6 and 7.7 show the comparison of our results for the η and η' slopes, respectively, together with the other experimental and theoretical determinations. Our

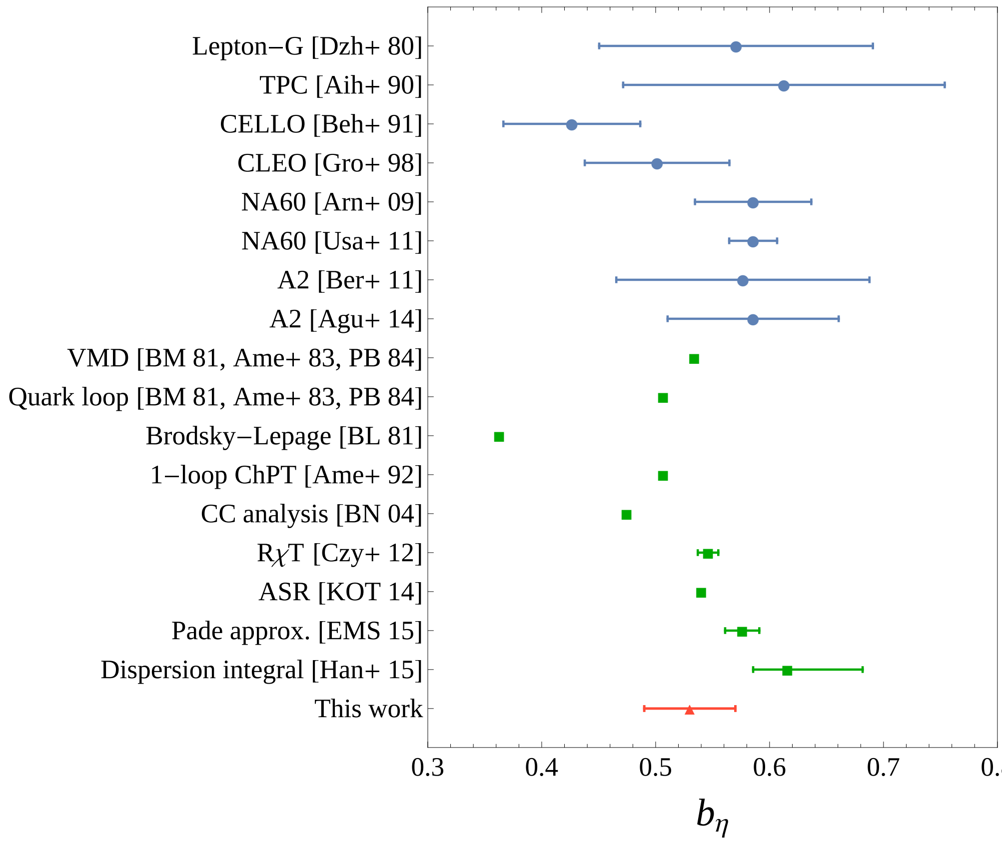

Figure 7.6: Comparison of the results for b_η.

values $b_\eta = 0.53(4)$ from the fit up to 0.40 GeV and $b_{\eta'} = 1.47(22)$ from fit I agree within the errors with most of the other theoretical and experimental results. In general, our result for b_η is slightly lower than the other determinations, whereas our value for $b_{\eta'}$ is slightly higher than the other results. From Tab. 7.6 one can observe that a decreasing fit range leads to values for b_η which come closer to the other theoretical and experimental determinations.

The main results for the curvatures of η and η' are displayed in Tabs. 7.6 and 7.7, respectively. The η curvature is reduced if the fit range is restricted to smaller q^2 values. The η' curvature decreases if the time-like range is decreased. As the space-like fit range becomes smaller, the fit is dominated

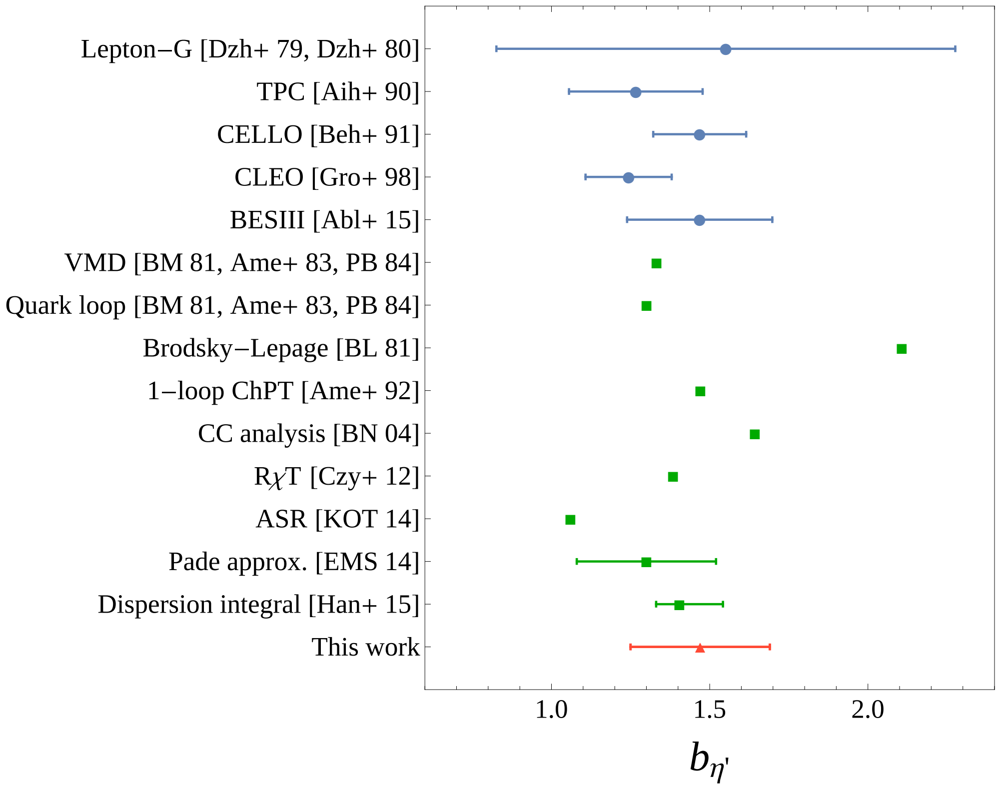

Figure 7.7: Comparison of the results for $b_{\eta'}$.

by the steeply rising time-like data and the curvature is almost twice as large. The main contributions to the curvature stem from the C_P terms. If we put them to zero, the remaining curvature is given by the loop contributions, which is rather small.

Our values for the curvature can be compared with other theoretical determinations. An analysis of the data using Padé approximants finds $c_\eta = 0.339(15)_{\text{stat}}(5)_{\text{sys}}$ [EMS 15] and $c_{\eta'} = 1.72(47)_{\text{stat}}(34)_{\text{sys}}$ [EMS 14]. If we use a simple VMD estimate as given in Eq. (7.25) with $\Lambda_P = 0.77$ GeV [Hac 08], we obtain $c_\eta = 0.26$ and $c_{\eta'} = 2.40$. Our values for c_η are mostly larger than the other predictions. Only if the fit range is decreased, our results come to agreement with Ref. [EMS 15], whereas the naive VMD prediction is even smaller. In the cases including the full space-like data, the η' curvature is slightly smaller than the one from Ref. [EMS 14], but shows agreement within the errors. The VMD prediction for $c_{\eta'}$ is larger and lies on the upper end of the error band in Ref. [EMS 14]. None of our values reaches within the errors, which are only the ones provided by the fit, the VMD value. The results for $c_{\eta'}$ in the cases where the space-like fit range is restricted are much larger than the ones from the fit to all space-like data as well as the ones from the other references.

7.3 Single Dalitz decays

Having performed the numerical evaluation of the single-virtual TFFs of η and η', we are now able to calculate the decay widths of the decays to one photon and a lepton pair. Since there are no low-energy data for the π^0 TFF available, we have not studied the π^0 TFF at NNLO. In addition, our analysis focuses more on the η-η' system. Therefore, here, we do not consider the single Dalitz decay $\pi^0 \to \gamma e^+e^-$. To obtain the invariant amplitude for the decay $P \to \gamma l^+l^-$, where $P = \eta,\ \eta'$ and $l = e,\ \mu$, we use Eq. (7.1) and therein define q_1^μ, with $q_1^2 = s$, and $\epsilon_1^\mu = (e/s)[\bar{u}\gamma^\mu v]$ as virtual-photon momentum and polarization, respectively. The momentum of the real photon is denoted by q_2 with $q_2^2 = 0$, and ϵ_2 is its polarization. The decay width can be written as [Hac 08]

$$\Gamma(P \to \gamma l^+l^-) = \int_{4m_l^2}^{M_P^2} ds \frac{\sqrt{\lambda[M_P^2, s, 0]}\sqrt{\lambda[s, m_l^2, m_l^2]}}{1024 M_P^3 \pi^4 s} \int d\Omega_{ll} \overline{\sum} |\mathcal{M}|^2. \quad (7.28)$$

Defining the leptonic tensor

$$L^{\mu\nu} = \sum_{\text{spin}} [\bar{u}\gamma^\mu v][\bar{u}\gamma^\nu v]^* \quad (7.29)$$

	$\Gamma_{\eta\to\gamma e^+e^-}$ [eV]	$\mathrm{BR}^{\mathrm{rel}}_{\eta\to\gamma e^+e^-}$ $[10^{-2}]$	$\Gamma_{\eta'\to\gamma e^+e^-}$ [eV]	$\mathrm{BR}^{\mathrm{rel}}_{\eta'\to\gamma e^+e^-}$ $[10^{-2}]$
LO	10.10 ± 0.02	1.63 ± 0.00	90.59 ± 0.20	1.80 ± 0.01
LO Qexp	3.22 ± 0.01	1.61 ± 0.01	150.06 ± 0.33	1.80 ± 0.01
NLO 1	9.90 ± 1.50	1.68 ± 1.17	80.88 ± 22.62	2.05 ± 6.37
NLO 2	8.39 ± 1.23	1.68 ± 3.43	71.02 ± 20.39	1.66 ± 5.13
NLO 3	7.46 ± 2.58	1.66 ± 2.11	85.25 ± 48.00	1.68 ± 2.59
NLO Qexp	8.52 ± 8.96	1.64 ± 23.38	70.65 ± 135.12	1.62 ± 35.22
Full	8.66 ± 0.24	1.68 ± 0.08	85.54 ± 3.58	1.96 ± 0.14
Cp=0	8.68 ± 0.34	1.68 ± 0.09	81.44 ± 4.41	1.87 ± 0.15
Exp. [Oli+ 14]	9.04 ± 0.63	1.75 ± 0.10	92.86 ± 9.09	2.13 ± 0.16

Table 7.8: Decay widths and relative BRs for $\eta^{(\prime)} \to \gamma e^+e^-$.

and employing the identity

$$\int \frac{d\Omega_{ll}}{4\pi} L_{\mu\mu'} = \frac{4}{3}\left(1 + \frac{2m_l^2}{q^2}\right)(q_\mu q_{\mu'} - q^2 g_{\mu\mu'}), \quad q^2 = s, \tag{7.30}$$

one obtains

$$\Gamma(P \to \gamma l^+l^-)$$
$$= \frac{e^2}{384 M_P^3 \pi^3} \int_{4m_l^2}^{M_P^2} ds \frac{\sqrt{1 - \frac{4m_l^2}{s}}(M_P^2 - s)^3(2m_l^2 + s)}{s^2} |F(P \to \gamma l^+l^-)|^2. \tag{7.31}$$

To evaluate this expression numerically, we make use of the LECs determined in Secs. 7.2.1 and 7.2.2. At NNLO, we employ the LECs determined from the first fits, i.e., fitting the η TFF up to 0.47 GeV and the η' TFF in the range $-0.53\ \mathrm{GeV}^2 \le q^2 \le 0.43\ \mathrm{GeV}^2$ (I). The results for the decay widths to one photon and a lepton pair are shown in Tabs. 7.8 and 7.9. The errors are calculated from the errors of the LECs which are assumed to be uncorrelated. They can be viewed as upper limits for the errors. Taking the correlations into account is beyond the scope of this thesis. In addition, a systematic error should be added as explained in Sec. 4.5.

The values for $\Gamma_{\eta\to\gamma e^+e^-}$ and $\Gamma_{\eta'\to\gamma e^+e^-}$ behave like the corresponding values for the decays to two real photons. The disagreement of the two-photon-decay widths in some scenarios and the experimental data is reflected in the values for $\Gamma_{\eta^{(\prime)}\to\gamma e^+e^-}$ as well. Therefore, we calculate the relative branching ratios (BR)

$$\mathrm{BR}^{\mathrm{rel}}_{P\to\gamma l^+l^-} = \frac{\Gamma_{P\to\gamma l^+l^-}}{\Gamma_{P\to\gamma\gamma}}, \tag{7.32}$$

	$\Gamma_{\eta\to\gamma\mu^+\mu^-}$ [eV]	$\mathrm{BR}^{\mathrm{rel}}_{\eta\to\gamma\mu^+\mu^-}$ $[10^{-4}]$	$\Gamma_{\eta'\to\gamma\mu^+\mu^-}$ [eV]	$\mathrm{BR}^{\mathrm{rel}}_{\eta'\to\gamma\mu^+\mu^-}$ $[10^{-3}]$
LO	0.34 ± 0.00	0.55 ± 0.00	8.65 ± 0.02	1.72 ± 0.01
LO Qexp	0.11 ± 0.00	0.55 ± 0.00	14.32 ± 0.03	1.72 ± 0.01
NLO 1	0.44 ± 0.06	0.75 ± 0.52	14.47 ± 3.11	3.66 ± 11.37
NLO 2	0.38 ± 0.06	0.76 ± 1.56	3.15 ± 1.37	0.74 ± 2.29
NLO 3	0.33 ± 0.10	0.73 ± 0.92	4.50 ± 3.39	0.89 ± 1.44
NLO Qexp	0.33 ± 0.33	0.63 ± 9.05	2.48 ± 5.46	0.57 ± 12.38
Full	0.42 ± 0.01	8.14 ± 0.37	13.36 ± 1.03	3.07 ± 0.30
Cp=0	0.42 ± 0.01	8.14 ± 0.37	9.91 ± 0.60	2.28 ± 0.19
Exp. [Oli+ 14]	0.41 ± 0.05	7.87 ± 1.02	21.38 ± 5.43	4.91 ± 1.24

Table 7.9: Decay widths and relative BRs for $\eta^{(\prime)} \to \gamma\mu^+\mu^-$.

using the values for $\Gamma_{P\to\gamma\gamma}$ obtained in the different scenarios. The results are shown in Tabs. 7.8 and 7.9. Now, the values for the relative BRs do not vary very much within the different cases and orders. The η relative BR is very close to the experimental value, while the η' relative BR is somewhat smaller than the experimental result, especially in most of the NLO cases. This is related to the value of the η' slope. The slope is very large in the NLO 1 case, which leads to a large relative BR, and the negative values for $b_{\eta'}$ in the other NLO cases are reflected in a reduced relative BR even compared to the LO value. The decay width of $P \to \gamma e^+e^-$ receives its main contribution at values where the virtual photon is in the vicinity of its mass shell. Therefore, the η and η' relative BRs are well described already at LO. The decay $P \to \gamma\mu^+\mu^-$ provides a better probe of the virtual behavior of the TFF at larger photon virtualities. However, the values for $\Gamma_{\eta\to\gamma\mu^+\mu^-}$ are still related to the two-photon-decay widths, but the higher-order corrections in q^2, parametrized by slope and curvature, become important. Here, we calculate the relative BRs as well. The LO relative BR of the η is now lower than the experimental value and increases at NLO and NNLO. Especially at NNLO, we obtain very good agreement with the data for both $\Gamma_{\eta\to\gamma\mu^+\mu^-}$ and $\mathrm{BR}^{\mathrm{rel}}_{\eta\to\gamma\mu^+\mu^-}$. The LO relative BR for $\eta' \to \gamma\mu^+\mu^-$ is only 30% of the experimental value. In the NLO scenarios it becomes even smaller except for NLO 1. This is related to the slope of the η' which is very large in the NLO 1 scenario, but poorly described in the other NLO cases with even negative values. The full NNLO value is larger than the LO one and most of the NLO values. However, it is still smaller than the experimental result. If we neglect the $C_{\eta'}$ term, the relative BR decreases again. This is connected to the description of the

	$\mathrm{BR}^{\mathrm{rel}}_{\eta\to\gamma e^+e^-}$ $[10^{-2}]$	$\mathrm{BR}^{\mathrm{rel}}_{\eta\to\gamma\mu^+\mu^-}$ $[10^{-4}]$
QED [MT 73]	1.63 ± 0	5.54 ± 0
Quark model [Lih 11]	1.77 ± 0	7.48 ± 0
Hidden gauge [Pet 10]	1.666 ± 0.002	7.75 ± 0.09
Mod. VMD [Pet 10]	1.662 ± 0.002	7.54 ± 0.11
Padé approx. [EG 15]	1.68 ± 0.15	8.30 ± 1.42
This work	1.68 ± 0.08	8.14 ± 0.37
Exp. [Oli+ 14]	1.75 ± 0.10	7.87 ± 1.02

Table 7.10: Comparison of theoretical determinations of the η relative BRs.

	$\mathrm{BR}^{\mathrm{rel}}_{\eta'\to\gamma e^+e^-}$ $[10^{-2}]$	$\mathrm{BR}^{\mathrm{rel}}_{\eta'\to\gamma\mu^+\mu^-}$ $[10^{-3}]$
Hidden gauge [Pet 10]	2.10 ± 0.02	4.45 ± 0.15
Mod. VMD [Pet 10]	2.06 ± 0.02	4.11 ± 0.18
Padé approx. [EG 15]	1.99 ± 0.16	3.36 ± 0.26
This work	1.96 ± 0.14	3.07 ± 0.30
Exp. [Oli+ 14]	2.13 ± 0.16	4.91 ± 1.24

Table 7.11: Comparison of theoretical determinations of the η' relative BRs.

η' TFF data. The time-like TFF is underestimated for higher values of q^2 and even more so if one does not take the $(q^2)^2$ term into account. The decay width of $\eta' \to \gamma\mu^+\mu^-$ receives contributions in q^2 ranges where vector-meson resonances become important [EG 15], which are not included in our framework.

Our full NNLO results for the relative BRs are compared with other theoretical determinations. The QED prediction for $\eta \to \gamma l^+l^-$, $l = e,\ \mu$, is provided in Ref. [MT 73]. Reference [Lih 11] studied the single Dalitz decays of the η within the light-front quark model. All four decays $\eta^{(\prime)} \to \gamma l^+l^-$, $l = e,\ \mu$, have been calculated including vector mesons in the hidden gauge model and a modified VMD model [Pet 10]. Reference [EG 15] predicts the decay widths by means of a data-driven approach using Padé approximants. The results for the η and η' relative BRs can be found in Tabs. 7.10 and 7.11, respectively.

Our values for $\mathrm{BR}^{\mathrm{rel}}_{\eta\to\gamma e^+e^-}$ and $\mathrm{BR}^{\mathrm{rel}}_{\eta'\to\gamma e^+e^-}$ agree well with the other determinations. In the case of $\mathrm{BR}^{\mathrm{rel}}_{\eta\to\gamma\mu^+\mu^-}$, as already stated, the simple QED prediction is too small. Here, our result agrees with the other works, except for Ref. [Lih 11] which gives a slightly smaller value. Our result for $\mathrm{BR}^{\mathrm{rel}}(\eta' \to \gamma\mu^+\mu^-)$ is smaller than the others. It agrees within errors with Ref. [EG 15], and the determinations including vector mesons are larger.

Chapter 8

$\eta^{(\prime)} \to \pi^+\pi^-\gamma^{(*)}$

At leading order, the decays $\eta^{(\prime)} \to \pi^+\pi^-\gamma^{(*)}$ are determined by the chiral box anomaly, which is contained in the Wess-Zumino-Witten Lagrangian. However, since the dynamical range of the decay involving a real photon, $4M_\pi^2 \le s_{\pi\pi} \le M_{\eta^{(\prime)}}^2$, is far from the chiral limit, higher-order corrections become important and their influence needs to be studied. Besides the decay widths, also the decay spectra have been measured for both the η and the η' decay. The photon-energy spectrum of $\eta \to \pi^+\pi^-\gamma$ is provided by the WASA@COSY collaboration [Adl+ 12]. Earlier measurements have been performed in Refs. [Gor+ 70, Lay+ 73], but are presented without acceptance corrections. The $\pi^+\pi^-$ invariant-mass spectrum of $\eta' \to \pi^+\pi^-\gamma$ has been measured by the Crystal Barrel collaboration [Abe+ 97]. The decays $\eta^{(\prime)} \to \pi^+\pi^-l^+l^-$, where $l = e,\ \mu$, probe the decays involving a virtual photon $\eta^{(\prime)} \to \pi^+\pi^-\gamma^*$ and provide information on the substructure of the decaying meson. For these decays, the decay widths $\Gamma(\eta^{(\prime)} \to \pi^+\pi^-e^+e^-)$ have been measured [Oli+ 14], whereas for $\Gamma(\eta^{(\prime)} \to \pi^+\pi^-\mu^+\mu^-)$ only upper limits are provided [Oli+ 14].

8.1 Calculation of the invariant amplitude

The invariant amplitude can be parametrized by

$$\mathcal{M} = -iF\epsilon_{\mu\nu\alpha\beta}\epsilon^\mu p_1^\nu p_2^\alpha q^\beta, \tag{8.1}$$

where q^μ and ϵ^μ denote the momentum and polarization of the photon, respectively, and p_1^μ, p_2^μ are the momenta of the pions with $s_{\pi\pi} = (p_1 + p_2)^2$. To obtain the invariant amplitude up to NNLO, we have to evaluate the Feynman diagrams shown in Fig. 8.1, where the vertices are obtained from

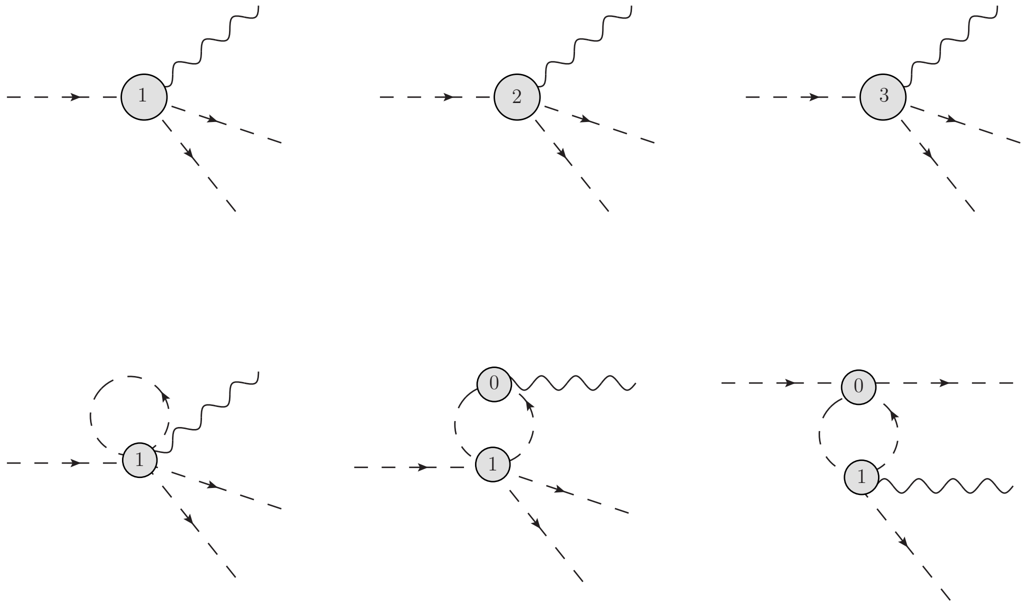

Figure 8.1: Feynman diagrams for $\eta^{(\prime)} \to \pi^+\pi^-\gamma^*$ up to NNLO. Dashed lines refer to pseudoscalar mesons and wiggly lines to photons. The numbers k in the interaction blobs refer to vertices derived from the corresponding Lagrangians $\mathcal{L}^{(k)}$.

the Lagrangians given in Chapter 4. We start the calculation by considering the general case of the quark-charge matrix $Q(N_c)$ for arbitrary N_c (see Sec. 4.4.1). However, in the calculation of the Feynman diagrams, it turns out that, due to the flavor structure, the N_c-dependent part of $Q(N_c)$ gives no contribution to the matrix element. Again, we employ the *Mathematica* package FEYNCALC [MBD 91] for the calculation of the Feynman diagrams. At LO, the form factors F are given by

$$F(\eta \to \pi^+\pi^-\gamma^*) = \frac{1}{4\sqrt{3}\pi^2 F_\pi^3}\left(\cos(\theta^{[0]}) - \sqrt{2}\sin(\theta^{[0]})\right), \tag{8.2}$$

$$F(\eta' \to \pi^+\pi^-\gamma^*) = \frac{1}{4\sqrt{3}\pi^2 F_\pi^3}\left(\sin(\theta^{[0]}) + \sqrt{2}\cos(\theta^{[0]})\right), \tag{8.3}$$

where $\theta^{[0]} = -19.6°$ is the LO mixing angle. At NLO, the form factors F read

$$
\begin{aligned}
&F(\eta \to \pi^+\pi^-\gamma^*) \\
&= \frac{1}{4\sqrt{3}\pi^2 F_\pi^3}\Big(\Big(\cos(\theta^{[1]}) - \sqrt{2}\sin(\theta^{[1]})\Big)\left(1 + c_{14}M_\eta^2 + c_{13}M_\pi^2 - c_{14}q^2 + c_{15}s_{\pi\pi}\right) \\
&\quad -\sqrt{2}\sin(\theta^{[1]})c_2\Big), \qquad (8.4) \\
&F(\eta' \to \pi^+\pi^-\gamma^*) \\
&= \frac{1}{4\sqrt{3}\pi^2 F_\pi^3}\Big(\Big(\sin(\theta^{[1]}) + \sqrt{2}\cos(\theta^{[1]})\Big)\left(1 + c_{14}M_{\eta'}^2 + c_{13}M_\pi^2 - c_{14}q^2 + c_{15}s_{\pi\pi}\right) \\
&\quad +\sqrt{2}\cos(\theta^{[1]})c_2\Big), \qquad (8.5)
\end{aligned}
$$

where

$$
\begin{aligned}
c_2 &= -48\pi^2\tilde{L}_1 - \frac{\Lambda_1}{2}, \\
c_{13} &= -1024\pi^2\left(L_{13}^{6,\epsilon} + L_{14}^{6,\epsilon} + L_5^{6,\epsilon} + \frac{L_6^{6,\epsilon}}{2}\right), \\
c_{14} &= 512\pi^2 L_{13}^{6,\epsilon}, \\
c_{15} &= 512\pi^2\left(2L_{13}^{6,\epsilon} + L_{14}^{6,\epsilon}\right), \qquad (8.6)
\end{aligned}
$$

and $\theta^{[1]}$ is the mixing angle calculated up to NLO, given in Eq. (5.33) in Sec. 5.1. The parameter c_2 represents a QCD-scale-invariant combination of OZI-rule-violating parameters [KL 00]. Since the expressions at NNLO are very long, we only display the loop corrections, corresponding to the loop diagrams in Fig. 8.1, in Appendix B.2. However, the tree-level contributions can be provided as a *Mathematica* notebook. Similar to the case of the two-photon decays (see Sec. 7.1), at NNLO, we have to deal with a proliferation of LECs and the fact that the $\mathcal{O}(p^8)$ Lagrangian has not been constructed. Therefore, we make an ansatz for the form factors at NNLO:

$$F_\eta(s_{\pi\pi}) = F_\eta^{\mathrm{LO}} + \frac{1}{4\sqrt{3}\pi^2 F_\pi^3}\left(b_\eta + c_\eta s_{\pi\pi} + d_\eta s_{\pi\pi}^2\right) + loops_\eta(s_{\pi\pi}), \qquad (8.7)$$

$$F_{\eta'}(s_{\pi\pi}) = F_{\eta'}^{\mathrm{LO}} + \frac{1}{4\sqrt{3}\pi^2 F_\pi^3}\left(b_{\eta'} + c_{\eta'} s_{\pi\pi} + d_{\eta'} s_{\pi\pi}^2\right) + loops_{\eta'}(s_{\pi\pi}), \qquad (8.8)$$

where F_P^{LO} are the LO form factors given in Eqs. (8.2) and (8.3), and the expression $loops_P(s_{\pi\pi})$ refers to the $s_{\pi\pi}$-dependent parts of the loop corrections. The parameters b_P and c_P receive contributions from the higher-order Lagrangians in Chapter 4 as well as from, in principle, the $\mathcal{O}(p^8)$ Lagrangian.

In addition, the LECs and loop contributions originating from the η-η' mixing are also absorbed in b_P and c_P. The parameters d_P consist solely of terms from the $\mathcal{O}(p^8)$ Lagrangian. However, the most general form factor at NNLO could depend on a second kinematic variable t or u. This dependence would be introduced by the $\mathcal{O}(p^8)$ Lagrangian. For simplicity, we ignore those contributions in the following and employ the ansatz in Eqs. (8.7) and (8.8).

A measurable observable of the decay is provided by the differential cross section as a function of the photon energy

$$\omega = \frac{1}{2}\left(M_P - \frac{s_{\pi\pi}}{M_P}\right), \tag{8.9}$$

which takes the form [Hac 08]

$$\frac{d\Gamma}{d\omega} = \frac{M_P\omega^3(M_P^2 - 4M_\pi^2 - 2M_P\omega)}{384\pi^3}\sqrt{1 - \frac{4M_\pi^2}{M_P^2 - 2M_P\omega}}|F(P \to \pi^+\pi^-\gamma)|^2. \tag{8.10}$$

The full decay width can be obtained by integration

$$\Gamma(P \to \pi^+\pi^-\gamma) = \int_0^{\frac{1}{2}(M_P - 4M_\pi^2/M_P)} d\omega \frac{d\Gamma}{d\omega}. \tag{8.11}$$

8.2 Numerical analysis

To evaluate our results numerically we need to fix the LECs. This is done in a successive way, starting at LO and proceeding to NLO and, finally, to NNLO.

8.2.1 LO

At LO, we can directly calculate the decay widths by using Eq. (8.11) together with the form factors in Eqs. (8.2) and (8.3). The LO results are

$$\Gamma(\eta \to \pi^+\pi^-\gamma) = 36 \text{ eV}, \tag{8.12}$$
$$\Gamma(\eta' \to \pi^+\pi^-\gamma) = 3.4 \text{ keV}, \tag{8.13}$$

which, in particular for the η', are a lot smaller than the experimental values $\Gamma(\eta \to \pi^+\pi^-\gamma) = (55.3\pm2.4)$ eV [Oli+ 14] and $\Gamma(\eta' \to \pi^+\pi^-\gamma) = (57.6\pm2.8)$ keV [Oli+ 14]. Employing Equation (8.10) with the LO form factors, we also determine the spectra at LO and compare them to the experimental data.

Since the data are provided in arbitrary units, we multiply our LO results for the spectra by a normalization constant A_P, $P = \eta,\ \eta'$, and determine this constant through a fit to the data. For $\eta \to \pi^+\pi^-\gamma$ we use the full photon-energy spectrum provided by Ref. [Adl+ 12], and for $\eta' \to \pi^+\pi^-\gamma$ we fit our results to the $\pi^+\pi^-$ invariant-mass spectrum, measured in Ref. [Abe+ 97], up to 0.59 GeV. The results are shown in Fig. 8.2. As one can clearly see, the LO description is very poor and it is crucial to take higher-order corrections into account.

8.2.2 NLO

At NLO, we determine the appearing LECs through a fit to the experimental spectra of the decays. It is not possible to independently determine all NLO LECs in the expressions for the NLO form factors in Eqs. (8.4) and (8.5). We are only able to fix those linear combinations of LECs which accompany independent $s_{\pi\pi}$ structures. The NLO form factors in terms of these linear combinations of LECs are given by

$$F_\eta(s_{\pi\pi}) = \frac{1}{4\sqrt{3}\pi^2 F_\pi^3}\left(\left(\cos(\theta^{[1]}) - \sqrt{2}\sin(\theta^{[1]})\right)(1 + c_{15}s_{\pi\pi}) + c_3\right), \quad (8.14)$$

$$F_{\eta'}(s_{\pi\pi}) = \frac{1}{4\sqrt{3}\pi^2 F_\pi^3}\left(\left(\sin(\theta^{[1]}) + \sqrt{2}\cos(\theta^{[1]})\right)(1 + c_{15}s_{\pi\pi}) + c_4\right), \quad (8.15)$$

where $\theta^{[1]}$ is the mixing angle calculated up to NLO, given in Eq. (5.33) in Sec. 5.1, and

$$\begin{aligned} c_3 &= \left(\cos(\theta^{[1]}) - \sqrt{2}\sin(\theta^{[1]})\right)\left(c_{13}M_\pi^2 + c_{14}M_\eta^2\right) - \sqrt{2}\sin(\theta^{[1]})\, c_2, \\ c_4 &= \left(\sin(\theta^{[1]}) + \sqrt{2}\cos(\theta^{[1]})\right)\left(c_{13}M_\pi^2 + c_{14}M_{\eta'}^2\right) + \sqrt{2}\cos(\theta^{[1]})\, c_2. \end{aligned} \quad (8.16)$$

We now have to determine four parameters c_3, c_4, c_{15}, and the NLO mixing angle $\theta^{[1]}$. For $\theta^{[1]}$ we employ our value from the NLO I analysis in Sec. 5.4.2. The constants c_3, c_4, and c_{15} are determined through a fit to experimental data. We use the decay width of $\eta \to \pi^+\pi^-\gamma$, the photon-energy spectrum of the η decay, and the $\pi^+\pi^-$ invariant-mass spectrum of the η' decay. Since we are not able to describe the full η' spectrum, we do not include the η' decay width in our fit. We perform three simultaneous fits to the data for the η decay width [Oli+ 14], the full η spectrum from Ref. [Adl+ 12], and to the η' spectrum from Ref. [Abe+ 97] up to 0.59 GeV (I), 0.64 GeV (II), and 0.72 GeV (III). Since the experimental spectra are provided in arbitrary units, we multiply our fit functions, i.e., Eq. (8.10) with the form factors from Eqs. (8.14) and (8.15), by normalization constants A_P. The results for the fit parameters are given in Tab. 8.1, where the errors are the ones provided by the *Mathematica* fit routine NonlinearModelFit.

Fit	A_η $[10^{10}]$	$A_{\eta'}$ $[10^5]$	c_3	c_4	c_{15} $[\text{GeV}^{-2}]$
I	1.43 ± 0.09	-0.59 ± 0.56	-0.68 ± 0.06	-1.06 ± 1.02	5.78 ± 0.32
II	1.43 ± 0.09	-1.17 ± 0.49	-0.68 ± 0.06	-1.68 ± 0.38	5.78 ± 0.32
III	1.43 ± 0.09	-2.83 ± 0.58	-0.68 ± 0.06	-2.35 ± 0.16	5.78 ± 0.34

Table 8.1: Fit parameters at NLO.

The parameters A_η and c_3 appear only in the η form factor. Therefore, they are fixed by the η data, which remain the same in all three cases and do not lead to a change of the parameters. Also c_{15}, which appears in both the expression for the η and the η' form factor, seems to be determined by the η spectrum, since it does not depend on the fit range of the η' spectrum. The variation of the η' fit range is then reflected in the variation of $A_{\eta'}$ and c_4. A VMD estimate from SU(3) ChPT predicts $c_{15} = 2.53\ \text{GeV}^{-2}$ [Hac 08]. Our value for c_{15} is more than twice as large.

The NLO results for the η and η' spectra are shown in Fig. 8.2 together with the LO results obtained in Sec. 8.2.1 and the experimental data. The 1σ error bands of the fits of the η' spectra are displayed in Fig. 8.3.

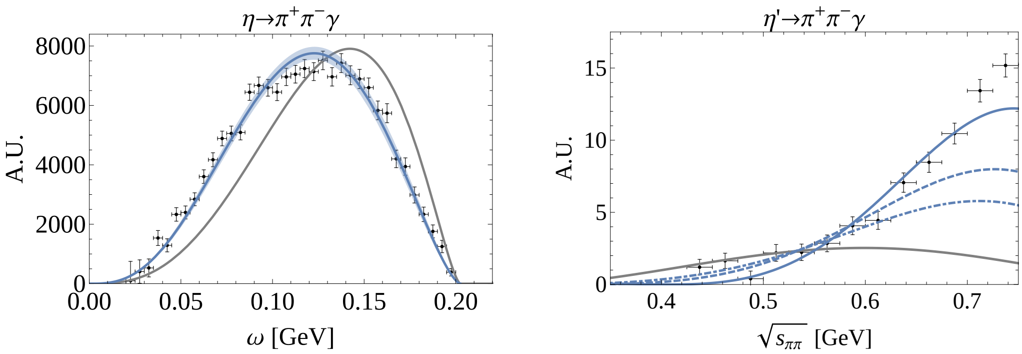

Figure 8.2: Left: Photon-energy spectrum of $\eta \to \pi^+\pi^-\gamma$ at LO (gray) and NLO (blue). The blue band is the 1σ error band. The experimental data are taken from Ref. [Adl+ 12]. Right: Invariant-mass spectrum of the $\pi^+\pi^-$ system in $\eta' \to \pi^+\pi^-\gamma$ at LO (gray) and NLO (blue) fitted up to 0.59 GeV (dash-dotted), 0.64 GeV (dashed), 0.72 GeV (solid). The experimental data are taken from Ref. [Abe+ 97].

For both the η and the η' spectrum, the NLO description is a clear improvement in comparison to the LO result. At NLO, increasing the fit range

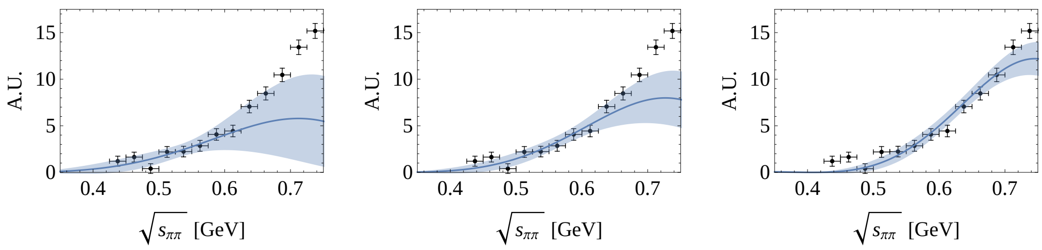

Figure 8.3: Invariant-mass spectrum of the $\pi^+\pi^-$ system in $\eta' \to \pi^+\pi^-\gamma$ with the 1σ error band at NLO fitted up to 0.59 GeV (left), 0.64 GeV (middle), 0.72 GeV (right). The experimental data are taken from Ref. [Abe+ 97].

of the η' spectrum leads to a better description of the data at higher $s_{\pi\pi}$, but it worsens at lower $s_{\pi\pi}$. The error bands become smaller as more data are included in the fit.

8.2.3 NNLO

At NNLO, we employ the ansatz for the form factors in Eqs. (8.7) and (8.8). Since the form factors for η and η' each have their specific set of LECs, we perform the fits to their data separately. The normalization A_η and the LECs b_η, c_η, d_η are fixed through a simultaneous fit to the η decay width [Oli+ 14] and the photon-energy spectrum [Adl+ 12]. We consider four different scenarios. The first is the full NNLO calculation (Full). Then we switch off the loop contributions (W/O loops). Finally, we put the d_η term to zero, and we also discuss the case without d_η and without loop contributions. The results are shown in Tab. C.6 in Appendix C. Then, all four scenarios are discussed for the η'. Since we cannot describe the full η' spectrum, we do not include the decay width in the fit. Therefore, when the loop contributions are switched off, we are not able to extract the overall normalization separately. In those cases, we can only fit the spectrum induced by the form factor

$$F_{\eta'}(s_{\pi\pi}) = F_{\eta'}^{\mathrm{LO}} + \frac{1}{4\sqrt{3}\pi^2 F_\pi^3}\left(\tilde{c}_{\eta'} s_{\pi\pi} + \tilde{d}_{\eta'} s_{\pi\pi}^2\right) \tag{8.17}$$

multiplied by the normalization constant $\tilde{A}_{\eta'}$. The relation to the parameters given in Eq. (8.8) (without $loops_P(s_{\pi\pi})$), with the original normalization $A_{\eta'}$, takes the form

$$\sqrt{\tilde{A}_{\eta'}} = \frac{\sin(\theta^{[0]}) + \sqrt{2}\cos(\theta^{[0]}) + b_{\eta'}}{\sin(\theta^{[0]}) + \sqrt{2}\cos(\theta^{[0]})}\sqrt{A_{\eta'}},$$
$$\tilde{c}_{\eta'} = \frac{\sin(\theta^{[0]}) + \sqrt{2}\cos(\theta^{[0]})}{\sin(\theta^{[0]}) + \sqrt{2}\cos(\theta^{[0]}) + b_{\eta'}} c_{\eta'},$$
$$\tilde{d}_{\eta'} = \frac{\sin(\theta^{[0]}) + \sqrt{2}\cos(\theta^{[0]})}{\sin(\theta^{[0]}) + \sqrt{2}\cos(\theta^{[0]}) + b_{\eta'}} d_{\eta'}, \tag{8.18}$$

where $\theta^{[0]} = -19.6°$ is the LO mixing angle. In the scenarios including loops, the loop contributions provide additional independent $s_{\pi\pi}$ structures, so we can try to extract the LECs and the overall normalization separately. The results with and without loops are provided in Tabs. C.7 and C.8 in Appendix C, respectively.

Figure 8.4 shows our LO, NLO, and NNLO predictions for the η spectrum together with the experimental data. The description of the spectrum

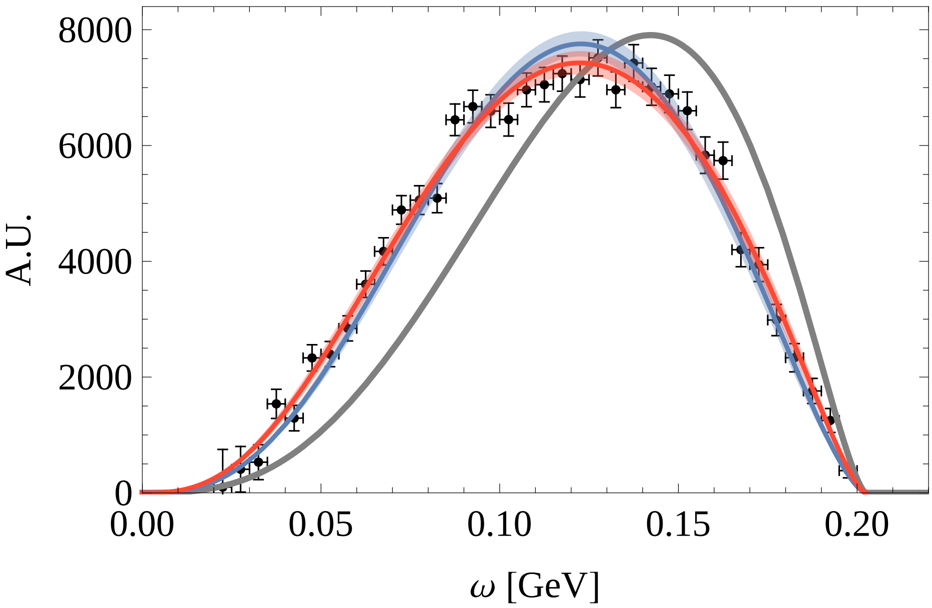

Figure 8.4: Photon-energy spectrum of $\eta \to \pi^+\pi^-\gamma$ at LO (gray), NLO (blue) and NNLO (red). For the NLO and NNLO results the corresponding 1σ error bands are shown. The experimental data are taken from Ref. [Adl+ 12].

improves gradually from LO to NLO to NNLO. We find that the contributions of the loops to the shape of the spectrum are very small and can be compensated by a change of the LECs. The improved description of the data from NLO to NNLO is due to the inclusion of the $s_{\pi\pi}^2$ term.

Figure 8.5 shows the results of the fits of the NNLO expression for the η' spectrum without $s_{\pi\pi}^2$ term to the experimental data in the three different fit ranges. The corresponding error bands are displayed in Fig. D.3 in Appendix D. Here, we observe a better description of the data compared to the NLO

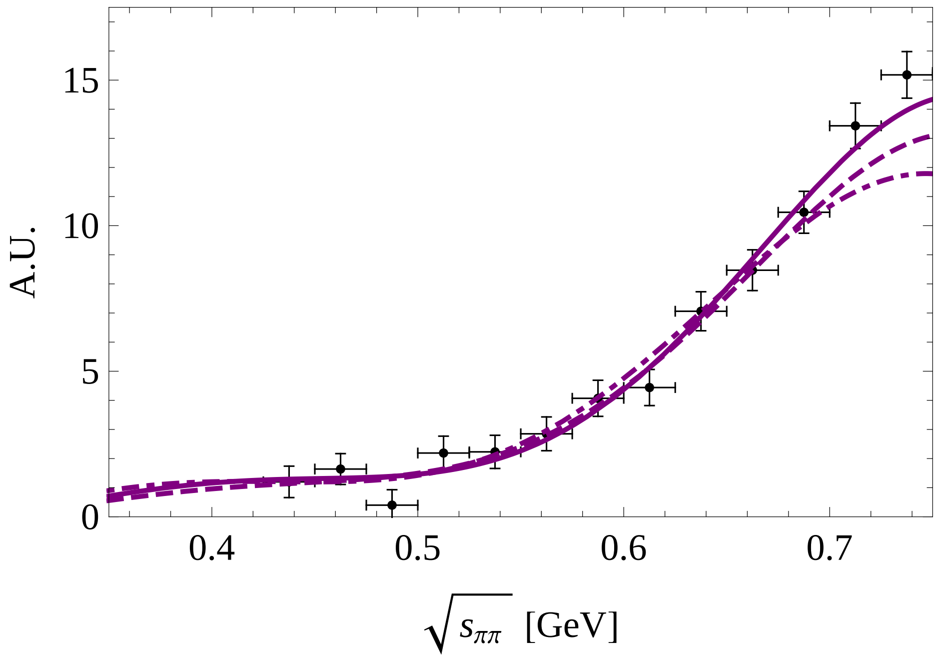

Figure 8.5: Invariant-mass spectrum of the $\pi^+\pi^-$ system in $\eta' \to \pi^+\pi^-\gamma$ at NNLO with $d_{\eta'} = 0$, fitted up to 0.59 GeV (dash-dotted), 0.64 GeV (dashed), 0.72 GeV (solid). The experimental data are taken from Ref. [Abe+ 97].

calculation due to the inclusion of the loop corrections. Taking the $s_{\pi\pi}^2$ term into account in the full NNLO expression tends to make the fit unstable, in particular in the cases where the fit range is small. Therefore, we discuss here only the results of the fits up to 0.72 GeV (III) and the results of the other fits are shown in Fig. D.4 in Appendix D. Figure 8.6 shows a comparison of our NLO, NNLO without $d_{\eta'}$ term, and full NNLO results for the η' spectrum fitted up to 0.72 GeV. At such high values of $s_{\pi\pi}$, the inclusion of the $d_{\eta'}$ term yields a better description of the data compared to NNLO with $d_{\eta'} = 0$. However, as can be seen in Fig. 8.6, even the full NNLO result is not able to describe the whole spectrum. This problem originates in the fact that, since the invariant mass of the pion pair reaches values as high as 0.8 GeV, vector-meson degrees of freedom become important. Since we do not consider vector mesons as explicit degrees of freedom in our calculation, we cannot reproduce the whole spectrum correctly.

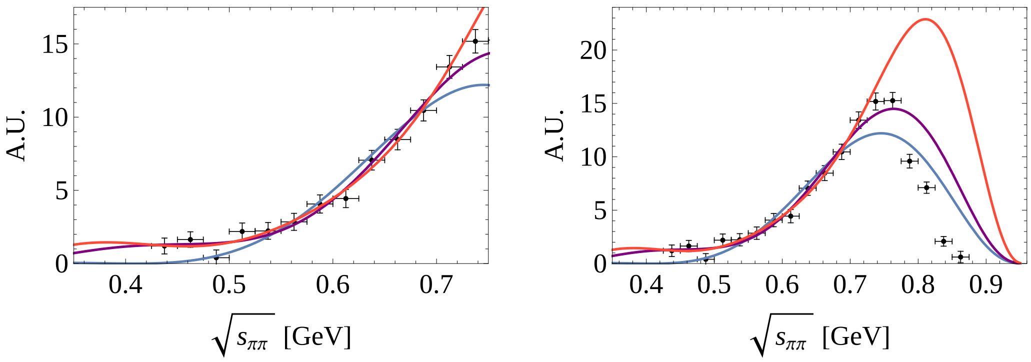

Figure 8.6: Invariant-mass spectrum of the $\pi^+\pi^-$ system in $\eta' \to \pi^+\pi^-\gamma$ at NLO (blue), NNLO with $d_{\eta'} = 0$ (purple), and full NNLO (red) fitted up to 0.72 GeV. The left plot shows the spectrum up to 0.75 GeV and the right plot the full spectrum. The experimental data are taken from Ref. [Abe+ 97].

Comparison with other works

The decay $\eta \to \pi^+\pi^-\gamma$ has been studied in one-loop ChPT using the LO η-η' mixing in Refs. [BBC 90, Hac 08]. They have found that $\mathcal{O}(p^6)$ corrections are crucial to describe the data, and that the contributions of the contact terms dominate over the loop corrections. We agree with these findings. Reference [BN 04b] investigates the decays $\eta^{(\prime)} \to \pi^+\pi^-\gamma$ in an approach that combines ChPT with a coupled-channel Bethe-Salpeter equation which generates vector mesons dynamically. They also observe the importance of $\mathcal{O}(p^6)$ contact terms in order to describe the data for the η decay. The η' data however, cannot be described by just adjusting the $\mathcal{O}(p^6)$ contact terms. In the decay $\eta' \to \pi^+\pi^-\gamma$, vector mesons play an important role and, after the inclusion of the coupled-channel approach, the experimental η' spectrum can be reproduced. The effects of vector mesons have been taken into account by a momentum dependent vector-meson-dominance model [Pic 92] or in a more elaborate way in the context of Hidden Local Symmetries [Ben+ 03, Ben+ 10]. References [VH 98, Hol 02] apply an Omnes function on top of the one-loop results to include the effects of p-wave pion scattering. Another approach consists in the combination of ChPT with dispersion theory allowing for a controlled inclusion of resonance physics [Sto+ 12]. Due to the inclusion of pion-pion rescattering in the final state both the η and the η' spectrum can be well described. Reference [KP 15] augments this analysis of the $\eta \to \pi^+\pi^-\gamma$ decay by the a_2 tensor meson.

8.3 $\eta^{(\prime)} \to \pi^+\pi^- l^+ l^-$

In the following, we investigate the decays involving a virtual photon $\eta^{(\prime)} \to \pi^+\pi^-\gamma^*$, which are connected to the decays $\eta^{(\prime)} \to \pi^+\pi^- l^+ l^-$, with a lepton pair $l = e,\ \mu$. The matrix element for the decay $\eta^{(\prime)} \to \pi^+\pi^-\gamma^*$ is given by

$$\mathcal{M} = -iF\epsilon_{\mu\nu\alpha\beta}\epsilon^\mu p_+^\nu p_-^\alpha q^\beta, \tag{8.19}$$

where q^μ and ϵ^μ denote the momentum and polarization of the photon, respectively, and p_+^μ, p_-^μ are the momenta of the pions. The decay $\eta^{(\prime)} \to \pi^+\pi^- l^+ l^-$ proceeds via a two-step mechanism [PR 93, BN 07]. The first decay is $\eta^{(\prime)} \to \pi^+\pi^-\gamma^*$ which is followed by $\gamma^* \to l^+ l^-$. We can obtain the invariant amplitude for $\eta^{(\prime)} \to \pi^+\pi^- l^+ l^-$ from a modification of the one in Eq. (8.19). The photon is now off shell and we replace its polarization vector ϵ^μ by $(e/q^2)\bar{u}(k^-)\gamma^\mu v(k^+)$, where $k^\pm$ are the lepton momenta. After this modification the invariant amplitude reads

$$\mathcal{M} = -iF\epsilon_{\mu\nu\alpha\beta}p_+^\nu p_-^\alpha q^\beta \left[\frac{e}{q^2}\bar{u}(k^-)\gamma^\mu v(k^+)\right]. \tag{8.20}$$

The form factors F have been calculated in Sec. 8.1. We can then calculate the differential decay rates of $\eta^{(\prime)} \to \pi^+\pi^- l^+ l^-$ in terms of the normalized invariant mass of the pion pair $x = (p^+ + p^-)^2/M_P^2 \equiv s_{\pi\pi}/M_P^2$ and the normalized invariant mass of the lepton pair $y = (k^+ + k^-)^2/M_P^2 \equiv q^2/M_P^2$, where $P = \eta,\ \eta'$. The differential decay width is given by [PR 93]

$$\frac{d^2\Gamma}{dxdy} = \frac{e^2 M_P^7}{18(4\pi)^5}\frac{\lambda^{3/2}(1,x,y)\lambda^{1/2}(y,\nu^2,\nu^2)\lambda^{3/2}(x,\mu^2,\mu^2)}{x^2y^2}\left(\frac{1}{4}+\frac{\nu^2}{2y}\right)|F|^2, \tag{8.21}$$

where $\lambda(x,y,z) = x^2+y^2+z^2-2xy-2xz-2yz$, $\mu = M_\pi/M_P$, and $\nu = m_l/M_P$. The spectrum with respect to x is obtained by integrating over y

$$\frac{d\Gamma}{dx} = \int_{4m_l^2/M_P^2}^{1-2\sqrt{x}+x} dy \frac{d^2\Gamma}{dxdy}, \tag{8.22}$$

whereas the integration over x leads to the spectrum with respect to y

$$\frac{d\Gamma}{dy} = \int_{4M_\pi^2/M_P^2}^{1-2\sqrt{y}+y} dx \frac{d^2\Gamma}{dxdy}. \tag{8.23}$$

The full decay width of $\eta^{(\prime)} \to \pi^+\pi^- l^+ l^-$ is given by

$$\Gamma(P \to \pi^+\pi^- l^+ l^-) = \int_{4M_\pi^2/M_P^2}^{1-2\sqrt{4m_l^2/M_P^2}+4m_l^2/M_P^2} dx \int_{4m_l^2/M_P^2}^{1-2\sqrt{x}+x} dy \frac{d^2\Gamma}{dxdy}. \tag{8.24}$$

8.3.1 Numerical analysis

While at LO the numerical evaluation of the results can be performed directly, at NLO we need to fix four constants c_3, c_4, c_{15}, and c_{14}. For the parameters c_3, c_4, c_{15} we employ the values determined from the decays to real photons $\eta^{(\prime)} \to \pi^+\pi^-\gamma$ at NLO in Tab. 8.1. The parameter c_{14} is multiplied by the photon virtuality q^2 and needs to be fixed using data for the decays $\eta^{(\prime)} \to \pi^+\pi^-l^+l^-$ involving a virtual photon. The only available data for these decays are the decay widths for $\eta^{(\prime)} \to \pi^+\pi^-e^+e^-$ [Oli+ 14], while for the decay widths of $\eta^{(\prime)} \to \pi^+\pi^-\mu^+\mu^-$ only upper limits exist [Oli+ 14]. The spectra of these decays have not been measured. Since we are not able to describe the full $\eta' \to \pi^+\pi^-\gamma$ spectrum due to the importance of resonant contributions, we also expect that the description of the $\eta' \to \pi^+\pi^-e^+e^-$ decay is not appropriate in our framework. Therefore, if we want to determine c_{14} from experimental data, we are left with only the decay width of $\eta \to \pi^+\pi^-e^+e^-$. Our naive attempt is to fix c_{14} to the experimental value of $\Gamma(\eta \to \pi^+\pi^-e^+e^-) = 350 \pm 20$ meV [Oli+ 14], which results in $c_{14} = (-9.67 \pm 33.06)\ \mathrm{GeV}^{-2}$. However, it turns out that $\Gamma(\eta \to \pi^+\pi^-e^+e^-)$ is not very sensitive to the value of c_{14} and the NLO result for $c_{14} = 0$ is already close to the experimental value. This can be also seen in the left plot of Fig. 8.7 which shows the $\pi^+\pi^-$ invariant-mass spectrum. The curves for $c_{14} = -9.67\ \mathrm{GeV}^{-2}$ and for $c_{14} = 0$

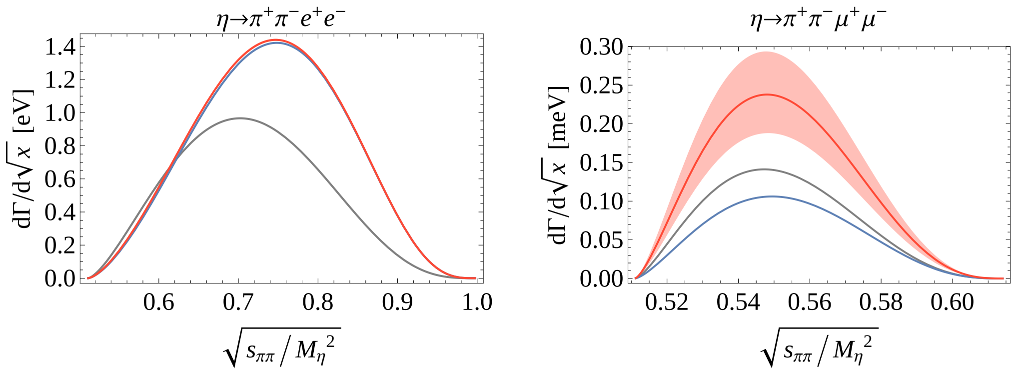

Figure 8.7: Invariant-mass spectra of the $\pi^+\pi^-$ system in $\eta \to \pi^+\pi^-l^+l^-$ at LO (gray), NLO with $c_{14} = 0$ (blue) and NLO (red). The bands correspond to the assumption of an 33% error in c_{14}.

are very similar. Moreover, the error of c_{14} due to the experimental error of $\Gamma(\eta \to \pi^+\pi^-e^+e^-)$ is very large. Therefore, in the following discussions, we consider only the systematic error of c_{14}. The red band shows the variation assuming an 33% error in c_{14}, which is also rather small. A naive VMD estimate for c_{14} is given by $c_{14} = -2.53\ \text{GeV}^{-2}$ [Hac 08], which is roughly of the same order of magnitude as our value $c_{14} = -9.67\ \text{GeV}^{-2}$. Figure 8.7 shows also the prediction for the $\pi^+\pi^-$ invariant-mass spectrum of $\eta \to \pi^+\pi^-\mu^+\mu^-$. Due to the larger invariant mass of the muon pair the photon virtuality

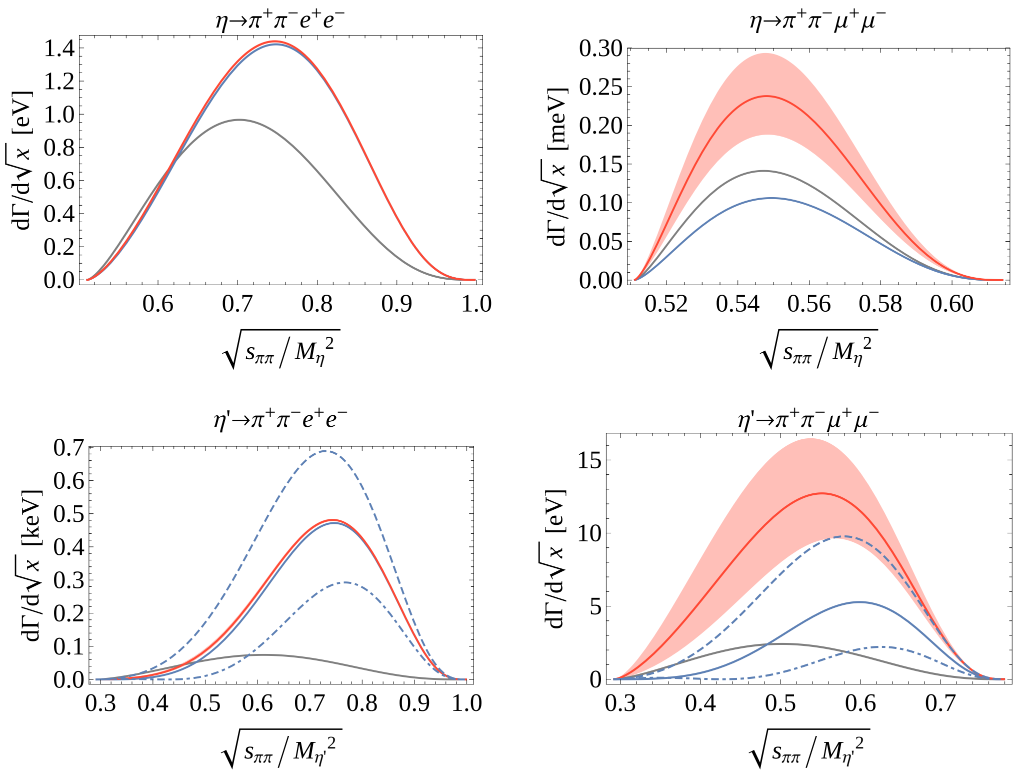

Figure 8.8: Invariant-mass spectra of the $\pi^+\pi^-$ system at LO (gray), NLO with $c_{14} = 0$ (blue) and NLO with $c_{14} = -9.67\ \text{GeV}^{-2}$ (red). The values for c_4 are taken from fit I (dashed), II (solid), III (dash-dotted).

is increased and the decay is more sensitive to c_{14}. Here, the error band is large and the result is different from the LO result and the one for $c_{14} = 0$. This decay would be better suited to determine c_{14}, but unfortunately no experimental data exist. From this analysis we conclude that our value for c_{14} cannot be well determined from $\Gamma(\eta \to \pi^+\pi^- e^+ e^-)$ and might not be very sensible. In the following, in order to obtain an estimate of the influence of c_{14}, we employ the naive value of $c_{14} = -9.67\ \text{GeV}^{-2}$ with an error of 33%. We show the invariant-mass spectra of the $\pi^+\pi^-$ and l^+l^- systems at NLO for all four decays $\eta^{(\prime)} \to \pi^+\pi^- l^+ l^-$ in Figs. 8.8 and 8.9, respectively. They are compared to the LO results and the NLO results for $c_{14} = 0$. For the η' decays we also show the predictions for the three different values of c_4

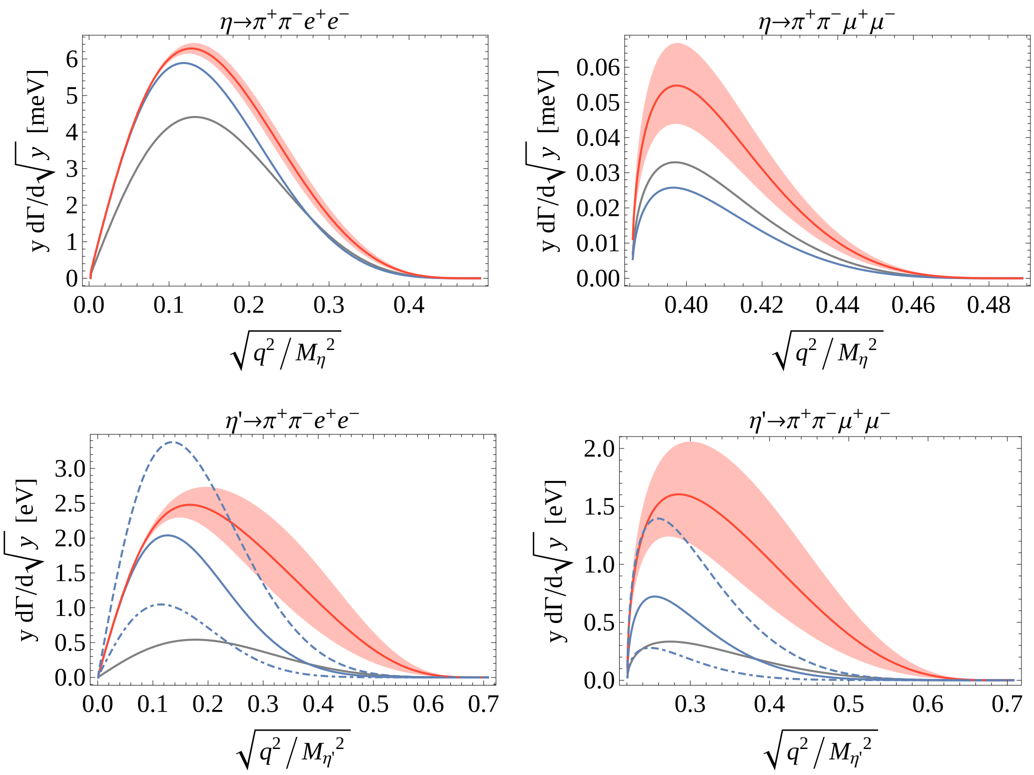

Figure 8.9: Invariant-mass spectra of the l^+l^- system at LO (gray), NLO with $c_{14} = 0$ (blue) and NLO with $c_{14} = -9.67\ \text{GeV}^{-2}$ (red). The values for c_4 are taken from fit I (dashed), II (solid), III (dash-dotted).

determined in Tab. 8.1 in Sec. 8.2.2 corresponding to the different fit ranges of the $\eta' \to \pi^+\pi^-\gamma$ spectrum.

In general, the LO and NLO spectra differ a lot. The NLO corrections tend to produce steeper and larger peaks compared to the LO predictions. The curves for $c_{14} = 0$ and $c_{14} = -9.67\ \mathrm{GeV}^{-2}$ coincide approximately for the decays involving an e^+e^- pair and differ in the cases with a muon pair. The different values for c_4 have a very strong influence on the η' spectra.

At NNLO, in addition to the parameters determined from $\eta^{(\prime)} \to \pi^+\pi^-\gamma$ more unknown LECs, multiplying possible structures in the form factors like $(q^2)^2$ or $q^2 s_{\pi\pi}$, appear. Therefore, we do not numerically evaluate the full NNLO expressions. At this order the loops start contributing. For completeness, in order to provide an estimate of the size of the loop corrections, we evaluate the scenario where we just add the loops to the LO expressions. The corresponding spectra are shown in Figs. D.5 and D.6 in Appendix D. We observe rather large effects of the loops on the spectra comparable in size to the NLO corrections.

Finally, we integrate the spectra and obtain predictions for the full decay widths of $\eta' \to \pi^+\pi^- l^+ l^-$. The results are displayed in Tab. 8.2. Since this is only a first study of the decays $\eta^{(\prime)} \to \pi^+\pi^- l^+ l^-$ to obtain a rough estimate of the higher-order corrections, we do not provide errors for the results of the decay widths. The values of the η decay widths do not change in the

	$\Gamma_{\eta\to\pi^+\pi^-e^+e^-}$ [10^{-10} GeV]	$\Gamma_{\eta'\to\pi^+\pi^-e^+e^-}$ [10^{-7} GeV]	$\Gamma_{\eta\to\pi^+\pi^-\mu^+\mu^-}$ [10^{-15} GeV]	$\Gamma_{\eta'\to\pi^+\pi^-\mu^+\mu^-}$ [10^{-9} GeV]
LO	2.34	0.26	7.20	0.59
NLO II	3.51	1.37	12.23	3.17
NLO c14=0 I	3.46	1.31	5.50	1.06
NLO c14=0 II	3.46	2.06	5.50	2.18
NLO c14=0 III	3.46	0.72	5.50	0.37
LO+Loops	1.81	1.13	5.16	2.50
Data [Oli+ 14]	3.5 ± 0.2	$4.8^{+2.6}_{-2.0}$	$< 4.7 \cdot 10^5$	< 5.7
VMD [PR 93]	3.8	-	-	-
[FFK 00]	4.72	3.56	15.72	3.96
CC [BN 07]	$3.89^{+0.10}_{-0.13}$	$4.31^{+0.38}_{-0.64}$	$9.8^{+5.8}_{-3.5}$	$3.2^{+2.0}_{-1.6}$
Hidden gauge [Pet 10]	4.11 ± 0.27	4.3 ± 0.46	11.33 ± 0.67	4.36 ± 0.63
Modif. VMD [Pet 10]	3.96 ± 0.22	4.49 ± 0.33	11.32 ± 0.54	4.77 ± 0.54

Table 8.2: Results for the decay widths of $\eta^{(\prime)} \to \pi^+\pi^- l^+ l^-$. At NLO, the value of c_4 is determined by the fits I-III in Sec. 8.2.2.

scenarios "NLO c14=0 I-III", since they correspond to a variation of c_4 which only appears in the η' form factor. The NLO corrections increase the value for $\Gamma_{\eta\to\pi^+\pi^-e^+e^-}$ compared to the LO one, providing results that are close to the experimental value. The LO value for $\Gamma_{\eta'\to\pi^+\pi^-e^+e^-}$ is very small. The NLO results depend quite strongly on the different values determined for c_4 and are only up to 40% of the experimental value. This is connected to the importance of vector mesons, which we have not taken into account explicitly. In addition, already the full NNLO contributions might improve our result. For $c_{14} = -9.67$ GeV^{-2}, the NLO value for $\Gamma_{\eta\to\pi^+\pi^-\mu^+\mu^-}$ is larger than the LO one, while the NLO value for $c_{14} = 0$ is even smaller than the LO result. However, the experimental limit is five orders of magnitude larger than our determinations. In the case of $\eta' \to \pi^+\pi^-\mu^+\mu^-$, the NLO values tend to increase in comparison to the LO one. As for the decays involving an electron pair, the NLO results depend strongly on c_4. The experimental limit is only twice as large as our largest results. In addition, the loops lead to a further increase of the decay width. Therefore, it could be possible to achieve a good description of this decay even in our framework without vector mesons. Since both a pion pair and a muon pair have to be created, their invariant masses do not reach values where the contributions of vector mesons start dominating. For both η decay widths the loop corrections decrease about 25% in comparison to the LO values, whereas the loops add a large positive contribution to the LO result for the η' decay widths.

Comparison with other works

In Table 8.2 we compare our results for the decay widths with other theoretical predictions. In Reference [PR 93], the decay $\eta \to \pi^+\pi^-e^+e^-$ has been studied in a chiral model that incorporates vector mesons explicitly. Reference [FFK 00] calculated various decays of light unflavored mesons using a meson-exchange model based on VMD. A chiral unitary approach that combines ChPT with a coupled-channel Bethe-Salpeter equation has been applied to the decays $\eta^{(\prime)} \to \pi^+\pi^-l^+l^-$ in Ref. [BN 07]. Reference [Pet 10] investigates the decays within the hidden gauge and a modified VMD model. The results of Refs. [BN 07, Pet 10] agree within their errors which are quite large in some cases, and the agreement is better for the decays involving e^+e^- than for those with $\mu^+\mu^-$. The results of Ref. [FFK 00] show larger deviations. Our NLO results for $\Gamma_{\eta\to\pi^+\pi^-e^+e^-}$ are slightly smaller than the other theoretical values which are larger than the experimental value. The other theoretical predictions agree within errors with the experimental value for $\Gamma_{\eta'\to\pi^+\pi^-e^+e^-}$, but they are slightly smaller and Ref. [FFK 00] shows the greatest deviation. All theory values for the decays involving a muon pair are below the experimental limits. In general, our NLO results for $\Gamma_{\eta'\to\pi^+\pi^-e^+e^-}$, $\Gamma_{\eta\to\pi^+\pi^-\mu^+\mu^-}$, and $\Gamma_{\eta'\to\pi^+\pi^-\mu^+\mu^-}$ are substantially lower than the other theoretical predictions. This can be explained by the fact that we, as opposed to the other works, have not taken the explicit contributions of vector mesons into account.

References [PR 93, BN 07, Pet 10] provide also plots of their predicted spectra. The invariant-mass spectra of the $\pi^+\pi^-$ and e^+e^- systems in $\eta \to \pi^+\pi^-e^+e^-$ agree with each other and with our NLO results for the spectra. For the spectra of $\eta \to \pi^+\pi^-\mu^+\mu^-$ with respect to $\sqrt{s_{\pi\pi}}$ and $\sqrt{q^2}$ we find qualitative agreement of our NLO results with Refs. [BN 07, Pet 10], with the difference that our peaks are a little bit higher than those of the other works. Our NLO $\pi^+\pi^-$ invariant-mass spectrum of $\eta' \to \pi^+\pi^-e^+e^-$ is much broader and lower than those in Refs. [BN 07, Pet 10], which exhibit a steep peak around 750 MeV. Less pronounced is the behavior in the e^+e^- invariant-mass spectrum, but also there our peak is broader and lower. Here, the influence of the explicit vector mesons which are included Refs. [BN 07, Pet 10] can be clearly seen. The spectra for $\eta' \to \pi^+\pi^-\mu^+\mu^-$ agree quite well between Ref. [BN 07] and our results. Only our peak in the invariant-mass spectrum of the $\mu^+\mu^-$ system is broader than in Ref. [BN 07].

In order to test the different approaches to the decays $\eta^{(\prime)} \to \pi^+\pi^-l^+l^-$, more experimental data on the decays is highly desirable. Experimental data on the differential decay spectra of any of the decays $\eta^{(\prime)} \to \pi^+\pi^-l^+l^-$ or the decays widths of $\eta^{(\prime)} \to \pi^+\pi^-\mu^+\mu^-$ would allow for an improved determination of the parameter c_{14} and might even facilitate the determination of LECs at NNLO.

Chapter 9

Conclusions

In this thesis we have studied the η-η' system in LN_cChPT. All calculations have been performed at the one-loop level, corresponding to NNLO calculations in the simultaneous expansion in external momenta, quark masses, and $1/N_c$. In the LN_c limit, the U$(1)_A$ anomaly contribution to the η' mass vanishes. Therefore, in the combined chiral and LN_c expansions, we have been able to include the η' as a ninth Goldstone boson in the effective theory.

Due to the explicit breaking of the SU(3) flavor symmetry caused by the difference of up-, down-, and strange-quark masses in the isopin-symmetric limit ($m_u = m_d \neq m_s$), the physical η and η' states are mixed singlet and octet states. We have calculated the η-η' mixing at the one-loop level up to NNLO in the simultaneous chiral and LN_c expansions. To that end, we have performed successive transformations to convert the starting effective Lagrangian in terms of octet and singlet fields into a diagonal Lagrangian in terms of the physical fields. We have derived a general expression for the η-η' mixing for a Lagrangian containing higher-derivative terms up to and including fourth order in the four momentum and general kinetic and mass terms, which have been determined in a one-loop calculation. In addition, we have calculated the axial-vector decay constants of the η-η' system at NNLO and determined the angles θ_8, θ_0 and the constants F_8, F_0 of the two-angle scheme.

Then, we have performed the numerical analysis of the results successively at LO, NLO, and NNLO. To that end, we have considered the masses M_π^2, M_K^2, M_η^2, $M_{\eta'}^2$, the decay constants F_π, F_K, the mixing angle θ, and the decay constants of the η-η' system. At NLO and especially at NNLO, we have to deal with a proliferation of unknown LECs. At NLO, we have been able to determine all appearing LECs by fixing the corresponding NLO expressions to the physical values of M_π^2, M_K^2, M_η^2, $M_{\eta'}^2$, F_π, F_K, and employing the quark mass ratio $\hat{m}/m_s$. At NNLO, however, this approach is no longer possible since the number of LECs becomes too large. This problem has been solved by our second strategy, which consists of using values for some LECs, L_i and C_i, determined in SU(3) ChPT. We have applied the appropriate matching relations between SU(3) and U(3) ChPT in order to obtain values for the LECs in U(3) ChPT. One OZI-rule-violating parameter has been determined by fixing it to M_η^2, the other five OZI-rule-violating LECs were set to zero. In general, we have found that the influence of the OZI-rule-violating parameters is rather large and their values need to be different from zero. Taking only LECs which appear in the SU(3) sector into account is not sufficient. Furthermore, the loop corrections have been found to be substantial and are rather of the order of magnitude of NLO corrections than NNLO corrections, questioning the convergence of LN_cChPT or the organization of the power counting.

Having fixed the LECs, we have obtained numerical results for the mixing angle and the decay constants of the η-η' system and compared them to other phenomenological determinations. While we find agreement for some parameters, the appearing discrepancies stem from the different treatments of OZI-rule-violating LECs, which are mostly neglected in the other works, or from the fact that the other determinations were performed in an NLO framework. Providing precise numerical results for the η-η' mixing at NNLO remains a challenge, due to the large number of unknown LECs. In the future, a determination of the NNLO LECs may be achieved with the help of Lattice QCD.

Having derived an expression for the η-η' mixing, we have been able to study two anomalous decays of the η-η' system, namely $\eta^{(\prime)} \to \gamma^{(*)}\gamma^{(*)}$ and $\eta^{(\prime)} \to \pi^+\pi^-\gamma^{(*)}$. As a benchmark for the investigation of higher-order corrections to anomalous processes or the future inclusion of vector mesons, we have first performed an explicit verification of the anomalous Ward identities at the one-loop level up to NNLO. To that end, we have calculated the three-point Green function involving one axial-vector current and two vector currents (AVV) with all three legs off shell. We have explicitly confirmed the normal Ward identities satisfied by the diagonal components of the vector currents and the anomalous Ward identities of the axial-vector current at the one-loop level.

The next step was the calculation of the decays $\eta^{(\prime)} \to \gamma^*\gamma^{(*)}$ and $\eta^{(\prime)} \to \pi^+\pi^-\gamma^{(*)}$ at the one-loop level up to NNLO. Besides the loop corrections, all contact terms appearing at NNLO have been calculated, except for those of the $\mathcal{O}(p^8)$ Lagrangian, which has not been constructed yet. However, in the expressions for the form factors describing the decays, possible structures originating from the $\mathcal{O}(p^8)$ Lagrangian have been introduced phenomenologically, accompanied by free parameters. The numerical analyses of the decays have been performed successively at LO, NLO, and NNLO. At NLO, we employed the values for the LECs and mixing angle determined in the NLO analysis of the η-η' mixing. The other LECs were fitted to the available experimental data for the decays.

We first considered the two-photon decays $\eta^{(\prime)} \to \gamma^{(*)}\gamma^{(*)}$. At NLO, the LECs from the odd-intrinsic-parity sector were fixed to the experimental data of the decay widths to real photons and the slope parameters of π^0, η, η'. We have found that the NLO results are not sufficient to describe all data simultaneously. If the N_c expansion of the quark-charge matrix is taken into account, the results worsen. At NNLO, the LECs have been determined through a fit to the experimental data for the η and η' transition form factors. We have achieved a good description of the η TFF up to 0.45 GeV and of the η' TFF between -0.25 GeV^2 and 0.3 GeV^2, which is mainly caused by the inclusion of $(q^2)^2$ terms, whereas loops do not play an important role. In addition, we have calculated the slopes and the curvatures of the TFFs and the decay widths of $\eta^{(\prime)} \to \gamma l^+l^-$, where $l = e,\ \mu$, and compared them to other works. In general, our NNLO results for those quantities tend to agree with the other experimental and theoretical determinations.

To numerically evaluate the $\eta^{(\prime)} \to \pi^+\pi^-\gamma$ decays, we have determined the LECs from the odd-intrinsic-parity sector through a fit to the decay width and the full decay spectrum of the η and to parts of the η' decay spectrum, since we are not able to adequately describe the full η' spectrum. In the case of the η, the description of the spectrum gradually improves from LO, which is far off, to NLO and NNLO, where the experimental data are well described. The higher-order contact terms play an important role and the improvement from NLO and NNLO is mainly caused by the $s_{\pi\pi}^2$ term in the form factor, whereas the loops have only a very small influence. Also in the case of the η' decay, the results gradually improve from LO to NLO and NNLO. Here, the influence of the loops is more important and the inclusion of the $s_{\pi\pi}^2$ term improves the results only if we try to describe the spectrum at high values of the $\pi^+\pi^-$ invariant mass. At NNLO, we have achieved a good description of the η' spectrum up to $\sqrt{s_{\pi\pi}} = 0.7$ GeV. At these high values of $s_{\pi\pi}$, our approach reaches its limit, since resonant contributions of vector mesons become important.

Finally, we have considered the decays $\eta^{(\prime)} \to \pi^+\pi^-l^+l^-$, $l = e,\ \mu$, which probe the decays $\eta^{(\prime)} \to \pi^+\pi^-\gamma^*$ involving a virtual photon. At NLO, the LEC c_{14}, which accompanies the photon virtuality, could only been fixed to the decay width of $\eta \to \pi^+\pi^-e^+e^-$, which is, however, not very sensitive to this parameter since the exchanged photon is close to its mass shell. As a first study, we have then evaluated the decay spectra of all four decays with respect to the invariant masses of the $\pi^+\pi^-$ and l^+l^- systems at NLO.

The NLO corrections modify the spectra substantially in comparison to the LO results. Unfortunately no experimental data for the spectra are available. We have compared our results with other theoretical determinations and find agreement in some cases. Discrepancies arise when the influence of vector-meson degrees of freedom becomes important, which have been taken into account in the other works. At NNLO, due to the appearance of additional LECs which cannot be fixed, we only evaluated the spectra for the scenario where we just added the loop corrections to the LO results. We have found that the loop contributions are of the same order of magnitude as the NLO corrections.

To further test the various theoretical approaches, more experimental information on the decay widths of $\eta^{(\prime)} \to \pi^+\pi^-\mu^+\mu^-$ or the differential spectra of any of the four decays is highly desirable. More data would also allow for a better determination of the LECs at NLO and maybe even at NNLO.

In conclusion, we have achieved a good description of the anomalous decays of the η-η' system in the low-energy region. In order to extend the range of applicability of our theory and in particular in order to describe the decay spectrum of $\eta' \to \pi^+\pi^-\gamma$, the inclusion of vector mesons as explicit degrees of freedom is necessary. The vector mesons should be included consistently in terms of constraints and renormalizability and one needs to make sure that the (anomalous) Ward identities are still satisfied. This approach could also reduce the number of independent couplings.

Appendix A

Definitions

A.1 Gell-Mann matrices

The Gell-Mann matrices λ_a ($a = 1, \ldots, 8$) are the generators of the group SU(3). An explicit representation is given by:

$$\lambda_1 = \begin{pmatrix} 0 & 1 & 0 \\ 1 & 0 & 0 \\ 0 & 0 & 0 \end{pmatrix}, \qquad \lambda_2 = \begin{pmatrix} 0 & -i & 0 \\ i & 0 & 0 \\ 0 & 0 & 0 \end{pmatrix}, \qquad \lambda_3 = \begin{pmatrix} 1 & 0 & 0 \\ 0 & -1 & 0 \\ 0 & 0 & 0 \end{pmatrix},$$
$$\lambda_4 = \begin{pmatrix} 0 & 0 & 1 \\ 0 & 0 & 0 \\ 1 & 0 & 0 \end{pmatrix}, \qquad \lambda_5 = \begin{pmatrix} 0 & 0 & -i \\ 0 & 0 & 0 \\ i & 0 & 0 \end{pmatrix}, \qquad \lambda_6 = \begin{pmatrix} 0 & 0 & 0 \\ 0 & 0 & 1 \\ 0 & 1 & 0 \end{pmatrix},$$
$$\lambda_7 = \begin{pmatrix} 0 & 0 & 0 \\ 0 & 0 & -i \\ 0 & i & 0 \end{pmatrix}, \qquad \lambda_8 = \sqrt{\frac{1}{3}} \begin{pmatrix} 1 & 0 & 0 \\ 0 & 1 & 0 \\ 0 & 0 & -2 \end{pmatrix}. \tag{A.1}$$

The Gell-Mann matrices are Hermitian, traceless 3×3 matrices satisfying the commutation relations

$$\left[\frac{\lambda_a}{2}, \frac{\lambda_b}{2}\right] = i f_{abc} \frac{\lambda_c}{2}, \tag{A.2}$$

where f_{abc} are the totally antisymmetric structure constants of SU(3). The non-vanishing structure constants are displayed in Tab. A.1. The anti-

abc	123	147	156	246	257	345	367	458	678
f_{abc}	1	$\frac{1}{2}$	$-\frac{1}{2}$	$\frac{1}{2}$	$\frac{1}{2}$	$\frac{1}{2}$	$-\frac{1}{2}$	$\frac{1}{2}\sqrt{3}$	$\frac{1}{2}\sqrt{3}$

Table A.1: Non-vanishing structure constants of SU(3).

abc	118	146	157	228	247	256	338	344
d_{abc}	$\frac{1}{\sqrt{3}}$	$\frac{1}{2}$	$\frac{1}{2}$	$\frac{1}{\sqrt{3}}$	$-\frac{1}{2}$	$\frac{1}{2}$	$\frac{1}{\sqrt{3}}$	$\frac{1}{2}$
abc	355	366	377	448	558	668	778	888
d_{abc}	$\frac{1}{2}$	$-\frac{1}{2}$	$-\frac{1}{2}$	$-\frac{1}{2\sqrt{3}}$	$-\frac{1}{2\sqrt{3}}$	$-\frac{1}{2\sqrt{3}}$	$-\frac{1}{2\sqrt{3}}$	$-\frac{1}{\sqrt{3}}$

Table A.2: Non-vanishing d_{abc}.

commutation relations of the Gell-Mann matrices read

$$\{\lambda_a, \lambda_b\} = \frac{4}{3}\delta_{ab}\mathbb{1} + 2d_{abc}\lambda_c, \tag{A.3}$$

where the totally symmetric d_{abc} are summarized in Tab. A.2. The product of two Gell-Mann matrices satisfies

$$\lambda_a\lambda_b = \frac{2}{3}\delta_{ab}\mathbb{1} + h_{abc}\lambda_c, \tag{A.4}$$

where $h_{abc} = d_{abc} + if_{abc}$, and the trace reads

$$\mathrm{Tr}(\lambda_a\lambda_b) = 2\delta_{ab}. \tag{A.5}$$

Moreover, it is convenient to introduce a ninth matrix

$$\lambda_0 = \sqrt{\frac{2}{3}}\mathbb{1}, \tag{A.6}$$

such that Eq. (A.5) is still satisfied by the nine matrices λ_a. Then, the set $\{i\lambda_a | a = 0, \ldots, 8\}$ provides a basis of the Lie algebra u(3) of U(3).

A.2 Loop integrals

In this section, we define the loop integrals which are needed for the calculations in this thesis. All loop integrals are reduced to scalar integrals [PV 79] employing the *Mathematica* package FEYNCALC [MBD 91]. Therefore, we only display the scalar integrals, which are defined in dimensional regularization:

Integral with one internal line

$$A_0(m^2) = \frac{(2\pi\mu)^{4-n}}{i\pi^2}\int \frac{d^nk}{k^2 - m^2 + i0^+}. \tag{A.7}$$

Integral with two internal lines

$$B_0(p^2, m_1^2, m_2^2) = \frac{(2\pi\mu)^{4-n}}{i\pi^2} \int \frac{d^n k}{[k^2 - m_1^2 + i0^+][(k+p)^2 - m_2^2 + i0^+]}. \quad \text{(A.8)}$$

The explicit expressions for these integrals read

$$A_0(m^2) = (-16\pi^2)\left[2m^2\lambda + \frac{m^2}{8\pi^2}\ln\left(\frac{m}{\mu}\right)\right], \quad \text{(A.9)}$$

$$B_0(p^2, m_1^2, m_2^2) = (-16\pi^2)\left\{2\lambda + \frac{\ln\left(\frac{m_1}{\mu}\right)}{8\pi^2} + \frac{1}{16\pi^2}\right. \quad \text{(A.10)}$$

$$\left.\times\left[-1 + \frac{p^2 - m_1^2 + m_2^2}{p^2}\ln\left(\frac{m_2}{m_1}\right) + \frac{2m_1 m_2}{p^2}F(\Omega)\right]\right\}, \quad \text{(A.11)}$$

where

$$\lambda = \frac{1}{16\pi^2}\left\{\frac{1}{n-4} - \frac{1}{2}[\ln(4\pi) + \Gamma'(1) + 1]\right\}, \quad \text{(A.12)}$$

$$\Omega = \frac{p^2 - m_1^2 - m_2^2}{2m_1 m_2} \quad \text{(A.13)}$$

and

$$F(\Omega) = \begin{cases} \sqrt{\Omega^2 - 1}\,\ln\left(-\Omega - \sqrt{\Omega^2 - 1}\right) & \text{for } \Omega \le -1, \\ \sqrt{1 - \Omega^2}\,\arccos(-\Omega) & \text{for } -1 \le \Omega \le 1, \\ \sqrt{\Omega^2 - 1}\,\ln\left(\Omega + \sqrt{\Omega^2 - 1}\right) - i\pi\sqrt{\Omega^2 - 1} & \text{for } 1 \le \Omega. \end{cases} \quad \text{(A.14)}$$

If not otherwise stated, we evaluate the loop integrals at the renormalization scale $\mu = 1$ GeV. Furthermore, some useful relations between the scalar integrals are given by:

$$B_0(0, m_1^2, m_2^2) = \frac{A_0(m_1^2) - A_0(m_2^2)}{m_1^2 - m_2^2}, \quad \text{(A.15)}$$

$$B_0(0, m^2, m^2) = \frac{A_0(m^2)}{m^2} - 1, \quad \text{(A.16)}$$

$$B_0(m^2, m^2, 0) = \frac{A_0(m^2)}{m^2} + 1. \quad \text{(A.17)}$$

A.3 Building blocks and transformation behavior

In the following, a decomposition of the U(3) building blocks in SU(3) and U(1) components is provided. The effective dynamical degrees of freedom are contained in the U(3) matrix

$$U = \exp\left(i\sum_{a=0}^{8}\frac{\phi_a\lambda_a}{F}\right) = e^{\frac{i}{3}\psi}\hat{U}, \tag{A.18}$$

where

$$\det(\hat{U}) = 1, \quad \det(U) = e^{i\psi}, \quad \psi = -i\ln(\det(U)). \tag{A.19}$$

The external fields s, p, l_μ, and r_μ are Hermitian, color-neutral 3×3 matrices coupling to the corresponding quark bilinears, and θ is a real field coupling to the winding number density [GL 85]. The traceless components of r_μ and l_μ are defined as

$$\begin{aligned} r_\mu &= \hat{r}_\mu + \frac{1}{3}\langle r_\mu\rangle, \quad \langle\hat{r}_\mu\rangle = 0, \\ l_\mu &= \hat{l}_\mu + \frac{1}{3}\langle l_\mu\rangle, \quad \langle\hat{l}_\mu\rangle = 0. \end{aligned} \tag{A.20}$$

We parametrize the group elements $(V_L, V_R) \in \mathrm{U}(3)_L \times \mathrm{U}(3)_R$ in terms of

$$\begin{aligned} V_R &= \exp\left(-i\sum_{a=0}^{8}\theta_{Ra}\frac{\lambda_a}{2}\right) = e^{-\frac{i}{3}\theta_R}\hat{V}_R, \\ \det\left(\hat{V}_R\right) &= 1, \quad \theta_R = i\ln\left(\det\left(V_R\right)\right), \\ V_L &= \exp\left(-i\sum_{a=0}^{8}\theta_{La}\frac{\lambda_a}{2}\right) = e^{-\frac{i}{3}\theta_L}\hat{V}_L, \\ \det\left(\hat{V}_L\right) &= 1, \quad \theta_L = i\ln\left(\det\left(V_L\right)\right). \end{aligned} \tag{A.21}$$

We define $v_\mu = \frac{1}{2}(r_\mu + l_\mu)$, $a_\mu = \frac{1}{2}(r_\mu - l_\mu)$, and $\chi = 2B(s+ip)$. Under the group $G = \mathrm{U}(3)_L \times \mathrm{U}(3)_R$, the transformation properties of the dynamical degrees of freedom and of the external fields read

$$
\begin{aligned}
U &\mapsto V_R U V_L^\dagger, \\
\psi &\mapsto \psi - i\ln(\det(V_R)) + i\ln(\det(V_L)) = \psi - (\theta_R - \theta_L), \\
r_\mu &\mapsto V_R r_\mu V_R^\dagger + iV_R \partial_\mu V_R^\dagger, \\
\hat{r}_\mu &\mapsto \hat{V}_R \hat{r}_\mu \hat{V}_R^\dagger + i\hat{V}_R \partial_\mu \hat{V}_R^\dagger, \\
\langle r_\mu \rangle &\mapsto \langle r_\mu \rangle - \partial_\mu \theta_R, \\
l_\mu &\mapsto V_L l_\mu V_L^\dagger + iV_L \partial_\mu V_L^\dagger, \\
\hat{l}_\mu &\mapsto \hat{V}_L \hat{l}_\mu \hat{V}_L^\dagger + i\hat{V}_L \partial_\mu \hat{V}_L^\dagger, \\
\langle l_\mu \rangle &\mapsto \langle l_\mu \rangle - \partial_\mu \theta_L, \\
\langle a_\mu \rangle &\mapsto \langle a_\mu \rangle - \frac{1}{2}(\partial_\mu \theta_R - \partial_\mu \theta_L), \\
\chi &\mapsto V_R \chi V_L^\dagger, \\
\theta &\mapsto \theta + (\theta_R - \theta_L).
\end{aligned} \tag{A.22}
$$

The covariant derivatives are defined according to the transformation behavior of the object to which they are applied:

$$
\begin{aligned}
D_\mu U &= \partial_\mu U - ir_\mu U + iUl_\mu \mapsto V_R D_\mu U V_L^\dagger, \\
D_\mu U^\dagger &= \partial_\mu U^\dagger + iU^\dagger r_\mu - il_\mu U^\dagger \mapsto V_L D_\mu U^\dagger V_R^\dagger, \\
D_\mu \hat{U} &= \partial_\mu \hat{U} - i\hat{r}_\mu \hat{U} + i\hat{U}\hat{l}_\mu, \\
D_\mu \psi &= \partial_\mu \psi - 2\langle a_\mu \rangle \mapsto D_\mu \psi, \\
D_\mu U &= e^{\frac{i}{3}\psi}\left(D_\mu \hat{U} + \frac{i}{3} D_\mu \Psi \hat{U}\right), \\
D_\mu \theta &= \partial_\mu \theta + 2\langle a_\mu \rangle \mapsto D_\mu \theta.
\end{aligned} \tag{A.23}
$$

Appendix B

Additional expressions

This appendix provides explicit higher-order expressions for the quantities calculated in this thesis. The loop functions are defined in Appendix A.2. If not otherwise stated, we evaluate the loop integrals at the renormalization scale $\mu = 1$ GeV.

B.1 η-η' mixing

The pion decay constant F in the chiral limit is given by

$$\begin{aligned}
F = F_\pi \Bigg[& 1 - \frac{4M_\pi^2 L_5}{F_\pi^2} \\
& - \frac{1}{F_\pi^4}\left(4\left(2M_\pi^4\left(3\left(L_5\right)^2 - 8L_8L_5 + \left(C_{14}+C_{17}\right)F_\pi^2\right) + F_\pi^2\left(2M_K^2 + M_\pi^2\right)L_4\right)\right) \\
& - \frac{A_0\left(M_K^2\right) + 2A_0\left(M_\pi^2\right)}{32\pi^2F_\pi^2}\Bigg]
\end{aligned} \tag{B.1}$$

in terms of the physical decay constant F_π and the physical pion and kaon masses, M_π and M_K, respectively. The expression for the LO pion mass $\overset{\circ}{M}{}_\pi^2$

reads

$$
\begin{aligned}
\overset{\circ}{M}{}_{\pi}^{2} &= 2B\hat{m} \\
&= M_\pi^2 \Bigg[1 + \frac{8M_\pi^2\left(L_5 - 2L_8\right)}{F_\pi^2} \\
&\quad + \frac{1}{F_\pi^4}\left(8\left(2M_\pi^4\left(8\left(L_5-2L_8\right)^2 + \left(2C_{12}+C_{14}+C_{17}-3C_{19}-2C_{31}\right)F_\pi^2\right)\right.\right. \\
&\quad \left.\left. +2F_\pi^2 M_K^2\left(L_4-2L_6\right) + F_\pi^2 M_\pi^2\left(L_4-2L_6\right)\right)\right) \\
&\quad + \frac{1}{192F_\pi^2}\left(\left(2\sqrt{2}\sin(2\theta^{[0]}) + \cos(2\theta^{[0]}) - 3\right)A_0\left(M_\eta^2\right)\right. \\
&\quad \left. - \left(2\sqrt{2}\sin(2\theta^{[0]}) + \cos(2\theta^{[0]}) + 3\right)A_0\left(M_{\eta'}^2\right) + 6A_0\left(M_\pi^2\right)\right)\Bigg],
\end{aligned}
\tag{B.2}
$$

and the LO kaon mass $\overset{\circ}{M}{}_{K}^{2}$ is given by

$$
\begin{aligned}
\overset{\circ}{M}{}_{K}^{2} &= B(\hat{m} + ms) \\
&= M_K^2 \Bigg[1 + \frac{8M_K^2\left(L_5 - 2L_8\right)}{F_\pi^2} \\
&\quad + \frac{1}{F_\pi^4}\left(8\left(4M_K^4\left(2\left(L_5-4L_8\right)\left(L_5-2L_8\right) + \left(C_{12}+C_{14}-3C_{19}-C_{31}\right)F_\pi^2\right)\right.\right. \\
&\quad + 2M_K^2\left(F_\pi^2\left(L_4-2L_6+2\left(-C_{14}+C_{17}+3C_{19}\right)M_\pi^2\right) + 4M_\pi^2 L_5\left(L_5-2L_8\right)\right) \\
&\quad \left.\left. -F_\pi^2 M_\pi^2\left(2\left(L_6+\left(-C_{14}+C_{17}+3C_{19}\right)M_\pi^2\right) - L_4\right)\right)\right) \\
&\quad + \frac{1}{192F_\pi^2 M_K^2}\left(\sin^2(\theta^{[0]})\left(\left(3M_{\eta'}^2 + M_\pi^2\right)A_0\left(M_{\eta'}^2\right) - 4M_K^2 A_0\left(M_\eta^2\right)\right)\right. \\
&\quad + \sqrt{2}\left(2M_K^2 - M_\pi^2\right)\sin(2\theta^{[0]})\left(A_0\left(M_{\eta'}^2\right) - A_0\left(M_\eta^2\right)\right) \\
&\quad \left. + \cos^2(\theta^{[0]})\left(\left(3M_\eta^2 + M_\pi^2\right)A_0\left(M_\eta^2\right) - 4M_K^2 A_0\left(M_{\eta'}^2\right)\right)\right)\Bigg].
\end{aligned}
\tag{B.3}
$$

In loop contributions, we always use the LO mixing angle

$$
\theta^{[0]} = -\arctan\left(\frac{2\sqrt{2}\left(M_K^2 - M_\pi^2\right)}{3\left(\frac{1}{3}\left(M_\pi^2 - 4M_K^2\right) + M_{\eta'}^2\right)}\right),
\tag{B.4}
$$

which yields $\theta^{[0]} = -19.6°$. The ratio of the physical kaon and pion decay constants is given by

$$
\begin{aligned}
&F_K/F_\pi \\
&= 1 + \frac{4\left(M_K^2 - M_\pi^2\right) L_5}{F_\pi^2} \\
&+ \frac{1}{F_\pi^4}\left(8\left(\left(3M_K^4 + 2M_\pi^2 M_K^2 - 3M_\pi^4\right)(L_5)^2 + 8\left(M_\pi^4 - M_K^4\right) L_8 L_5\right.\right. \\
&\left.\left.+2F_\pi^2\left(M_K^2 - M_\pi^2\right)\left(C_{14} M_K^2 + C_{17} M_\pi^2\right)\right)\right) \\
&+ \frac{1}{128\pi^2 F_\pi^2}\left(2A_0\left(M_K^2\right) + 3\cos^2(\theta^{[0]}) A_0\left(M_\eta^2\right) + 3\sin^2(\theta^{[0]}) A_0\left(M_{\eta'}^2\right)\right. \\
&\left.-5A_0\left(M_\pi^2\right)\right)
\end{aligned}
\tag{B.5}
$$

In the following, the NNLO expressions for the matrix $\mathcal{C}_A$ defined in Eq. (5.2) in Sec. 5.1, the kinetic matrix $\mathcal{K}_B$ and the mass matrix $\mathcal{M}_B$ defined in Eq. (5.11) are provided. The components of $\mathcal{C}_A$ are given by

$$c_8 = \frac{32C_{12}\left(4M_K^2 - M_\pi^2\right)}{3F_\pi^2}, \tag{B.6}$$

$$c_1 = \frac{32C_{12}\left(2M_K^2 + M_\pi^2\right)}{3F_\pi^2}, \tag{B.7}$$

$$c_{81} = \frac{64\sqrt{2}C_{12}\left(M_\pi^2 - M_K^2\right)}{3F_\pi^2}. \tag{B.8}$$

At NNLO, both tree and loop corrections occur. The second-order tree contributions to the kinetic matrix read

$$
\begin{aligned}
\delta_8^{(2,\mathrm{tr})} = \frac{1}{3F_\pi^4}&\left[8\left(2\left(8\left(2M_K^4 + 2M_\pi^2 M_K^2 - M_\pi^4\right)(L_5)^2 + 8\left(M_\pi^4 - 4M_K^4\right) L_8 L_5\right.\right.\right. \\
&\left.+ (C_{14} + C_{17}) F_\pi^2\left(8M_K^4 - 8M_\pi^2 M_K^2 + 3M_\pi^4\right)\right) \\
&\left.\left.+3F_\pi^2\left(2M_K^2 + M_\pi^2\right) L_4\right) + 32C_{12} F_\pi^2\left(8M_K^4 - 8M_\pi^2 M_K^2 + 3M_\pi^4\right)\right],
\end{aligned}
\tag{B.9}
$$

$$
\begin{aligned}
\delta_1^{(2,\mathrm{tr})} = \frac{1}{3F_\pi^4}&\left[8\left(3F_\pi^2\left(2M_K^2 + M_\pi^2\right) L_4 + 16\left(M_K^4 + M_\pi^2 M_K^2 + M_\pi^4\right)(L_5)^2\right.\right. \\
&- 16\left(2M_K^4 + M_\pi^4\right) L_8 L_5 \\
&\left.+2(C_{14} + C_{17})\left(4M_K^4 - 4M_\pi^2 M_K^2 + 3M_\pi^4\right) + 3L_{18}\left(2M_K^2 + M_\pi^2\right)\right)\Big) \\
&\left.+32C_{12} F_\pi^2\left(4M_K^4 - 4M_\pi^2 M_K^2 + M_0^2\left(2M_K^2 + M_\pi^2\right) + 3M_\pi^4\right)\right],
\end{aligned}
\tag{B.10}
$$

$$\delta_{81}^{(2,\mathrm{tr})} = -\frac{1}{3F_\pi^4}\Big[8\sqrt{2}\left(M_K^2 - M_\pi^2\right)\left(16L_5\left(\left(M_K^2 + 2M_\pi^2\right)L_5 - 2\left(M_K^2 + M_\pi^2\right)L_8\right)\right.$$
$$\left. + F_\pi^2\left(8\left(C_{14} + C_{17}\right)M_K^2 + 3L_{18}\right)\right)$$
$$+ 32\sqrt{2}C_{12}F_\pi^2\left(4M_K^2 + M_0^2\right)\left(M_K^2 - M_\pi^2\right)\Big], \tag{B.11}$$

and the loop contributions

$$\delta_8^{(2,\mathrm{lo})} = \frac{A_0\left(M_K^2\right)}{16\pi^2F_\pi^2}, \quad \delta_1^{(2,\mathrm{lo})} = 0, \quad \delta_{81}^{(2,\mathrm{lo})} = 0. \tag{B.12}$$

The second-order tree contributions to the mass matrix are

$$\Delta M_8^{2\,(2,\mathrm{tr})}$$
$$= \frac{1}{3F_\pi^4}\Big[16\left(16M_K^6\left(8\left(L_5 - 2L_8\right)L_8 + \left(3C_{19} + 2C_{31}\right)F_\pi^2\right)\right.$$
$$+ 8M_\pi^2M_K^4\left(16\left(L_8\right)^2 - 3\left(3C_{19} + 2C_{31}\right)F_\pi^2\right) + 4M_\pi^4M_K^2\left(32L_8\left(L_8 - L_5\right)\right.$$
$$\left. + 3\left(3C_{19} + 2C_{31}\right)F_\pi^2\right) + M_\pi^6\left(24\left(3L_5 - 4L_8\right)L_8 - \left(3C_{19} + 2C_{31}\right)F_\pi^2\right)$$
$$\left. + 8F_\pi^2\left(M_K^2 - M_\pi^2\right)^2L_7 + F_\pi^2\left(8M_K^4 + 2M_\pi^2M_K^2 - M_\pi^4\right)L_6\right)\Big], \tag{B.13}$$

$$\Delta M_1^{2\,(2,\mathrm{tr})}$$
$$= \frac{1}{3F_\pi^4}\Big[16\left(F_\pi^2\Lambda_2\left(2M_K^4 + M_\pi^4\right)\left(L_5 - 2L_8\right) + F_\pi^2\left(2M_K^2 + M_\pi^2\right)^2L_6\right.$$
$$+ F_\pi^2\left(2M_K^2 + M_\pi^2\right)^2L_7 - 128M_K^6\left(L_8\right)^2 + 64M_K^6L_5L_8 + 64M_\pi^2M_K^4\left(L_8\right)^2$$
$$+ 64M_\pi^4M_K^2\left(L_8\right)^2 - 64M_\pi^4M_K^2L_5L_8 - 96M_\pi^6\left(L_8\right)^2 + 72M_\pi^6L_5L_8$$
$$+ 24C_{19}F_\pi^2M_K^6 + 16C_{31}F_\pi^2M_K^6 - 36C_{19}F_\pi^2M_\pi^2M_K^4 - 24C_{31}F_\pi^2M_\pi^2M_K^4$$
$$+ 18C_{19}F_\pi^2M_\pi^4M_K^2 + 12C_{31}F_\pi^2M_\pi^4M_K^2 + 3C_{19}F_\pi^2M_\pi^6 + 2C_{31}F_\pi^2M_\pi^6$$
$$\left. - 12F_\pi^2L_{25}M_K^4 + 12F_\pi^2L_{25}M_\pi^2M_K^2 - 9F_\pi^2L_{25}M_\pi^4\right)\Big]$$
$$+ 6(2M_K^2 + M_\pi^2)v_2^{(2)}, \tag{B.14}$$

$$\Delta M_{81}^{2\,(2,\mathrm{tr})}$$
$$= -\frac{1}{3F_\pi^4}\Big[16\sqrt{2}\left(M_K^2 - M_\pi^2\right)\left(2\left(4M_K^4\left(8\left(L_5 - 2L_8\right)L_8 + \left(3C_{19} + 2C_{31}\right)F_\pi^2\right)\right.\right.$$
$$+ M_\pi^2\left(F_\pi^2\left(L_6 + L_7 - 2\left(3C_{19} + 2C_{31}\right)M_K^2\right) + 32M_K^2\left(L_5 - L_8\right)L_8\right)$$
$$\left. + F_\pi^2M_K^2\left(2\left(L_6 + L_7\right) - 3L_{25}\right) + \left(3C_{19} + 2C_{31}\right)F_\pi^2M_\pi^4\right)$$
$$\left.\left. + F_\pi^2\Lambda_2\left(M_K^2 + M_\pi^2\right)\left(L_5 - 2L_8\right)\right)\right], \tag{B.15}$$

and the loop corrections are given by

$$\Delta M_8^{2\,(2,\mathrm{lo})} = \frac{1}{576F_\pi^2}\Big(2\sqrt{2}\left(8M_K^2 - 5M_\pi^2\right)\sin(2\theta^{[0]})\left(A_0\left(M_\eta^2\right) - A_0\left(M_{\eta'}^2\right)\right)$$
$$+\left(8M_K^2 - 5M_\pi^2\right)\cos(2\theta^{[0]})\left(A_0\left(M_\eta^2\right) - A_0\left(M_{\eta'}^2\right)\right)$$
$$+3\left(8M_K^2 - 3M_\pi^2\right)\left(A_0\left(M_\eta^2\right) + A_0\left(M_{\eta'}^2\right)\right)$$
$$+6M_\pi^2\left(3A_0\left(M_\pi^2\right) - 2A_0\left(M_K^2\right)\right)\Big), \tag{B.16}$$

$$\Delta M_1^{2\,(2,\mathrm{lo})} = \frac{1}{144F_\pi^2}\Big(2\sqrt{2}\left(M_K^2 - M_\pi^2\right)\sin(2\theta^{[0]})\left(A_0\left(M_\eta^2\right) - A_0\left(M_{\eta'}^2\right)\right)$$
$$+\left(M_K^2 - M_\pi^2\right)\cos(2\theta^{[0]})\left(A_0\left(M_\eta^2\right) - A_0\left(M_{\eta'}^2\right)\right)$$
$$+3M_K^2\left(4A_0\left(M_K^2\right) + A_0\left(M_\eta^2\right) + A_0\left(M_{\eta'}^2\right)\right) + 9M_\pi^2 A_0\left(M_\pi^2\right)\Big), \tag{B.17}$$

$$\Delta M_{81}^{2\,(2,\mathrm{lo})} = \frac{1}{576F_\pi^2}\Big(4\left(4M_K^2 - M_\pi^2\right)\sin(2\theta^{[0]})\left(A_0\left(M_{\eta'}^2\right) - A_0\left(M_\eta^2\right)\right)$$
$$+\sqrt{2}\left(4M_K^2 - M_\pi^2\right)\cos(2\theta^{[0]})\left(A_0\left(M_{\eta'}^2\right) - A_0\left(M_\eta^2\right)\right)$$
$$-3\sqrt{2}\Big(\left(4M_K^2 - 3M_\pi^2\right)\left(A_0\left(M_\eta^2\right) + A_0\left(M_{\eta'}^2\right)\right)$$
$$+\left(8M_K^2 - 4M_\pi^2\right)A_0\left(M_K^2\right) - 6M_\pi^2 A_0\left(M_\pi^2\right)\Big)\Big). \tag{B.18}$$

The NNLO expressions for the decay constants of the η-η' system are given by

$$F_\eta^8 = F_\pi\cos(\theta^{[2]}) + \frac{1}{3F_\pi}\left(8\left(M_K^2 - M_\pi^2\right)L_5\left(\sqrt{2}\sin(\theta^{[2]}) + 2\cos(\theta^{[2]})\right)\right)$$
$$+\frac{\cos(\theta^{[2]})}{48\pi^2F_\pi^3}\Big[256\pi^2\left(\left(4M_K^4 + 8M_\pi^2M_K^2 - 9M_\pi^4\right)(L_5)^2 + 16\left(M_\pi^4 - M_K^4\right)L_8L_5\right.$$
$$\left.+4\left(C_{14} + C_{17}\right)F_\pi^2M_K^2\left(M_K^2 - M_\pi^2\right)\right) + 3F_\pi^2\left(A_0\left(M_K^2\right) - A_0\left(M_\pi^2\right)\right)\Big]$$
$$+\frac{\sin(\theta^{[2]})}{3F_\pi^3}\Big[2\sqrt{2}\left(M_K^2 - M_\pi^2\right)\left(F_\pi^2\left(-\Lambda_1L_5 + 16\left(C_{14} + C_{17}\right)M_K^2 + 6L_{18}\right)\right.$$
$$\left.+16L_5\left(\left(M_K^2 + 3M_\pi^2\right)L_5 - 4\left(M_K^2 + M_\pi^2\right)L_8\right)\right)\Big]$$
$$+\frac{C_{12}}{3F_\pi\left(4M_K^2 - 3M_{\eta'}^2 - M_\pi^2\right)}\Big[16\left(M_K^2 - M_\pi^2\right)\Big(-2\left(M_K^2 - M_\pi^2\right)M_{\eta'}^2$$
$$\times\left(\sqrt{2}\sin(\theta^{[2]}) - 4\cos(\theta^{[2]})\right) + 3\sqrt{2}M_\pi^2\left(M_\pi^2 - 2M_K^2\right)\sin(\theta^{[2]})$$
$$+3\sqrt{2}M_{\eta'}^4\sin(\theta^{[2]})\Big)\Big], \tag{B.19}$$

$$
\begin{aligned}
F^8_{\eta'} = {} & F_\pi \sin(\theta^{[2]}) - \frac{1}{3F_\pi}\left(8\left(M_K^2 - M_\pi^2\right)L_5\left(\sqrt{2}\cos(\theta^{[2]}) - 2\sin(\theta^{[2]})\right)\right) \\
& - \frac{\cos(\theta^{[2]})}{3F_\pi^3}\left[2\sqrt{2}\left(M_K^2 - M_\pi^2\right)\left(F_\pi^2\left(-\Lambda_1 L_5 + 16\left(C_{14}+C_{17}\right)M_K^2 + 6L_{18}\right)\right.\right. \\
& \left.\left. +16L_5\left(\left(M_K^2 + 3M_\pi^2\right)L_5 - 4\left(M_K^2 + M_\pi^2\right)L_8\right)\right)\right] \\
& + \frac{\sin(\theta^{[2]})}{48\pi^2 F_\pi^3}\left[256\pi^2\left(\left(4M_K^4 + 8M_\pi^2 M_K^2 - 9M_\pi^4\right)\left(L_5\right)^2 + 16\left(M_\pi^4 - M_K^4\right)L_8 L_5\right.\right. \\
& \left. +4\left(C_{14}+C_{17}\right)F_\pi^2 M_K^2\left(M_K^2 - M_\pi^2\right)\right) + 3F_\pi^2\left(A_0\left(M_K^2\right) - A_0\left(M_\pi^2\right)\right)\Big] \\
& + \frac{C_{12}}{3F_\pi}\left[16\left(\frac{1}{4M_K^2 - 3M_{\eta'}^2 - M_\pi^2}\left[\sqrt{2}\left(M_K^2 - M_\pi^2\right)\cos(\theta^{[2]})\right.\right.\right. \\
& \left(-2M_K^2\left(7M_{\eta'}^2 + 5M_\pi^2\right) + 16M_K^4 + 3M_{\eta'}^4 + 2M_\pi^2 M_{\eta'}^2 + 3M_\pi^4\right)\Big] \\
& \left.\left. - \sin(\theta^{[2]})\left(-4M_K^2\left(M_{\eta'}^2 + 2M_\pi^2\right) + 8M_K^4 + M_\pi^2\left(M_{\eta'}^2 + 3M_\pi^2\right)\right)\right)\right],
\end{aligned} \tag{B.20}
$$

$$
\begin{aligned}
F^0_\eta = {} & -\frac{1}{6F_\pi}\left[16\left(M_K^2 - M_\pi^2\right)L_5\left(\sin(\theta^{[2]}) + \sqrt{2}\cos(\theta^{[2]})\right) + 3F_\pi^2\left(\Lambda_1 + 2\right)\sin(\theta^{[2]})\right] \\
& - \frac{\cos(\theta^{[2]})}{3F_\pi^3}\left[2\sqrt{2}\left(M_K^2 - M_\pi^2\right)\left(F_\pi^2\left(-\Lambda_1 L_5 + 16\left(C_{14}+C_{17}\right)M_K^2\right.\right.\right. \\
& \left.\left.\left. +6\left(L_{18} + 2L_{46} + 2L_{53}\right)\right) + 16L_5\left(\left(M_K^2 + 3M_\pi^2\right)L_5 - 4\left(M_K^2 + M_\pi^2\right)L_8\right)\right)\right] \\
& + \frac{\sin(\theta^{[2]})}{96\pi^2 F_\pi^3}\left[2\left(2\pi^2\left(32\left(4L_5\left(8\left(M_K^4 - M_\pi^4\right)L_8 + \left(-2M_K^4 - 4M_\pi^2 M_K^2 + 3M_\pi^4\right)L_5\right)\right.\right.\right.\right. \\
& + F_\pi^2\left(M_\pi^2\left(8\left(C_{14}+C_{17}\right)M_K^2 - 3\left(L_{18} + L_{46} + L_{53}\right)\right) - 8\left(C_{14}+C_{17}\right)M_K^4\right. \\
& \left.\left. -6\left(L_{18} + L_{46} + L_{53}\right)M_K^2\right)\right) + 32F_\pi^2\Lambda_1\left(M_K^2 + 2M_\pi^2\right)L_5 + 3F_\pi^4\Lambda_1^2\Big) \\
& \left. +3F_\pi^2 A_0\left(M_\pi^2\right)\right) + 3F_\pi^2 A_0\left(M_K^2\right)\Big] \\
& + \frac{C_{12}}{3F_\pi\left(4M_K^2 - 3M_{\eta'}^2 - M_\pi^2\right)}\left[16\left(\sin(\theta^{[2]})\left(4M_K^2 - 3M_{\eta'}^2 - M_\pi^2\right)\right.\right. \\
& \times\left(2M_K^2\left(M_{\eta'}^2 - 3M_\pi^2\right) + M_\pi^2\left(M_{\eta'}^2 + 3M_\pi^2\right)\right) + \sqrt{2}\left(M_K^2 - M_\pi^2\right)\cos(\theta^{[2]}) \\
& \left.\left. \times\left(2M_K^2\left(M_{\eta'}^2 + 3M_\pi^2\right) - 2M_\pi^2 M_{\eta'}^2 - 3M_{\eta'}^4 - 3M_\pi^4\right)\right)\right],
\end{aligned} \tag{B.21}
$$

$$
\begin{aligned}
F^0_{\eta'} =& \frac{1}{6F_\pi}\Big[16\left(M_K^2 - M_\pi^2\right)L_5\left(\cos(\theta^{[2]}) - \sqrt{2}\sin(\theta^{[2]})\right) + 3F_\pi^2\left(\Lambda_1 + 2\right)\cos(\theta^{[2]})\Big] \\
& \frac{\cos(\theta^{[2]})}{96\pi^2 F_\pi^3}\big[2\left(2\pi^2\left(32\left(4L_5\left(\left(2M_K^4 + 4M_\pi^2 M_K^2 - 3M_\pi^4\right)L_5 + 8\left(M_\pi^4 - M_K^4\right)L_8\right)\right.\right.\right. \\
& + F_\pi^2\left(M_\pi^2\left(3\left(L_{18} + L_{46} + L_{53}\right) - 8\left(C_{14} + C_{17}\right)M_K^2\right) + 8\left(C_{14} + C_{17}\right)M_K^4\right. \\
& \left.\left. +6\left(L_{18} + L_{46} + L_{53}\right)M_K^2\right)\right) - 32F_\pi^2\Lambda_1\left(M_K^2 + 2M_\pi^2\right)L_5 - 3F_\pi^4\Lambda_1^2\Big) \\
& \left. -3F_\pi^2 A_0\left(M_\pi^2\right)\right) - 3F_\pi^2 A_0\left(M_K^2\right)\big] \\
& - \frac{\sin(\theta^{[2]})}{3F_\pi^3}\Big[2\sqrt{2}\left(M_K^2 - M_\pi^2\right)\left(F_\pi^2\left(-\Lambda_1 L_5 + 16\left(C_{14} + C_{17}\right)M_K^2\right.\right. \\
& \left.\left. +6\left(L_{18} + 2L_{46} + 2L_{53}\right)\right) + 16L_5\left(\left(M_K^2 + 3M_\pi^2\right)L_5 - 4\left(M_K^2 + M_\pi^2\right)L_8\right)\right)\Big] \\
& + \frac{C_{12}}{3F_\pi\left(4M_K^2 - 3M_{\eta'}^2 - M_\pi^2\right)}\Big[16\left(M_K^2 - M_\pi^2\right)\left(\sqrt{2}\sin(\theta^{[2]})\right. \\
& \times\left(-2M_K^2\left(7M_{\eta'}^2 + 5M_\pi^2\right) + 16M_K^4 + 3M_{\eta'}^4 + 2M_\pi^2 M_{\eta'}^2 + 3M_\pi^4\right) \\
& \left. -8\left(M_K^2 - M_\pi^2\right)\cos(\theta^{[2]})\left(2M_K^2 - M_{\eta'}^2\right)\right)\Big],
\end{aligned}
\tag{B.22}
$$

in terms of the physical masses M_π^2, M_K^2, $M_{\eta'}^2$ and the physical pion decay constant F_π. The mixing angle $\theta^{[2]}$ is the NNLO mixing angle given in Eq. (5.33) in Sec. 5.1. In the case where the loop contributions are added to the NLO results, the parameters of the two-angle scheme can be simplified to read

$$
F_8 = F_\pi + \frac{1}{48\pi^2 F_\pi}\left[256\pi^2\left(M_K^2 - M_\pi^2\right)L_5 + 3A_0\left(M_K^2\right) - 3A_0\left(M_\pi^2\right)\right], \tag{B.23}
$$

$$
\begin{aligned}
F_0 =& F_\pi + \frac{1}{96\pi^2 F_\pi}\left[16\pi^2\left(16M_K^2\left(L_5 + 3L_{18}\right) + 8M_\pi^2\left(3L_{18} - 2L_5\right) + 3F_\pi^2\Lambda_1\right)\right. \\
& \left. -3A_0\left(M_K^2\right) - 6A_0\left(M_\pi^2\right)\right],
\end{aligned}
\tag{B.24}
$$

$$
\theta_8 = \theta^{[2]} + \arctan\left(-\frac{4\sqrt{2}\left(M_K^2 - M_\pi^2\right)\left(2L_5 + 3L_{18}\right)}{3F_\pi^2}\right), \tag{B.25}
$$

$$
\theta_0 = \theta^{[2]} - \arctan\left(-\frac{4\sqrt{2}\left(M_K^2 - M_\pi^2\right)\left(2L_5 + 3L_{18}\right)}{3F_\pi^2}\right). \tag{B.26}
$$

B.2 Anomalous decays

In the case without the N_c expansion of the quark-charge matrix Q, the loop contributions to the form factors of the two-photon decays given by the loop diagrams in Fig. 7.1 read

$$
\begin{aligned}
&F(\pi^0 \to \gamma^*\gamma^*) \\
&= \frac{1}{1152\pi^4 F_\pi^3}\Big[3\left(q_1^2 - 4M_K^2\right)B_0\left(q_1^2, M_K^2, M_K^2\right) \\
&\quad + 3\left(q_2^2 - 4M_K^2\right)B_0\left(q_2^2, M_K^2, M_K^2\right) + 3\left(\left(q_1^2 - 4M_\pi^2\right)B_0\left(q_1^2, M_\pi^2, M_\pi^2\right)\right. \\
&\quad \left. + \left(q_2^2 - 4M_\pi^2\right)B_0\left(q_2^2, M_\pi^2, M_\pi^2\right)\right) + 24A_0\left(M_K^2\right) + 24A_0\left(M_\pi^2\right) \\
&\quad +4\left(-6\left(M_K^2 + M_\pi^2\right) + q_1^2 + q_2^2\right)\Big],
\end{aligned} \tag{B.27}
$$

$$
\begin{aligned}
&F(\eta \to \gamma^*\gamma^*) \\
&= \frac{1}{1152\sqrt{3}\pi^4 F_\pi^3}\Big[\left(\sqrt{2}\sin(\theta^{[0]}) - \cos(\theta^{[0]})\right)\left(q_2^2\left(-\left(3B_0\left(q_2^2, M_K^2, M_K^2\right)\right.\right.\right. \\
&\quad \left.\left. +3B_0\left(q_2^2, M_\pi^2, M_\pi^2\right) + 4\right)\right) + 3\left(4M_K^2 - q_1^2\right)B_0\left(q_1^2, M_K^2, M_K^2\right) \\
&\quad + 4\left(3M_K^2 B_0\left(q_2^2, M_K^2, M_K^2\right) + 3M_\pi^2 B_0\left(q_2^2, M_\pi^2, M_\pi^2\right) + 6\left(M_K^2 + M_\pi^2\right) - q_1^2\right) \\
&\quad \left. +3\left(4M_\pi^2 - q_1^2\right)B_0\left(q_1^2, M_\pi^2, M_\pi^2\right)\right) + 6\left(\cos(\theta^{[0]}) - 7\sqrt{2}\sin(\theta^{[0]})\right)A_0\left(M_K^2\right) \\
&\quad +6A_0\left(M_\pi^2\right)\left(7\cos(\theta^{[0]}) - 10\sqrt{2}\sin(\theta^{[0]})\right)\Big],
\end{aligned} \tag{B.28}
$$

$$
\begin{aligned}
&F(\eta' \to \gamma^*\gamma^*) \\
&= \frac{1}{1152\sqrt{3}\pi^4 F_\pi^3}\Big[-\left(\sin(\theta^{[0]}) + \sqrt{2}\cos(\theta^{[0]})\right)\left(q_2^2\left(-\left(3B_0\left(q_2^2, M_K^2, M_K^2\right)\right.\right.\right. \\
&\quad \left.\left. +3B_0\left(q_2^2, M_\pi^2, M_\pi^2\right) + 4\right)\right) + 3\left(4M_K^2 - q_1^2\right)B_0\left(q_1^2, M_K^2, M_K^2\right) \\
&\quad + 4\left(3M_K^2 B_0\left(q_2^2, M_K^2, M_K^2\right) + 3M_\pi^2 B_0\left(q_2^2, M_\pi^2, M_\pi^2\right) + 6\left(M_K^2 + M_\pi^2\right) - q_1^2\right) \\
&\quad \left. +3\left(4M_\pi^2 - q_1^2\right)B_0\left(q_1^2, M_\pi^2, M_\pi^2\right)\right) + 6\left(\sin(\theta^{[0]}) + 7\sqrt{2}\cos(\theta^{[0]})\right)A_0\left(M_K^2\right) \\
&\quad +6A_0\left(M_\pi^2\right)\left(7\sin(\theta^{[0]}) + 10\sqrt{2}\cos(\theta^{[0]})\right)\Big].
\end{aligned} \tag{B.29}
$$

Including the N_c expansion of Q, the loop contributions are given by

$$
\begin{aligned}
&F(\pi^0 \to \gamma^*\gamma^*) \\
&= \frac{1}{2304\pi^4 F_\pi^3}\Big[3\left(q_1^2 - 4M_K^2\right)B_0\left(q_1^2, M_K^2, M_K^2\right) \\
&\quad +3\left(q_2^2 - 4M_K^2\right)B_0\left(q_2^2, M_K^2, M_K^2\right) + 24A_0\left(M_K^2\right) + 2\left(-12M_K^2 + q_1^2 + q_2^2\right)\Big],
\end{aligned} \tag{B.30}
$$

$$
\begin{aligned}
&F(\eta \to \gamma^*\gamma^*)\\
&= \frac{1}{4608\sqrt{3}\pi^4 F_\pi^3}\Big[\sqrt{2}\sin(\theta^{[0]})\left(2\left(2\left(q_2^2\left(-\left(3B_0\left(q_2^2, M_K^2, M_K^2\right) + 3B_0\left(q_2^2, M_\pi^2, M_\pi^2\right) + 4\right)\right)\right.\right.\right.\\
&\quad + 3\left(4M_K^2 - q_1^2\right)B_0\left(q_1^2, M_K^2, M_K^2\right) + 4\left(3M_K^2 B_0\left(q_2^2, M_K^2, M_K^2\right)\right.\\
&\quad \left. +3M_\pi^2 B_0\left(q_2^2, M_\pi^2, M_\pi^2\right) + 6\left(M_K^2 + M_\pi^2\right) - q_1^2\right) + 3\left(4M_\pi^2 - q_1^2\right)B_0\left(q_1^2, M_\pi^2, M_\pi^2\right)\Big)\\
&\quad -129A_0\left(M_\pi^2\right)\Big) - 177A_0\left(M_K^2\right)\Big) + 2\cos(\theta^{[0]})\left(3\left(4M_K^2 - q_1^2\right)B_0\left(q_1^2, M_K^2, M_K^2\right)\right.\\
&\quad + 3\left(4M_K^2 - q_2^2\right)B_0\left(q_2^2, M_K^2, M_K^2\right) + 6\left(\left(q_1^2 - 4M_\pi^2\right)B_0\left(q_1^2, M_\pi^2, M_\pi^2\right)\right.\\
&\quad \left.+\left(q_2^2 - 4M_\pi^2\right)B_0\left(q_2^2, M_\pi^2, M_\pi^2\right)\right) - 24A_0\left(M_K^2\right) + 48A_0\left(M_\pi^2\right)\\
&\quad \left.+2\left(12\left(M_K^2 - 2M_\pi^2\right) + q_1^2 + q_2^2\right)\right)\Big],
\end{aligned} \tag{B.31}
$$

$$
\begin{aligned}
&F(\eta' \to \gamma^*\gamma^*)\\
&= \frac{1}{4608\sqrt{3}\pi^4 F_\pi^3}\Big[2\sin(\theta^{[0]})\left(3\left(4M_K^2 - q_1^2\right)B_0\left(q_1^2, M_K^2, M_K^2\right)\right.\\
&\quad + 3\left(4M_K^2 - q_2^2\right)B_0\left(q_2^2, M_K^2, M_K^2\right) + 6\left(\left(q_1^2 - 4M_\pi^2\right)B_0\left(q_1^2, M_\pi^2, M_\pi^2\right)\right.\\
&\quad \left.+\left(q_2^2 - 4M_\pi^2\right)B_0\left(q_2^2, M_\pi^2, M_\pi^2\right)\right) - 24A_0\left(M_K^2\right) + 48A_0\left(M_\pi^2\right)\\
&\quad \left.+2\left(12\left(M_K^2 - 2M_\pi^2\right) + q_1^2 + q_2^2\right)\right) + \sqrt{2}\cos(\theta^{[0]})\left(4\left(3\left(q_1^2 - 4M_K^2\right)B_0\left(q_1^2, M_K^2, M_K^2\right)\right.\right.\\
&\quad + 3\left(q_2^2 - 4M_K^2\right)B_0\left(q_2^2, M_K^2, M_K^2\right) + 3\left(\left(q_1^2 - 4M_\pi^2\right)B_0\left(q_1^2, M_\pi^2, M_\pi^2\right)\right.\\
&\quad \left.\left.+\left(q_2^2 - 4M_\pi^2\right)B_0\left(q_2^2, M_\pi^2, M_\pi^2\right)\right) + 4\left(-6\left(M_K^2 + M_\pi^2\right) + q_1^2 + q_2^2\right)\right)\\
&\quad \left.+177A_0\left(M_K^2\right) + 258A_0\left(M_\pi^2\right)\right)\Big].
\end{aligned} \tag{B.32}
$$

Without the N_c expansion of Q, the NNLO tree-level contributions to the η TFF take the form

$$
\begin{aligned}
&F(\eta \to \gamma^*\gamma^*)\\
&= \frac{2\cos(\theta^{[0]})}{9\sqrt{3}\pi^2 F_\pi^5}\Big[2F_\pi^2\Big(3\left(M_K^2-M_\pi^2\right)\left(4\left(C_{14}+C_{17}\right)M_K^2+512\pi^2F_\pi^2L_9^{6,\epsilon}+3L_{18}\right)\\
&\quad -1024\pi^2\left(4M_K^4-7M_\pi^4\right)L_8^{6,\epsilon}L_8\Big)+L_5\Big(96\left(M_\pi^4-M_K^4\right)L_8\\
&\quad +F_\pi^2\Big(3072\pi^2M_\pi^2\left(2M_K^2-3M_\pi^2\right)L_8^{6,\epsilon}-\left(M_K^2-M_\pi^2\right)\Big(32\pi^2\left(3K_1+32\left(q_1^2+q_2^2\right)L_{19}^{6,\epsilon}\right)\\
&\quad +9\Lambda_1\Big)\Big)\Big)-6\left(4M_K^4-24M_\pi^2M_K^2+23M_\pi^4\right)\left(L_5\right)^2\Big]\\
&\quad +\frac{8\sin(\theta^{[0]})}{72\sqrt{6}\pi^2F_\pi^5}\Big[\Big(L_5\Big(192\left(M_\pi^4-M_K^4\right)L_8\\
&\quad +F_\pi^2\Big(-2048\pi^2\left(q_1^2+q_2^2\right)\left(M_K^2-M_\pi^2\right)L_{19}^{6,\epsilon}+12288\pi^2M_\pi^2\left(M_K^2+M_\pi^2\right)L_8^{6,\epsilon}\\
&\quad -9\Lambda_1\left(3M_K^2+M_\pi^2\right)+192\pi^2K_1\left(M_\pi^2-M_K^2\right)\Big)\Big)-32\pi^2F_\pi^2\Big(512\left(M_K^4+2M_\pi^4\right)L_8^{6,\epsilon}L_8\\
&\quad +3F_\pi^2\left(q_1^2+q_2^2\right)\left(8\Lambda_1L_{19}^{6,\epsilon}+3L_{239}\right)\Big)-48\left(M_K^4-6M_\pi^2M_K^2+2M_\pi^4\right)\left(L_5\right)^2\Big)\\
&\quad +48F_\pi^2\Big(8\left(C_{14}+C_{17}\right)\left(M_K^2-M_\pi^2\right)M_K^2+9L_{18}\left(M_K^2+M_\pi^2\right)\Big)\\
&\quad +F_\pi^4\Big(-32\pi^2\Lambda_1\left(128\left(M_K^2+2M_\pi^2\right)L_8^{6,\epsilon}+9K_1\right)+24\pi^2\Big(1024\left(2M_K^2+M_\pi^2\right)L_9^{6,\epsilon}\\
&\quad +\Lambda_{442}\left(M_K^2+2M_\pi^2\right)\Big)-27\Lambda_1^2\Big)\Big]\\
&\quad +\frac{C_{12}}{3\sqrt{3}\pi^2F_\pi^3\left(4M_K^2-3M_{\eta'}^2-M_\pi^2\right)}\Big[4\sqrt{2}\sin(\theta^{[0]})\Big(-9\left(M_K^2+M_\pi^2\right)M_{\eta'}^4\\
&\quad -2\left(M_K^4-8M_\pi^2M_K^2+7M_\pi^4\right)M_{\eta'}^2+32M_K^6-22M_\pi^2M_K^4-7M_\pi^4M_K^2+15M_\pi^6\Big)\\
&\quad +8\cos(\theta^{[0]})\Big(6\left(M_\pi^2-M_K^2\right)M_{\eta'}^4+\left(-8M_K^4+16M_\pi^2M_K^2+M_\pi^4\right)M_{\eta'}^2+32M_K^6\\
&\quad -76M_\pi^2M_K^4+50M_\pi^4M_K^2-15M_\pi^6\Big)\Big], \qquad \text{(B.33)}
\end{aligned}
$$

where $K_1=-16\pi^2(\tilde{L}_2+2\tilde{L}_3)$.

The loop contributions to the form factors of the decays $\eta^{(\prime)}\to\pi^+\pi^-\gamma^*$ given by the loop diagrams in Fig. 8.1 read

$$
\begin{aligned}
&F(\eta\to\pi^+\pi^-\gamma^*)\\
&=\frac{1}{768\sqrt{3}\pi^4F_\pi^5}\Big[2\cos(\theta^{[0]})\Big(3\left(q^2-4M_K^2\right)B_0\left(q^2,M_K^2,M_K^2\right)\\
&\quad +2\left(s_{\pi\pi}-4M_K^2\right)B_0\left(s_{\pi\pi},M_K^2,M_K^2\right)+\left(s_{\pi\pi}-4M_\pi^2\right)B_0\left(s_{\pi\pi},M_\pi^2,M_\pi^2\right)\\
&\quad +2A_0\left(M_K^2\right)+22A_0\left(M_\pi^2\right)+2\left(-10M_K^2-2M_\pi^2+q^2+s_{\pi\pi}\right)\Big)\\
&\quad -\sqrt{2}\sin(\theta^{[0]})\Big(\left(s_{\pi\pi}-4M_K^2\right)B_0\left(s_{\pi\pi},M_K^2,M_K^2\right)+2\Big(\left(s_{\pi\pi}-4M_\pi^2\right)\\
&\quad \times B_0\left(s_{\pi\pi},M_\pi^2,M_\pi^2\right)-2M_K^2-4M_\pi^2+s_{\pi\pi}\Big)+22A_0\left(M_K^2\right)+44A_0\left(M_\pi^2\right)\Big)\Big]
\end{aligned}
$$

(B.34)

and

$$
\begin{aligned}
&F(\eta' \to \pi^+\pi^-\gamma^*) \\
&= \frac{1}{768\sqrt{3}\pi^4 F_\pi^5}\Big[2\sin(\theta^{[0]})\left(3\left(q^2-4M_K^2\right)B_0\left(q^2,M_K^2,M_K^2\right)\right. \\
&\quad + 2\left(s_{\pi\pi}-4M_K^2\right)B_0\left(s_{\pi\pi},M_K^2,M_K^2\right)+\left(s_{\pi\pi}-4M_\pi^2\right)B_0\left(s_{\pi\pi},M_\pi^2,M_\pi^2\right) \\
&\quad \left. +2A_0\left(M_K^2\right)+22A_0\left(M_\pi^2\right)+2\left(-2\left(5M_K^2+M_\pi^2\right)+q^2+s_{\pi\pi}\right)\right) \\
&\quad +\sqrt{2}\cos(\theta^{[0]})\left(\left(s_{\pi\pi}-4M_K^2\right)B_0\left(s_{\pi\pi},M_K^2,M_K^2\right)+2\left(\left(s_{\pi\pi}-4M_\pi^2\right)\right.\right. \\
&\quad \left.\left.\times B_0\left(s_{\pi\pi},M_\pi^2,M_\pi^2\right)-2M_K^2-4M_\pi^2+s_{\pi\pi}\right)+22A_0\left(M_K^2\right)+44A_0\left(M_\pi^2\right)\right)\Big]. \qquad \text{(B.35)}
\end{aligned}
$$

Appendix C

Additional parameters

	μ [GeV]	L_5 [10^{-3}]	L_8 [10^{-3}]	$\tilde{\Lambda}$	L_{25} [10^{-3}]
NLO I	-	1.86 ± 0.06	0.78 ± 0.05	-0.34 ± 0.05	0 ± 0
NLO+Lps I	0.77	1.37 ± 0.06	0.85 ± 0.05	0.52 ± 0.05	0 ± 0
NLO+Lps I	1	0.75 ± 0.06	0.55 ± 0.05	1.09 ± 0.04	0 ± 0
NLO II	0.77	1.20 ± 0.10	0.55 ± 0.20	0.02 ± 0.13	0 ± 0
NLO II	1	0.58 ± 0.10	0.24 ± 0.20	0.41 ± 0.13	0 ± 0
NLO+Lps II	0.77	1.20 ± 0.10	0.55 ± 0.20	1.34 ± 0.13	0 ± 0
NLO+Lps II	1	0.58 ± 0.10	0.24 ± 0.20	1.34 ± 0.13	0 ± 0
NNLO w/o Ci	0.77	1.20 ± 0.10	0.55 ± 0.20	0 ± 0	0.55 ± 0.08
NNLO w/o Ci	1	0.58 ± 0.10	0.24 ± 0.20	0 ± 0	0.50 ± 0.08
NNLO w/ Ci	0.77	1.01 ± 0.06	0.52 ± 0.10	0 ± 0	0.84 ± 0.04
NNLO w/ Ci	1	0.39 ± 0.06	0.21 ± 0.10	0 ± 0	0.80 ± 0.04

Table C.1: Summary of the results for the LECs determined in the numerical analysis of the η-η' mixing in Sec. 5.4.

	μ [GeV]	L_4 [10^{-3}]	L_6 [10^{-3}]	L_7 [10^{-3}]	L_{18} [10^{-3}]
NLO I	-	0 ± 0	0 ± 0	0 ± 0	0 ± 0
NLO+Lps I	0.77	0 ± 0	0 ± 0	0 ± 0	0 ± 0
NLO+Lps I	1	0 ± 0	0 ± 0	0 ± 0	0 ± 0
NLO II	0.77	0 ± 0	0 ± 0	0 ± 0	0 ± 0
NLO II	1	0 ± 0	0 ± 0	0 ± 0	0 ± 0
NLO+Lps II	0.77	0.21 ± 0	0.10 ± 0	0 ± 0	-0.41 ± 0
NLO+Lps II	1	0 ± 0	0 ± 0	0 ± 0	0 ± 0
NNLO w/o Ci	0.77	0.00 ± 0.30	0.04 ± 0.40	0.00 ± 0.20	-0.41 ± 0
NNLO w/o Ci	1	-0.21 ± 0.30	-0.07 ± 0.40	0.00 ± 0.20	0 ± 0
NNLO w/ Ci	0.77	0.30 ± 0	0.18 ± 0.05	0.00 ± 0.09	-0.41 ± 0
NNLO w/ Ci	1	0.09 ± 0	0.07 ± 0.05	0.00 ± 0.09	0 ± 0

Table C.2: Input LECs used in Sec. 5.4.

	μ [GeV]	C_{12} [10^{-3}]	C_{14} [10^{-3}]	C_{17} [10^{-3}]	C_{19} [10^{-3}]	C_{31} [10^{-3}]
NLO I	-	0 ± 0	0 ± 0	0 ± 0	0 ± 0	0 ± 0
NLO+Lps I	0.77	0 ± 0	0 ± 0	0 ± 0	0 ± 0	0 ± 0
NLO+Lps I	1	0 ± 0	0 ± 0	0 ± 0	0 ± 0	0 ± 0
NLO II	0.77	0 ± 0	0 ± 0	0 ± 0	0 ± 0	0 ± 0
NLO II	1	0 ± 0	0 ± 0	0 ± 0	0 ± 0	0 ± 0
NLO+Lps II	0.77	0 ± 0	0 ± 0	0 ± 0	0 ± 0	0 ± 0
NLO+Lps II	1	0 ± 0	0 ± 0	0 ± 0	0 ± 0	0 ± 0
NNLO w/o Ci	0.77	0 ± 0	0 ± 0	0 ± 0	0 ± 0	0 ± 0
NNLO w/o Ci	1	0 ± 0	0 ± 0	0 ± 0	0 ± 0	0 ± 0
NNLO w/ Ci	0.77	-0.33 ± 0	-0.12 ± 0	-0.12 ± 0	-0.47 ± 0	0.24 ± 0
NNLO w/ Ci	1	-0.33 ± 0	-0.12 ± 0	-0.12 ± 0	-0.47 ± 0	0.24 ± 0

Table C.3: Input LECs used in Sec. 5.4 in GeV^{-2}.

	q_{max} [GeV]	A_η	B_η [GeV^{-2}]	C_η [GeV^{-4}]
Full	0.47	-0.17 ± 0.02	2.16 ± 0.18	11.57 ± 1.46
Full	0.40	-0.17 ± 0.02	2.44 ± 0.23	8.37 ± 2.21
Full	0.35	-0.17 ± 0.02	2.46 ± 0.32	8.01 ± 3.91
Full Qexp	0.47	0.66 ± 0.02	2.23 ± 0.18	11.65 ± 1.46
Full Qexp	0.40	0.66 ± 0.02	2.51 ± 0.23	8.44 ± 2.21
Full Qexp	0.35	0.66 ± 0.02	2.53 ± 0.32	8.09 ± 3.91
W/O loops	0.47	-0.17 ± 0.02	2.84 ± 0.17	12.30 ± 1.44
W/O loops	0.40	-0.17 ± 0.02	3.06 ± 0.23	9.75 ± 2.21
W/O loops	0.35	-0.17 ± 0.02	3.02 ± 0.32	10.31 ± 3.90
W/O loops Qexp	0.47	0.66 ± 0.02	2.84 ± 0.17	12.30 ± 1.44
W/O loops Qexp	0.40	0.66 ± 0.02	3.06 ± 0.23	9.75 ± 2.21
W/O loops Qexp	0.35	0.66 ± 0.02	3.02 ± 0.32	10.31 ± 3.90
Cp=0	0.47	-0.17 ± 0.03	3.41 ± 0.12	0 ± 0
Cp=0	0.40	-0.17 ± 0.03	3.24 ± 0.11	0 ± 0
Cp=0	0.35	-0.17 ± 0.03	3.08 ± 0.11	0 ± 0
Cp=0 Qexp	0.47	0.66 ± 0.03	3.49 ± 0.12	0 ± 0
Cp=0 Qexp	0.40	0.66 ± 0.03	3.32 ± 0.11	0 ± 0
Cp=0 Qexp	0.35	0.66 ± 0.03	3.16 ± 0.11	0 ± 0
W/O loops Cp=0	0.47	-0.17 ± 0.03	4.17 ± 0.13	0 ± 0
W/O loops Cp=0	0.40	-0.17 ± 0.03	4.00 ± 0.11	0 ± 0
W/O loops Cp=0	0.35	-0.17 ± 0.03	3.82 ± 0.11	0 ± 0
W/O loops Cp=0 Qexp	0.47	0.66 ± 0.03	4.17 ± 0.13	0 ± 0
W/O loops Cp=0 Qexp	0.40	0.66 ± 0.03	4.00 ± 0.11	0 ± 0
W/O loops Cp=0 Qexp	0.35	0.66 ± 0.03	3.82 ± 0.11	0 ± 0

Table C.4: Fit parameters for the η TFF determined in Sec. 7.2.2.

	Fit	$A_{\eta'}$	$B_{\eta'}$ [GeV^{-2}]	$C_{\eta'}$ [GeV^{-4}]
Full	I	-0.06 ± 0.02	1.08 ± 0.18	1.18 ± 0.37
Full	II	-0.06 ± 0.01	0.95 ± 0.16	0.92 ± 0.33
Full	III	-0.06 ± 0.01	1.12 ± 0.11	2.89 ± 0.50
Full	IV	-0.06 ± 0.01	1.04 ± 0.11	2.43 ± 0.51
Full Qexp	I	-0.29 ± 0.02	1.07 ± 0.18	1.17 ± 0.37
Full Qexp	II	-0.29 ± 0.01	0.95 ± 0.16	0.91 ± 0.33
Full Qexp	III	-0.29 ± 0.01	1.11 ± 0.11	2.89 ± 0.50
Full Qexp	IV	-0.29 ± 0.01	1.03 ± 0.11	2.42 ± 0.51
W/O loops	I	-0.06 ± 0.02	1.23 ± 0.18	1.30 ± 0.37
W/O loops	II	-0.06 ± 0.01	1.10 ± 0.16	1.04 ± 0.33
W/O loops	III	-0.06 ± 0.01	1.27 ± 0.11	3.03 ± 0.48
W/O loops	IV	-0.06 ± 0.01	1.19 ± 0.11	2.59 ± 0.50
W/O loops Qexp	I	-0.29 ± 0.02	1.23 ± 0.18	1.30 ± 0.37
W/O loops Qexp	II	-0.29 ± 0.01	1.10 ± 0.16	1.04 ± 0.33
W/O loops Qexp	III	-0.29 ± 0.01	1.27 ± 0.11	3.03 ± 0.48
W/O loops Qexp	IV	-0.29 ± 0.01	1.19 ± 0.11	2.59 ± 0.50
Cp=0	I	-0.06 ± 0.02	0.55 ± 0.10	0 ± 0
Cp=0	II	-0.06 ± 0.02	0.54 ± 0.08	0 ± 0
Cp=0	III	-0.06 ± 0.02	0.78 ± 0.21	0 ± 0
Cp=0	IV	-0.06 ± 0.02	0.72 ± 0.17	0 ± 0
Cp=0 Qexp	I	-0.29 ± 0.02	0.54 ± 0.10	0 ± 0
Cp=0 Qexp	II	-0.29 ± 0.02	0.53 ± 0.08	0 ± 0
Cp=0 Qexp	III	-0.29 ± 0.02	0.77 ± 0.21	0 ± 0
Cp=0 Qexp	IV	-0.29 ± 0.02	0.71 ± 0.17	0 ± 0
W/O loops Cp=0	I	-0.06 ± 0.02	0.64 ± 0.10	0 ± 0
W/O loops Cp=0	II	-0.06 ± 0.02	0.63 ± 0.09	0 ± 0
W/O loops Cp=0	III	-0.06 ± 0.02	0.91 ± 0.22	0 ± 0
W/O loops Cp=0	IV	-0.06 ± 0.02	0.85 ± 0.18	0 ± 0
W/O loops Cp=0 Qexp	I	-0.29 ± 0.02	0.64 ± 0.10	0 ± 0
W/O loops Cp=0 Qexp	II	-0.29 ± 0.02	0.63 ± 0.09	0 ± 0
W/O loops Cp=0 Qexp	III	-0.29 ± 0.02	0.91 ± 0.22	0 ± 0
W/O loops Cp=0 Qexp	IV	-0.29 ± 0.02	0.85 ± 0.18	0 ± 0

Table C.5: Fit parameters for the η' TFF determined in Sec. 7.2.2. The fit ranges are: -0.53 GeV$^2 \leq q^2 \leq 0.43$ GeV^2 (I), -0.53 GeV$^2 \leq q^2 \leq 0.40$ GeV^2 (II), -0.50 GeV$^2 \leq q^2 \leq 0.43$ GeV^2 (III), -0.50 GeV$^2 \leq q^2 \leq 0.40$ GeV^2 (IV).

	A_η [10^{10}]	b_η	c_η [GeV^{-2}]	d_η [GeV^{-4}]
Full	1.29 ± 0.05	0.09 ± 0.17	-4.60 ± 2.13	34.35 ± 6.35
W/O loops	1.45 ± 0.07	-0.01 ± 0.17	-3.30 ± 2.02	31.49 ± 6.01
dp=0	1.28 ± 0.07	-2.03 ± 0.06	-8.41 ± 0.41	0 ± 0
dp=0 w/o loops	1.43 ± 0.09	-0.84 ± 0.06	7.24 ± 0.41	0 ± 0

Table C.6: Fit parameters for the η spectrum at NNLO determined in Sec. 8.2.

	$A_{\eta'}$ [10^6]	$b_{\eta'}$	$c_{\eta'}$ [GeV^{-2}]	$d_{\eta'}$ [GeV^{-4}]
Full I	-48.57 ± 16.05	-0.59 ± 0.49	-3.20 ± 4.11	4.77 ± 8.76
Full II	-45.34 ± 4.93	-0.34 ± 0.23	-5.05 ± 1.70	7.84 ± 2.90
Full III	-44.38 ± 14.19	-1.31 ± 0.11	1.32 ± 0.75	-2.59 ± 0.92
dp=0 I	-47.21 ± 6.75	-1.19 ± 0.07	0.20 ± 0.31	0 ± 0
dp=0 II	-45.03 ± 5.37	-0.88 ± 0.05	-0.80 ± 0.17	0 ± 0
dp=0 III	-42.57 ± 4.43	-0.85 ± 0.03	-0.89 ± 0.08	0 ± 0

Table C.7: Fit parameters for the η' spectrum at NNLO including loops determined in Sec. 8.2.

	$\tilde{A}_{\eta'}$ [10^5]	$\tilde{c}_{\eta'}$ [GeV^{-2}]	$\tilde{d}_{\eta'}$ [GeV^{-4}]
W/O loops I	-19.06 ± 28.20	-5.93 ± 1.14	12.73 ± 1.67
W/O loops II	-11.27 ± 10.94	-5.27 ± 0.70	11.75 ± 1.35
W/O loops III	-7.53 ± 4.04	-4.88 ± 0.27	11.73 ± 1.35
dp=0 w/o loops I	-0.01 ± 0.13	50.58 ± 325.28	0 ± 0
dp=0 w/o loops II	-0.28 ± 0.52	-14.14 ± 10.36	0 ± 0
dp=0 w/o loops III	-3.78 ± 1.80	-5.98 ± 0.86	0 ± 0

Table C.8: Fit parameters for the η' spectrum at NNLO without loops determined in Sec. 8.2.

Appendix D

Additional plots

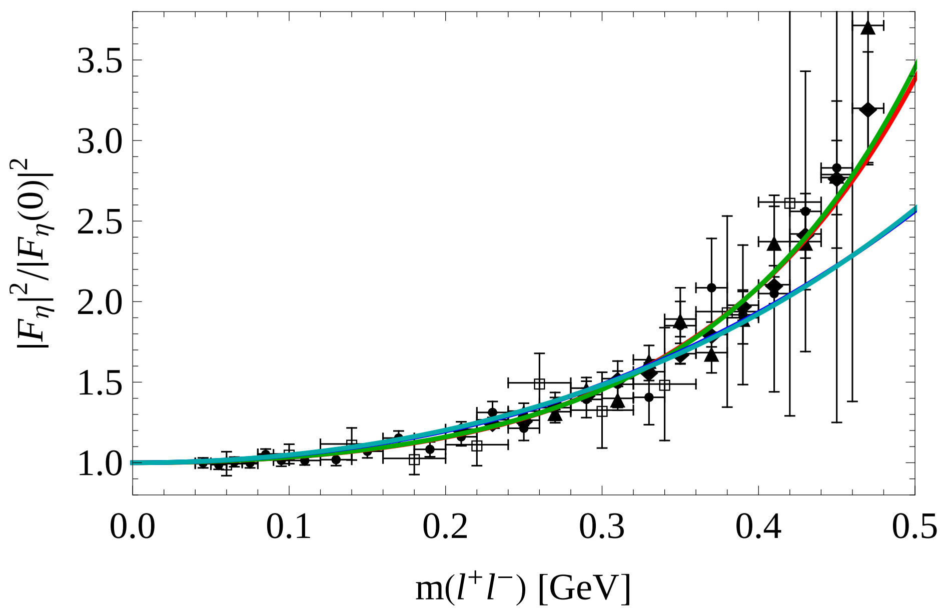

Figure D.1: η TFF fitted up to 0.47 GeV. The red line is the full NNLO calculation, the green line the NNLO result without loops. The blue lines coincide and are the NNLO results with $C_\eta = 0$ including loops (dark blue) and without loops (light blue). The experimental data are taken from Refs. [Arn+ 09] (▲), [Ber+ 11] (□), [Agu+ 14] (■), [Arn+ 16] (♦).

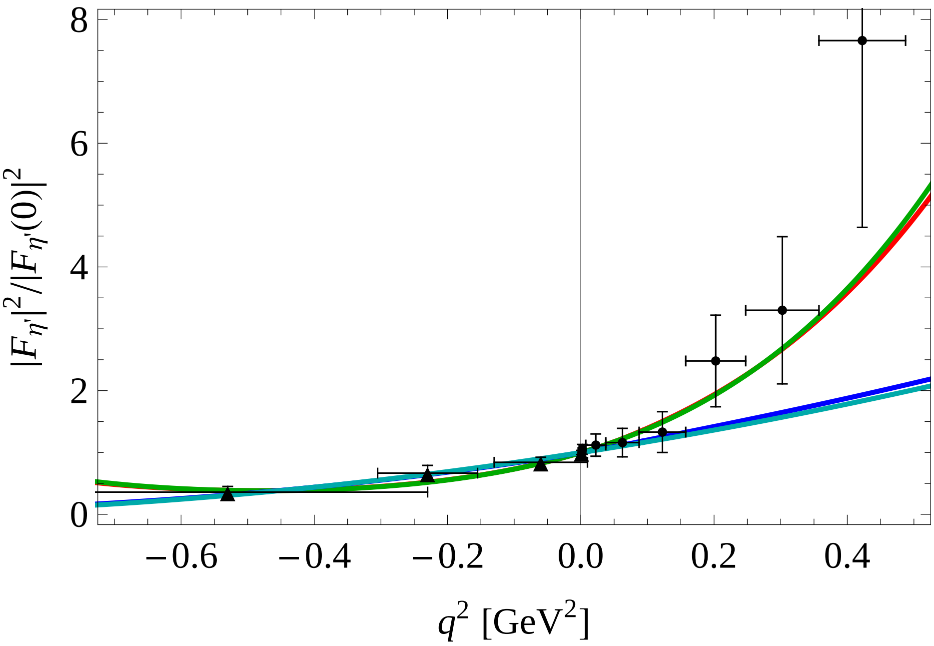

Figure D.2: η' TFF fitted between -0.53 GeV^2 and 0.43 GeV^2. The red line is the full NNLO calculation and the green line the NNLO result without loops. The blue lines are the NNLO results with $C_{\eta'} = 0$ including loops (dark blue) and without loops (light blue). The time-like data are taken from Ref. [Abl+ 15] (•) and the space-like data from Ref. [Acc+ 98] (▲).

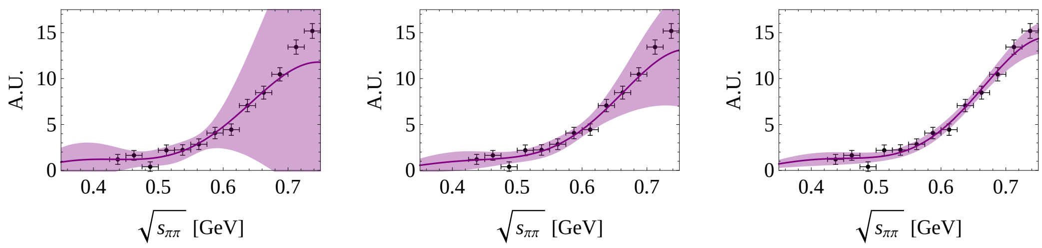

Figure D.3: Invariant-mass spectrum of the $\pi^+\pi^-$ system in $\eta' \to \pi^+\pi^-\gamma$ at NNLO with $d_{\eta'} = 0$ fitted up to 0.59 GeV (left), 0.64 GeV (middle), 0.72 GeV (right) including the 1σ error bands. The experimental data are taken from Ref. [Abe+ 97].

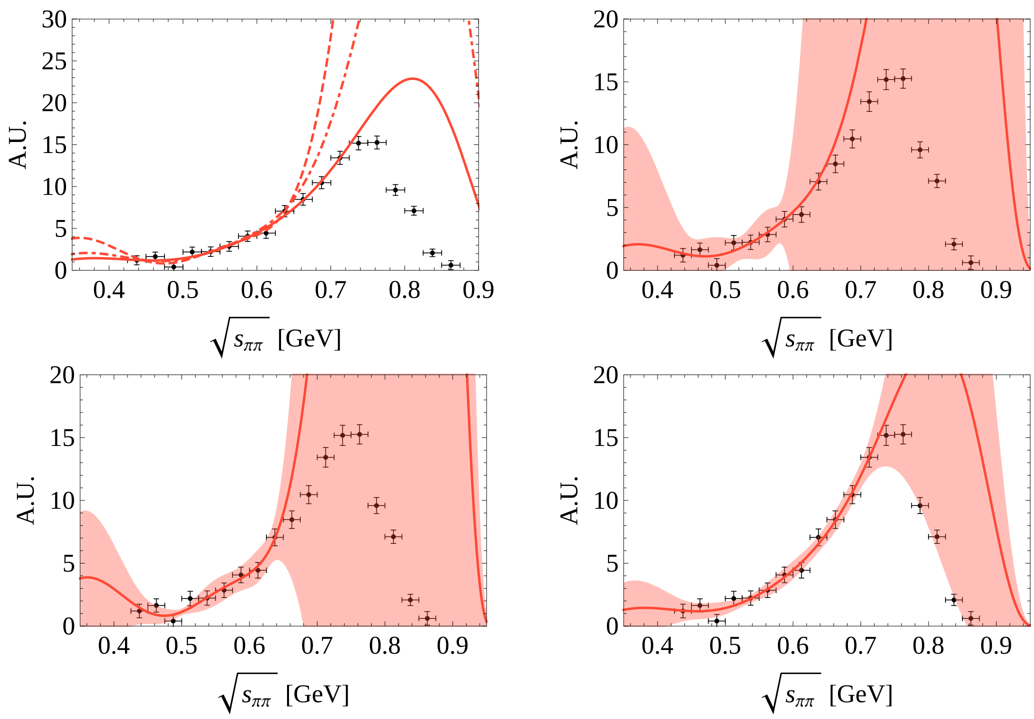

Figure D.4: Upper-left plot: Invariant-mass spectrum of the $\pi^+\pi^-$ system in $\eta' \to \pi^+\pi^-\gamma$ at NNLO fitted up to 0.59 GeV (dash-dotted), 0.64 GeV (dashed), 0.72 GeV (solid). Upper-right plot: 1σ error band for the fit up to 0.59 GeV. Lower-left plot: 1σ error band for the fit up to 0.64 GeV. Lower-right plot: 1σ error band for the fit up to 0.72 GeV. The experimental data are taken from Ref. [Abe+ 97].

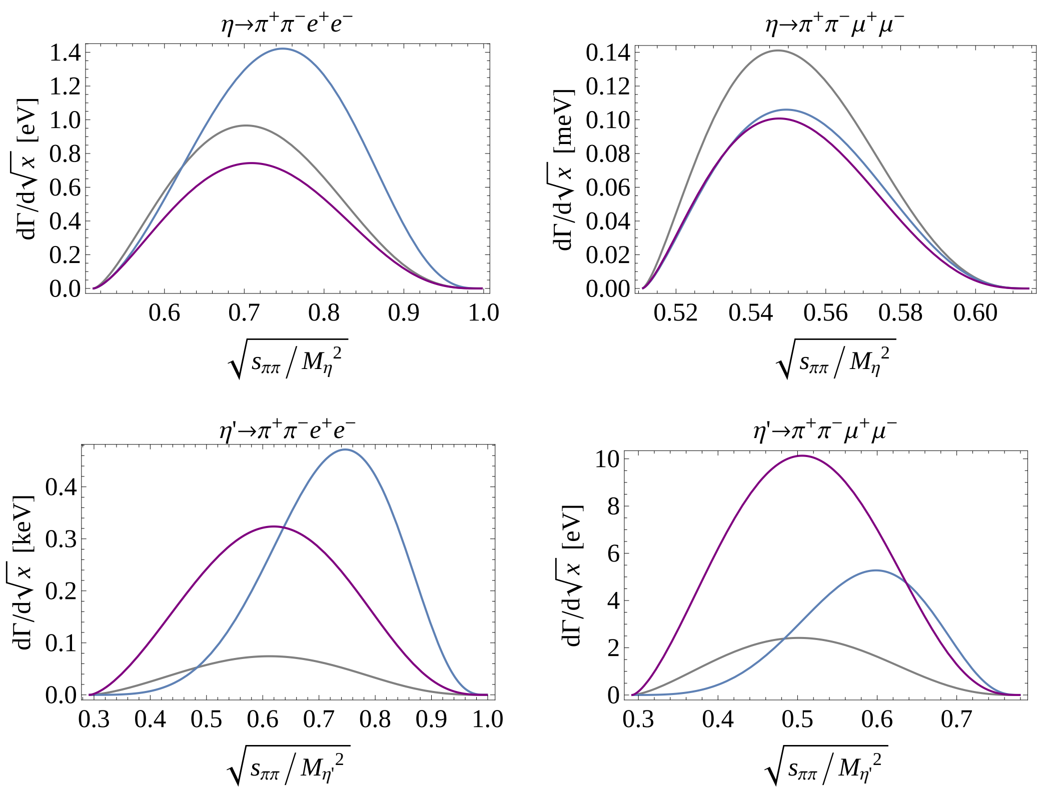

Figure D.5: Invariant-mass spectra of the $\pi^+\pi^-$ system at LO (gray), NLO with $c_{14} = 0$ (blue), and LO with loops added (purple).

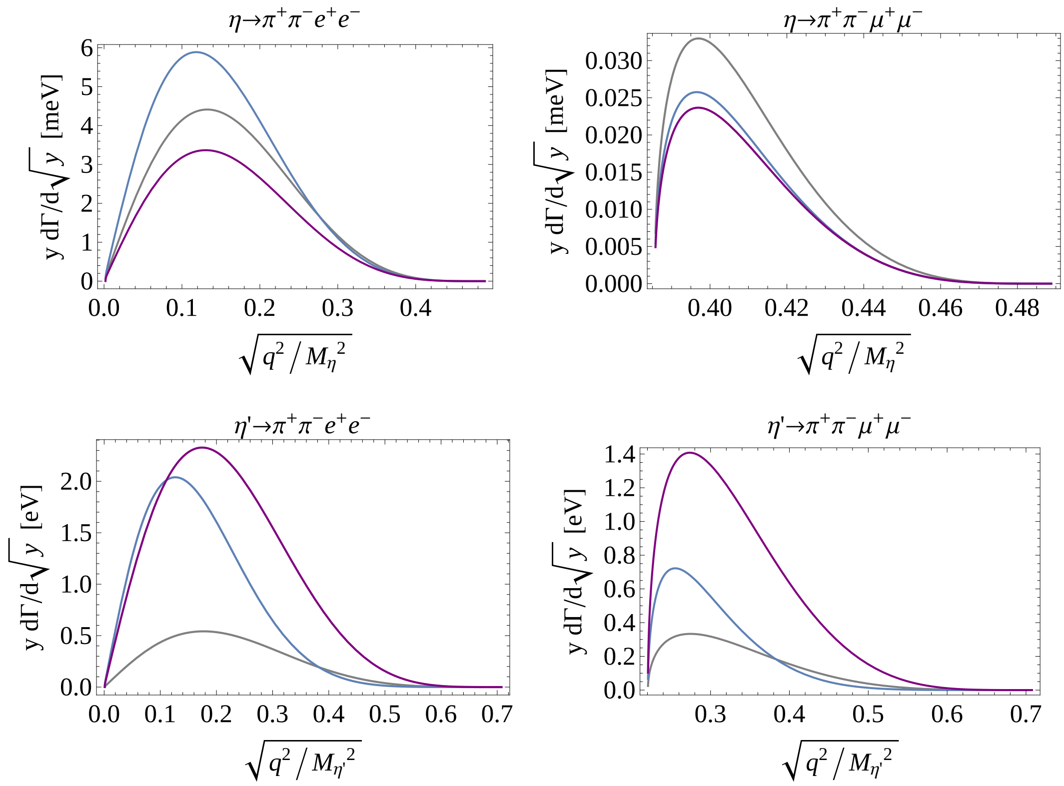

Figure D.6: Invariant-mass spectra of the l^+l^- system at LO (gray), NLO with $c_{14} = 0$ (blue), and LO with loops added (purple).

Bibliography

[AB 69] S. L. Adler and W. A. Bardeen, Phys. Rev. **182**, 1517 (1969).

[Abe+ 97] A. Abele *et al.* [Crystal Barrel Collaboration], Phys. Lett. B **402**, 195 (1997).

[Abl+ 15] M. Ablikim *et al.* [BESIII Collaboration], Phys. Rev. D **92**, no. 1, 012001 (2015) [arXiv:1504.06016 [hep-ex]].

[Acc+ 98] M. Acciarri *et al.* [L3 Collaboration], Phys. Lett. B **418**, 399 (1998).

[Adl 69] S. L. Adler, Phys. Rev. **177**, 2426 (1969).

[Adl+ 12] P. Adlarson *et al.* [WASA-at-COSY Collaboration], Phys. Lett. B **707**, 243 (2012) [arXiv:1107.5277 [nucl-ex]].

[AF 89] R. Akhoury and J. M. Frere, Phys. Lett. B **220**, 258 (1989).

[Agu+ 14] P. Aguar-Bartolome *et al.* [A2 Collaboration], Phys. Rev. C **89**, no. 4, 044608 (2014) [arXiv:1309.5648 [hep-ex]].

[Aih+ 90] H. Aihara *et al.* [TPC/Two Gamma Collaboration], Phys. Rev. Lett. **64**, 172 (1990).

[Alt 81] G. Altarelli, Phys. Rept. **81**, 1 (1982).

[Amb+ 11] F. Ambrosino *et al.* [KLOE and KLOE-2 Collaborations], Phys. Lett. B **702**, 324 (2011) [arXiv:1105.6067 [hep-ex]].

[Ame+ 83] L. Ametller, L. Bergstrom, A. Bramon, and E. Masso, Nucl. Phys. B **228**, 301 (1983).

[Ame+ 92] L. Ametller, J. Bijnens, A. Bramon, and F. Cornet, Phys. Rev. D **45**, 986 (1992).

[Aok+ 14] S. Aoki, Y. Aoki, C. Bernard, T. Blum, G. Colangelo, M. Della Morte, S. Dürr, and A. X. El Khadra *et al.*, Eur. Phys. J. C **74**, no. 9, 2890 (2014) [arXiv:1310.8555 [hep-lat]].

[Arn+ 09] R. Arnaldi *et al.* [NA60 Collaboration], Phys. Lett. B **677**, 260 (2009) [arXiv:0902.2547 [hep-ph]].

[Arn+ 16] R. Arnaldi *et al.* [NA60 Collaboration], Phys. Lett. B **757**, 437 (2016) [arXiv:1608.07898 [hep-ex]].

[Ams+ 14] C. Amsler, T. DeGrand, and B. Krusche, *Quark Model*, in Ref. [Oli+ 14], p 259.

[Bak 06] C. A. Baker *et al.*, Phys. Rev. Lett. **97**, 131801 (2006) [hep-ex/0602020].

[Bar 69] W. A. Bardeen, Phys. Rev. **184**, 1848 (1969).

[BBC 88] J. Bijnens, A. Bramon, and F. Cornet, Phys. Rev. Lett. **61**, 1453 (1988).

[BBC 90] J. Bijnens, A. Bramon, and F. Cornet, Phys. Lett. B **237**, 488 (1990).

[BCE 99] J. Bijnens, G. Colangelo, and G. Ecker, JHEP **9902**, 020 (1999).

[BDC 00] M. Benayoun, L. DelBuono, and H. B. O'Connell, Eur. Phys. J. C **17**, 593 (2000).

[BE 14] J. Bijnens and G. Ecker, Ann. Rev. Nucl. Part. Sci. **64**, 149 (2014).

[Beh+ 91] H. J. Behrend *et al.* [CELLO Collaboration], Z. Phys. C **49**, 401 (1991).

[Ben+ 03] M. Benayoun, P. David, L. DelBuono, P. Leruste, and H. B. O'Connell, Eur. Phys. J. C **31**, 525 (2003) [nucl-th/0306078].

[Ben+ 10] M. Benayoun, P. David, L. DelBuono, and O. Leitner, Eur. Phys. J. C **65**, 211 (2010) [arXiv:0907.4047 [hep-ph]].

[Ber+ 11] H. Berghauser *et al.*, Phys. Lett. B **701**, 562 (2011).

[BES 97] A. Bramon, R. Escribano, and M. D. Scadron, Phys. Lett. B **403**, 339 (1997) [hep-ph/9703313].

[BES 99] A. Bramon, R. Escribano, and M. D. Scadron, Eur. Phys. J. C **7**, 271 (1999) [hep-ph/9711229].

[BFT 96] P. Ball, J. M. Frere, and M. Tytgat, Phys. Lett. B **365**, 367 (1996) [hep-ph/9508359].

[BGT 02] J. Bijnens, L. Girlanda, and P. Talavera, Eur. Phys. J. C **23**, 539 (2002) [hep-ph/0110400].

[BH 13] A. M. Bernstein and B. R. Holstein, Rev. Mod. Phys. **85**, 49 (2013) [arXiv:1112.4809 [hep-ph]].

[Bij 93] J. Bijnens, Int. J. Mod. Phys. A **8**, 3045 (1993).

[BJ 69] J. S. Bell and R. Jackiw, Nuovo Cim. A **60**, 47 (1969).

[BL 81] S. J. Brodsky and G. P. Lepage, Phys. Rev. D **24**, 1808 (1981).

[BL 05] B. Borasoy and E. Lipartia, Phys. Rev. D **71**, 014027 (2005) [hep-ph/0410141].

[BM 81] A. Bramon and E. Masso, Phys. Lett. B **104**, 311 (1981).

[BN 04a] B. Borasoy and R. Nißler, Eur. Phys. J. A **19**, 367 (2004) [hep-ph/0309011].

[BN 04b] B. Borasoy and R. Nißler, Nucl. Phys. A **740**, 362 (2004) [hep-ph/0405039].

[BN 07] B. Borasoy and R. Nißler, Eur. Phys. J. A **33**, 95 (2007) [arXiv:0705.0954 [hep-ph]].

[Bor 04] B. Borasoy, Eur. Phys. J. C **34**, 317 (2004).

[BW 01] O. Bär and U. J. Wiese, Nucl. Phys. B **609**, 225 (2001) [hep-ph/0105258].

[Col 66] S. Coleman, J. Math. Phys. **7**, 787 (1966).

[Col+ 11] G. Colangelo *et al.*, Eur. Phys. J. C **71**, 1695 (2011) [arXiv:1011.4408 [hep-lat]].

[Col+ 14] G. Colangelo, M. Hoferichter, B. Kubis, M. Procura, and P. Stoffer, Phys. Lett. B **738**, 6 (2014) [arXiv:1408.2517 [hep-ph]].

[Col+ 15] G. Colangelo, M. Hoferichter, M. Procura, and P. Stoffer, JHEP **1509**, 074 (2015) [arXiv:1506.01386 [hep-ph]].

[Cre 90] M. Creutz, Quarks, Gluons and Lattices (Cambridge University Press, Cambridge, 1990).

[CW 80] S. R. Coleman and E. Witten, Phys. Rev. Lett. **45**, 100 (1980).

[Czy+ 12] H. Czyz, S. Ivashyn, A. Korchin, and O. Shekhovtsova, Phys. Rev. D **85**, 094010 (2012) [arXiv:1202.1171 [hep-ph]].

[DW 89] J. F. Donoghue and D. Wyler, Nucl. Phys. B **316**, 289 (1989).

[Dzh+ 79] R. I. Dzhelyadin *et al.*, Phys. Lett. B **88**, 379 (1979) [JETP Lett. **30**, 359 (1979)].

[Dzh+ 80] R. I. Dzhelyadin *et al.*, Phys. Lett. B **94**, 548 (1980) [Sov. J. Nucl. Phys. **32**, 516 (1980)] [Yad. Fiz. **32**, 998 (1980)].

[Eck+ 89a] G. Ecker *et al.*, Nucl. Phys. B **321**, 311 (1989).

[Eck+ 89b] G. Ecker *et al.*, Phys. Lett. B **223**, 425 (1989).

[EF 05] R. Escribano and J. M. Frere, JHEP **0506**, 029 (2005).

[EFS 02] T. Ebertshäuser, H. W. Fearing, and S. Scherer, Phys. Rev. D **65**, 054033 (2002) [hep-ph/0110261].

[EG 15] R. Escribano and S. Gonzalez-Solis, arXiv:1511.04916 [hep-ph].

[EGM 15] R. Escribano, S. Gonzalez-Solis, P. Masjuan, and P. Sanchez-Puertas, arXiv:1512.07520 [hep-ph].

[EMS 11] R. Escribano, P. Masjuan, and J. J. Sanz-Cillero, JHEP **1105**, 094 (2011).

[EMS 14] R. Escribano, P. Masjuan, and P. Sanchez-Puertas, Phys. Rev. D **89**, no. 3, 034014 (2014).

[EMS 15] R. Escribano, P. Masjuan, and P. Sanchez-Puertas, Eur. Phys. J. C **75**, no. 9, 414 (2015).

[ET 82] D. Espriu and R. Tarrach, Z. Phys. C **16**, 77 (1982).

[FFK 00] A. Fäßler, C. Fuchs, and M. I. Krivoruchenko, Phys. Rev. C **61**, 035206 (2000) [nucl-th/9904024].

[FGL 73] H. Fritzsch, M. Gell-Mann, and H. Leutwyler, Phys. Lett. B **47**, 365 (1973).

[FJ 77] H. Fritzsch and J. D. Jackson, Phys. Lett. B **66**, 365 (1977).

[Fra 55] E. S. Fradkin, Zh. Eksp. Teor. Fiz. **29**, 258 (1955) [Sov. Phys. JETP **2**, 361 (1956)].

[FKS 98] T. Feldmann, P. Kroll, and B. Stech, Phys. Rev. D **58**, 114006 (1998).

[FKS 99] T. Feldmann, P. Kroll, and B. Stech, Phys. Lett. B **449**, 339 (1999).

[FS 96] H. W. Fearing and S. Scherer, Phys. Rev. D **53**, 315 (1996).

[FS 00] H. W. Fearing and S. Scherer, Phys. Rev. C **62**, 034003 (2000).

[Fuj 79] K. Fujikawa, Phys. Rev. Lett. **42**, 1195 (1979).

[Fuj 80] K. Fujikawa, Phys. Rev. D **21**, 2848 (1980) [Phys. Rev. D **22**, 1499 (1980)].

[GBH 02] J. L. Goity, A. M. Bernstein, and B. R. Holstein, Phys. Rev. D **66**, 076014 (2002) [hep-ph/0206007].

[Geo 84] H. Georgi, Weak Interactions and Modern Particle Theory (Benjamin/Cummings, Menlo Park, 1984).

[GK 87] F. J. Gilman and R. Kauffman, Phys. Rev. D **36**, 2761 (1987) Erratum: [Phys. Rev. D **37**, 3348 (1988)].

[GL 84] J. Gasser and H. Leutwyler, Annals Phys. **158**, 142 (1984).

[GL 85] J. Gasser and H. Leutwyler, Nucl. Phys. B **250**, 465 (1985).

[Gol 61] J. Goldstone, Nuovo Cim. **19**, 154 (1961).

[Gor+ 70] M. Gormley, E. Hyman, W. Y. Lee, T. Nash, J. Peoples, C. Schultz, and S. Stein, Phys. Rev. D **2**, 501 (1970).

[Gro+ 98] J. Gronberg *et al.* [CLEO Collaboration], Phys. Rev. D **57**, 33 (1998) [hep-ex/9707031].

[GT 58] M. Goldberger and S. Treiman, Phys. Rev. **110**, 1178 (1958).

[Guo+ 15] X. K. Guo, Z. H. Guo, J. A. Oller, and J. J. Sanz-Cillero, JHEP **1506** 175, (2015).

[Gup 53] S. Gupta, Proc. Phys. Soc. London Sect. A **66**, 129 (1953).

[GW 73a] D. J. Gross and F. Wilczek, Phys. Rev. Lett. **30**, 1343 (1973).

[GW 73b] D. J. Gross and F. Wilczek, Phys. Rev. D **8**, 3633 (1973).

[Hac 08] C. Hacker, PhD Thesis, Johannes Gutenberg-Universität, Mainz (2008).

[Hah 01] T. Hahn, Comput. Phys. Commun. **140**, 418 (2001) [hep-ph/0012260].

[Han+ 15] C. Hanhart, A. Kupść, U.-G. Meißner, F. Stollenwerk, and A. Wirzba, Eur. Phys. J. C **73**, no. 12, 2668 (2013) Erratum: [Eur. Phys. J. C **75**, no. 6, 242 (2015)] [arXiv:1307.5654 [hep-ph]].

[Her+ 97] P. Herrera-Siklody, J. I. Latorre, P. Pascual, and J. Taron, Nucl. Phys. B **497**, 345 (1997).

[Her 98] P. Herrera-Siklody, Phys. Lett. B **442**, 359 (1998).

[Her+ 98] P. Herrera-Siklody, J. I. Latorre, P. Pascual, and J. Taron, Phys. Lett. B **419**, 326 (1998) [hep-ph/9710268].

[HL 15] T. Husek and S. Leupold, Eur. Phys. J. C **75**, no. 12, 586 (2015) [arXiv:1507.00478 [hep-ph]].

[Hol 02] B. R. Holstein, Phys. Scripta T **99**, 55 (2002) [hep-ph/0112150].

[Hoo 74a] G. 't Hooft, Nucl. Phys. B **72**, 461 (1974).

[Hoo 74b] G. 't Hooft, Nucl. Phys. B **75**, 461 (1974).

[HP 99] T. Hahn and M. Perez-Victoria, Comput. Phys. Commun. **118**, 153 (1999) [hep-ph/9807565].

[Iiz 66] J. Iizuka, Suppl. Prog. Theor. Phys. **37**, 21 (1966).

[IKS 66] J. Iizuka, K. Okada, and O. Shito, Prog. Theor. Phys. **35**, 1061 (1966).

[Isg 76] N. Isgur, Phys. Rev. D **13**, 122 (1976).

[Jac 86] R. Jackiw, Helv. Phys. Acta **59**, 835 (1986).

[JGW 14] S. Z. Jiang, F. J. Ge, and Q. Wang, Phys. Rev. D **89** (2014) 7, 074048 [arXiv:1401.0317 [hep-ph]].

[JN 09] F. Jegerlehner and A. Nyffeler, Phys. Rept. **477**, 1 (2009) [arXiv:0902.3360 [hep-ph]].

[KL 98] R. Kaiser and H. Leutwyler, In *Adelaide 1998, Nonperturbative methods in quantum field theory* 15-29 [hep-ph/9806336].

[KL 00] R. Kaiser and H. Leutwyler, Eur. Phys. J. C **17**, 623 (2000).

[Kod 80] J. Kodaira, Nucl. Phys. B **165**, 129 (1980).

[KOT 14] Y. Klopot, A. Oganesian, and O. Teryaev, JETP Lett. **99**, 679 (2014) [arXiv:1312.1226 [hep-ph]].

[KP 15] B. Kubis and J. Plenter, Eur. Phys. J. C **75**, no. 6, 283 (2015) [arXiv:1504.02588 [hep-ph]].

[Lay+ 73] J. G. Layter, J. A. Appel, A. Kotlewski, W. Y. Lee, S. Stein, and J. J. Thaler, Phys. Rev. D **7**, 2565 (1973).

[Leb 99] R. F. Lebed, Czech. J. Phys. **49**, 1273 (1999) [nucl-th/9810080].

[Leu 94] H. Leutwyler, Annals Phys. **235**, 165 (1994) [hep-ph/9311274].

[Leu 96] H. Leutwyler, Phys. Lett. B **374**, 163 (1996).

[Leu 98] H. Leutwyler, Nucl. Phys. Proc. Suppl. **64**, 223 (1998).

[Lih 11] C. C. Lih, J. Phys. G **38**, 065001 (2011) [arXiv:0912.2147 [hep-ph]].

[LSZ 55] H. Lehmann, K. Symanzik, and W. Zimmermann, Nuovo Cim. **1**, 205 (1955).

[Man 85] J. L. Manes, Nucl. Phys. B **250**, 369 (1985).

[Man 97] A. V. Manohar, *Large N QCD*, in *Probing the Standard Model of Particle Interactions.* Proceedings, Summer School in Theoretical Physics, NATO Advanced Study Institute, 68th session, Les Houches, France, July 28 - September 5, 1997, Pt. 1, 2, edited by R. Gupta, A. Morel, E. de Rafael, and F. David (Elsevier, Amsterdam, 1999), hep-ph/9802419.

[Mas 12] P. Masjuan, Phys. Rev. D **86**, 094021 (2012) [arXiv:1206.2549 [hep-ph]].

[MBD 91] R. Mertig, M. Bohm, and A. Denner, Comput. Phys. Commun. **64**, 345 (1991).

[Mou 95] B. Moussallam, Phys. Rev. D **51**, 4939 (1995).

[MP 78] W. J. Marciano and H. Pagels, Phys. Rept. **36**, 137 (1978).

[MS 16] P. Masjuan and P. Sanchez-Puertas, JHEP **1608**, 108 (2016) [arXiv:1512.09292 [hep-ph]].

[MT 73] T. Miyazaki and E. Takasugi, Phys. Rev. D **8**, 2051 (1973).

[Mue 90] A. H. Mueller, Phys. Lett. B **234**, 517 (1990).

[Nec 09] S. Necco, PoS CONFINEMENT **8**, 024 (2008) [arXiv:0901.4257 [hep-lat]].

[Nyf 16] A. Nyffeler, arXiv:1602.03398 [hep-ph].

[Oli+ 14] K. A. Olive *et al.* [Particle Data Group Collaboration], Chin. Phys. C **38**, 090001 (2014).

[Oku 63] S. Okubo, Phys. Lett. **5**, 165 (1963).

[Oku 77] S. Okubo, Phys. Rev. D **16**, 2336 (1977).

[PB 84] A. Pich and J. Bernabeu, Z. Phys. C **22**, 197 (1984).

[Pet 10] T. Petri, arXiv:1010.2378 [nucl-th].

[Pic 92] C. Picciotto, Phys. Rev. D **45**, 1569 (1992).

[Pol 73] H. D. Politzer, Phys. Rev. Lett. **30**, 1346 (1973).

[PR 93] C. Picciotto and S. Richardson, Phys. Rev. D **48**, 3395 (1993).

[PS 95] M. E. Peskin and D. V. Schroeder, An Introduction to Quantum Field Theory (Westview Press, Boulder, 1995).

[PV 49] W. Pauli and F. Villars, Rev. Mod. Phys. **21**, 434 (1949).

[PV 79] G. Passarino and M. J. G. Veltman, Nucl. Phys. B **160**, 151 (1979).

[Sak 69] J. J. Sakurai, Currents and Mesons (The University of Chicago Press, Chicago, 1969).

[Sch 51] J. S. Schwinger, Phys. Rev. **82**, 664 (1951).

[Sch 62] J. S. Schwinger, Phys. Rev. **128**, 2425 (1962).

[Sch 03] S. Scherer, Adv. Nucl. Phys. **27**, 277 (2003).

[SF 95] S. Scherer and H. W. Fearing, Phys. Rev. D **52**, 6445 (1995).

[SS 12] S. Scherer and M. R. Schindler, Lect. Notes Phys. **830**, 1 (2012).

[Ste 49] J. Steinberger, Phys. Rev. **76**, 1180 (1949).

[Sto+ 12] F. Stollenwerk, C. Hanhart, A. Kupść, U. G. Meißner, and A. Wirzba, Phys. Lett. B **707**, 184 (2012) [arXiv:1108.2419 [nucl-th]].

[Sut 67] D. G. Sutherland, Nucl. Phys. B **2**, 433 (1967).

[Tak 57] Y. Takahashi, Nuovo Cim. **6**, 371 (1957).

[Tre+ 86] S. Treiman, E. Witten, R. Jackiw, and B. Zumino, 1986, Current Algebra and Anomalies (World Scientific, Singapore).

[Usa+ 11] G. Usai [NA60 Collaboration], Nucl. Phys. A **855**, 189 (2011).

[Vel 67] M. Veltman, Proc. R. Soc. Edinburgh, Sect. A **301**, 107 (1967).

[VH 98] E. P. Venugopal and B. R. Holstein, Phys. Rev. D **57**, 4397 (1998) [hep-ph/9710382].

[War 50] J. C. Ward, Phys. Rev. **78**, 182 (1950).

[Wei 67] S. Weinberg, Phys. Rev. Lett. **19**, 1264 (1967).

[Wei 68] S. Weinberg, Phys. Rev. **166**, 1568 (1968).

[Wei 73] S. Weinberg, Phys. Rev. Lett. **31**, 494 (1973).

[Wei 79] S. Weinberg, Physica A **96**, 327 (1979).

[Wei 95] S. Weinberg, The Quantum Theory of Fields Volume I (Cambridge University Press, Cambridge, 1995).

[Wil 74] K. G. Wilson, Phys. Rev. D **10**, 2445 (1974).

[Wit 79] E. Witten, Nucl. Phys. B **160**, 57 (1979).

[Wit 83] E. Witten, Nucl. Phys. B **223**, 422 (1983).

[WS 88] A. Widom and Y. Srivastava, Am. J. Phys. **56**, 824 (1988).

[WZ 71] J. Wess and B. Zumino, Phys. Lett. B **37**, 95 (1971).

[Zee 03] A. Zee, Quantum field theory in a nutshell (Princeton University Press, Princeton, 2003).

[Zwe 84] G. Zweig, CERN Report No. 8419 TH 412, 1964, reprinted in Developments in the Quark Theory of Hadrons, edited by D.B. Lichtenberg and S.P. Rosen (Hadronic Press, Massachusetts, 1980).